



The  
University  
Of  
Sheffield.

**Cellular uptake  
of PMPC-PDPA polymersomes  
in mammalian cells**

**Maria Milagros Avila Olias**

Faculty of Science

Department of Biomedical Science

June 2014

Submitted in partial fulfilment of the PhD degree  
for the Department of Biomedical Sciences,  
The University of Sheffield



# Acknowledgements

First of all I would like to express my sincerest thanks to my supervisors Prof. Giuseppe Battaglia and Prof. Elizabeth Symthe for their exceptional guidance and encouragement and all the resources presented to me during my PhD. I have to extend my gratitude to Dr. Louise Robson and Prof. Walter Marcotti for their great advisory labour, to Ibercaja Obra Social and the BBSRC for funding my PhD, and to Dr. Andrew Furley and the Department of Biomedical Science for the academic support and stimulating academic and scientific atmosphere. I will always be proud to be an alumna of The University of Sheffield and therefore I am very grateful to everyone that made it possible for me to complete my PhD at this university.

I would also like to thank the following people without whom the work presented in this thesis would not be possible:

Biocompatibles UK Ltd. for the MPC polymer and Prof. Steve Armes group members and ex-members Dr. Nicholas Warren and Dr. Jeppe Madsen, for the synthesis and characterisation of the PMPC-PDPA copolymers used on this thesis. Thanks to Dr. Jens Gaitzsch (Prof. Battaglia group) for the same reason.

Prof. Jane McKeating (The University of Birmingham) for kindly providing me with CD81 antibody, ITX5061 antagonist, and Huh 7 cells. Thanks for her useful discussion of the results and for sharing with me her knowledge in viral entry.

I have to specially thank Dr. Irene Canton for her training in different laboratory techniques and her priceless advice in experimental design and scientific writing. Thanks particularly for the work done together with the scavenger receptors.

Thanks to James Robertson for providing me with tubular polymersomes for my studies and for his enthusiasm for science, it has been a pleasure to work with him. Thanks to Dr. Nisa Patikarnmothon for helping me with the chemical inhibition studies and for her inestimable friendship, and to Sophie Nyberg for her help with the siRNA knockdown screening in *Drosophila* cells.

Dr. Svet Tsokov and Chris Hill (BMS Electron Microscope Unit), Dr. Stephen Brown (Sheffield RNAi Screening Facility), Sue Clark (Flow Cytometry facilities) and Dr. Darren Robinson (BMS Light Microscopy Facility). Thanks to all of them for their training and technical support.

Big thanks to all members (past and present) in Prof. Battaglia and Prof. Smythe groups for the stimulating scientific discussion, training and technical support and friendship. Thanks especially to Dr. Tian Xhiaohe, Dr. Filipe Ferreira, Dr. Russell Pearson, Gavin Fullstone, and Pornpen Panomwan.

Finally, my deepest gratitude to my family for its unconditionally trust in my capabilities and its infinite support and love, and to my friends in Sheffield whom have proven to be a second family, specially to my dearest friends Georgia and Natasja, as well as Janet, Iñigo, Isa, Jandia, Yianis, Vasilis, Julian, Francesca and Angela. Thank you.

## Summary

Polymersomes (synthetic polymeric vesicles), formed by the self-assembly of amphiphilic block copolymers in water attract great attention as drug delivery systems and as diagnostic/imaging tools. Our group has shown that 2-(methacryloyloxy)ethyl phosphorylcholine-block-2-(diisopropylamino)ethyl methacrylate (PMPC-PDPA) polymersomes are of special interest due to their ability to encapsulate a wide range of therapeutic molecules including anticancer compounds, antibiotics, antibodies, and nucleic acids, and their capacity to deliver their cargo intracellularly, both *in vitro* and *in vivo*, without promoting cellular toxicity or stress.

The favourable uptake kinetics and toxicological profile of PMPC-PDPA polymersomes justify a thorough study on the cellular interactions and mechanisms underlying their uptake, which was the aim of this thesis.

Exploring different polymersome production methods we studied the impact that the physical properties of PMPC-PDPA polymersomes (nanoparticle size and shape) have on their cellular uptake. Using flow cytometry and fluorescence microscopy we demonstrated that both spherical and tubular polymersomes could be used as intracellular delivery vectors. In addition, spherical and tubular polymersomes presented different uptake kinetic profiles, opening new avenues to modulate the temporal delivery of a cargo.

In a parallel line of work we identified receptor-mediated endocytosis as a common pathway for the internalisation of PMPC-PDPA polymersome in mammalian cells. Studying polymersome uptake in the presence of antagonists and neutralising antibodies, we identified two families of transmembrane proteins mediating PMPC-PDPA polymersome endocytosis and the specific receptors facilitating polymersome uptake. In addition, different endocytic pathways and molecules (i.e. dynamin, BAR domain proteins) were investigated in relation with polymersome internalisation by means of chemical inhibitors, dominant negative proteins and siRNA knockdown. Polymersome endocytosis seems to be dominated by a high level of promiscuity and the ability of PMPC-PDPA polymersome to induce their uptake, which could be translated in new therapeutic applications with a great clinical impact.

## Publications

James D. Robertson, Guy Yealland, **Milagros Avila-Olias**, Luca Chierico, Oliver Bandman, Stephen A. Renshaw, Giuseppe Battaglia

pH-Sensitive Tubular Polymersomes: Formation and Applications in Cellular Delivery  
*ACS Nano*, **2014**, ahead of print

Helen E. Colley\*, Vanessa Hearnden\*, **Milagros Avila-Olias\***, Denis Cecchin, Irene Canton, Jeppe Madsen, Sheila MacNeil, Nicholas Warren, Ke Hu, Jane A. McKeating, Steven P. Armes, Craig Murdoch, Martin H. Thornhill, and Giuseppe Battaglia

\* Authors contributed equally to this study

Polymersome-mediated delivery of combination anti-cancer therapy to head and neck cancer cells: 2D and 3D *in vitro* evaluation.

*Molecular Pharmaceutics*, 11, 1176-1188, **2014**

**Milagros Avila-Olias**, Carla Pegoraro, Giuseppe Battaglia, and Irene Canton

Inspired by nature: fundamentals in nanotechnology design to overcome biological barriers.

*Therapeutic Delivery* 4, 27-43, **2013**

Russell T. Pearson, **Milagros Avila-Olias**, Adrian S. Joseph, Sophie Nyberg and Giuseppe Battaglia

Smart Polymersomes: Formation, Characterization and Applications

Chapter 7 in *Smart Materials for Drug Delivery*, RSC Publishing, 1, 179-207, **2013**

# Contents

<b>Abbreviations</b>	<b>11</b>
<b>List of Figures</b>	<b>15</b>
<b>List of Tables</b>	<b>17</b>
<b>Chapter 1: Introduction</b>	<b>19</b>
<b>1.1 Nanotechnology for drug delivery</b>	<b>19</b>
<b>1.2 Transport across the plasma membrane</b>	<b>23</b>
1.2.1 Diffusion	23
1.2.2 Endocytosis	23
1.2.2.1 Detachment of the endocytic vesicle from the plasma membrane. Membrane fission.	27
<b>1.3 Soft nanoparticles as intracellular delivery vectors</b>	<b>36</b>
1.3.1 Polymersomes	38
1.3.1.1 Molecular fundamentals in polymersome self-assembly	38
1.3.1.2 Polymersome-Cell interactions	41
1.3.1.3 PMPC-PDPA polymersomes	43
<b>Chapter 2: Aim and Objectives</b>	<b>53</b>
<b>Chapter 3: Materials and Methods</b>	<b>55</b>
<b>3.1 PMPC-PDPA polymersomes</b>	<b>55</b>
3.1.1 Polymersome preparation	55
3.1.1.1 Copolymers	55
3.1.1.2 Methods of polymersome production	56
3.1.2 Polymersome purification	58
3.1.2.1 Gel Permeation Chromatography	58

3.1.2.2 Polymersome purification by centrifugation at increasing Relative Centrifugal Force	59
3.1.3 Polymersome physical characterisation	60
3.1.3.1 Polymer concentration, UV-Vis Spectroscopy	60
3.1.3.2 Size and shape characterisation	62
<b>3.2 Cell culture</b>	<b>63</b>
3.2.1 Mammalian cells	63
3.2.2 Insect cells	63
<b>3.3 Biological experimental procedures</b>	<b>64</b>
3.3.1 Detection and analysis techniques	64
3.3.1.1 Flow cytometry	64
3.3.1.2 Fluorescence microscopy	67
3.3.1.3 Western blotting	70
3.3.2 Cell viability	71
3.3.2.1 MTT assay	71
3.3.2.2 Live/Dead cell viability assay	73
3.3.3 Perturbation of the cellular uptake of PMPC-PDPA polymersomes	74
3.3.3.1 Polymersome uptake in the presence of chemical inhibitors of endocytosis	74
3.3.3.2 Polymersome uptake in the presence of known ligands for scavenger receptors	76
3.3.3.3 Polymersome uptake in the presence of blocking antibodies. Antibodies against scavenger receptors CD36 and SR-Bs, and tetraspanin CD81	78
3.3.4 Cellular transfection	79
3.3.4.1 Mutant K44A dynamin	79
3.3.4.2 siRNA knockdown	80
<b>3.4 Statistics</b>	<b>82</b>
<b>Chapter 4: Uptake of PMPC-PDPA polymersomes in mammalian cells. Effect of nanoparticle size and nanoparticle shape in polymersome internalisation</b>	<b>83</b>
<b>4.1 Introduction</b>	<b>83</b>



<b>4.2 Results</b>	<b>84</b>
4.2.1 General characteristics of the uptake of spherical PMPC-PDPA polymersomes in mammalian cells	84
4.2.2 Uptake kinetics of spherical PMPC-PDPA polymersomes with different diameters	88
4.2.3 Uptake kinetics of tubular PMPC-PDPA polymersomes	93
<b>4.3 Discussion</b>	<b>99</b>
<b>Chapter 5: Receptor-mediated endocytosis of PMPC-PDPA polymersomes by scavenger receptors and tetraspanins</b>	<b>103</b>
<b>5.1 Introduction</b>	<b>103</b>
<b>5.2 Results</b>	<b>105</b>
5.2.1 Effect of ligands for scavenger receptors A and B in PMPC-PDPA polymersome uptake	105
5.2.2 Scavenger receptors type B: Role of SR-BI, SR-BII and CD36 in PMPC-PDPA polymersomes uptake	107
5.2.3 Tetraspanin CD81 in PMPC-PDPA polymersome uptake.	116
<b>5.3 Discussion</b>	<b>125</b>
<b>Chapter 6: Characterising the mechanism of receptor-mediated endocytosis of PMPC-PDPA polymersomes</b>	<b>131</b>
<b>6.1 Introduction</b>	<b>131</b>
<b>6.2 Results</b>	<b>132</b>
6.2.1 Investigation of PMPC-PDPA polymersome endocytosis using chemical inhibitors	132
6.2.1.1 Prescreen. Selection of chemical inhibitors to map different endocytic routes and definition of their treatment window	133
6.2.1.2. Final screen	145
6.2.2 Role of dynamin in PMPC-PDPA polymersome internalisation.	148

5.2.3 BAR domain proteins in PMPC-PDPA polymersome internalisation. siRNA screening in Drosophila cells	156
<b>6.3 Discussion</b>	<b>167</b>
6.3.1 Investigation of PMPC-PDPA polymersome endocytosis through chemical inhibitors	167
6.3.2 Implication of dynamin in PMPC-PDPA polymersome internalisation	169
6.3.3 BAR domain proteins in PMPC-PDPA polymersome internalisation. siRNA screening in Drosophila cells	171
6.3.4 Final remarks	172
<b>Chapter 7: Conclusions, final discussion and future perspectives</b>	<b>175</b>
<b>7.1 Summary of findings</b>	<b>175</b>
7.1.1 Effects of polymersome size and shape in PMPC-PDPA polymersome uptake	175
7.1.2 Identification of the cellular receptors targeted by PMPC-PDPA polymersomes	176
7.1.3 Dynamin-independent internalisation of PMPC-PDPA polymersomes	177
<b>7.2 Final discussion and future perspectives</b>	<b>178</b>
<b>References</b>	<b>185</b>

# Abbreviations

ADP	adenosine diphosphate
ANOVA	analysis of variance
AP2	adaptor protein 2
ARF	ADP-ribosylation factor
Arp2/3	actin-related protein2/3
ATP	adenosine triphosphate
ATRP	atom transfer radical polymerisation
AUC	area under the curve
BAR	Bin1/amphiphysin/Rvs167
BSA	bovine serum albumin
CAC	critical aggregation concentration
CCD	charge-coupled device
CCPs	clathrin coated pits
CCVs	clathrin coated vesicles
Cdc42	cell division cycle 42
cDNA	complementary DNA
CME	clathrin-mediated endocytosis
CO <sub>2</sub>	carbon dioxide
CPP	cell-penetrating peptide
CPZ	chlorpromazine
DAPI	4',6-diamidino-2-phenylindole
DLS	dynamic light scattering
DMEM	dulbecco's modified eagle's medium
DMSO	dimethyl sulfoxide
DNA	deoxyribonucleic acid
ECL	enhanced chemiluminescence
EDTA	ethylenediaminetetraacetic acid
EIPA	5-(N-ethyl-N-isopropyl) amiloride
Em	emission

EMEM	eagle's minimal essential medium
Ex	excitation
F	fucoidan
FCS	fetal calf serum
GPI-Aps	glycosylphosphatidylinositol-anchored proteins
GRAF	GTPase regulator associated with focal adhesion kinase
GTP	guanosine-5'-triphosphate
HCl	hydrogen chloride
HDF	human dermal fibroblast
HDL	high density lipoprotein
He-Ne	Helium-Neon
HRP	horseradish peroxidase
IgG	immunoglobulin G
IL-2R	interleukin-2 cytokine receptor
IPA-3	1,1-Disulfanediyldinaphthalen-2-ol
LDL	low density lipoprotein
LUT	look-up-table
MDC	monodansylcadaverine
MFI	median fluorescence intensity
MHC	major histocompatibility complex
MTT	3-(4,5-Dimethylthiazol-2-yl)-2,5-diphenyltetrazolium bromide
NaCl	sodium chloride
NaOH	sodium hydroxide
NF- $\kappa$ B	nuclear factor kappa-light-chain-enhancer of activated B cells
NH <sub>4</sub> Cl	ammonium chloride
NPs	nanoparticles
ns	non-statistical significant difference
N-WASP	Neural Wiskott-Aldrich syndrome protein
PAK	serine/threonine-protein kinase
PBS	phosphate buffered saline buffer
PDPA	poly(2-(diisopropylamino)ethyl methacrylate)
PEG	polyethylene glycol
PEO	polyethylene oxide

PI(4,5)P2	phosphatidyl-4,5-bisphosphate
PI	polyinosinic acid
PI	propidium iodide
pKa	acid dissociation constant
PMPC	poly(2-(methacryloyloxy)ethyl phosphorylcholine)
rac	Ras-related C3 botulinum toxin substrate 1
RAFT	reversible addition-fragmentation chain transfer
RCF	relative centrifugal force
RhoA	Ras homolog gene family, member A
RIPA	radioimmunoprecipitation assay
RNA	ribonucleic acid
SCrs	scavenger receptors
SDS	sodium dodecyl sulfate
siRNA	silencing RNA
SR-Bs	scavenger receptors class B type I (SR-BI) and type II (SR-BII)
TBS	tris-buffered saline buffer
TEM	transmission electron microscope
UV-Vis	ultraviolet-visible
WT	wild type

## Symbols

% (v/v)	volume by volume percent
% (wt/v)	weight by volume percent
% (wt/wt)	weight by weight percent
°C	centigrade
g	gram
g/mol	grams per mole
IU	international units
kDa	kiloDalton
kPa	kiloPascal
mg	milligram

$\mu\text{g}$	microgram
$\mu\text{l}$	microlitre
$\mu\text{m}$	micrometre
$\text{mA}$	milliamps
$\text{min}$	minutes
$\text{ml}$	millilitre
$\text{mM}$	millimolar
$\text{ms}$	millisecond
$\text{nm}$	nanometre
$\text{V}$	volt

## List of Figures

Figure 1.1: Mechanisms of endocytosis identified in mammalian cells together with the approximated size of the endocytic vesicles formed.....	33
Figure 1.2: Molecular packing factor and associated geometries of self-assembled block copolymers .....	40
Figure 1.3: Arrangement of PMPC-PDPA block copolymers in aqueous solution above and below the PDPA pKa .....	46
Figure 1.4: Release of rhodamine octadecyl ester perchlorate B encapsulated in pH sensitive or pH insensitive polymersomes .....	47
Figure 1.5: Subcellular vesicular trafficking compartments, alongside their ionic and enzymatic composition.....	48
Figure 1.6: Proposed mechanism of endosomal escape and polymersome-mediated cytosolic delivery for PMPC-PDPA polymersomes.....	49
Figure 1.7: PMPC-PDPA mediated intracellular delivery of compounds with different hydrophilic profiles .....	50
Figure 1.8: Effect of polymersome size (diameter) and polymersome surface topology in PMPC-PDPA polymersome internalisation.....	51
Figure 3.1: Absorption spectrums and standard curves for PMPC-PDPA and rhodamine 6G-PMPC-PDPA block copolymers.....	61
Figure 3.2: MTT assays performed in FaDu and HeLa cells treated with rho-PMPC-PDPA polymersomes or the ligands for scavenger receptors, Fucoidan and Polyinosinic acid .....	72
Figure 3.3: Chemical structures of Fucoidan and Polyinosinic acid.....	77
Figure 3.4: Chemical structure of ITX5061.....	78
Figure 4.1: Uptake of spherical polymersomes in mammalian cells .....	86
Figure 4.2: Polymersome fractions of different sizes and micelles obtained after purification by centrifugation.....	91
Figure 4.3: Uptake of spherical PMPC-PDPA nanoparticles of different diameters in FaDu cells.....	92

Figure 4.4: Uptake of tubular PMPC-PDPA polymersomes in FaDu cells .....	96
Figure 4.5: PMPC-PDPA polymersome-mediated intracellular delivery of different compounds .....	97
Figure 5.1: Effect of Fucoidan and Polyinosinic acid on polymersome uptake in different cell types.....	106
Figure 5.2: Scavenger receptors type B: SR-BI, SR-BII and CD36 in polymersome uptake .....	113
Figure 5.3: Uptake of PMPC-PDPA polymersome in SR-Bs knockdown FaDu cells.	115
Figure 5.4: Uptake of polymersomes in the presence of a blocking antibody against CD81 .....	119
Figure 5.5: Cellular expression of the scavenger receptors SR-Bs and CD36 and the tetraspanin CD81 in mammalian cells .....	122
Figure 6.1: Cell viability levels after incubation with inhibitors (MTT assays).....	137
Figure 6.2: Live-Dead experiments I. Flow cytometry.....	142
Figure 6.3: Live-Dead experiments II. Fluorescence microscopy .....	144
Figure 6.4: Uptake of PMPC-PDPA polymersomes, transferrin, cholera toxin subunit B and dextran in the presence of inhibitors of endocytosis in HeLa cells.....	147
Figure 6.5: Polymersomes and transferrin uptake in mutant K44A dynamin HeLa cells .....	153
Figure 6.6: Polymersome uptake in FaDu cells expressing mutant K44A dynamin ....	155
Figure 6.7: Uptake of PMPC-PDPA polymersomes in knockdown SR2 <sup>+</sup> Drosophila cells. Fluorescent micrographs examples.....	161
Figure 6.8: Uptake of rhodamine-labelled PMPC-PDPA polymersomes in non- transfected, or transfected with non-targeting siRNA, SR2 <sup>+</sup> Drosophila cells.....	162
Figure 6.9: Uptake of PMPC-PDPA polymersomes in knockdown SR2 <sup>+</sup> Drosophila cells. Fluorescent intensity measurements .....	165



## List of Tables

Table 3.1: Chemical composition of PMPC <sub>25</sub> -PDPA <sub>70</sub> and rhodamine-PMPC <sub>25</sub> -PDPA <sub>70</sub> copolymers .....	56
Table 3.2: Stock solutions prepared for different chemical inhibitors.....	75
Table 3.3: Experimental conditions for cells incubated with polymersomes or control cargoes.....	76
Table 6.1: Chemical inhibitors of endocytosis.....	135
Table 6.2: Selected inhibitors and their associated incubation conditions (concentration and time) for live/dead assays .....	139
Table 6.3: Selected inhibitors and their associated incubation conditions (concentration and time) to investigate the mechanism of PMPC-PDPA polymersome endocytosis in HeLa cells .....	146
Table 6.4: Genes related to endocytosis and cellular trafficking investigated in a siRNA screening in SR2+ Drosophila cells .....	160



# Chapter 1: Introduction

## 1.1 Nanotechnology for drug delivery

Advances in biomedicine and medicinal chemistry have produced state-of-the-art therapeutic biomolecules and drugs with great potential for diagnosis and patient treatment that are highly specific towards their target (i.e.. antibodies and nucleic acids). Nonetheless, these molecules often present undesirable properties that can hamper their clinical use, such as poor solubility in water, which is a major problem since biological fluids are aqueous fluids<sup>3</sup>. In addition, therapeutic molecules can be unstable in certain biological environments. For example therapeutic proteins, which are quite sensitive to pH changes and the presence of proteases, or may be rapidly cleared from the body circulation by the immune system<sup>4</sup>. Moreover, some molecules with high therapeutic value, such as nucleic acids, act in the cell cytoplasm and are impermeable to the cell membrane and so cannot reach their target site by themselves<sup>5,6</sup>. Finally, some drugs are quite cytotoxic (i.e. anticancer chemicals) and therefore only the target tissue or group of cells should come in contact with them. Consequently, there is the need to engineer drug delivery systems able to protect the active compound within a biological environment and at the same time to limit its interactions with off-target sites, to transport it to the desired biological target and to efficiently release it at that site. Furthermore, no collateral toxicity must be derived from the use of such vector. Traditional drug formulations are frequently associated with poor protection of the compound of interest from the biological environment and lack of controlled release, spatially or temporally. This is translated in the need for frequent doses to reach a therapeutic effect, which in turn can result in unwanted side effects including drug resistance. Along these lines, nanotechnology has emerged as a promising way to improve drug delivery<sup>7</sup>. Nanotechnology (understanding and controlling matter at the nanoscale, where at least one dimension is between 1-100 nm) takes a multi-disciplinary approach to engineer nanoscopic devices that offer enhanced protection and transport of bioactive cargoes, increasing the ability to overcome biological barriers in order to release this cargo at the cellular or subcellular level, which are the sites of action for

most drugs and therapeutic biomolecules. In fact, several nanoparticles formulations are currently commercialised for the treatment of different diseases (table 1.1).

To deliver a cargo intracellularly is not an easy task, evolution has placed several barriers within the human body to protect it from external sources of danger, and to maintain the specific local conditions that the different biological processes need to operate. Nevertheless, there is communication between these compartments (i.e. plasma and interstitial fluid or cytoplasm and nucleus), and although the transport at their interface is strictly regulated it opens a window for the use of nanotechnology for enhanced drug delivery<sup>8</sup>. Nature itself is an example of nanotechnology at work, with viruses being the most effective intracellular nanoscopic delivery vectors described. Viruses rely in their ability to overcome all the biological barriers to be able to replicate, therefore, evolution has equipped them with a set of tools to evade the immune system, avoid rapid renal and hepatic clearance, and target a specific group of cells, sometimes beyond extremely tightly regulated barriers such as the blood brain barrier<sup>9,10</sup>. Finally, viruses are able to penetrate the cell membrane, to escape from endo-lysosomal intracellular vesicles and to cross the nuclear membrane, which comprise the main barriers to be overcome at the cellular level<sup>11</sup>. In the in-depth knowledge of the barriers mentioned and the examples of natural particles with the ability to cross them, nanoscientists have an invaluable source of inspiration that they can turn to in order to engineer better intracellular delivery systems<sup>12</sup>.

This thesis focuses on the study of nanoparticle transport across the plasma membrane, hence, the ways to move across this barrier will be described below.

<b>Product</b>	<b>Manufacturer/Distributor</b>	<b>Composition</b>	<b>Indication</b>
<b><i>Protein-Based Nanoparticles</i></b>			
<b>Abraxane</b>	Celgene Corporation	Albumin bound-paclitaxel	Head and neck, lung, ovarian, prostate, colon cancers, and metastatic breast cancer
<b><i>Lipid-Based Nanoparticles</i></b>			
<b>Abelect</b>	Sigma-Tau Pharmaceuticals, Inc.	Lipid complex formulation of amphotericin B	Fungal and parasite infections
<b>Amphotec</b>	Alkopharma	Liposomes encapsulating amphotericin B	
<b>Ambisome</b>	Gilead Sciences, Inc.	Liposomes encapsulating amphotericin B	
<b>Nyotran</b>	Aronex Pharmaceuticals	Liposomal formulation of nystatin	Fungal infections
<b>DepoCyt</b>	Sigma-Tau Pharmaceuticals, Inc.	Liposomes encapsulating cytarabine	Lymphomatous Meningitis
<b>Inflexal V</b>	Crucell	Adjuvant liposomes in influenza vaccine	Influenza
<b>Epaxal</b>	Crucell	Adjuvant liposomes in hepatitis A vaccine	Hepatitis A
<b>Daunoxome</b>	Galen	Liposomes encapsulating daunorubicin	Kaposi's sarcoma
<b>Doxil/Caelyx</b>	Janssen Products	Liposomes incorporating doxorubicin	Metastatic breast cancer, ovarian, Kaposi's sarcoma
<b>Lipodox</b>	TTY Biopharm		
<b>Myocet</b>	Enzon Pharmaceuticals		
<b>Lipoplatin Nanoplatin</b>	Regulon AE	Liposomes incorporating cisplatin	Pancreatic and lung cancer
<b>Visudyne</b>	Valeant Pharmaceuticals	Liposomes incorporating verteporfin	Age-related molecular degeneration, pathologic myopia, ocular histoplasmosis
<b>Estrasorb</b>	Novavax	Lipidic micellar nanoemulsion containing estradiol	Post-menopausal hot flashes
<b>DepoDur</b>	SkyePharma PLC and Endo Pharmaceuticals	Liposomes encapsulating morphine sulfate	Relief of postsurgical pain

<b>Product</b>	<b>Manufacturer/Distributor</b>	<b>Composition</b>	<b>Indication</b>
<b><i>Polymer-Based Nanoparticles</i></b>			
<b>Adagen</b>	Sigma-Tau Pharmaceuticals, Inc.	PEGylated adenosine deaminase enzyme	Adenosine deaminase (ADA) deficiency in patients with severe combined immunodeficiency disease
<b>Oncaspar</b>	Sigma-Tau Pharmaceuticals, Inc.	PEGylated L-asparaginase	Acute lymphoblastic leukemia
<b>PegIntron</b>	Merck	PEGylated interferon alpha	Hepatitis B and C
<b>Pegasys</b>	Roche		
<b>Somavert</b>	Pfizer	PEGylated modified version of the human growth hormone	Acromegaly
<b>Neulasta</b>	Amgen	PEGylated recombinant methionyl human granulocyte colony-stimulating factor	Severe neutropenia in patients under chemotherapy
<b>Macugen</b>	Pfizer	PEGylated anti-vascular endothelial growth factor (VEGF) aptamer	Neovascular wet age-related macular degeneration
<b>Mircera</b>	Roche	PEGylated erythropoietin	Anemia related with chronic kidney disease
<b>Omontys</b>	Affymax and Takeda,	PEGylated synthetic erythropoietin	
<b>Cimzia</b>	UCB	PEGylated monoclonal antibody anti-TNF	Severe rheumatoid arthritis, Crohn's disease, psoriatic arthritis, ankylosing spondylitis.
<b>Eligard</b>	Sanofi-Aventis	Leuprolide acetate in a poly (DL-lactide-co-glycolide) (PLGH) polymer formulation	Advanced prostate cancer
<b>Cynviloq</b>	Sorrento Therapeutics	Diblock copolymer micelles incorporating Paclitaxel	Metastatic breast cancer, non-small cell lung cancer, ovarian cancer
<b>Renagel</b>	Sanofi-Aventis	Polyallylamine crosslinked with epichlorohydrin	Hyperphosphatemia in patients with chronic kidney disease
<b>Renvela</b>			
<b>VivaGel</b>	Starpharme	Lysine-based dendrimer	Prevention of sexually transmitted infections

**Table 1.1: Examples of commercially available nanoparticle drug delivery systems.**

Adapted from<sup>1,2</sup>

## 1.2 Transport across the plasma membrane

### 1.2.1 Diffusion

The plasma membrane of mammalian cells is semi-permeable, therefore only a selected group of molecules can **passively diffuse** across it. This group include small (< 1kDa) lipophilic particles, such as fatty acids and steroids, gases, such as oxygen or carbon dioxide, and small non-charged polar molecules like water, ethanol, and urea. On the other hand, larger polar/apolar macromolecules such as glucose, amino acids, or nucleotides, and strongly charged molecules such as ions ( $K^+$ ,  $Na^+$ ,  $Ca^{2+}$ ,  $Cl^-$ ) require ion channels or small molecule transporters embedded within the membrane, which are highly specific towards the cargo transported, to diffuse through it. **Facilitated diffusion** does not require energy to operate when molecules move from areas of high concentration to areas of low concentration (i.e. glucose). Instead, energy, often in form of ATP, is needed to fuel facilitated diffusion against a concentration or electrochemical gradient (i.e.  $K^+$  /  $Na^+$  pump)<sup>13</sup>.

Passive and facilitated diffusion are non-compatible with the cellular uptake and release of high volume of fluids and macromolecules (i.e. proteins) very different in nature. These cargoes cross the plasma membrane through endocytosis (cellular uptake) or exocytosis (cellular release). These are energy-dependent processes associated with high rates of membrane remodelling in which cargoes are transported in and out the cell in membrane-enclosed vesicles.

### 1.2.2 Endocytosis

The term endocytosis was first coined in 1963 by de Duve, to name the cellular internalisation of particles and fluids through plasma membrane invaginations, resulting in intracellular vesicles containing the material endocytosed<sup>14</sup>. Therefore, endocytosis is best known as the energy-dependent process by which cells uptake fluids, molecules and macromolecules by the controlled deformation of the plasma membrane. However, its role in the biology of the cell is far more extensive. It regulates the lipo-protein composition of the plasma membrane, participates in the presentation of receptors in the

plasma membrane, cell signalling, cell motility and division<sup>15</sup>. Numerous diseases are related to defective endocytosis, and bacteria and viruses often exploit this pathway to enter cells<sup>16,17</sup>. Mechanisms of nanoparticle cellular internalisation have mostly been found to be energy-dependent processes, rather than passive diffusion through the membrane or membrane pores<sup>18</sup>. In addition, endocytosis has been identified as the primary cellular internalisation pathway for many nanoparticles formulations<sup>19</sup>. Endocytosis and its consequent subcellular sorting is a complex process with multiple cellular pathways often overlapping. Furthermore, the lack of enough specific markers and inhibitors for distinctive pathways, and the technical limitations to its in-depth study (i.e. imaging resolution thresholds, experimental protocols perturbing cell homeostasis) are responsible for the fact that only a small, although extremely significant part, of this important biological process has been decoded so far.

Endocytosis is traditionally divided into phagocytosis and pinocytosis. **Phagocytosis**, typically exclusive of specialised cells of the immune system such as macrophages and neutrophils, is normally associated with the internalisation of large solid particles. Membrane protrusions, driven by the rearrangement of the actin cytoskeleton, are usually projected to engulf the extracellular particle in vesicles called phagosomes. Phagosomes bypass early endosomes and fuse directly with lysosomes to form phagolysosomes<sup>20</sup> (figure 1.1). On the other hand, pinocytosis is a process present in almost all eukaryotic cells and it is regularly used for the uptake of fluids and particles smaller than 1  $\mu\text{m}$ . Pinocytosis can be further subdivided into several mechanisms defined by the specific lipids and proteins involved in each of them. The precise boundary between different pathways is an area of much debate, and the particular uptake mechanisms remain highly dependent on the cargo and the cell type. Figure 1.1 is a schematic representation of the currently identified endocytic routes, while table 1.2 lists different endocytic pathways, together with the vesicular morphology observed and a examples of cellular molecules involved in each of them. Table 1.2 does not include non-lysosomal pathways (and hence non-degradative pathways). However, it is important to mention that **transcytosis** has a central role in the transport of macromolecular nutrients across endothelial and epithelial barriers. Transcytosis allows the effective intracellular transport of macromolecules such as folate, chemokines and immunoglobulins, maintaining biologically active cargo from one side to the opposite side of a cell<sup>21</sup>.



Due to the relatively big diameter of the endocytic vesicles formed, **macropinocytosis** was one of the first pinocytic events observed<sup>22</sup>. Macropinocytosis involves the internalisation of a large quantity of external fluids by the extension of the plasma membrane, usually upon stimulation by growth factor receptors, bacteria, apoptotic bodies, necrotic cells or viruses, to form > 200 nm organelles known as macropinosomes. Macropinocytosis provides an effective uptake route for the non-selective endocytosis of macromolecules up to 1  $\mu\text{m}^3$ . In addition, it is associated with high cell surface ruffling (lamellipodia-like extensions, circular ruffles and blebs) and therefore with high rates of actin cytoskeleton reorganisation. Nonetheless, it is not macropinocytosis, but **clathrin-mediated endocytosis** (CME), discovered by Roth and Porter in 1964<sup>24</sup>, that is the most-studied and best-characterised endocytic pathway to date. CME is initiated at membrane sites enriched in phosphatidyl-4,5-bisphosphate (PI(4,5)P<sub>2</sub>), where adaptor proteins trigger the assembly of clathrin and accessory proteins into polygonal lattices that will grow to form clathrin coated pits (CCPs) upon cargo stimulation<sup>25,26</sup>. Clathrin coated vesicles are subsequently detached from the plasma membrane in a dynamin-dependent way and lose their clathrin coat before localising to early endosomes. At a given time CCPs occupy approximately 2% of the plasma membrane surface<sup>27,28</sup>, and the rate of plasma membrane internalisation through CME is close to 1–5% per minute<sup>29</sup>.

The first clathrin-independent pathway described, **caveolae-mediated endocytosis**, was originally observed in the early 1950's at the surface of endothelial cells<sup>30,31</sup>. It was named after the transmembrane cholesterol-binding protein coating the invaginations: caveolin. Three isoforms of caveolin have been identified, caveolin 1, caveolin 2 and caveolin 3<sup>32</sup>. Caveolin 1 and caveolin 3, the last one only present in muscle cells, are indispensable for the formation of the caveolae. The main function of caveolin 2 remains unclear. Caveolae are 50-80 nm flask-shaped invaginations (20-40 nm at the neck) displayed by the plasma membrane of many cells, except hepatocytes, neuronal cells and lymphocytes<sup>33</sup>. Caveolae present limited motility and dynamics<sup>33</sup> and are characterised by the presence of cholesterol and sphingolipid-rich domains (lipid-rafts domains). Actually, caveolae are important in cholesterol homeostasis regulation<sup>34</sup>. Although traditionally it has been considered that the main role of caveolae were to define a clathrin-independent endocytic pathway, as well as being important signalling

platforms, nowadays the hypothesis in which the main role of caveolae is to act as membrane tension regulators is gaining strength<sup>35,22</sup>. Nonetheless, it is clear that different cargoes can take advantage of caveolae to be internalised through endocytosis, especially by transcytosis<sup>36</sup>.

Advances in microscopy (sample preparation protocols and instrumentation) and molecular techniques, have permitted, in the last decade, the discovery of novel endocytic pathways, different from clathrin and caveolae-mediated endocytosis. Although these new routes remain largely unexplored, it seems that they could account for a high percentage of the total cellular endocytosis and plasma membrane turnover<sup>37</sup>. In addition, many of these pathways appear to be highly sensitive to cholesterol levels at the plasma membrane and be related to the uptake of glycosylphosphatidylinositol-anchored proteins (GPI-Aps) and glycosphingolipids. One of these pathways is defined by the presence of the ubiquitously expressed mammalian transmembrane proteins known as **flotillins** (flotilin 1, flotilin 2). Flotillins, associated with lipid rafts at the plasma membrane, define specific microdomains that resemble caveolae but that are different from them, as well as negative for the presence of clathrin<sup>38</sup>. Flotillin-positive domains are associated with the endocytosis of plasma membrane components such as CD59 (GPI-Ap)<sup>39,40</sup>. In addition, and similar to caveolae, they seem to function as signal transduction platforms and more importantly, as regulators of the cortical cytoskeleton<sup>41</sup>.

**Cell division cycle 42 (Cdc42)**, a small GTPase enzyme of the Ras superfamily of GTP-binding proteins, seems to define a specific endocytic route, first identified during the study of GPI-APs internalisation<sup>42</sup>. Cdc42 binding and hydrolysis of GTP (nucleotide guanine triphosphate) is crucial for cell growth regulation, cellular differentiation, and apoptosis, mostly through the rearrangement of the actin cytoskeleton. It directly binds to Neural Wiskott-Aldrich syndrome protein (N-WASP), which activates Arp2/3, which in turn nucleates new F-actin. Therefore Cdc42 endocytosis is very sensitive to inhibitors of actin polymerisation. Cdc42 interacts with multiple partners, among them Arf1 and GRAF1, a GTPase in which different domains associated with membrane deformation and vesicle scission can be identified. Cdc42 is one of the few dynamin-independent endocytic mechanisms identified so far together with Arf6-dependent endocytosis. **ADP-ribosylation factor 6 (Arf6)**, another small

GTPase ubiquitously expressed in mammalian cells<sup>43</sup>, is normally found in membrane ruffles. It contains a BAR domain which allows this protein to sense and promote membrane curvature<sup>44</sup>. Endocytosis of the GPI-linked protein CD59 and proteins from the major histocompatibility complex (MHC) class I occurs in an Arf6-dependent fashion. Finally, the internalisation mechanism followed by the **interleukin-2 cytokine receptor (IL-2R)** appears to outline a novel endocytic route. The involvement of the small G proteins rhoA and rac1, and the kinases PAK1, PAK2, and phosphatidylinositol-3-kinase are hallmarks of this pathway<sup>45</sup>. Vesicle scission from the plasma membrane is regulated by dynamin. N-WASP regulation of actin is also important for membrane remodelling associated with IL-2R endocytosis<sup>46</sup>. As pointed out above, the small GTPase RhoA (Ras homolog gene family) is closely related to IL-2R internalisation<sup>47</sup>. Moreover, both RhoA and IL-2R define  $\gamma$ c-cytokine receptor endocytosis. RhoA has a main role in actin cytoskeleton dynamics and therefore it is also found regulating other endocytic routes (table 1.2).

#### 1.2.2.1 Detachment of the endocytic vesicle from the plasma membrane.

##### Membrane fission

###### *1.2.2.1.1 Dynamin*

Dynamin is a large GTPase belonging to the dynamin superfamily<sup>48</sup>. It was discovered in the last decade of the 20th century and soon related to endocytosis through genetic loss-of-function studies in *Drosophila melanogaster*<sup>49,50</sup>. Three dynamins have been described in mammals. Dynamins 1 and 3 are mostly expressed in the nervous system and dynamin 2 is almost ubiquitously expressed. In addition to the GTPase domain that binds and hydrolyses GTP, dynamin has 4 more domains: the middle domain, the pleckstrin-homology domain (PH), the GTPase effector domain (GED) and the proline/arginine-rich domain (PRD). The middle and the GED domains are involved in oligomerization and regulation of the GTPase activity. The PH domain targets dynamin to the plasma membrane, and it is through the PRD domain that dynamin establishes direct interactions with other proteins involved in membrane remodelling and scission<sup>26</sup>. These domains are expected to fold into a hairpin-like three-dimensional structure where the G domain lies on a helical bundle, known as the bundle signalling element<sup>51</sup>

<sup>52</sup>. The helices of the middle and the GED domains form a stalk that connects the GTPase region and the PH domain<sup>53,54</sup>. The PH domain constitutes the ‘foot’ of the hairpin that interacts with the lipidic membrane<sup>55-57</sup>. The PRD domain is predicted to be unfolded and to get projected in opposite direction to the membrane at the conjunction between the BSE and the G domain<sup>58</sup>. Dynamin polymerisation is central to dynamin function. The stalks of two dynamin monomers dimerise in a cross-like fashion<sup>53,54</sup>. Dynamin dimers further polymerise and self-assemble as rings and spirals around the neck of endocytic buds<sup>59,60</sup>. G domain dimerisation, which is crucial for GTP hydrolysis, occurs between adjacent rungs of the dynamin helix<sup>52,61</sup>.

Dynamin is an important protein with a mechano-enzymatic activity mediating pinching off of endocytic membranes from the plasma membrane in mammalian cells<sup>48</sup>. Accordingly, it has been found driving the fission of endocytic vesicles in some of the best characterised endocytic pathways described to date<sup>62,63</sup> (table 1.2). Although there is extensive evidence of the ability of dynamin to tubulate membranes and generate membrane fission both in vitro and in vivo<sup>64-66</sup> the exact mechanism through which dynamin promotes membrane fission is still the subject of much debate<sup>57,67,68</sup>. Bridging the gap, a general consensus exists that dynamin polymerises around the neck of the spherical or tubular invagination in the form of short spirals, and that it undergoes a structural change following GTP hydrolysis which ultimately results in the scission of the endocytic vesicle from the plasma membrane<sup>25,69</sup>. Whilst dynamin is often indispensable for the scission of endocytic vesicles in vivo, it does not work alone, quite the opposite, it directly interacts with different proteins with the special mention of actin<sup>70,71</sup> and BAR domain proteins<sup>72,73</sup> that contribute to dynamin-mediated membrane fission<sup>74</sup>.

#### *1.2.2.1.2 BAR domain proteins*

As the name indicates, proteins belonging to the super family of BAR domain proteins contain a BAR domain within their structure that allow them to sense and/or induce membrane curvature, mainly through electrostatic interactions<sup>75</sup>. The first BAR domain protein identified was amphiphysin in 2004 by the McMahon group<sup>76</sup>, since then dozens of new members have been recognised<sup>77-83</sup>. Different subtypes have been identified

depending on their ability to bind to membrane with diverse curvatures. BAR/N-BAR proteins bind to membranes with high positive curvature (towards the cell cytoplasm, i.e. amphiphysin and arfaptin). F-BAR members bind to positive curved membranes, although flatter than the previous group (i.e. FCHo2)<sup>81</sup>, while I-BAR domain proteins recognise and bind to membranes with negative curvature (towards the extracellular space, i.e. IRSp53)<sup>84</sup>. The dimeric  $\alpha$ -helical coiled coils that constitute the BAR domain function as a rigid scaffold for the stabilisation or generation of curved membrane domains<sup>76,85</sup>. BAR domain dimers recruited to the membrane can interact among them to form higher-order assemblies, which tend to be more flexible structures in comparison to the isolated dimers, and offer new opportunities for the deformation of the membrane<sup>86</sup>. For example, CIP4 or FBP17 generate helical oligomers through lateral contacts, and contacts at the ends of their BAR domains<sup>85,87</sup>. Another example is the crosslinking of endophilin through the amphipathic helices present at the N-terminus of the dimers<sup>88</sup>.

BAR domain proteins have, in some cases, other domains within their structure that allow them to directly interact with different endocytic molecules. A well-studied example is amphiphysin that has an internal clathrin and adaptor-binding domain (CLAP) to bind to clathrin and the AP2 adaptor complex, and a C-terminal SH3 domain through which it binds to dynamin. It has been demonstrated that inhibiting dynamin-amphiphysin interaction inhibits clathrin-mediated endocytosis<sup>89</sup>. BAR domain proteins also serve as bridges between the plasma membrane and the cytoskeleton at different endocytic sites<sup>65,75,90</sup>, and they are implicated in actin polymerization and the intracellular trafficking of a cargo after scission from the plasma membrane via interaction with nucleation promoting factors (i.e. N-WASP)<sup>75</sup> and Rho-family GTPases<sup>90</sup> (i.e. Cdc42<sup>91</sup>, Arf6<sup>92</sup>).

Interestingly, it has been recently demonstrated, in a liposome vesiculation assay, the ability of BAR domain proteins containing amphipathic helices (N-BAR proteins such as endophilin and amphiphysin) to directly promote membrane scission<sup>93</sup>. This is in addition to their well-known capacity to generate membrane curvature through the same mechanism<sup>94</sup>. According to the published study, the ability of these proteins to promote membrane fission resides on their amphipathic helices, and it is proportional to the hydrophobicity and number of those helices. In line with this, they showed that Epsin, which although it is not a BAR domain protein, has an amphipathic helix (ENTH

domain) that inserts in the plasma membrane, can also generate membrane fission at the neck of clathrin coated vesicles in the absence of dynamin<sup>93</sup>.

### *1.2.2.1.3 Actin, lipid-phase separation and the energy-state of the plasma membrane*

Actin is an ATPase highly abundant in most eukaryotic cells, where it can be found as monomeric globular G-actin and as polymeric filamentous F-actin. Actin filaments are formed by polymerisation of G-actin giving rise to the actin cytoskeleton. Therefore actin is crucial to preserve the cell shape. In addition, actin polymerisation and the growth of actin filaments in a polarised fashion generate a force needed to maintain cell polarity and to drive cell remodelling when necessary (i.e. motility, division, muscle contraction and endocytosis)<sup>95</sup>. Actin is an important player in endocytosis in mammalian cells, where it is involved at different stages of the internalisation process, from early invagination, to movement of the endocytosed vesicle away from the plasma membrane, being able to drive membrane fission in some types of clathrin-independent endocytosis<sup>96</sup>. Actin is crucial in phagocytosis<sup>97</sup> and macropinocytosis<sup>98</sup>, it is involved in the generation of caveolae and their endocytosis<sup>99,100</sup>, and it is also implicated in CME, and clathrin and caveolae-independent endocytosis<sup>101</sup> (table 1.2).

The specific role of actin is especially controversial in CME in mammalian cells<sup>102</sup>, and therefore much research has been committed to study actin in this pathway. In yeast, actin is essential for early plasma membrane invagination in CME<sup>103</sup>. Actin is also important in the successive endocytic stages including the scission of the CCP, which seems to be driven by Vps1 and amphiphysins<sup>104,105</sup>. Vsp1 is the yeast homologue of the human dynamin, the main molecule responsible for the detachment of CCPs in mammalian cells<sup>48</sup>. Thanks to the extensive investigation on this field we now know that dynamin interacts directly and indirectly with actin at the endocytic site<sup>106-108</sup> and that actin is important, although the level of importance seems to be quite cell-type dependent, in dynamin-mediated fission of the endocytic vesicle<sup>70,109</sup>. The current understanding, inspired by the fact that actin may be essential in yeast CME to overcome the turgor pressure<sup>103</sup>, is that actin is needed for the successful internalisation of clathrin coated vesicles at endocytic sites under high local membrane tension providing the extra force required in such situations<sup>110</sup>. This could be easily extended to

other endocytic routes, complementing the fact that actin could be facilitating membrane fission by actively driving lipid phase separation<sup>96,111</sup>. In line with this, not only proteins, but also lipids seem to have a decisive role in membrane invagination and membrane scission through **lipid-phase separation** at the plasma membrane. Phase separation, also known as formation of lipids domains or lipid clustering, creates a repulsive tension at the boundary of the domain with the surrounding membrane, which is known as line tension. A way to minimise this tension is to bud the domain out of the membrane, providing the line tension is higher than the energy necessary to bend the membrane (bending energy). Theoretical models and *in vitro* studies raise the idea that in extreme cases, when the line tension is high and the radius at the bud neck smaller than a threshold (approx. 5 nm) the vesicle could undergo spontaneous fission<sup>67,112,113</sup>. Otherwise, the bud might be detached with the help of the proteins mentioned above or it could remain connected to the plasma membrane helping to minimise line tension. As follows from this argument, the local **energy-state of the plasma membrane**, which in turn is influenced by the arrangement of lipids, transmembrane and peripheral proteins, is a key parameter to have in consideration, and it could be indicating the essential requirements for effective membrane fission in each situation. Scission has to be overall an energetically favourable process. The scission of an endocytic vesicle is a way to relax the tension built up in a membrane under high local curvature and therefore it should be accompanied by a relaxation of the free energy of the system<sup>114,115</sup>.





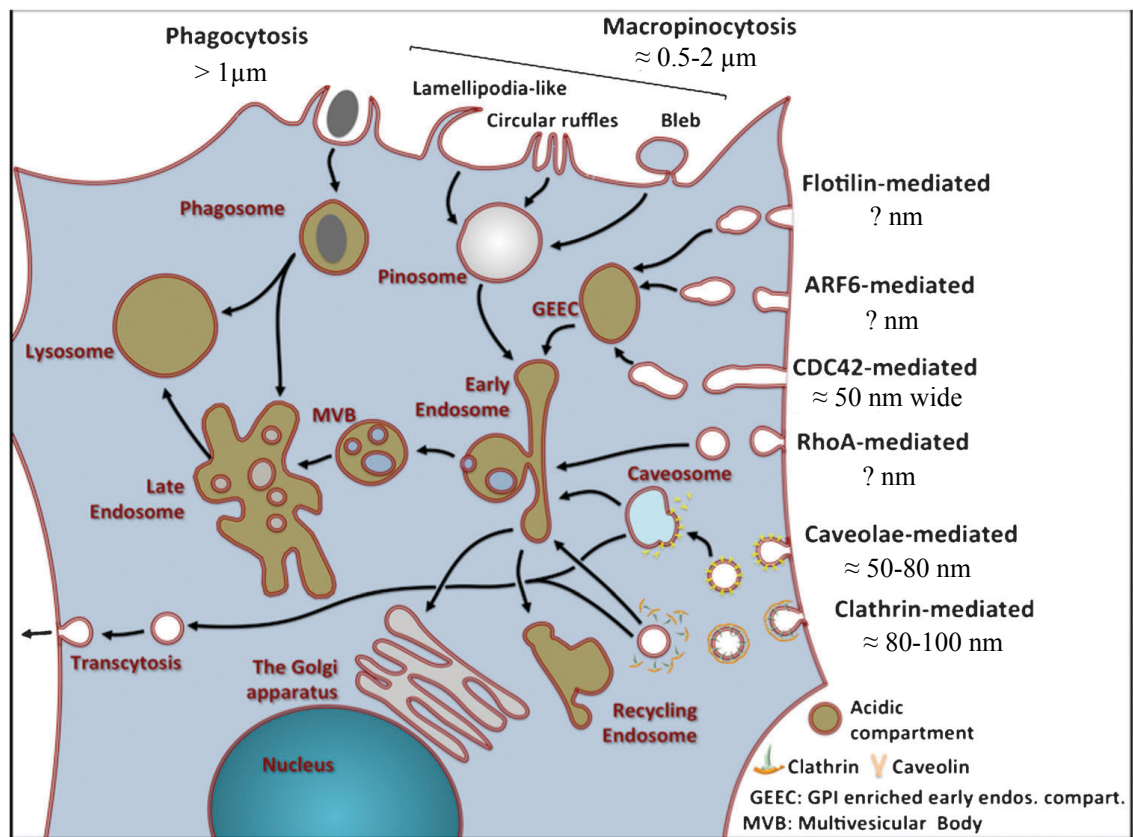


**Figure 1.1: Mechanisms of endocytosis identified in mammalian cells together with the approximated size of the endocytic vesicles formed.**

Adapted from Canton and Battaglia 2012 with permission of The Royal Society of Chemistry(<http://dx.doi.org/10.1039/C2CS15309B>).

Pinocytosis									
Pathway	Phagocytosis	Macropinocytosis	Clathrin mediated	Caveolae mediated	Flotillin mediated	Cdc42 mediated	Arf6 mediated	IL-2R/ RhoA mediated	
Av. invagination diameter	5-10 $\mu$ m	0.5-10 $\mu$ m	dictated by cargo	50-80 nm	?	0.2-0.6 $\mu$ m length x 30-50 nm wide	?	?	?
Max. size of cargo endocytosed	> 1 $\mu$ m	$\leq$ 1 $\mu$ m	80-100 nm	100 nm	?	?	?	?	?
Endocytic vesicle morphology	dictated by cargo	irregular	spherical	flask shape, tubule-vesicular	similar to caveolae (?)	tubular	tubular and spherical	?	?
Dynamin-mediated scission	controversy	Yes (Lamellipodia and circular ruffles) No (Blebs)	yes	yes	controversy	no	no	yes	yes
Actin involvement	yes	yes	yes	yes	yes	yes	yes	yes	yes
Trafficking through EEs	no	yes	yes	yes	yes	yes	yes	yes	yes
Implicated	Rac1 RhoA Arf6 CDC42 tyrosine kinases	Rac1 Pak1 PI3K Ras Src CDC42 PKC cholesterol	AP2 AP108 Epsin FCHO SNX9 amphiphysin intersectin synaptojanin	CAV1 Src PKC- $\alpha$ cholesterol	Flotilin 1 Flotilin 2 Src kinases (Fyn kinase) cholesterol	CDC42 PIK3 GRAF1 Arf1 CAV1	Arf6 PIK3	RhoA Rac1 PAK1 PAK2	

Pathway	Phagocytosis	Pinocytosis						IL-2R/ RhoA mediated
		Macropinocytosis	Clathrin mediated	Caveolae mediated	Flotillin mediated	Cdc42 mediated	Arf6 mediated	
<b>Examples of biological cargoes</b>	mimi virus herpex virus simplex1	fluid phase uptake GPI-Aps RTKs vaccinia virus HIV adenovirus2&3 echo virus1 ebola virus Kaposi's sarcoma- associated herpesvirus, poxvirus	transferrin, RTKs GPCRs anthrax toxin SFV HCV dengue reovirus rhinovirus 2 phleboviruses influenza A adenovirus 2&5	GPI-Aps Integrins (i.e β1) SV40 papillomavirus echo virus	CD59 (GPI-AP) proteoglycans	fluid phase uptake GPI-Aps VacA toxin	MHC I β1 integrin E-cadherin GPI-Aps (CD59) carboxypeptidaseE	IL2Rβ, IL-2R- αβ FcεRI, γc- cytokine receptor

**Table 1.2: Morphological and molecular characteristics of different endocytic pathways and examples of biological cargoes**

ARF6: ADP-ribosylation factor -6. CAV: caveolin. EEs: early endosomes. FcεRI: IgE receptor FcεRI. FCHO: Fer/Cip4 homology domain-only protein GPCRs: G protein-coupled receptors. GPI-Aps: glycosylphosphatidylinositol-anchored proteins. HCV: hepatitis C virus. IL-2R: interleukin-2 receptor. MCH I: major histocompatibility complex I. P13K: phosphatidylinositol 3-kinase. PKC-α: protein kinase C-α. RTK: receptor tyrosine kinase. SFV: semliki forest virus. Src: src kinases. SNX9: sorting nexin 9. SV40: simian virus 40. VacA: helicobacter pylori vacuolatin toxin.

### 1.3 Soft nanoparticles as intracellular delivery vectors

Nanotechnology has already provided different examples of nanoparticles (NPs) able to deliver their cargo intracellularly both in cell cultures and *in vivo* animal models, some of which are currently marketed products (table 1.1). Depending on the material that the nanoparticle is comprised and on the methods of assembly we can distinguish between hard metal nanoparticles (gold, silver, iron, quantum dots) and carbon-based NPs (fullerene, carbon nanotubes), characterised by the strong ionic, metallic or covalent bonds holding the particle together, and soft nanoparticles, such as lipid-based nanoparticles (micelles, liposomes) and polymer-based nanoparticles (micelles, dendrimers, polymersomes) supported by weak interactions including hydrogen bonds, hydrophobic effect or columbic forces<sup>116</sup>. This thesis focuses on polymersomes, and therefore the main characteristics of different colloidal soft nanoparticles with great potential to improve the intracellular delivery of diagnostic and therapeutic molecules will be introduced below.

**Liposomes**, vesicles made by natural amphiphilic molecules known as phospholipids, were first produced in the early 60s by Bangham and Horn<sup>117</sup>, and have remained as the gold standard in synthetic biology for the intracellular delivery of different compounds since then. Liposomes have the ability to encapsulate hydrophilic and hydrophobic cargoes while self-assembling in physiological solutions, they are relatively easy to size-tune and composed of well-characterised building blocks. However, these nanoparticles present short shelf-life during storage due to their reduced chemical and physical stability, and poor biostability as they present very reduced blood circulation times. Polymeric science at the nanoscale allows for the creation of similar delivery systems to liposomes but from a completely synthetic nature, the **polymersome**, which will be described in detail in the next section. Another interesting alternative to liposomes is the exosome. **Exosomes** are endocytic-derived vesicles,  $\approx 40\text{--}100$  nm in diameter, firstly observed in 1983<sup>118</sup>, which are secreted by most cell types *in vitro*. Exosomes present high stability in blood and shielding from immunogenicity due to their self-origin. Interestingly, exosomes derived from dendritic cells carry on their surface tetraspanins including CD9, which has been found to facilitate direct membrane fusion with the target cell and cargo release bypassing lysosomal degradation<sup>119</sup>.

Although the use of exosomes as intracellular delivery vectors is recent, there are interesting reports showing exosome-mediated delivery of a small anti-inflammatory drug<sup>120</sup> and interfering siRNA<sup>121</sup>.

**Dendrimers** are spherical hyperbranched macromolecules formed by repeated polymerisation around a central synthetic polymeric core. Since the synthesis of the first dendrimers in 1978<sup>122</sup> various generations of these polymeric nanoparticles have been produced. Dendrimer generation refers to the number of repeated branching cycles performed during particle synthesis, with the molecular weight of the nanoparticle nearly doubling in each new generation. High generation dendrimers present many cavities that can be used to accommodate therapeutic molecules<sup>123</sup>, at the same time they boast a higher number of functional groups on their surface allowing further dendrimer customisation<sup>124</sup>. Synthesis of dendrimers is a laborious process with numerous steps, however, this is rewarded by obtaining nanoparticle populations with narrow size and shape distributions.

It is important to highlight that in order to improve specificity towards the target site and to promote or enhance the cellular uptake of the nanocarrier, many nanoparticles are currently conjugated on their surface with ligands for the targeting of cellular markers. These ligands include small molecules, proteins and peptides, antibodies or antibody fragments, and aptamers. Among them, conjugation of nanoparticles with **cell-penetrating peptide** (CPP) has emerged as a promising technology to cross the plasma membrane by direct translocation or endocytosis<sup>125</sup>. CPPs derive from proteins able to translocate across cellular membranes. The most common CPP used in intracellular delivery derives from the HIV-1 Tat protein<sup>126</sup>. Novel CPP delivery vectors have been engineered for the transmembrane delivery of oligonucleotides, peptides, peptide nucleic acids, proteins, low-molecular-mass drugs, and nanoparticles such as liposomes<sup>127</sup>. The association of CPPs to nanocarriers has also been used for the development of new cellular imaging tools or biosensors<sup>128</sup>.

### 1.3.1 Polymersomes

The first self-assembly of block copolymer chains into polymeric vesicles (a.k.a polymersome) was reported in 1995 by Zhang and Eisenberg<sup>129</sup>. Since then much research has been conducted in polymersome design and production, and directed towards polymersome biomedical applications, especially as intracellular delivery nanovectors. Polymersomes are considered as the biomimetic analogues of natural phospholipid vesicles since they are formed from the self-assembly in water of synthetic polymeric amphiphiles. Therefore, they are able to entrap hydrophilic molecules within the aqueous core, hydrophobic compounds within the membrane, and amphiphilic substances across the membrane. Their high molecular weight entangled polymeric membranes provide them with enhanced mechanical properties (i.e. stability, flexibility and lower permeability) in comparison with liposomes<sup>130,131</sup>. As an example poly(ethylene oxide)-poly(ethyl ethylene) (PEO-b-PEE) membranes are around 5–50 times tougher than phosphatidylcholine membranes<sup>130</sup>. In addition, polymersome membranes thickness varies between 2 to 50 nm while lipid membranes are 3-5 nm thick<sup>132,133</sup>, and the diffusion coefficient of polymeric membranes is at least one order of magnitude inferior to that of lipidic membranes<sup>134</sup>. The soft nature of polymersomes equips them with a liquid-liquid interface, meaning that their interactions with the biological surroundings are characterised by surface energies with orders of magnitude comparable to those of biological systems<sup>116,135</sup>. Finally, their synthetic nature allows modification of their chemical composition relatively easily<sup>136</sup>, decoration of their external surface with biomolecules for active targeting, or making them stimuli-responsive<sup>134</sup>.

#### 1.3.1.1 Molecular fundamentals in polymersome self-assembly

An amphiphile is a molecule where two domains that behave in an opposite way in contact with water can be identified, with one part being hydrophilic and the other one hydrophobic. Therefore, in an aqueous solution the hydrophilic segment tends to maximise its contact with the surrounding water molecules while the hydrophobic part of the amphiphile tries to limit the contact with the water by staying in close proximity to other hydrophobic regions. This phenomenon is known as the hydrophobic effect<sup>137</sup>

and drives the self-assembly of block copolymers in aqueous solution into polymeric aggregates of different architectures when the copolymer concentration overcome the critical aggregation concentration (CAC). CAC corresponds to the minimum amphiphile concentration to form an aggregate. For high molecular weight amphiphilic copolymers CAC is virtually zero. This is translated in slow chain exchange and therefore high stability of the nanostructure formed. The most likely self-assembled morphology formed is dictated by the dimensionless molecular packing parameter  $p$ <sup>138</sup> (equation 1 and figure 1.2):

*Equation 1*

$$p = \frac{v}{a_o l_c}$$

Where  $v$  is the volume of the hydrophobic chains,  $l_c$  is the length of the hydrophobic tail, and  $a_o$  is the optimal surface area per molecule at the interface between the hydrophobic and hydrophilic domains.

Spherical micelles, monolayered particles consisting of a hydrophobic core surrounded by a soluble corona, are formed when  $p \leq 1/3$ ; when the hydrophobic fraction increases being  $p$  a value between  $1/3$  and  $1/2$  ( $1/3 < p \leq 1/2$ ) cylindrical micelles are formed instead. Finally,  $p$  values between  $1/2 < p \leq 1$  associate with the formation of bilayers with hydrophilic brushes at both sides and a thick hydrophobic core of interdigitated polymers. In order to protect the hydrophobic edges of the bilayer from the contact with the water the membrane rounds itself into a vesicle with an aqueous core, the polymersome<sup>139</sup>.

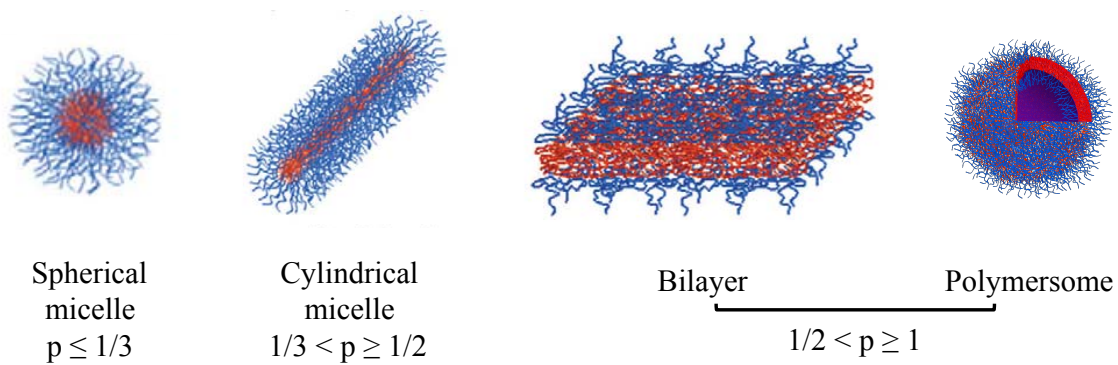


**Figure 1.2: Molecular packing factor and associated geometries of self-assembled block copolymers**

Hydrophilic regions are represented in blue while hydrophobic segments are shown in red. Polymersome representation is reproduced from LoPresti et al., 2009 with permission of The Royal Society of Chemistry (<http://dx.doi.org/10.1039/B818869F>). Spherical micelle, cylindrical micelle and bilayer representations are courtesy of Prof. Battaglia.



### 1.3.1.2 Polymersome-Cell interactions

Nanoparticles are characterised by a large surface area, through which they can establish multiple interactions with the surrounding biomolecules and cells. Therefore, small changes in their physicochemical properties (i.e. size, shape, surface topology and charge) could strongly affect their interactions with the cell membranes. Different groups have been interested in studying soft nanoparticle-cell interactions and how the physicochemical properties of the nanoparticle influence them. The information gathered has proved very useful to guide the design of improved formulations.

One of the most-studied parameters influencing the rate and mechanism of nanoparticle internalisation is nanoparticle **size**. Nowadays, a general agreement exists in that nanoparticles  $\leq 100$  nm in diameter tend to be internalised faster than particles  $>100$  nm<sup>140,141</sup>. Alongside size, nanoparticle **shape** greatly impacts nanoparticle-cell communication. Several studies have concluded that spherical nanoparticles are more efficiently internalised than their rod-shaped or cylindrical counterparts across a variety of cell cultures<sup>19,142-145</sup>. A reason for this behaviour can be found in the fact that spherical particles are characterised by an aspect ratio of one, meaning that particle orientation has no effect on their physical interaction with the cell. Ferrari and Decuzzi<sup>19</sup> found the fastest internalisation time for nanoparticles with aspect ratios close to one. Moreover, they observed that particles with large aspect ratios lead to “frustrated endocytosis”, where the particles become partially wrapped by the membrane but not successfully internalised. Previously, Champion and Mitragotri<sup>145</sup> had arrived at an interesting conclusion when studying the effect of particle shape on cellular internalisation. The angle created between the particle and the cell at the initial contact point, alongside with the volume of the particle, determines the internalisation efficiency. Spherical particles are characterised by a cellular contact angle of 45 degrees. Particles with smaller angles correspond to a more elliptical morphology, with the smaller edge oriented towards the cell. This interaction was easily internalised by phagocytes. On the other hand, phagocytes were unable to internalise elongated particles lying parallel to the cell (contact angles larger than 45 degrees) and would simply spread around them. Nonetheless, studies by DeSimone group<sup>146</sup> contradict this trend of less efficient internalisation at increasing aspect ratio. They found higher rates of endocytosis for rod-like nanoparticles compared with cubic-shaped particles,

highlighting the importance of particle curvature in nanoparticle cellular uptake. To our knowledge, there are no published studies that specifically address the effects of shape on the cellular polymersome internalisation. However, Discher and coworkers have studied the effect of nanoparticle shape in cellular uptake using block copolymer micelles, finding that spherical micelles and short “rod-like” filomicelles were taken up more readily by cells than highly elongated filomicelles<sup>144</sup>.

The plasma membrane of mammalian cells is covered by anionic polysaccharides (proteoglycans), which are responsible for its negative **charge**<sup>147</sup>. Therefore, cationic nanoparticles show a stronger affinity than anionic or neutral particles towards cell membranes. This has driven the design of cationic nanoparticles with the aim to enhance cellular uptake. However, cationic formulations have been related to cytotoxic effects more often than their anionic and neutral counterparts. This has been demonstrated for a diverse range of nanoparticle formulations including dendrimers<sup>148,149</sup>, gold nanoparticles<sup>150</sup> and liposomes<sup>51,151-153</sup>. Our group have studied the effect of surface charge on the cellular uptake of polymersomes, with similar results to the aforementioned formulations. Triblock copolymer poly(ethylene oxide)-poly(2-(diisopropylamino) ethyl methacrylate)-poly(2-(dimethylamino) ethyl methacrylate) (PEO-PDPA-PDMA) was used to produce polymersomes displaying either the neutral PEO or the cationic PDMA polymer on the outer surface. We observed that polymersomes with cationic corona were taken up faster than neutral polymersomes by primary cells in culture. However, the cationic formulation induced higher cellular toxicity<sup>154</sup>. The mechanism by which cationic nanoparticles cause this toxicity is not fully understood. It has been hypothesised that particles with a high density of positive charge would interact with phospholipids in the plasma membrane leading to severe membrane damage such as poration<sup>155,156</sup>. Nevertheless, there are also examples in the literature where the use of cationic polymeric nanoparticles was not related to cytotoxicity<sup>146,157,158</sup>. Although anionic formulations are generally associated with lower cytotoxicity than cationic ones, their negative charge favours the interaction with proteins and components of the extra-cellular matrix. Strong interactions with proteins can destabilise nanoparticle structure, promote particle aggregation and finally hinder their ability to be internalised. Strong interactions of both cationic and anionic nanoparticles with proteins have been observed<sup>159-163</sup>. An additional particle surface feature that is revealing crucial in nanoparticle-cell interactions is the **arrangement of**

**domains of defined chemistry at the nanoparticle surface**<sup>164</sup>. In line with this, our group has investigated the formation and internalisation of polymersomes with diverse surface topologies by blending PMPC-PDPA, and PEO-PDPA polymersome forming block copolymers<sup>165,166</sup>. It was observed that different surface topologies were related to drastic changes in the behaviour and rate of cellular internalisation. The uptake of 100% PEO-PDPA polymersomes was very moderate and relatively dependent on polymersome size with smaller particles internalised more rapidly than large ones, while the internalisation of 100% PMPC-PDPA polymersomes was more efficient and faster (polymersomes uptaken by the cell per hour) than in the former case, and strongly influenced by polymersome diameter. More interesting, blended polymersomes were more efficiently internalised by cells than formulations with uniform surfaces, and for the most efficiently internalised blended formulation, the uptake rates were hardly affected by polymersome diameter<sup>165,166</sup>.

### 1.3.1.3 PMPC-PDPA polymersomes

Most of the research conducted in Prof. Battaglia laboratory has been devoted to investigate polymersome formation, and nanoparticle intracellular delivery, using 2-(methacryloyloxy)ethyl phosphorylcholine-block-2-(diisopropylamino)ethyl methacrylate diblock copolymer, resulting in the formation of colloiddally-stable nanometre-sized PMPC-PDPA polymersomes at physiological pH<sup>167</sup>. The characteristics of the two polymers in this formulation provide the final nanoparticle with some desirable properties for a vector intended for the intracellular delivery of different compounds in mammalian cells. In the last decade, there has been a movement in biomedical sciences towards bio-mimicking. This can be translated to the nanotechnology field in the production of biocompatible, phospholipid-like materials. One of those materials is the highly hydrophilic, phosphocholine-containing vinyl monomer 2-(methacryloyloxy)ethyl phosphorylcholine (MPC). The clinical use of MPC-based macromolecules is approved by the FDA (U.S Food and Drug Administration). As a result, it is currently used for the coating of several medical devices/implants such as soft contact lenses<sup>168</sup>, cardiovascular stents<sup>169</sup>, hip replacement joints<sup>170</sup>, and blood pumps for implants<sup>171</sup>. While the PMPC is biocompatible, the PDPA is pH sensitive, which drives the self-assembly of copolymer chains (unimers) in solution into polymersomes when the pH overcomes the pKa value of the PDPA,  $\approx 6.4$

at physiological conditions<sup>172</sup>. The logarithmic expression of the acid dissociation constant, the pKa, indicates the pH value at which half of the acid is dissociated. In the case of the weak cationic polyelectrolyte PDPA, at pH < 6.4 half of the tertiary amines are protonated making the copolymer hydrophilic, whilst at pH ≥ 6.4 the PDPA is mostly deprotonated becoming hydrophobic and turning the copolymer into an amphiphile that self-assembles into nanovesicles (figure 1.3). This pH sensitivity allows polymersome formation and encapsulation of compounds with different hydrophilic/hydrophobic behaviour. Furthermore, it is also behind the intracellular disassembly of the nanovesicle and the cargo release. Figure 1.4 shows how cells incubated with PMPC-PDPA polymersomes encapsulating a fluorescent dye have become fluorescent, as the dye has been effectively released into the cell cytoplasm. On the other hand, when the cells were incubated with a non-pH sensitive formulation where the PDPA is replaced by poly(butylene glycol) (PBG) the situation was markedly different. The dye-loaded polymersomes were confined in membrane-enclosed compartments within the cell. Most likely these compartments correspond to endo-lysosomal vesicles, since the pH-sensitive formulation encounter in them the right stimulus for its disassembly, a low pH. In line with this, it is important to highlight that taking into account the pKa value of the PDPA polymer it is likely that polymersome disassembly occurs early in the endo-lysosomal route, presumably at the level of the early endosomes (figure 1.5). This is highly desirable for the intracellular delivery of functional biomolecules such as therapeutic proteins that are very sensitive to acidic pH and the presence of degradative enzymes and therefore they would be easily inactivated if released in the late endosomes or the lysosomes.

We believe that the mechanism of cytosolic release is triggered by nanoparticle disassembly inside the endosomes, which will produce a sudden and strong increase in the endosomal osmotic pressure. As an example, a standard 200 nm PMPC-PDPA polymersome produced in 100 mM PBS aqueous solution would be disassembled into  $1.7 \times 10^3$  copolymer chains and  $5 \times 10^5$  ionic species elevating the osmotic pressure to 2.5 kPa ( $1 \mu\text{m}^3$  endocytic vesicle)<sup>173</sup>. In order to compensate for the high pressure built up in the endosomal lumen, part of its content would be released into the cell cytoplasm until homeostatic conditions are reached again, all this without a permanent disruption of the endosomal membrane (figure 1.6). Although speculative, the proposed mechanism is in agreement with a couple of validated properties of PMPC-PDPA polymersomes. PMPC-PDPA polymersomes have excellent intracellular delivery

capability in mammalian cells. As figure 1.7 shows these polymersomes can encapsulate, and subsequently deliver, a wide range of different fluorescent compounds including hydrophilic propidium iodide, hydrophobic cholesterol and amphiphilic ceramides<sup>174</sup>. More interestingly, PMPC-PDPA polymersomes have been shown to be able to deliver *in vitro* and *in vivo* molecules with a high therapeutic profile such as antibiotics<sup>175</sup>, anticancer compounds<sup>176</sup>, DNA<sup>173,177</sup>, and antibodies<sup>177,178</sup>. Equally important, we have observed that the use of this polymersome formulation as a intracellular delivery vector does not promote cellular toxicity or stress, as incubation with PMPC-PDPA polymersomes did not significantly affect the normal mitochondrial metabolic activity or trigger NF- $\kappa$ B nuclear translocation<sup>166,173</sup>.

Motivated by the excellent intracellular delivery abilities of PMPC-PDPA polymersomes and the lack of collateral toxicity observed, the cellular interactions established by this nanoparticle formulation have started to be studied. As previously mentioned, both nanoparticle surface topology and nanoparticle size affect polymersome-cell interactions. We have discovered that efficiency of PMPC-PDPA polymersome internalisation (polymersomes/cell) is strongly influenced by nanoparticle size, decreasing as particle size increases. Polymersomes of 100 nm diameter were internalised almost 100 times better than 200 nm polymersomes and near 3 orders of magnitude more than 400 nm polymersomes<sup>166</sup>. The effect of different nanoparticle surface topologies in PMPC-PDPA polymersomes internalisation has also been investigated by blending this chemistry with another block of copolymers. Interestingly, when PMPC distribution at the surface of the vesicles is not continuous but patched the overall nanoparticle size is less important in the uptake rates, up to the point that for certain formulations the internalisation efficiency is hardly affected by the polymersome diameter<sup>165,166</sup> (figure 1.8). Our knowledge about the internalisation mechanism of PMPC-PDPA polymersomes is limited since the particular cellular uptake pathway for these nanoparticles is unknown. Nonetheless, it seems that PMPC-PDPA polymersomes enter the cell through an endocytic route. After general inhibition of endocytosis, both, by pre-incubating the cells at 4C° or with chloroquine, polymersome internalisation was not detected<sup>166</sup>. In addition, PMPC-PDPA polymersomes were able to enter more than 23 different cell types tested in the laboratory, of animal and human origin, including primary cell types and cell lines<sup>166</sup>, except red blood cells<sup>166</sup>, which are known for not undergoing endocytosis<sup>179,180</sup>.

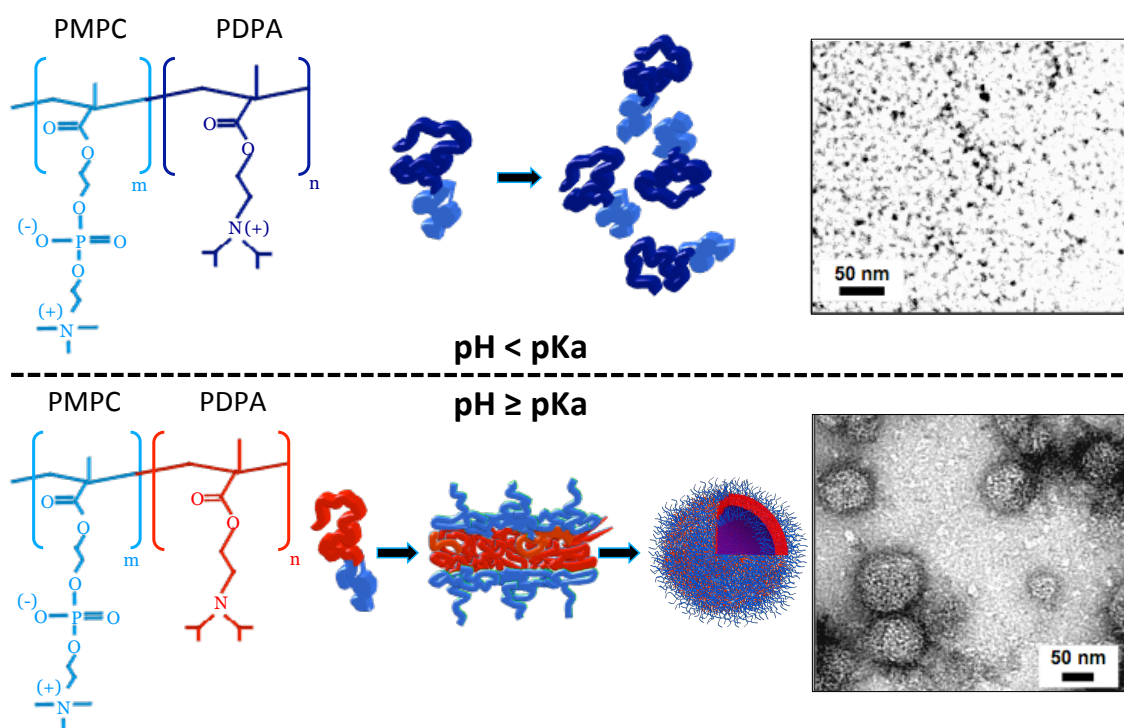


**Figure 1.3: Arrangement of PMPC-PDPA block copolymers in aqueous solution above and below the PDPA pKa**

Upper panel shows the chemical structure of both copolymers when the  $\text{pH} < \text{PDPA pKa}$ , with half of the tertiary amines in the PDPA polymer protonated. At this pH both polymers are hydrophilic and therefore copolymer chains are dissolved, as shown by the TEM micrograph on the right. The bottom panel displays the situation when the  $\text{pH} \geq \text{PDPA pKa}$ . As the PDPA becomes hydrophobic the copolymer chains self-assemble into bilayers that finally round up into vesicles, easily recognisable under the TEM. TEM micrographs are reproduced from Lomas et al., 2008 with permission of The Royal Society of Chemistry (<http://dx.doi.org/10.1039/B717431D>).

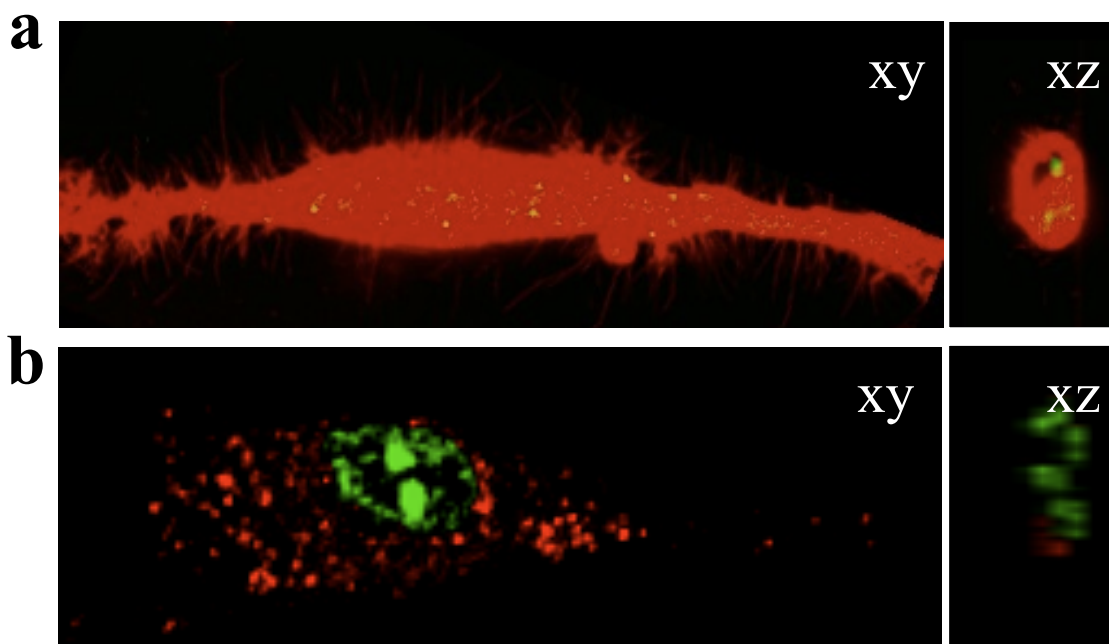


**Figure 1.4: Release of rhodamine octadecyl ester perchlorate B encapsulated in pH sensitive or pH insensitive polymersomes**

Confocal micrographs after 24 hours incubation of human dermal fibroblasts (HDFs) with either pH sensitive PMPC-PDPA polymersomes encapsulating a red fluorescent dye **a**), or pH insensitive PEG-PBG polymersomes encapsulating the same dye **b**). Green channel: DNA staining SYTO<sup>®</sup>9. Reproduced with permission from Massignani et al., 2009 (<http://dx.doi.org/10.1002/smll.200900578>). KGaA Copyright Wiley-VCH Verlag GmbH & Co. KGaA.

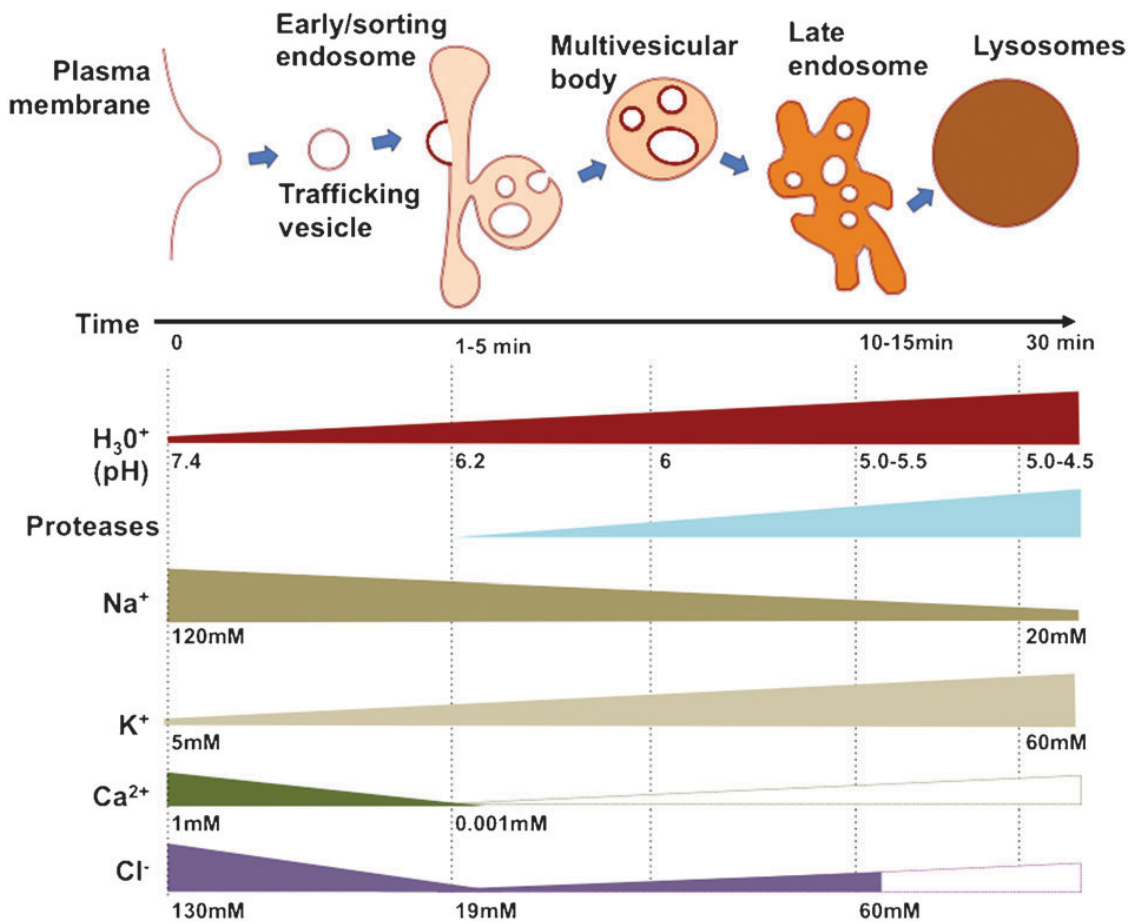


**Figure 1.5: Subcellular vesicular trafficking compartments, alongside their ionic and enzymatic composition**

Reproduced from Canton and Battaglia 2012 with permission of The Royal Society of Chemistry (<http://dx.doi.org/10.1039/C2CS15309B>).



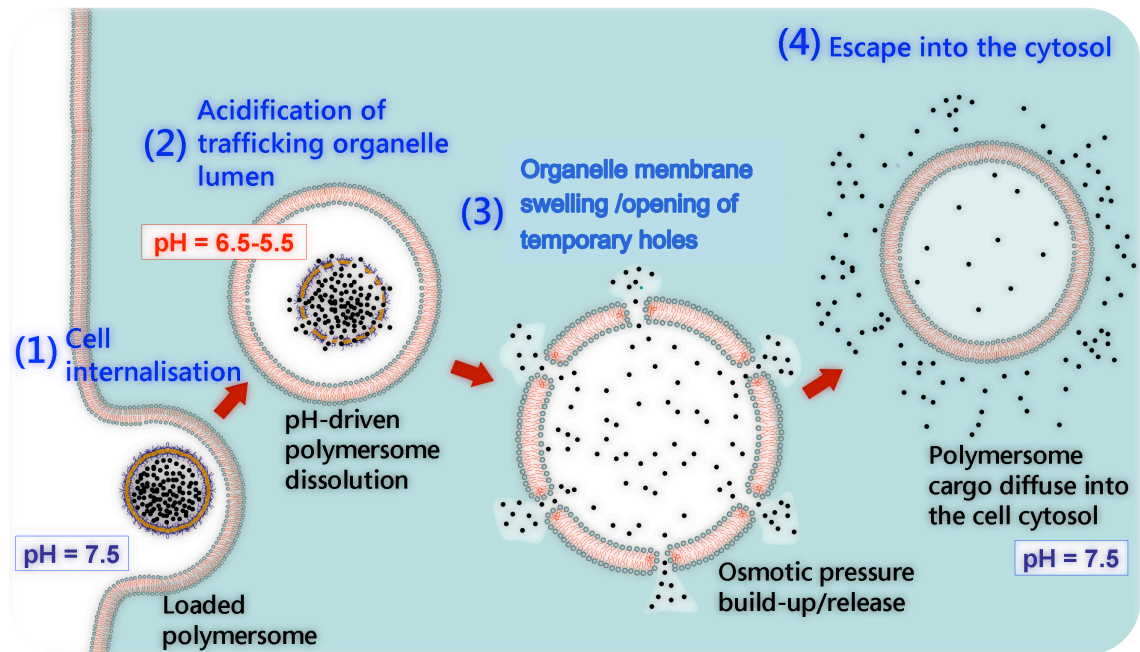


**Figure 1.6: Proposed mechanism of endosomal escape, and polymersome-mediated cytosolic delivery, for PMPC-PDPA polymersomes.**

Adapted from LoPresti et al., 2009 with permission of The Royal Society of Chemistry (<http://dx.doi.org/10.1039/B818869F>).

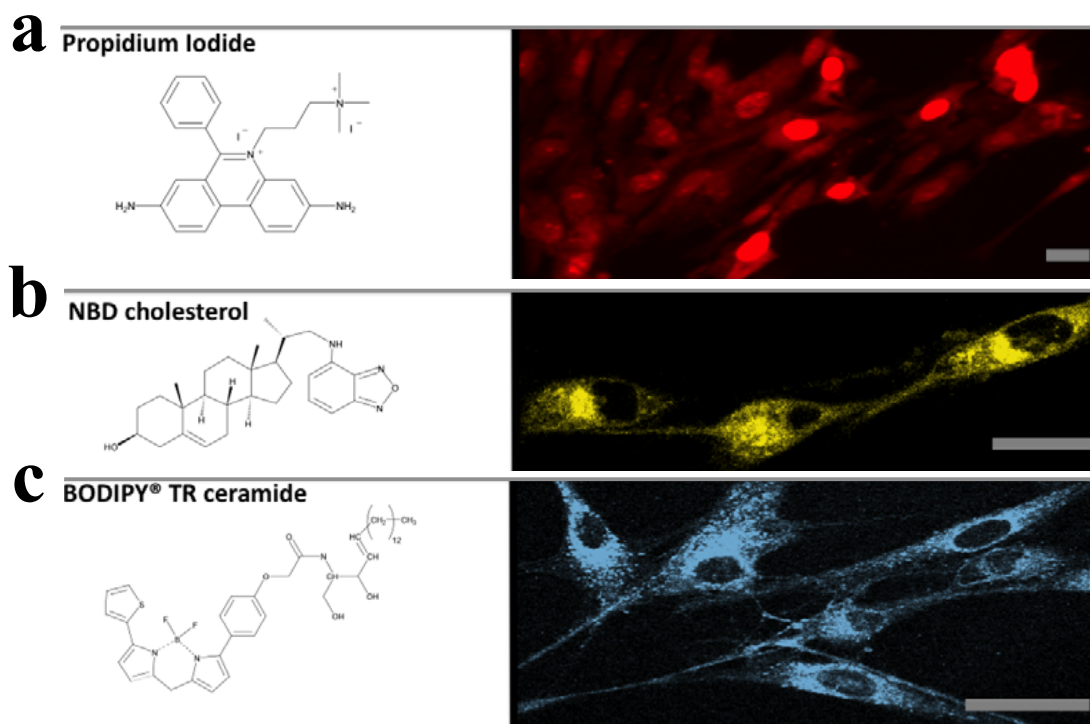


**Figure 1.7: PMPC-PDPA mediated intracellular delivery of compounds with different hydrophilic profiles**

Reproduced from Massignani et al., 2010.

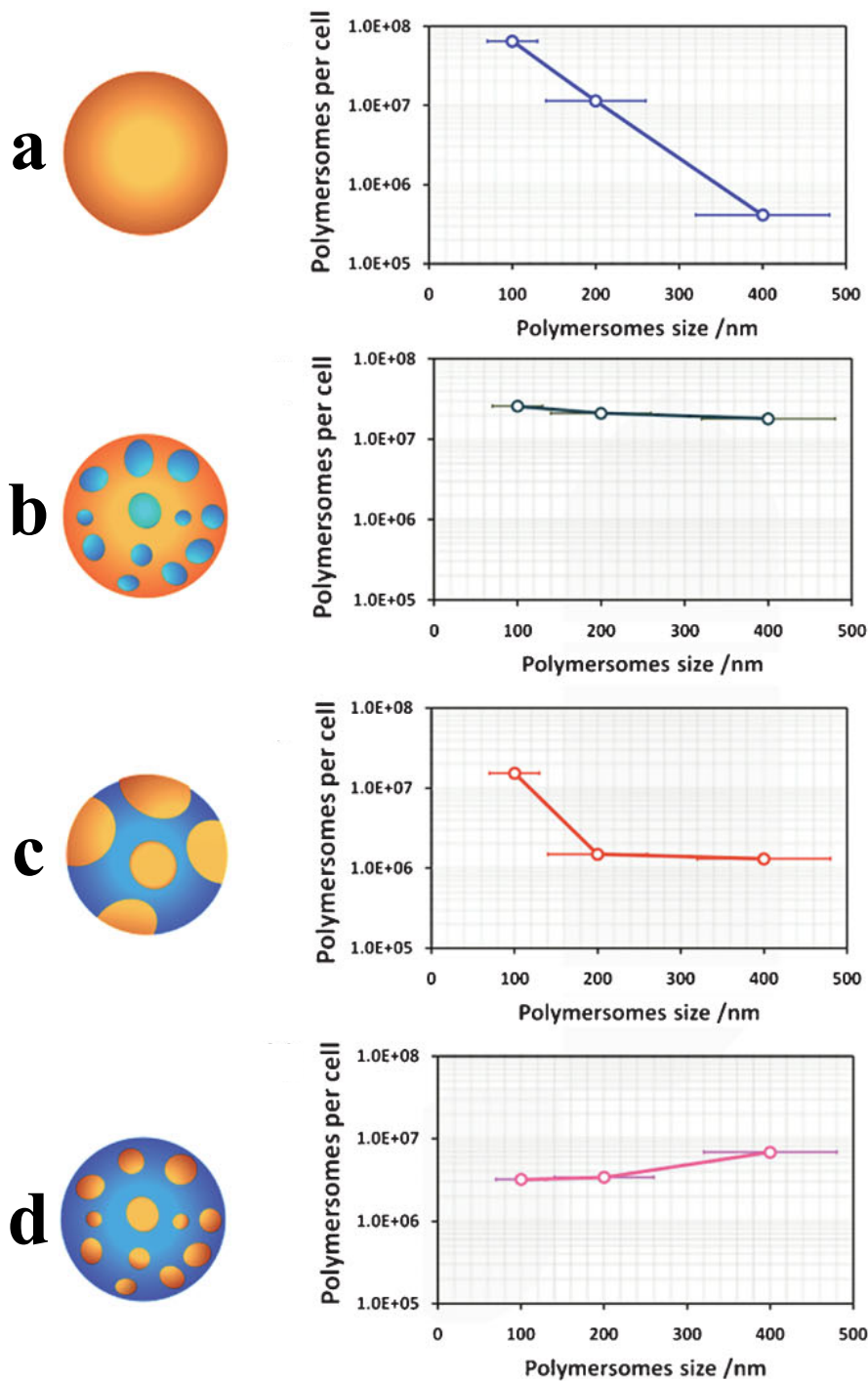


**Figure 1.8: Effect of polymersome size (diameter) and polymersome surface topology in PMPC-PDPA polymersome internalisation**

Polymersomes internalised per cell (HDFs) after 24 hours incubation with: **a)** 100% PMPC-PDPA polymersomes **b)** 75% PMPC-PDPA 25% PEG-PDPA **c)** 50% PMPC-PDPA 50% PEG-PDPA and **d)** 25% PMPC-PDPA 75% PEG-PDPA. Reproduced with permission from Massignani et al., 2009 (<http://dx.doi.org/10.1002/sml.200900578>). Copyright Wiley-VCH Verlag GmbH & Co. KGaA.



## Chapter 2: Aim and objectives

This thesis aims to elucidate and characterise the cellular internalisation mechanism, in mammalian cells, of PMPC-PDPA polymersomes developed in the group of Prof. Battaglia (Department of Chemistry, UCL; previously based in the Department of Biomedical Science, The University of Sheffield). According to the results reviewed in the previous chapter, PMPC-PDPA polymersomes have great potential as intracellular delivery vectors for a wide range of drugs and diagnostic compounds. The ultimate role of such vectors is to be internalised by the cells in order to deliver the encapsulated cargo at the appropriate subcellular compartment. Therefore, characterising nanovector-cell interactions and nanoparticle internalisation becomes a crucial step in effective pharmacokinetics.

Motivated by the early data obtained in our laboratory in the cellular uptake of PMPC-PDPA polymersomes, the internalisation of the nanoparticles will be investigated from two complementary approaches. On one hand, the physicochemical properties of these polymersomes will be studied in relation with their ability to influence their own uptake. On the other hand, it is our objective to identify the cellular factors assisting nanoparticle internalisation.

As previously presented, the size of the nanoparticles along with the surface chemistry, influences the cellular uptake of polymersomes. Subsequently, we hypothesise that the surface chemistry of the nanoparticle controls the binding to the cell surface. Once this binding is formed, there must be an optimal particle size in order to induce cell membrane deformation and polymersome endocytosis, in cooperation with the endocytic cellular machinery. In order to test this hypothesis the following points will be addressed:

- a) Identification of the cellular receptors or plasma membrane components mediating PMPC-PDPA polymersome binding to the plasma membrane.
- b) Further investigation of the effect that the nanoparticle size has in PMPC-PDPA polymersome uptake. Identification of the optimal size for the endocytosis of this formulation.

- c) Examination of the influence that polymersome shape has in PMPC-PDPA polymersome internalisation. Studies in spherical and tubular PMPC-PDPA polymersomes.
- d) Identification of the intracellular cell factors mediating PMPC-PDPA endocytosis, with special attention to the involvement of endocytic molecules able to sense or induce membrane curvature, or to mediated detachment of invaginated vesicles from the cell surface, such as dynamin, actin and BAR domain proteins.

## Chapter 3: Materials and Methods

Unless otherwise specified all chemicals used were acquired from Sigma-Aldrich<sup>®</sup> and all the antibodies were purchased from Abcam. Polystyrene tissue cultured treated 24 well plates and 6 well plates were purchased from Corning<sup>®</sup> Costar<sup>®</sup>. Tissue culture treated  $\mu$ -dishes for high-resolution microscopy were obtained from Ibidi<sup>®</sup> (80136) and flat bottom 96 well plates for fluorescence microscopy from Greiner bio-one. PBS tablets were acquired from Oxoid (Thermo Scientific), and diluted in ultrapure water (Milli-Q<sup>®</sup> Integral Water Purification System, Merck Millipore) to prepare 100 mM PBS solution (pH 7.4).

### 3.1 PMPC-PDPA polymersomes

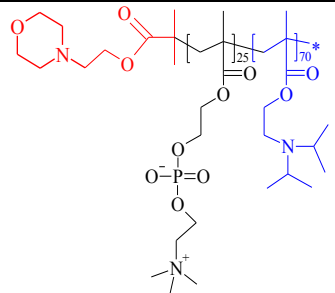
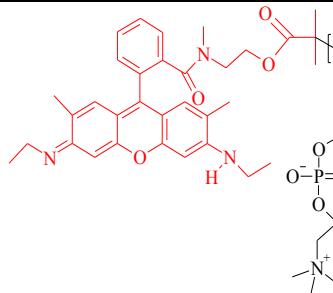
#### 3.1.1 Polymersome preparation

##### 3.1.1.1 Copolymers

2-(Methacryloyloxy)ethyl phosphorylcholine (MPC) polymer was kindly donated by Biocompatibles UK Ltd. 2-(Diisopropylamino)ethyl methacrylate (DPA) polymer was purchased from Scientific Polymer Products, Inc.

PMPC<sub>x</sub>-PDPA<sub>y</sub> and rhodamine 6G-labelled PMPC<sub>x</sub>-PDPA<sub>y</sub> (rho-PMPC-PDPA) copolymers were synthesized and kindly donated by Dr. J. Madsen and Dr. N. Warren in Prof. S. Armes group (Department of Chemistry, The University of Sheffield) and Dr. J. Gaitzsch from Prof. G. Battaglia group. The degree of polymerisation was 25 (x) and 62-70 (y) for PMPC-PDPA copolymers, depending on the batch, while a standard copolymer chain of rho-PMPC-PDPA was composed by 25 MPC monomers and 70 DPA monomers. PMPC<sub>25</sub>-PDPA<sub>62-70</sub> and rho-PMPC<sub>25</sub>-PDPA<sub>70</sub> will be referred as PMPC-PDPA and rho-PMPC-PDPA in this thesis.

PMPC-PDPA copolymers were obtained either by atom transfer radical polymerisation (ATRP)<sup>167</sup> or by reversible addition fragmentation chain transfer polymerization<sup>181,182</sup> as previously described, whereas rho-PMPC-PDPA was always prepared by ATRP<sup>183</sup>.

-	PMPC-PDPA	Rho-PMPC-PDPA
Structure		
Composition	PMPC <sub>25</sub> -PDPA <sub>70</sub>	Rho-PMPC <sub>25</sub> -PDPA <sub>70</sub>
Molecular weight (g/mol)	~22,300	~22,500

**Table 3.1: Chemical composition of PMPC<sub>25</sub>-PDPA<sub>70</sub> and rhodamine-PMPC<sub>25</sub>-PDPA<sub>70</sub> copolymers**

Chemical structures and molecular weights, obtained by nuclear magnetic resonance, for two representative batches of block copolymers used on this thesis.

### 3.1.1.2 Methods of polymersome production

Both unlabelled PMPC-PDPA and rhodamine-labelled PMPC-PDPA polymersomes were prepared and used in this thesis. When rhodamine-labelled polymersomes were required, they were produced by addition of 10 % (wt/wt) rho-PMPC-PDPA copolymer (equivalent to approx. 10% molar ratio) to already weighed PMPC-PDPA copolymer, unless otherwise specified.

#### 3.1.1.2.1 pH switch method

##### 3.1.1.2.1.1 Manual increase of the pH

PMPC-PDPA and rho-PMPC-PDPA copolymers (if needed) were weighed in a glass vial and dissolved in a 2:1 mixture of analytical purity grade chloroform/methanol (Fisher Scientific) at a concentration of 3 mg/ml. The solvent mixture was evaporated in a vacuum oven at 60°C overnight, resulting in the formation of a copolymer film in the walls of the vial. The film was rehydrated using sterile PBS at pH 2 to give an acidic 10 mg/ml polymer solution. The solution was then filtered into sterile vials using 0.2 µm



polyethersulfone filters (Minisart<sup>®</sup>, Sartorius). Polymersomes were formed at room temperature, by increasing the pH over the pKa of the DPA polymer (aprox.6.4) to a final pH of 7.4. This was done by manual dropwise addition of 1 M NaOH, mixing the solution by vortexing for 1 minute after every addition of NaOH. The polymersome dispersion obtained was finally sonicated for 30 minutes (Sonicor Instrument Corporation). Polymersome dispersion was characterised in terms of polymer concentration and polymersome size and shape, and stored at 4°C.

#### *3.1.1.2.1.2 Programmed increase of the pH*

PMPC-PDPA and rho-PMPC-PDPA copolymers (if needed) were weighed in a glass vial and dissolved in a 2:1 mixture of analytical purity grade chloroform/methanol (Fisher Scientific) at a concentration of 3 mg/ml. The solvent mixture was evaporated in a vacuum oven at 60°C overnight, resulting in the formation of a copolymer film in the walls of the vial. The film was rehydrated using sterile PBS at pH 2. The solution was then filtered into sterile vials using 0.2 µm polyethersulfone filters (Minisart<sup>®</sup>, Sartorius). Polymersomes were formed between 25-27°C, by increasing the pH over the pKa of the DPA polymer (aprox.6.4) to a final pH of 7.4. This was done with the help of a water bath and a heater/stirrer plate to monitor and control the temperature. In addition a LAMBDA VIT-FIT syringe pump (LAMBDA Laboratory Instruments) was programmed to standardise the dropwise addition of 0.5 M NaOH, to the polymer solution under continuous stirring. The polymersome dispersion obtained was finally sonicated for 30 minutes (Sonicor Instrument Corporation). Polymersome dispersion was characterised in terms of polymer concentration and polymersome size and shape, and stored at 4°C.

#### *3.1.1.2.2 Film rehydration method*

Tubular polymersomes used in chapter 4 were prepared by J. D. Robertson using the following method. PMPC-PDPA and rho-PMPC-PDPA copolymers were dissolved in a 2:1 mixture of analytical purity grade chloroform/methanol (Fisher Scientific). The solution was subsequently filtered into a sterile glass vial using a 0.2 µm nylon filter (GE Healthcare). A sterilised 0.2µm membrane filter (Millipore) was placed and secured at the top of the vial to allow solvent evaporation, while preserving sterile

conditions inside the vial. The solvent mixture was consequently evaporated in a desiccator overnight. The resulting polymer film was rehydrated under stirring conditions for 4 weeks in sterile PBS (pH 7.4) for a final polymer concentration of 10 mg/ml. The resultant nanoparticle dispersion was sonicated for 20 minutes at room temperature (Sonicor Instrument Corporation). Polymersome dispersion was characterised in terms of polymer concentration and polymersomes size and shape, and stored at 4°C.

### **3.1.2 Polymersome purification**

#### **3.1.2.1 Gel Permeation Chromatography**

Bulk polymersome dispersion, obtained by pH switch, was centrifuged at 500 RCF (rotational centrifugal force) in a 5424 microcentrifuge (Eppendorf). The resulting pellet was concentrated to 0.5 ml with the help of a sterilised hollow fiber module with 20 nm pores (MicroKros<sup>®</sup> Filter Modules X1-500S-200-04P, Spectrum Laboratories, Inc.) The 0.5 µL polymersome dispersion was immediately placed on top of a size-exclusion column packed with sterile Sepharose 4B in endotoxin free PBS (pH 7.4), which was also used to elute the polymersomes. Nanoparticles were collected in sterile 96 well plates (2 drops/well) as they came out for the column. The content of each well was characterised in terms of nanoparticle size by dynamic light scattering (DLS). According to DLS measurements, wells containing nanoparticles of similar sizes were mixed and further characterised by DLS, transmission electron microscope<sup>105</sup> and UV-Vis spectroscopy. Fractions of interest were stored at 10 mg/ml at 4°C.

### 3.1.2.2 Polymersome purification by centrifugation at increasing Relative Centrifugal Force

#### *3.1.2.2.1 Purification of spherical nanoparticles*

Bulk polymersome dispersion obtained by pH switch was circulated through a previously sterilised hollow fiber module with 50 nm pores using a KrosFlo<sup>®</sup> Research Ili Tangential Flow Filtration System (Spectrum Laboratories, Inc.) in order to remove the micelles from the dispersion (referred as fraction 6 in internalisation studies). The resulting dispersion was exposed to successive 20 minutes cycles of centrifugation at room temperature and increasing RCF in a 5424 microcentrifuge (Eppendorf) to separate it into different fractions, each of them enriched in spherical nanoparticles within a specific nanometer-size range. The bulk dispersion was first centrifuged at 2,000 RCF to pellet down any aggregates or big particles above the nm range. The remaining supernatant was then centrifuged at 5,000 RCF, the resulting pellet was resuspended in PBS and the sample was characterised in terms of nanoparticle size and shape and polymer concentration by DLS, TEM and UV-Vis spectroscopy, respectively. Characterised sample was stored at 4°C for subsequent internalisation experiments (fraction 1). The next centrifugation cycle was carried on the residual supernatant from the previous cycle, this time at 10,000 RCF. Pellet was processed as before (fraction 2) and the supernatant was centrifuged at 15,000 RCF. Pellet was resuspended, characterised and stored (fraction 3) while the supernatant was finally centrifuged at 20,000 RCF. The resuspended pellet and the supernatant were characterised and stored as before (fraction 4 and fraction 5 respectively).

#### *3.1.2.2.2. Purification of tubular nanoparticles*

To isolate tubular polymersomes, of the desired diameter and length, from the bulk dispersion obtained after the rehydration method, the dispersion was centrifuged at 2,000 RCF for 20 minutes. The remaining supernatant was then centrifuged at 15,000 RCF for another 20 minutes. The resuspended pellet was characterised in the same way as described above and storage at 4°C for subsequent studies.

### 3.1.3 Polymersome physical characterisation

#### 3.1.3.1 Polymer concentration, UV-Vis Spectroscopy

Polymersome samples were diluted in acidified PBS (standard PBS pH 7.4 acidified to pH 2 by dropwise addition of HCL 1M) to produce the disassembly of the nanoparticles into block copolymer chains. UV-Vis absorbance for each sample was measured in a Jasco UV-Vis V-630 Spectrophotometer between 190 nm and 600 nm, at a 400 nm/min scan speed, using a 10 mm quartz cuvette. Acidified PBS (pH 2) was used as a blank. Absorbance values at 540 nm (maximum absorbance for rho-PMPC-PDPA) and 217 nm (maximum absorbance for PMPC-PDPA) were used to calculate total polymer concentration using equations 3.1 and 3.2, which were derived from Lambert-Beer's Law (equation 2).

$$\text{Equation 2} \quad A = \varepsilon \cdot l \cdot C$$

Where A is the absorption,  $\varepsilon$  is the molar extinction coefficient ( $M \cdot cm$ )<sup>-1</sup>, l is the path length of the cuvette in which the sample is contained (cm) and C is the concentration of the sample (M).

On this thesis we used the following modification of the formula in 2 (equation 3):

$$\text{Equation 3} \quad A = \varepsilon \cdot C$$

Where l was not represented since it is a constant value equal to 1 cm. C was measured in mg/ml and  $\varepsilon$  was measured in ml/mg (mass absorption coefficient).

Mass absorption coefficients ( $\varepsilon$ ) are specific for a polymer at an individual wavelength, and were extracted from the standard curves calculated for each polymer batch (figure 3.1).

$$\text{Equation 3.1} \quad A_{217nm} = A_{217nm}^{NL} + A_{217nm}^L = \varepsilon_{217nm}^{NL} \cdot C^{NL} + \varepsilon_{217nm}^L \cdot C^L$$

$$\text{Equation 3.2} \quad A_{540nm} = A_{540nm}^L = \varepsilon_{540nm}^L \cdot C^L$$

NL refers to non-labelled polymer (PMPC-PDPA) and L refers to labelled polymer (rho-PMPC-PDPA). At 217 nm the final absorbance is influenced by the absorbance values of both labelled and unlabelled copolymers, while at 540 nm the final absorbance only depends on the rho-labelled polymer.

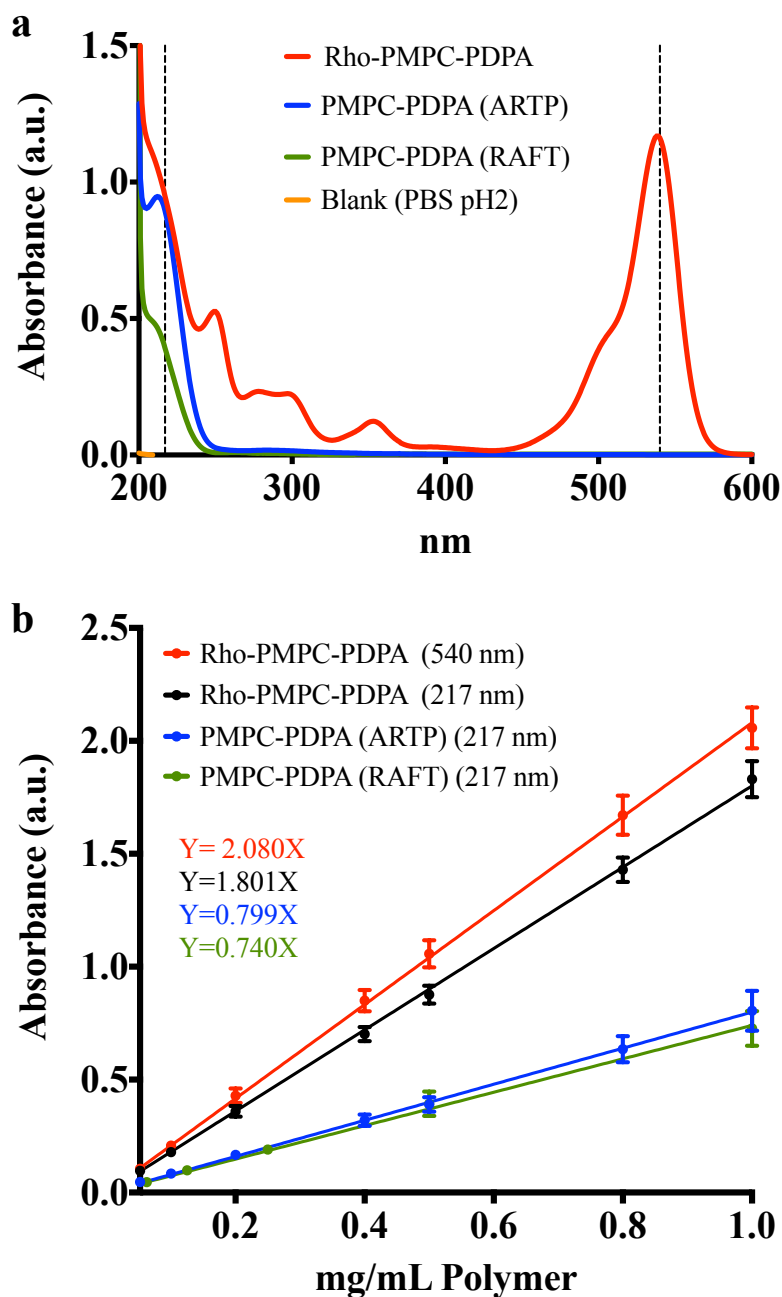


**Figure 3.1: Absorption spectra and standard curves for PMPC-PDPA and rhodamine 6G-PMPC-PDPA block copolymers**

**a)** Examples of absorption spectra, in aqueous solution at pH 2, for rho-PMPC-PDPA and PMPC-PDPA copolymers synthesised by ARTP or by RAFT. PBS pH 2 was used as blank. Vertical dashed lines at 217 nm and 540 nm represent absorbance maxima for PMPC-PDPA and rho-PMPC-PDPA copolymers. **b)** Examples of standard curves produced for PMPC-PDPA (at 217 nm) and rho-PMPC-PDPA (at 217 nm and 540 nm) copolymers. The equations for the regression lines are embedded on the graph.  $n=3$  experiments. Error bars:  $\pm$  SD.

### 3.1.3.2 Size and shape characterisation

#### *3.1.3.2.1 Dynamic Light Scattering*

Diluted polymersome samples in filtered PBS (pH 7.4) were placed in 1 ml polystyrene disposable cuvettes (Fisherbrand<sup>®</sup>) and their size distribution was measured in a Zetasizer Nano ZS (Malvern) at 25°C and at a scattering angle of 173°, using a 4mW He-Ne laser at 633 nm. Each sample was measured three times with a cycle consisting of 12–14 subcycles of 10 seconds duration each. Particle-size distributions were automatically provided by the Zetasizer.

#### *3.1.3.2.2 Transmission Electron Microscope*

Carbon-coated copper/palladium square mesh grids (Agar Scientific) were glow discharged by applying plasma to their surfaces for 30–40 seconds in a partly evacuated chamber. This procedure rendered their surfaces hydrophilic, facilitating the adsorption of aqueous nanoparticle suspensions. Subsequently, glow-discharged grids were treated with 5 µL of polymersomes dispersion (0.1 to 1 mg/ml) for 1 minute. Excess of dispersion was blotted away with filter paper and grids were consecutively positively stained with a 0.75 % (wt/v) phosphotungstic acid solution in ultrapure water (pH 7) for 5 seconds. Finally, grids were blotted with filter paper and dried using a vacuum system. Stained grids were imaged in a FEI Tecnai G2 Spirit electron microscope equipped with a high resolution Orius<sup>®</sup> CCD camera. Image analysis was performed using Gatan Digital Micrograph and Image J software packages.

## **3.2 Cell culture**

### **3.2.1 Mammalian cells**

Primary human dermofibroblasts (HDF), FaDu, HeLa, LADMAC and I-11.15 macrophages were purchased from the American Type Culture Collection (Manassas, VA, USA). The hepatocyte-derived cellular carcinoma cell line Huh7 was a kind gift from Prof. J. McKeating (The University of Birmingham).

FaDu, HeLa and HDF were cultured in Dulbecco's modified Eagle's medium (DMEM) supplemented with 10 % (v/v) fetal calf serum (FCS, Biosera), 2 mM L-glutamine, 100 IU/ml penicillin, 100 mg/ml streptomycin, and 0.625 mg/ml amphotericin B. In the case of Huh7 cells the above media formulation was supplemented with 1 % (v/v) non-essential amino acids and amphotericin B was not added to the media. LADMAC were cultured in Eagle's minimal essential medium (EMEM) supplemented with 10 % (v/v) FCS and 2 mM L-glutamine. 20 % (v/v) of LADMAC conditioned medium together with 10 % (v/v) FCS and 2 mM L-glutamine was used to supplement DMEM medium for the culture of I-11.15 macrophages.

Adherent FaDu, HeLa, HDF and Huh7 cells were detached using trypsin-EDTA and subcultured at ratios 1:5 to 1:10, 2 to 3 times per week. HDF were used for experimentation between passages 2-6 while HeLa, FaDu and Huh7 cells were used between passages 2-10. Before subculture, LADMAC cells were brought to suspension by tapping the sides of the flask. On the other hand, macrophages were gently detached with the help of a cell scraper.

### **3.2.2 Insect cells**

*Drosophila* S2R<sup>+</sup> cells supplied by the Sheffield RNAi Screening Facility (SRSF) were cultured in Schneider's *Drosophila* medium (Gibco<sup>®</sup>, life technologies<sup>™</sup>) supplemented with 10 % (v/v) FCS and 1 % (v/v) penicillin/streptomycin, in a CO<sub>2</sub>-free incubator at 25 °C. Cells were subcultured at a 1:4 ratio every 3 days. In order to do that, semi-adherent cells were helped to come in suspension by carefully banging the culture flask and pipetting up and down the cellular suspension to separate cellular clumps.

### 3.3 Biological experimental procedures

Incubation with PMPC-PDPA nanoparticle was always normalised by amount of polymer added per well, and concentration of polymer per well. Unlabelled or 10 % (wt/wt) rhodamine-labelled nanoparticles were normally diluted 10 times in media as they were added to the well or dish containing the cells. Cellular treatment, in terms of polymer concentration per well, ranged from 0.1 to 1 mg/ml depending on the experiment.

#### 3.3.1 Detection and analysis techniques

##### 3.3.1.1 Flow cytometry

###### 3.3.1.1.1 *Relative quantification of polymersome internalisation*

Processing and evaluation of cellular samples

Live cells were analysed by flow cytometry in order to determine relative polymersome internalisation were processed as follows: media was aspirated from the wells and cells were thoroughly washed with ice-cold PBS twice. Cells were then detached according to cell type (see page 63) and spun down at 153 RCF for 5 minutes. Cell pellets were carefully resuspended in ice-cold PBS (300-400  $\mu$ L/pellet) and analysed either in a FACSArray (BD Biosciences) using a 532 nm laser and a 585-642 nm filter to record the red fluorescence emitted, or in a FACSaria analyser (BD Biosciences) using a 488 nm laser and a 575-626 nm filter. 10,000 cells were measured per sample.

Data analysis

The median fluorescence intensity (MFI) value, obtained from the viable cell population for each condition, was normalised against (divided by) the MFI value of the negative control (cells that were treated only with PBS, or the main diluent used in the experiment). A value of 1 was subsequently subtracted from the normalised data so that untreated cells are always represented by 0 *normalised intensity ratios (a.u.)*.



In order to compare nanoparticle uptake under different conditions, or in the presence of diverse agents, data was represented as *% of normalised intensity ratios*. In this case the *normalised intensity ratio* for the positive control (cells treated only with polymersomes) was set to represent 100% uptake. The % of uptake for the rest of the conditions was calculated based on this.

In addition to MFI values, the percentage of fluorescent cells retrieved by the flow cytometer, at a certain time point or under a specific condition, was also used to investigate polymersome uptake. The percentage of fluorescent cells in the negative control (typically a low value between 0.3-1 %) was deducted from the % of fluorescent cells in each condition under study.

#### *3.3.1.1.1 Titration of polymersomes uptake in mammalian cells*

To titrate the cellular response, in terms of cellular uptake, to different concentrations of polymersomes, FaDu cells were seeded in 24 well plates and allowed to grow for one day before incubating them with increasing concentrations of rhodamine-labelled polymersome dispersion (0.1-1 mg/ml) during 90 minutes. Afterwards, cells were processed for flow cytometry as described above.

#### *3.3.1.1.2 Uptake of polymersomes in serum+ vs. serum- conditions*

In order to investigate the effect that the presence of serum in the media has during the uptake of polymersomes different cells types were pre-incubated in serum free media or media with serum for 30 minutes. Afterwards rhodamine-labelled polymersomes were added to the cells for a final concentration of 1mg/ml polymer per well and incubation was maintained for 1 hour. Subsequently, cells were processed for flow cytometry as described above. MFI values associated with the cells and % of fluorescent cells were recorded and analysed.

### *3.3.1.1.1.3 Uptake kinetics of spherical nanoparticles with different sizes and tubular polymersomes*

FaDu cells were seeded in 24 well plates and allowed to grow for one day. The next day the cells were incubated, for different time points up to 24 hours, with 0.1 mg/ml (final concentration per well) rhodamine-labelled spherical polymersomes of diverse diameters, micelles or tubular polymersomes.

In order to relate MFI values obtained by flow cytometry to the relative number of particles internalised, MFI values were normalised to mass of polymer per particle, in addition to the standard normalisation against the negative control described above. This specific value for each incubation condition was obtained by dividing the mass of polymer that the cells were treated with, by the number of particles that the cells were treated with. The number of particles was calculated based on the molecular weight of the copolymer, the number of polymer chains per particle, and the nanoparticle size distribution obtained by DLS in the case of spherical nanoparticles, or by manual analysis of multiple TEM micrographs, using ImageJ software in the case of tubular polymersomes.

### *3.3.1.1.2 Immunolabeling of surface receptors*

Cells were harvested from T75 flasks using a 0.02% EDTA solution, and gently scraping when appropriate. Detached cells were pelleted at 106 RCF and 4°C for 5 minutes, and resuspended in ice-cold 3% bovine serum albumin (BSA) in PBS (blocking buffer) at a cell density of  $1 \times 10^5$  cells/aliquot. Cells were then incubated with 3  $\mu$ g (equivalent to 0.03 mg/ml) of anti SR-BI<sup>184</sup> (PF-71, provided and used with the consent of Prof. McKeating at The University of Birmingham) or anti CD36 (ab80080), or 0.1  $\mu$ g (equivalent to 0.006 mg/ml) of anti CD81<sup>184</sup> (kindly donated by Prof. McKeating) for 30 minutes at 4°C. After washing off unbound primary antibody cells were incubated with fluorescently-labelled secondary antibody diluted in blocking buffer (ab97170 and ab6954 at 1:100 or ab97035 1:500) for another 30 minutes at 4°C. Finally, cells were washed to remove unbound secondary antibody and processed for

flow cytometry. Cells not treated with antibodies and cells treated only with secondary antibodies were used as controls.

### 3.3.1.2 Fluorescence microscopy

Fluorescent micrographs were processed using either ImageJ on-line free software or Volocity 3D image analysis software (PerkinElmer).

#### *3.3.1.2.1 Polymersome internalisation*

##### *3.3.1.2.1.1 Uptake of polymersomes at 37°C vs. 4°C*

Subconfluent HDF growing in 96 well plates were treated with 14 µg/ml (concentration per well) of Hoechst staining solution (Invitrogen™, Life Technologies™) for 20 minutes. Subsequently cells were washed twice with PBS and they were either placed on the fridge at 4°C or in an incubator at 37°C for 15 minutes. Rhodamine-labelled polymersomes were then added to the cells (1 mg/ml per well) and incubation was maintained at either temperature for another 20 minutes. Finally, media was aspirated and cells were thoroughly washed 3 times using PBS. Live cells in culture media without phenol red were imaged in a Zeiss LSM510 Meta inverted confocal microscope using a 561 nm laser, a 575-615 nm filter to record the red fluorescence emitted and a 40X water immersion lens.

##### *3.3.1.2.1.2 Internalisation of spherical polymersomes*

FaDu cells were seeded in a 96 well plate 24 hours prior to incubation with 0.5 mg/ml (concentration per well) rhodamine-labelled polymersomes for different time points up to 1 hour. Media was aspirated; cells were washed with PBS and left in culture media without phenol red for subsequent imaging. Live cells were imaged in a BD Pathway 855 spinning disk confocal (BD biosciences) using a 20X lens.

##### *3.3.1.2.1.3 Internalisation of tubular polymersomes*

FaDu cells were seeded in Ibidi<sup>®</sup>  $\mu$ -dishes for fluorescence microscopy 24 hours prior to experimentation. On the following day, cells were incubated with 0.1 mg/ml (final concentration per dish) of 30 % (wt/wt) rhodamine-labelled tubular polymersomes for either 5 or 9 hours. Media was removed and cells were thoroughly washed with PBS. Z-stacks of the cells were acquired in a Perkin-Elmer UltraVIEW VoX spinning disk confocal system running on an Olympus IX81 motorized microscope. A 514 nm laser and a 40X oil immersion lens were used to image the cells.

### *3.3.1.2.2 Polymersome-mediated intracellular delivery*

#### *3.3.1.2.2.1 Intracellular delivery by spherical polymersomes*

FaDu cells growing in Ibidi<sup>®</sup>  $\mu$ -dishes, or HeLa cells growing in a 96 well plate, were treated with 1 mg/ml of PMPC-PDPA polymersomes encapsulating rhodamine B octadecyl ester perchlorate (CellLuminate<sup>®</sup>) for 1 hour. Afterwards, the media was aspirated and cells were thoroughly washed with PBS. Live cells in culture media without phenol red were imaged in a Zeiss LSM510 Meta inverted confocal microscope equipped with a 561 nm laser, a 575-615 nm filter, and a 60X oil immersion lens.

#### *3.3.1.2.2.2 Intracellular delivery by tubular polymersomes*

BSA was fluorescently labelled with AlexaFluor<sup>®</sup>647 using a commercial kit from Invitrogen<sup>™</sup> (Life Technologies<sup>™</sup>) and encapsulated in tubular polymersomes by electroporation as previously described<sup>185</sup>. Encapsulation efficiency was determined to be 29% by fluorescence spectroscopy. Protein labelling and encapsulation was carried out by J. Robertson.

FaDu cells were seeded in Ibidi<sup>®</sup>  $\mu$ -dishes 24 hours prior to incubation with protein-encapsulated polymersomes at a final concentration of 0.5 mg/ml of polymer/dish (0.15  $\mu$ g of fluorescent BSA/dish) for 9 hours. Media was aspirated and cells were washed with PBS before being imaged in a Perkin-Elmer UltraVIEW VoX spinning disk confocal system running on an Olympus IX81 motorized microscope, using a 514 nm laser and a 40X oil immersion lens.

### 3.3.1.2.3 Immunofluorescence of cellular receptors

FaDu cells were seeded in sterile cover slides at a cell density of  $9 \times 10^4$ , and allowed to grow for either 1 or 2 days in order to reach 50% and 100% confluence respectively. Cells were fixed with 4 % paraformaldehyde at room temperature for 20 minutes. Fixation was then blocked during 3 cycles of 5 minutes incubation with 50 mM  $\text{NH}_4\text{Cl}$  in PBS at room temperature. Subsequent steps were always carried out at room temperature. The blocking solution was washed off with PBS (3 cycles of 5 minutes each). Cells were then permeabilised with a 0.1 % (v/v) solution of Triton X-100 in PBS for 4 minutes. Fixed cells were incubated with a 0.2 % (wt/v) blocking solution of fish skin gelatine in PBS during 30 minutes. Cells on the cover slides were then incubated with diluted primary antibody in blocking solution, 1/500 for anti SR-BI/SR-BII (ab36970) and anti CD81<sup>184</sup> (kind gift from Prof. McKeating, The University of Birmingham), and 1/250 for anti CD36 (ab78054, ab80080) in a humidifier chamber for 1 or 2 hours in the case of anti SR-BI/SR-BII (figures 5.5.b and 5.5.c-d respectively), 2 hours or overnight for anti CD36 (figures 5.5.b and 5.5.c-d respectively), and 1 hour for CD81 (figures 5.5.b-d). Unbound primary antibody was washed off using blocking solution (3 cycles, 5 minutes each). Cells were then incubated with diluted secondary antibodies in blocking solution in a humidified chamber protected from light as follows: 1/1000, 20 minutes or 40 minutes for anti SR-BI/SR-BII (ab6942, figures 5.5.b and 5.5.c-d respectively), 1/500 or 1/1000 for 60 minutes for anti CD36 (ab6955, figures 5.5.b and 5.5.c-d respectively), and 1/1000 during 20 minutes in the case of anti CD81 (ab6947). Unbound antibody was removed as before and cells were briefly incubated with nuclear staining (DAPI, from Molecular probes<sup>®</sup>, Life Technologies<sup>™</sup>) for 1 minute. Nuclear staining in excess was removed in 3 cycles of 5 minutes each, with blocking solution, followed by 3 washing cycles of 5 minutes with ultrapure water to remove salts. Cells on cover slides were mounted using Prolong Gold Antifade (Molecular probes<sup>®</sup>, Life Technologies<sup>™</sup>) and stored at  $-20^\circ\text{C}$ , 24 hours after. Z stacks of the cells were acquired in a Delta Vision microscope equipped with a 100X Olympus lens. A 457 nm laser was used to image the cellular nucleus and a 685 nm laser to detect the fluorescently labelled receptors.

### 3.3.1.3 Western blotting

To investigate protein levels of scavenger receptors B by western blotting, cells were first detached using either trypsin-EDTA (approx. 40 seconds) or a cell scraper. Subsequently they were spun down at 153 RCF for 5 minutes at 4°C and resuspended in lysis buffer (RIPA buffer from Sigma-Aldrich<sup>®</sup> complemented with fresh cOmplete protease inhibitor cocktail from Roche). Cells were then briefly vortexed (30s) and frozen down (-20°C) overnight. Defrosted pellets were briefly vortexed and spun down at high speed (20,000 RCF) for 10 minutes at 4°C, any pellet was discarded. Protein concentration was calculated by the Bradford protein dye-binding assay<sup>186</sup>. The cell pellet was mixed with diluted Bio-Rad Protein Assay reagent (Bio-Rad) and the absorbance of the mixture was measured in a spectrophotometer at 595 nm and compared to BSA standards. Denatured sample, containing 22 µg of protein, was mixed by vortex with Laemmli buffer (5X buffer: 1 M Tris-Cl pH 6.8, 2 g SDS, 10 ml glycerol, 2 ml β-mercaptoethanol, 50 mg bromophenol blue) and immediately denatured in a water bath at 37°C during 30 minutes. Denatured samples were loaded in 1 mm thick 8% acrylamide gels with a 20 % (wt/v) SDS content. Proteins in the gel were electrophoresed at 150 V for 40 minutes. Subsequently, they were transferred to a nitrocellulose membrane, either overnight at 22 V and room temperature, or during 75 minutes at 400 mA and 4°C. The membrane was then blocked during 60 minutes using 5 % (wt/v) dried milk in TBS (20 mM Tris-HCl pH 7.4, 137 mM NaCl). Next, it was incubated with anti SR-BI/SR-BII antibody (1:100, ab52629) or anti β-actin antibody (1:1000, A1778 Sigma-Aldrich<sup>®</sup>) diluted in blocking solution (5 % wt/v dried milk in TBS) for 90 minutes at room temperature. Unbound primary antibody was washed off using 0.05 % (v/v) Tween<sup>®</sup>20 in TBS (3 cycles of 5 minutes each). The membrane was then incubated with HRP-conjugated secondary antibodies (sc-2004 and sc-2006, Santa Cruz Biotechnology, Inc.) diluted 1:5000 in blocking solution for 60 minutes at room temperature. Unbound antibody was washed off as before. Finally, protein bands were revealed using either ECL, in the case of β-actin, or ECL prime for SR-BI/SR-BII (GE Healthcare Life Sciences) according to manufacturer instructions. Chemiluminescence was detected using an UVI-prochemi camera.

### 3.3.2 Cell viability

#### 3.3.2.1 MTT assay

The MTT assay<sup>187</sup> is based on the ability of living cells to reduce the yellow tetrazole 3-(4,5-Dimethylthiazol-2-yl)-2,5-diphenyltetrazolium bromide (MTT) to a purple formazan salt. Cellular metabolic activity can be determined by spectrophotometry following formazan solubilisation. The mitochondrial activity of a population of cells is an indirect indication of the cellular viability of those cells.

Following cellular incubation with the compound, where its toxicity is to be determined, the media was aspirated and the cells were washed twice with PBS. Cells were then incubated with fresh 0.5 mg/ml MTT solution in PBS (1ml/well) at 37°C and 5% CO<sub>2</sub> for 50 minutes. After incubation, the MTT solution was carefully disposed of and the purple formazan crystals were solubilised with the help of 300 µL/well of acidified isopropanol (25 µL of concentrated HCL per 20 ml of isopropanol). Solubilised formazan was transferred to a 96 well plate (150 µL/well) and its absorbance at 540 nm was read in an ELx800 Absorbance Microplate Reader (BioTek Instruments, Inc.) using a 630 nm wavelength as a reference.

Control cells were treated with PBS, or the main diluent used in the study. Absorbance at 540 nm associated with the control group was assigned to represent 100 % viable cells; percentages for the rest of the conditions were calculated accordingly.

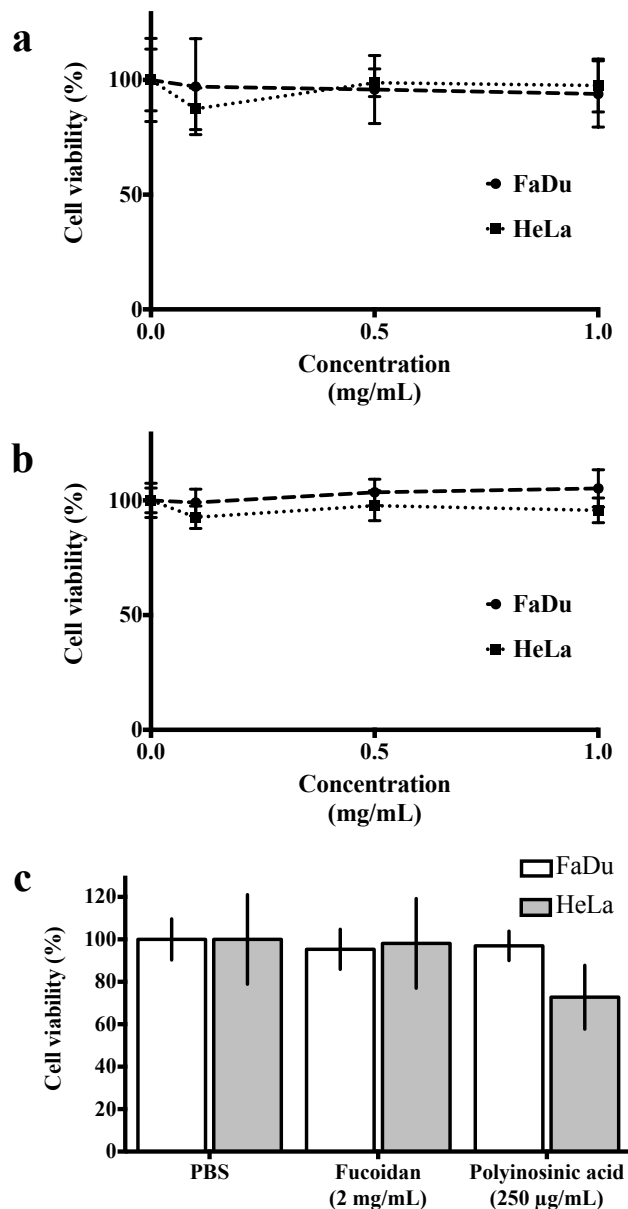


**Figure 3.2: MTT assays performed in FaDu and HeLa cells treated with rho-PMPC-PDPA polymersomes or the ligands for scavenger receptors, Fucoidan and Polyinosinic acid**

**a-b)** Cell viability levels after 24 hours incubation with different concentrations of rho-PMPC-PDPA polymersomes. In both cases the rho-PMPC-PDPA copolymer used for the nanoparticle production was obtained by ARTP, while the PMPC-PDPA copolymer was produced by ARTP in **a)** and by RAFT in **b)**. **c)** Cell viability after 2 hours incubation with Fucoidan or Polyinosinic acid (see section 3.3.3.2.1) n=3 experiments. Error bars:  $\pm$  sem. No statistical difference was found between control cells (10 % (v/v) PBS treated) and treated cells (polymersomes or scavenger ligands) using one-way ANOVA in a, b and c.



### 3.3.2.2 Live/Dead cell viability assay

Propidium iodide (PI) (Ex/Em: 536 nm/617nm) and SYTO<sup>®</sup>9 (Ex/Em: 480 nm/500 nm), acquired from Invitrogen<sup>™</sup> (Life Technologies<sup>™</sup>), were used to investigate cytotoxicity induced by different inhibitors of endocytosis in HeLa cells.

#### 3.3.2.2.1 *Flow cytometry*

After incubation of subconfluent cells, growing in 24 well plates, with the compounds under study or the appropriated controls, media from the wells was aspirated and cells were thoroughly washed with PBS 3 times. Cells were then incubated with a solution 50  $\mu$ M of PI for 10 minutes at room temperature. PI solution was disposed of and cells were prepared for flow cytometry. Analysis was carried out in a FACSArray (BD Biosciences) using the 532 nm laser and a 585-642 nm bandpass filter to record the red fluorescence emitted.

#### 3.3.2.2.2 *Fluorescence microscopy*

After incubation of subconfluent cells, growing in 96 well plates, with the compounds under study or the appropriate controls, media from the wells was aspirated and cells were thoroughly washed with PBS 3 times. Cells were then incubated with a solution containing 50  $\mu$ M PI plus 2  $\mu$ M SYTO<sup>®</sup>9, for 10 minutes at room temperature. The solution containing fluorescent dyes in excess was removed and cells were rinsed twice with PBS. Cells in culture media with out phenol red were imaged at 20X in a BD Pathway 855 spinning disk confocal (BD biosciences).

### **3.3.3 Perturbation of the cellular uptake of PMPC-PDPA polymersomes**

Different approaches were used to try to inhibit polymersome uptake in mammalian cells including the use of chemical compounds, ligands and small antagonists for scavenger receptors and antibodies targeting the extracellular loop of either CD36, SR-BI/SR-BII scavenger receptors or tetraspanin CD81.

#### **3.3.3.1 Polymersome uptake in the presence of chemical inhibitors of endocytosis**

##### *3.3.3.1.1 Preparation of stock solutions*

Inhibitors were dissolved in ultrapure water (chlorpromazine) or dimethyl sulfoxide (DMSO) (monodansylcadaverine, dynasore, sertraline, filipin, genistein, cytochalasin D, latrunculin B, IPA-3, EIPA, bafilomicin A1) to yield stock solutions 1mM to 16  $\mu$ M (stock solution 1, Table 3.1). Stock solutions were filtered using sterile 0.20  $\mu$ m filters (GE Healthcare) and stored according to manufacture instructions.

For experiments involving the use of chemical inhibitors (MTTs, live-dead cell viability assays and experiments looking at polymersome uptake in cells treated with chemical inhibitors), solutions containing the inhibitor were diluted ten times in media with serum as they were added to the cells. To facilitate the experimental work stock solutions 1 were diluted in ultrapure water to produce stock solutions 2 (Table 3.1). Stock solutions 2 are 10 times concentrate solutions compared with the inhibitor concentration on well and were freshly prepared before each experiment.

Inhibitor	Stock solution 1	Stock solution 2
Chlorpromazine	1 mM	50 $\mu$ M
		100 $\mu$ M
		200 $\mu$ M
Monodansylcadaverine	1mM	250 $\mu$ M
		500 $\mu$ M
Filipin	1.5 mM	10 $\mu$ M
		50 $\mu$ M
		100 $\mu$ M
Genistein	18.5 mM	0.5 mM
		1 mM
		2 mM
Dynasore	15 mM	0.5 mM
		0.8 mM
		1 mM
Sertraline	1mM	50 $\mu$ M
		200 $\mu$ M
		500 $\mu$ M
Nocodazole	10 M	3 $\mu$ M
		30 $\mu$ M
		333 $\mu$ M
Latrunculin B	2.5 mM	10 $\mu$ M
		50 $\mu$ M
		100 $\mu$ M
Cytochalasin D	2 mM	1 $\mu$ M
		10 $\mu$ M
		20 $\mu$ M
1,1'-Disulfanediylidinaphthalen-2-ol (IPA-3)	1mM	100 $\mu$ M
		250 $\mu$ M
		500 $\mu$ M
5-(N-ethyl-N-isopropyl) amiloride (EIPA)	1mM	250 $\mu$ M
		500 $\mu$ M
Bafilomycin A1	16 $\mu$ M	0.1 $\mu$ M
		0.5 $\mu$ M
		1 $\mu$ M

**Table 3.2: Stock solutions prepared for different chemical inhibitors**

AlexaFluor<sup>®</sup>647 conjugates of transferrin, cholera toxin subunit B and 10kDa dextran were purchased from Invitrogen<sup>™</sup> (Life Technologies<sup>™</sup>), diluted in ultrapure water or PBS according to manufacturer indications, and used as control cargoes for different endocytic pathways.

### 2.3.3.1.2 Screen

Subconfluent HeLa cells growing in 6 well plates were pre-incubated with inhibitors (see table 6.3 for concentrations) for 15 minutes at 37°C and 5% CO<sub>2</sub>. Afterwards, rhodamine-labelled polymersomes, control cargoes (table 3.3 for concentrations), or PBS, were added to the cells, doubling the total volume of the wells and therefore reducing to half the concentration of inhibitors/well. Incubation under these conditions was maintained during 20 minutes at 37°C and 5% CO<sub>2</sub>. Finally, media was aspirated, cells were thoroughly washed three times with ice cold PBS, detached with the help of a cell scraper, and immediately processed for flow cytometry. Cells were analysed in a FacsArray (BD Biosciences) using the 532 nm laser and a 585-642 nm filter to capture the fluorescence emitted by cells treated with rhodamine-labelled polymersomes or a 633nm laser and 661-716 nm filter in the case of cells treated with AlexaFluor<sup>®</sup>647 conjugates.

-	Concentration/well (µg/ml)	Amount/well (µg)
Polymersomes	200	320
Transferrin	5	8
Cholera toxin subunit B	10	16
10 kDa Dextran	100	160

**Table 3.3: Experimental conditions for cells incubated with polymersomes or control cargoes**

### 3.3.3.2 Polymersome uptake in the presence of known ligands for scavenger receptors

#### 3.3.3.2.1 Ligands for scavenger receptors type A and B. Fucoïdan and Polyinosinic acid

Stock solutions, 10 times concentrated, of Fucoïdan (from *Fucus vesiculosus* F5631, Sigma-Aldrich<sup>®</sup>) and Polyinosinic acid (P4154, Sigma-Aldrich<sup>®</sup>) were prepared in endotoxin free PBS, filtered and storage at -20°C until use.

Subconfluent cells growing in 24 well plates were incubated with Fucoidan (2 mg/ml) or Polyinosinic acid (0.25, mg/ml) for one hour. Rhodamine-labelled polymersomes were then added to the cells at 1 mg/ml (final polymer concentration/well) and incubation was continued for another hour. Media was aspirated, cells were thoroughly washed with PBS and processed for flow cytometry. Cells incubated only with PBS and cells incubated with polymersomes in the absence of Fucoidan and Polyinosinic acid were used as negative and positive controls for uptake respectively.

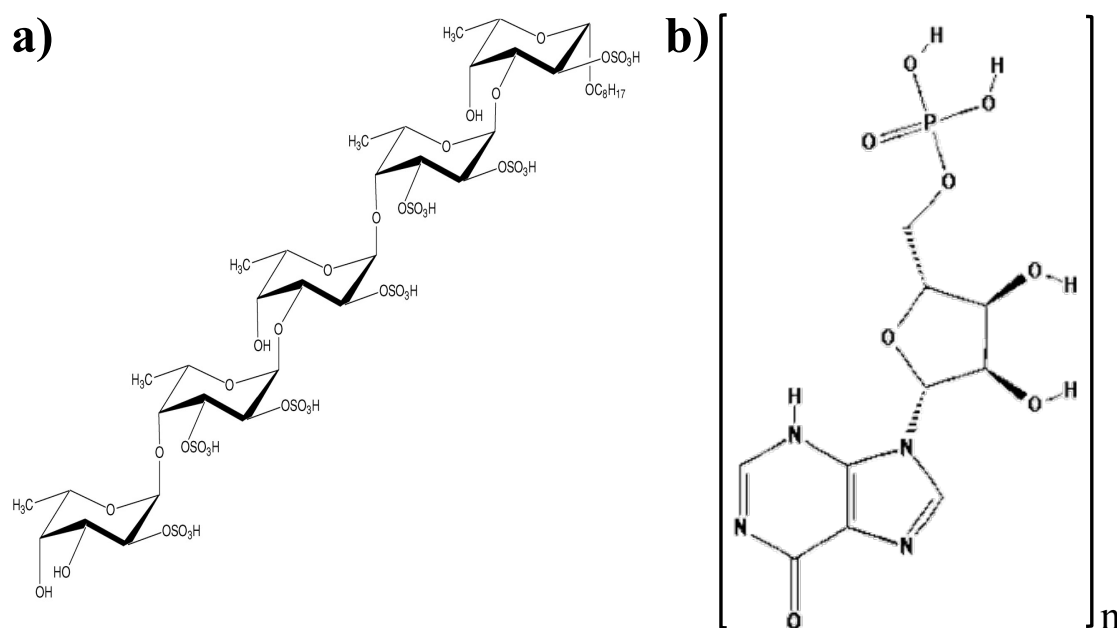


**Figure 3.3: Chemical structures of Fucoidan and Polyinosinic acid.**

**a)** Fucoidan from *Fucus vesiculosus*. Reproduced from Ale et al., 2011<sup>188</sup>. **b)** Polyinosinic acid. Adapted from PubChem Compound database, unique chemical structure identifier CID: 8582.

### 3.3.3.2.2 SR-Bs antagonist ITX5061

ITX5061 solution was a kind gift from Prof. McKeating (The University of Birmingham).

HDF were seeded into 24 well plates and allowed to grow for two days until they were 80% confluent. Cells were then incubated with different concentrations of ITX5061 (1-20  $\mu$ M) for 1 hour prior to incubation with rho-labelled polymersomes for another hour in the presence of the antagonist. Media was aspirated and cells were processed for flow cytometry.

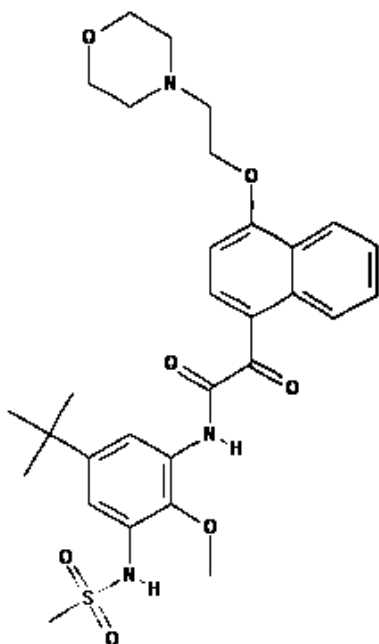


**Figure 3.4: Chemical structure of ITX5061.**

Adapted from PubChem Compound database, unique chemical structure identifier CID: 56843466.

### 3.3.3.3 Polymersome uptake in the presence of blocking antibodies. Antibodies against scavenger receptors CD36 and SR-Bs, and tetraspanin CD81

Subconfluent cells growing in 24 well plates were incubated with anti-SR-BI/SR-BII antibody (ab36970, 0.3 mg/ml or 0.5 mg/ml), anti-CD36 antibody (0.04 mg/ml or 0.02 mg/ml), anti SR-BI/SR-BII plus anti CD36 (ab78054, 0.3 mg/ml) or anti-CD81 antibody<sup>184</sup> (kind gift from Prof. McKeating, The University of Birmingham, 0.006 mg/ml). An unspecific IgG (ab37415) at the same concentration as the targeting antibodies was included as control. Rhodamine-labelled polymersomes (1 mg/ml final concentration per well) were added to the previous cells and incubation was maintained for another hour. Media was then aspirated and cells were processed and measured for flow cytometry. Cells incubated either with PBS, or polymersomes, in the absence of any antibody, were used as negative and positive controls for uptake respectively.

### **3.3.4 Cellular transfection**

#### **3.3.4.1 Mutant K44A dynamin**

##### *3.3.4.1.1 Flow cytometry*

Cells were seeded in 24 well plates and allowed to grow for 24 hours in antibiotic free DMEM media. The following morning the media was replaced with OPTI-MEM<sup>®</sup> media (Life Technologies<sup>™</sup>). Transfection complexes were prepared using lipofectamine<sup>®</sup> 2000 (Invitrogen<sup>™</sup>, Life Technologies<sup>™</sup>) following the standard protocol supplied by the manufacturer. Ratio cDNA:lipofectamine was 1:2 and final cDNA concentration per well was 1 µg/ml for both wild type (WT) and mutant K44A dynamin constructs. Detailed preparation of WT and K44A constructs is described elsewhere<sup>72</sup>. Following incubation for 12 hours, transfection media was replaced with complete DMEM media and cells were incubated with rhodamine-labelled polymersomes (1 mg/ml final polymer concentration/well) for one hour. Afterwards the media was aspirated and cells were washed twice with ice cold PBS. Cells were then processed for flow cytometry and analysed in FACS Aria analyser (BD Biosciences) using a 488 nm laser and a 575-626 nm filter to record red fluorescence associated with cells after incubation with fluorescent polymersomes. The expression of a cerulean blue fluorescent reporter gene included in the cDNA was used to identify transfected cells within the total cell population. Therefore, cells were also excited with a 405 nm laser and their fluorescence recorded between 450-550 nm.

Control conditions included untransfected cells, treated or not with polymersomes, and WT and K44A transfected cells not treated with polymersomes.

##### *3.3.4.1.2 Fluorescence microscopy*

Cells growing in a 96 well plate were 70-80% confluent at the moment of the transfection with TurboFect<sup>™</sup> (Fermentas, Thermo Scientific). Transfection with either WT or K44A cDNA constructs was carried out according with the protocol supplied by

the manufacturer for a 96 well plate format. Ratio cDNA:Turbofect™ was 1:1 % (v/v) and 0.2 µg of cDNA were added per well. Transfection was prolonged for 8 hours. HeLa cells transfected with WT or K44A dynamin as well as non-transfected cells, were incubated in serum free media with either 25 µg/ml of AlexaFluor® 647 transferrin (Ex/Em: 652/668 nm) for 20 minutes or 1 mg/ml of CelLuminate® (PMPC-PDPA polymersomes encapsulating rhodamine B octadecyl ester perchlorate, Ex/Em: 554/578 approx.) during 1 hour. Afterwards, media was aspirated and cells were washed twice with PBS and left in culture media without phenol red. Cells were immediately imaged in a Zeiss LSM510 Meta inverted confocal microscope using a 60X oil immersion lens. A 405 nm laser line was used to verify the presence of transfected cells while excitation with the 561 nm and the 633 lasers was used to investigate the cellular uptake of CelLuminate® and AlexaFluor® 647 transferrin, respectively. Confocal images and Z-stacks obtained were analysed using Image J software.

### 3.3.4.2 siRNA knockdown

#### *3.3.4.2.1 siRNA knockdown by electroporation*

Cells were transfected either with On-TARGET plus Human SCARB1 siRNA pool or On-TARGET plus non-targeting siRNA pool (Dharmacon, Thermo Scientific) by electroporation using the Neon™ Transfection System (Invitrogen™, Life Technologies™).

FaDu cells were allowed to grow in a T75 flask with complete medium until they were 70-90% confluent. On the day of the transfection cells were rinsed with PBS, detached from the flask, pelleted and counted. Different siRNA concentrations were tested with  $3 \times 10^5$  cells transfected per condition. Cells were electroporated with one pulse of 30 ms at 1350 V and immediately transferred to a 6 well plate with antibiotic free media. Transfection was prolonged for either 24, 36 or 48 hours. In any case, transfection media was replaced with fresh media without antibiotics 24 hours after transfection. Protein knockdown was investigated by western blotting.



### 3.3.4.2.2 siRNA knockdown screen in *Drosophila* cells

Two 384 well plates, procured by the RNAi screening facilities at The University of Sheffield, were used for the screen. One contained siRNAs targeting genes of *Caenorhabditis elegans* (*C.elegans*), which have no homology with *Drosophila* genes (non-targeting siRNAs). The other plate comprised the siRNAs for the knockdown of the genes under study. Each well on the plate had 5  $\mu\text{L}$  of a 0.05  $\mu\text{g}/\text{ml}$  solution of siRNA in water (0.25  $\mu\text{g}$  siRNA/well). Sealed plates were stored at  $-20^{\circ}\text{C}$  or  $-80^{\circ}\text{C}$  until their use.

On the day of the transfection, plates containing the siRNAs were thawed at room temperature and centrifuged at 153 RCF for 1 minute before removing the seals. 20  $\mu\text{L}$  of a suspension containing  $6 \times 10^5$  SR2<sup>+</sup> cells in serum free media were added to each well and incubated for 1 hour. Afterwards, 30  $\mu\text{L}$  of complete Schneider's media was added to the cells. Transfection under these premises was prolonged for 3 days in a CO<sub>2</sub>-free incubator at 25°C. To study polymersome internalisation in transfected cells, the media from the wells was aspirated and replaced with 50  $\mu\text{L}$  of serum free media containing 5  $\mu\text{g}$  of rhodamine labelled PMPC-PDPA polymersomes. Cells were incubated with polymersomes for 1 hour, afterwards the media was aspirated and cells were washed with PBS. Cells were fixed with 6 % formaldehyde and stained with Hoescht (Invitrogen<sup>TM</sup>, Life Technologies<sup>TM</sup>) during 10 minutes. Finally, the solution containing the fixative and the nuclear staining was aspirated and cells were washed with PBS. Cells in PBS were imaged in an ImageXpress Micro XLS Widefield High Content Screening System (Molecular Devices) using a 40x objective and two lasers lines configured to excite and record the fluorescence of DAPI and Cy3 dyes. The two fluorescent channels were used to generate a quantification mask for image analysis using MetaXpress<sup>®</sup> (Molecular Devices).

### **3.4 Statistics**

Unpaired T-test was used to test for statistical difference between two sets of data. One-way ANOVA was employed when it was necessary to compare more than two sets of data. Bonferroni test was used after ANOVA if statistical significance was found between the groups. Statistical significance from either statistical test used was represented as follows:  $p < 0.05$  (\*),  $p < 0.01$  (\*\*),  $p < 0.001$  (\*\*\*)

# **Chapter 4: Uptake of PMPC-PDPA polymersomes in mammalian cells. Effect of nanoparticle size and nanoparticle shape in polymersome internalisation**

Part of this chapter has been published as:

pH-Sensitive Tubular Polymersomes: Formation and Applications in Cellular Delivery.

James D. Robertson, Guy Yealland, **Milagros Avila-Olias**, Luca Chierico, Oliver Bandman, Stephen A. Renshaw, Giuseppe Battaglia

ACS Nano, **2014**

## **4.1 Introduction**

The cellular interactions and subsequent internalisation of a synthetic particle can be studied, similar to natural particles, by two complementary approaches. It is crucial to identify the cellular structures implicated in internalisation and at the same time it is essential to understand whether and how the inherent properties of the particle influence its uptake. Although traditionally the cellular internalisation of a biological cargo has been preferentially investigated on the basis of the first approach mentioned, and allocated to well-defined uptake pathways, it is nowadays becoming widely accepted and increasingly important that the cargo features are crucial in determining how it will be ultimately internalised, and therefore the uptake mechanism should be specifically characterised for each cargo with its set of defined properties<sup>135,189</sup>. According to this, the physicochemical properties of PMPC-PDPA polymersomes in relation to their uptake in mammalian cells, have started to be investigated. As presented in the introduction chapter, it has been demonstrated that the efficiency of PMPC-PDPA polymersome internalisation (polymersomes/cell) is strongly influenced by nanoparticle size and nanoparticle surface topology. To extend further our understanding of the effect that the physical properties of PMPC-PDPA polymersomes have in their

internalisation in mammalian cells, specifically polymersome shape and polymersome size below 100 nm, I carried out the studies presented in the next section of this chapter.

According to the experimental knowledge gained in recent years in our laboratory FaDu cells, an epithelial adherent cell line established from the pharynx of a patient with squamous cell carcinoma<sup>190</sup>, present a faster uptake of PMPC-PDPA polymersomes compared with other cell types. Hence I have used FaDu cells as a model cell type for further studies and most of the experiments presented in this thesis were conducted on them. In addition, FaDus are clinically relevant in the context of oral cancer and their enhanced uptake of PMPC-PDPA polymersomes could open new avenues for the treatment of this type of tumours, which remains very challenging<sup>191</sup>, adding an extra motivation for the study of polymersome internalisation in this cancer cell line.

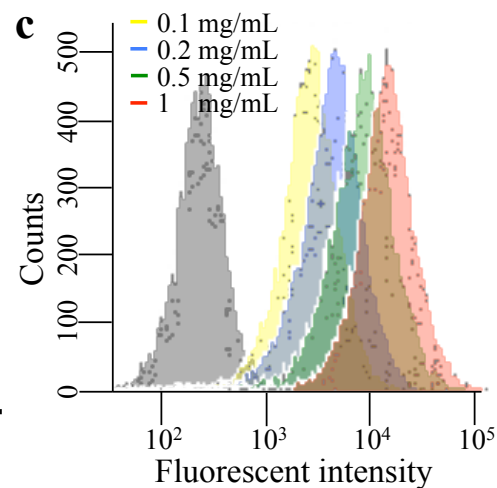
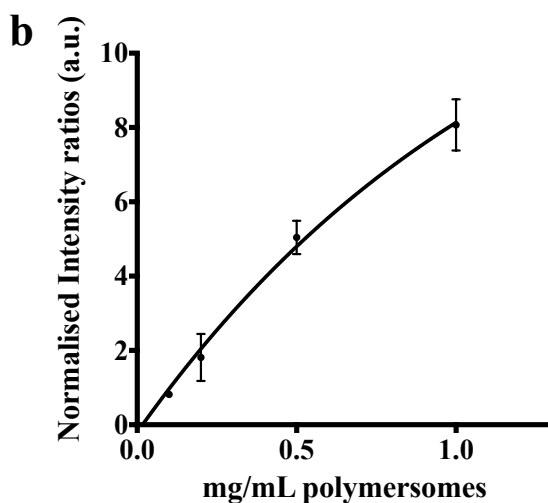
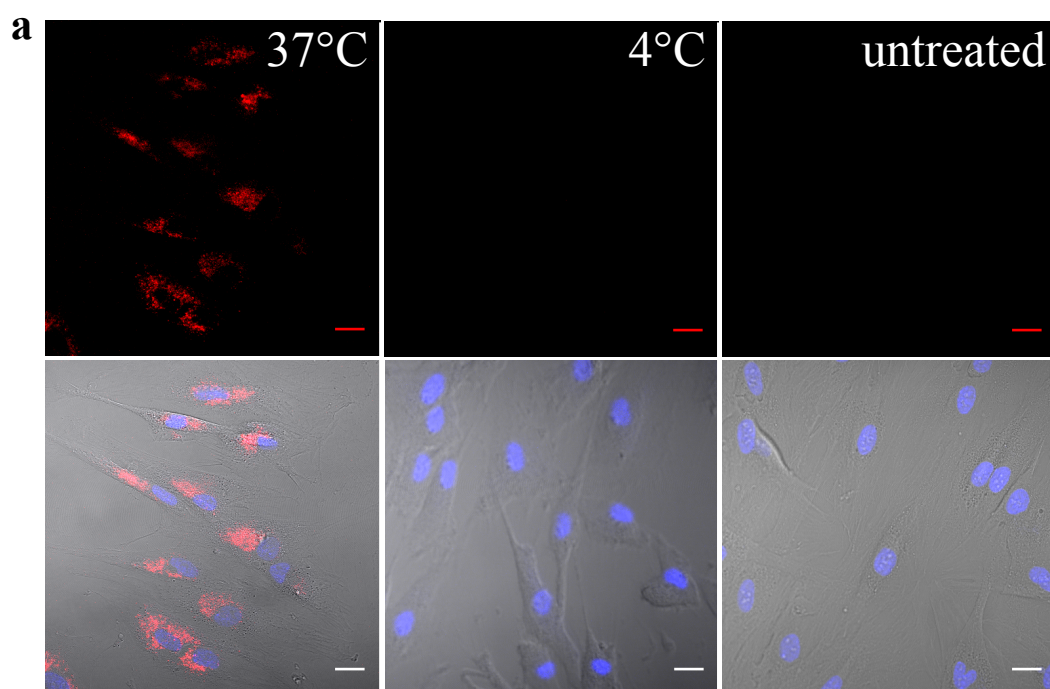
## **4.2 Results**

### **4.2.1 General characteristics of the uptake of spherical PMPC-PDPA polymersomes in mammalian cells**

To validate whether PMPC-PDPA polymersomes are internalised by an energy-dependent process I incubated primary human dermal fibroblasts (HDFs) with rhodamine-labelled polymersomes at either 37°C or 4°C for 20 minutes, and subsequently explored cellular uptake by confocal microscopy. As shown in figure 4.1.a, cells that were incubated with fluorescent-labelled polymersomes at 37°C have become fluorescent. On the other hand, in cells that were incubated with the nanoparticles at 4°C, temperature at which the energy-dependent process of the cell are paused as a consequence of the reduced metabolic activity, there was no evident polymersome uptake and cells looked very similar to control cells, that were not incubated with the nanoparticles. Next, I measured the cellular uptake following incubation with increasing concentrations of polymersome dispersion. Cells were incubated with fluorescent-labelled polymersomes, up to 1.5 hours, and cellular uptake was investigated by flow cytometry. As expected, cellular internalisation increases as cells are incubated with increasing nanoparticle concentrations (figures 4.1.b-c) and, as

figure 4.1.b shows, at 1 mg/ml of polymersomes/well we are close to reaching saturation of the cellular uptake.

Based on the experiments presented above together with the information derived from previous and current research in Prof. Battaglia group, it seems that the cellular uptake of PMPC-PDPA polymersomes in mammalian cells is a relatively fast process. In order to gain a qualitative insight into the internalisation kinetics of these nanoparticles I investigated the uptake of rhodamine-labelled polymersomes by confocal microscopy in FaDu cells. As figure 4.1.d shows, polymersomes were rapidly internalised. Cellular internalisation can start to be observed 5 minutes after incubation with fluorescent nanoparticles and it increases during the experimental time-course.



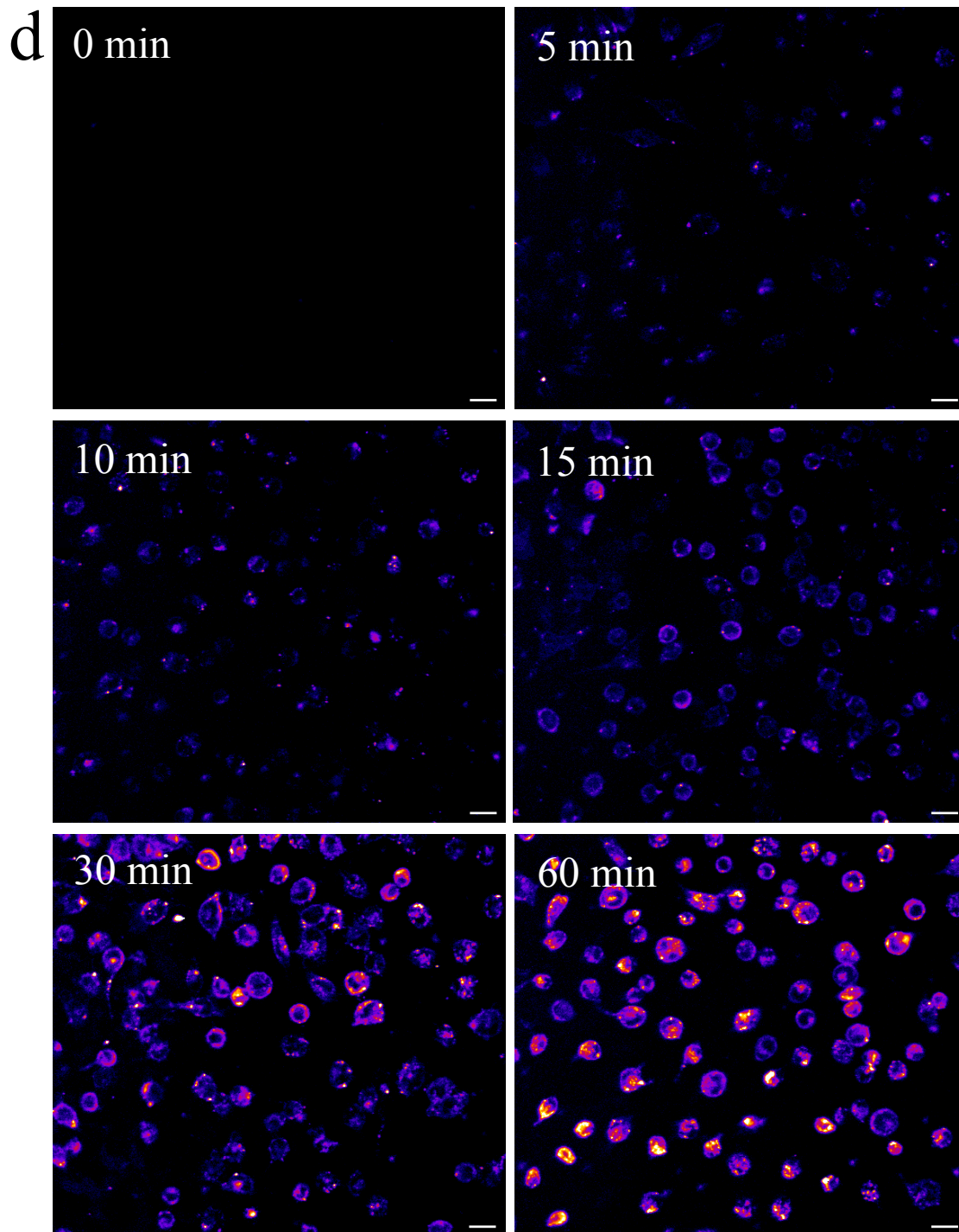


**Figure 4.1: Uptake of spherical polymersomes in mammalian cells**

**a)** Confocal micrographs of HDFs following 20 minutes incubation with 1 mg/ml of rhodamine-labelled polymersomes at either 37°C or 4°C. Untreated cells are included as control. Scale bars: 20µm. **b)** Titration of polymersomes uptake in FaDu cells. Cells were incubated with increasing concentrations of rhodamine-labelled polymersomes for 90 minutes. Chart shows median fluorescence intensity (MFI) values associated with the cells as measured by flow cytometry. n=3 experiments. Error bars: ± SD. **c)** Representative histograms obtained by flow cytometry showing fluorescent intensity associated with cells after incubation with increasing concentrations of fluorescent polymersomes for 90 minutes. Untreated cells are represented in grey. **d)** Confocal images of FaDu cells after incubation with 0.5 mg/ml of fluorescent-labelled polymersomes at the time points indicated. Micrographs display the FIRE LUT from ImageJ software. Scale bars: 25 µm.

## 4.2.2 Uptake kinetics of spherical PMPC-PDPA polymersomes with different diameters

Once I had acquired information about the general characteristics of the uptake of PMPC-PDPA polymersomes in mammalian cells, I decided to move on into the investigation of the impact that the physical characteristics of these nanoparticles have in their cellular internalisation, I did so by exploring the effect of nanoparticle size in the first instance.

Two main protocols are routinely conducted in the laboratory for the production of polymersomes, the *pH switch method* and the *film rehydration method*. On the former, we start from an acidic aqueous solution of copolymers chains and gradually raise the pH of the solution to physiological pH (7.4) by the dropwise addition of NaOH 1 M. We have usually observed in the laboratory that when polymersomes are produced in this way we end up with a dispersion of spherical nanoparticles with a heterogeneous size distribution (figures 4.2.b-c). We tried to purify this bulk dispersion to isolated aliquots of spherical nanoparticles, each of them containing particles within a different size range, for successive cellular internalisation studies.

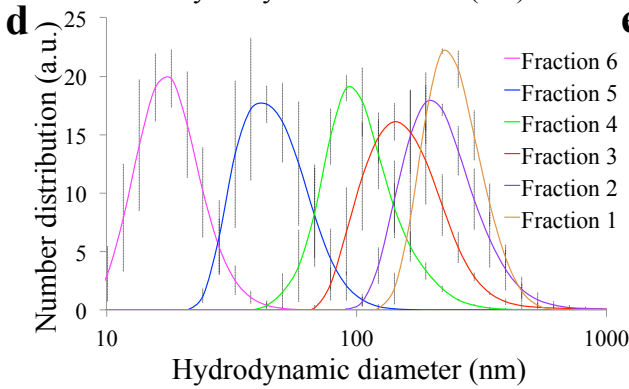
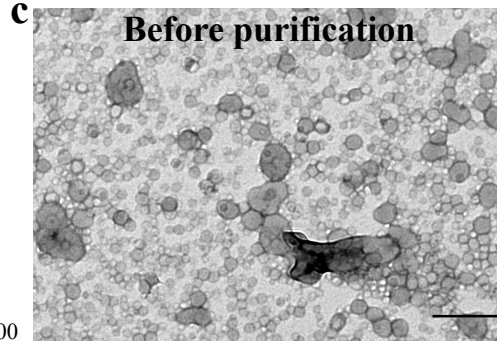
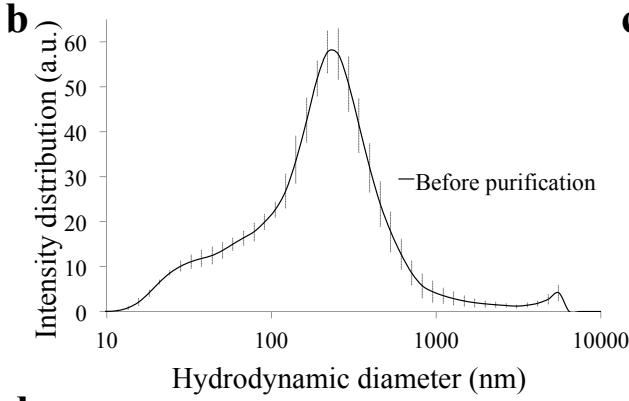
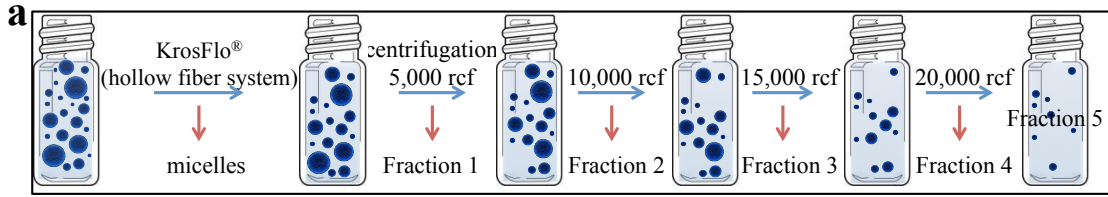
The purification process is represented in figure 4.2.a and consists of a combination of tangential flow filtration and successive cycles of centrifugation at increasing relative centrifugal force (RCF). First we removed the micelles, which constitute the fraction of smaller nanoparticles in suspension (fraction 6), by recirculating, for several hours, the bulk nanoparticle dispersion through a filtration module with a 50 nm pore threshold. The theoretical diameter of a micelle formed by PMPC<sub>25</sub>-PDPA<sub>70</sub> block copolymers is approximately 33.4 nm. This value is the sum of two fully stretched MPC chains (brush conformation), each of them with a length of 6.25 nm, and two coiled coil DPA chains that form the hydrophobic core of the micelle, each of them circa 10.44 nm long<sup>192,193</sup> (specific lengths of the polymer chains are Prof. Battaglia personal communications). Nanoparticles used for the experiments reported in this section were made using copolymers with slightly shorter DPA chains (PMPC<sub>25</sub>-PDPA<sub>65</sub>) hence, micelles formed by this polymer are expected to be less than 33.4 nm in diameter.

The main dispersion, virtually free of micelles, underwent successive 20 minutes cycles of centrifugation at increasing RCF. After each cycle the nanoparticle pellet was carefully resuspended in sterile PBS and stored at 4°C for internalisation studies while



the supernatant was put through the next cycle of centrifugation. At the end of the purification process we have separated the starting nanoparticle dispersion into 6 fractions, each of them enriched in nanoparticles of a certain size (figure 4.2.e). All fractions were characterised in terms of size and shape by dynamic light scattering (DLS) and transmission electron microscope <sup>105</sup> (figures 4.2.d, f). The combination of the hollow structure of the polymersomes and the drying process to which the polymersomes adsorbed onto the grids for TEM are exposed to, can lead to the collapse of the spherical architecture typical of hydrated polymersomes. This is more likely to happen with bigger polymersomes and can make them appear as non-spherical particles under the TEM microscope as shown for fraction 1 in figure 4.2.f.

Following characterisation of the fractions, I investigated the uptake kinetics of polymersomes of different sizes (fractions 1-5) and polymeric micelles (fraction 6) in FaDu cells at different time points up to 24 hours using flow cytometry. The fluorescence intensity associated with the cells after nanoparticle incubation was normalised by the mass of polymer per particle, like this the uptake represented will be proportional to the number of particles internalised rather than to the amount of polymer. Normalising in this way I take into account that not all the cells were incubated with the same number of particles (figure 4.3a) and the difference in polymer per particle between particles of different sizes. As shown in figure 4.3.b nanoparticles of different sizes were not internalised with the same efficacy. If we plot the area under the curve for the uptake profiles in figure 4.3.b against the average nanoparticle size of each fraction, it seems to be an optimal particle diameter for polymersome internalisation, in terms of the relative number of nanoparticles internalised in a period of time, around 60 nm (figure 4.3.c).



**e**

Fraction	Average size based on number distribution (nm)
1	240 ± 30
2	220 ± 52
3	170 ± 13
4	110 ± 11
5	50 ± 10
6	20 ± 4

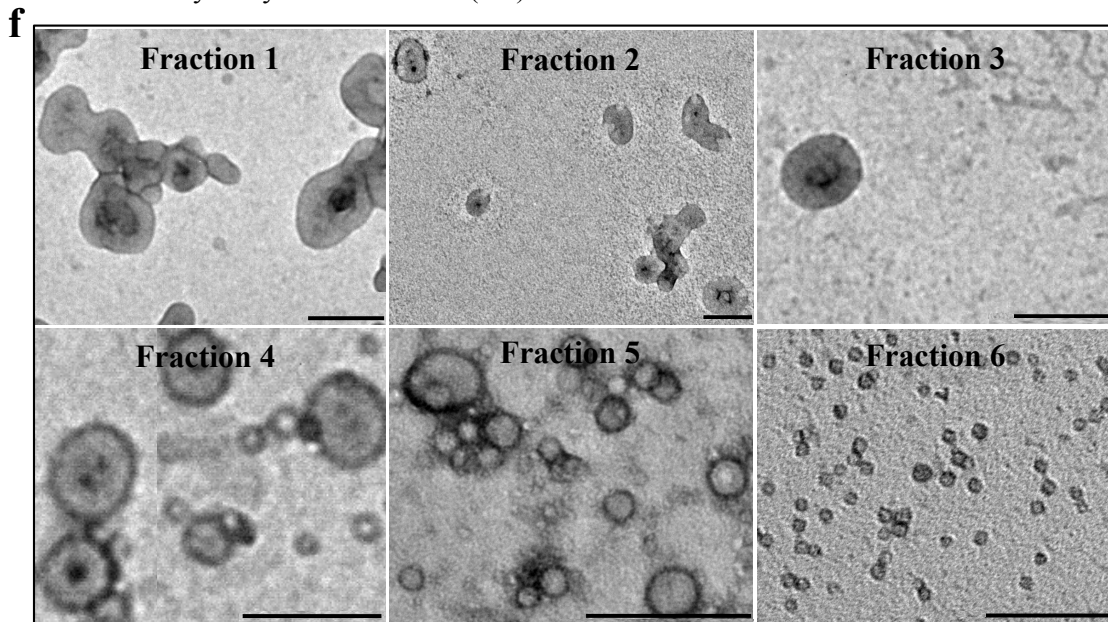


**Figure 4.2: Polymersome fractions of different sizes and micelles obtained after purification by centrifugation**

**a)** Schematic representation of the purification process. A hollow fiber system is used to remove the micelles from the bulk nanoparticle dispersion followed by cycles of centrifugation at increasing centrifugal force; after each cycle a sample (fraction #) enriched in polymersomes of a certain size is collected. **b)** Size distribution measured by DLS of the bulk nanoparticle dispersion before purification.  $n=3$  batches of nanoparticles. Errors bars:  $\pm$  sem. **c)** TEM micrograph of the nanoparticle dispersion before purification. Scale bar: 200 nm. **d)** DLS traces showing the size distribution of the different fractions obtained after purification.  $n=3$  different batches of nanoparticles. Errors bars:  $\pm$  sem. **e)** Average size of the fractions measured by DLS.  $n=3$  batches of nanoparticles. Errors bars:  $\pm$  sem. **f)** TEM micrographs of the different fractions obtained after purification. Scale bars: 200 nm

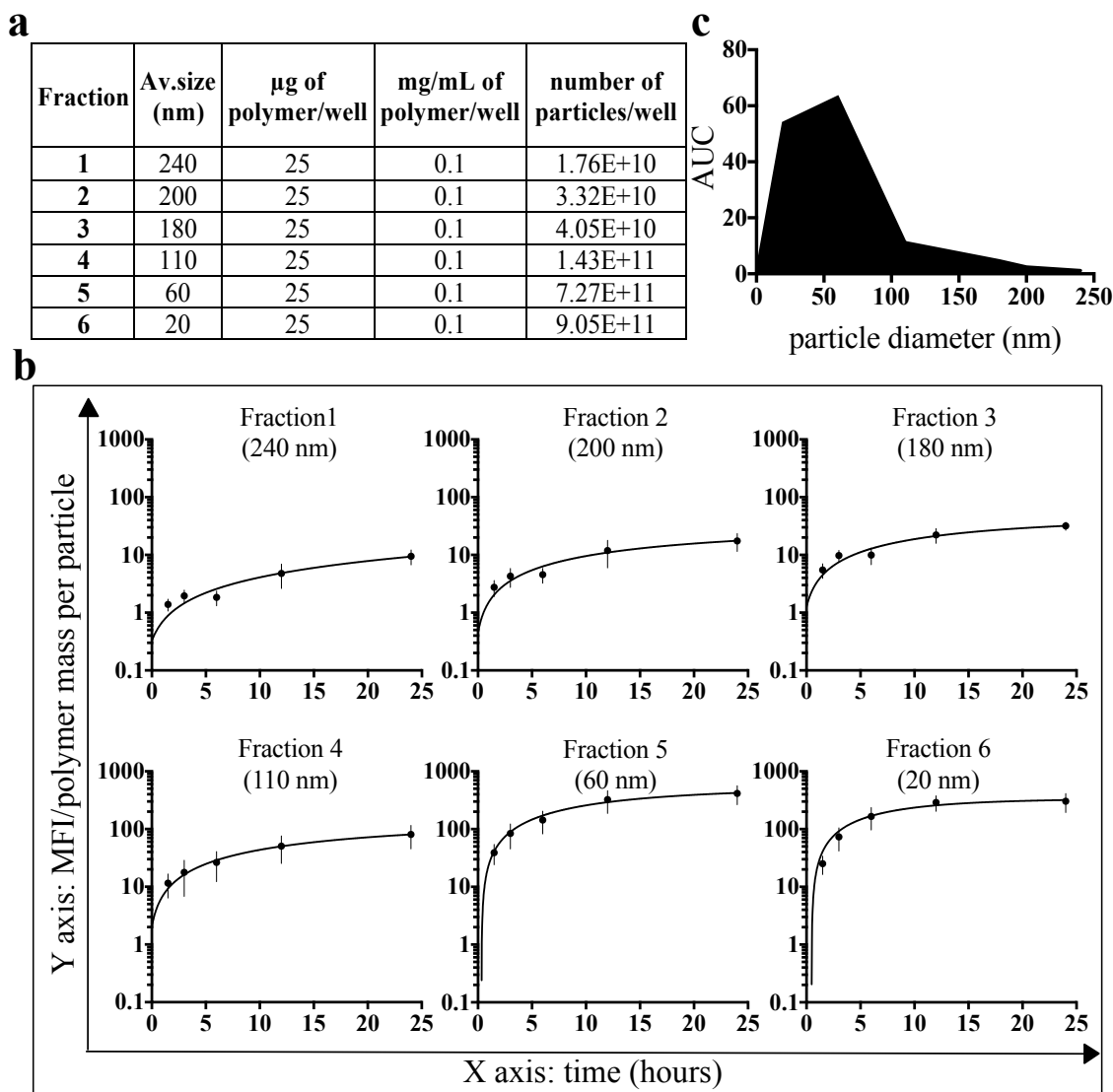


**Figure 4.3: Uptake of spherical PMPC-PDPA nanoparticles of different diameters in FaDu cells**

**a)** Table displaying the different nanoparticle fractions that the cells were incubated with and the average nanoparticle diameter for each fraction. Cellular treatment is presented as amount of polymer/well, concentration of polymer/well and number of particles/well. **b)** Uptake kinetics for nanoparticles of different diameters. MFI values measured by flow cytometry are normalised to the relative number of particles taken up for each fraction at different time points up to 24 hours. Points on the graphs were fitted to a one-phase decay non-linear regression curve using PRISM<sup>®</sup> software.  $n=3$  experiments. Errors bars:  $\pm$  sem. **c)** Cellular uptake as the relative number of nanoparticles of a specific diameter internalised after 24 hours. The chart displays the area under the curve for each plot in **b** against the average nanoparticle size of the fraction.

### 4.2.3 Uptake kinetics of tubular PMPC-PDPA polymersomes

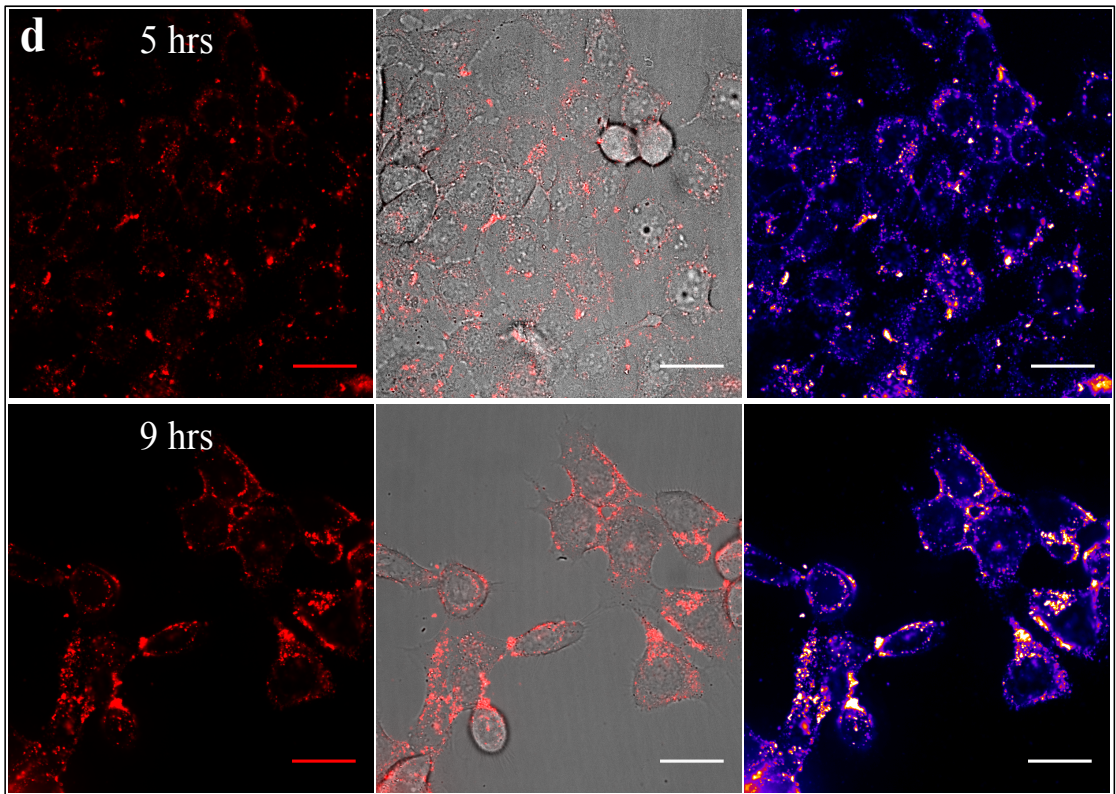
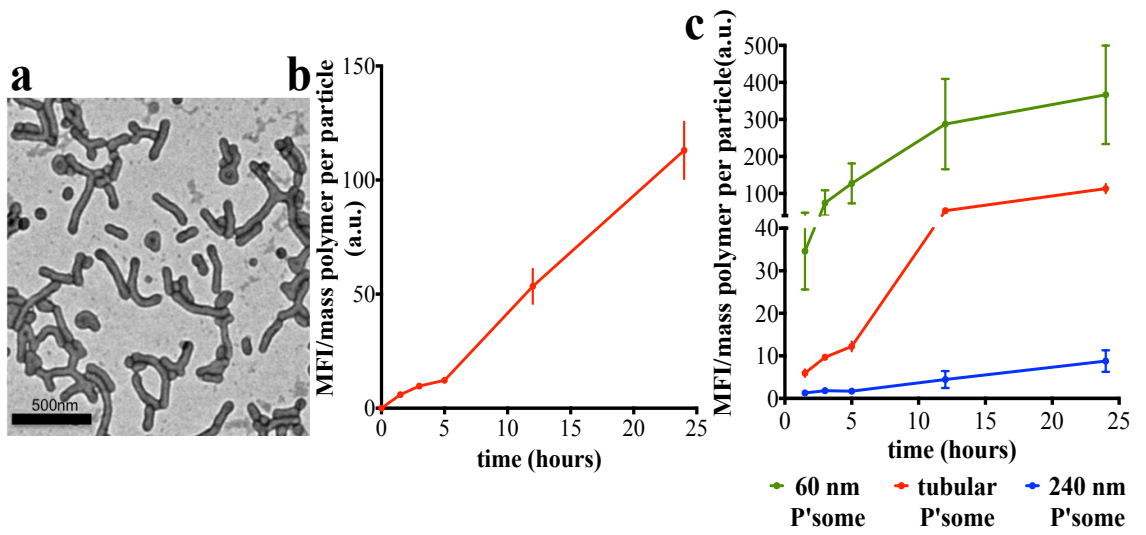
Polymersomes can be produced by the *film rehydration* method. Using this approach the copolymers are firstly dissolved in an organic solvent mixture in a glass vial and subsequently left under vacuum overnight to achieve solvent evaporation. The thin polymer film formed on the walls of the vial is then forced into solution by stirring it with PBS (pH 7.4) up to 4 weeks. Interestingly, polymersome dispersions obtained in this way mainly consist of tubular polymersomes. We have just started to understand how these tubular polymersomes are made, and the current knowledge of our group of the forces driving the formation of tubular structures from the polymer film is detailed in a recently published paper<sup>194</sup>. Briefly, it is a spinodal decomposition, where the thermal and mechanical fluctuations experienced by the polymeric film under stirring create pressure gradients across it, leading to film perforation and subsequent dewetting. The continuous hydration and swelling of the polymer, the balance between hydrophilic and hydrophobic forces and the shear stress, govern the successive transitions. The bicontinuous polymeric network comes into solution and forms a connected tubular network, from where branched tubular structures detach and finally break up into tubular polymersomes.

For the purpose of the present research the opportunity to work with tubular polymersomes gave me the possibility to investigate the effect of nanoparticle shape in the internalisation of PMPC-PDPA polymersomes. In order to do that the nanoparticle dispersion obtained was first centrifuged at 2,000 RCF for 20 minutes to remove nanotubes and any membranous assemblies close to, or above the  $\mu\text{m}$  range. The remaining supernatant was then centrifuged at 15,000 RCF for another 20 minutes. The resuspended pellet in PBS resulting from the last centrifugation was characterised by TEM. A representative micrograph is displayed in figure 4.4.a, showing that this fraction is almost exclusively composed by tubular polymersomes, which are characterised by an average diameter of 60 nm and an average length of 240 nm. While the diameter is kept almost constant among all the tubular nanoparticles examined, the nanoparticles present a broad length distribution. The cellular uptake of these fluorescent-tubular nanoparticles was investigated by flow cytometry in FaDu cells, the resulting uptake profile is shown in figure 4.4.b. A biphasic uptake kinetic can be observed where a moderate increase in fluorescence signal up to 5 hours was followed a by a great and rapid increase in fluorescent signal. This seems different from the kinetic

profile previously observed for spherical particles. On figure 4.4.c the uptake profile of the tubular polymersomes under study is compared with spherical polymersomes with diameters that mimic the average tube diameter, 60 nm, or the average tube length, 240 nm. Differences with the internalisation behaviour of the spherical counterparts are especially noticeable between tubular polymersomes and 60 nm spherical polymersomes where a rapid increase in fluorescence is followed by a single plateau.

We believe that the two phases detected by flow cytometry in the uptake of tubular polymersomes could correspond to a first step of binding of the tubes to the cell surface followed by a slow internalisation of the elongated nanoparticles. Binding and final internalisation would be spaced enough in time so as to be detected separately. In order to test this hypothesis I tried to visualise the two phases looking under the microscope at cells that were incubated with fluorescent tubular polymersomes for either 5 or 9 hours. Representative confocal micrographs from these experiments are shown in figure 4.4.d where it is observed that after 9 hours incubation with rhodamine-labelled tubular polymersomes there is evident fluorescence inside of the cells while after 5 hours incubation the fluorescent signal is mainly observed at the cell periphery. 3D reconstructions from single cells in figure 4.4.e show in more detail the state of tubular polymersome internalisation at both time points. At 9 hours there is abundant fluorescence coming from different focal planes of the cell, as particularly observed in the bottom montage displaying all the successive slices from the Z-stack. Although at 5 hours the fluorescent signal is, as expected, less intense and not so evident through the cell cytoplasm, some internalisation has already started to occur.

To investigate the potential of these tubular polymersomes as intracellular drug delivery systems, tubular nanoparticles encapsulating fluorescent BSA were prepared, and thoroughly purified by gel permeation chromatography to remove any non-encapsulated protein from the nanoparticle dispersion. This is important, since BSA alone can be used as an endocytic probe<sup>195</sup>. Cells were incubated with purified polymersomes encapsulating fluorescent-BSA for 9 hours before exploring protein intracellular delivery by confocal microscopy (figure 4.5.b).



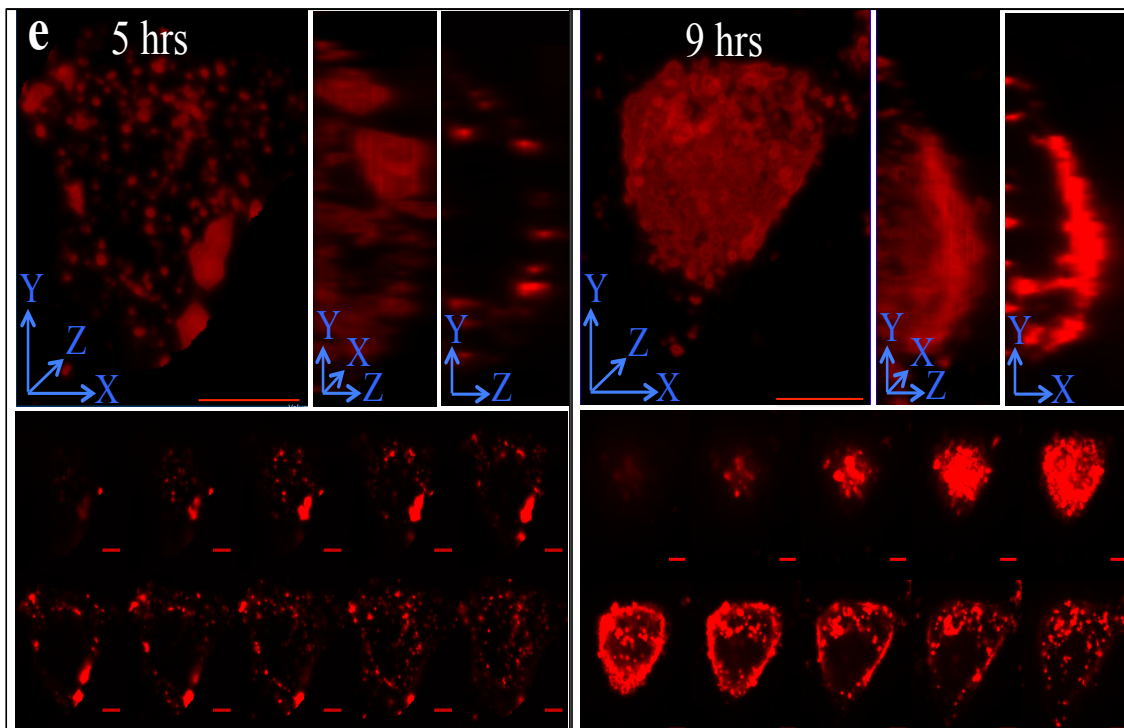


**Figure 4.4: Uptake of tubular PMPC-PDPA polymersomes in FaDu cells**

**a)** TEM micrograph of tubular polymersomes used for *in vitro* uptake. Reprinted with permission from Robertson et al., 2014. Copyright 2014 American Chemical Society. **b)** Uptake kinetics profile of tubular polymersomes (60 nm x 240 nm). **c)** Uptake kinetics profiles of tubular polymersomes (60 nm x 240 nm), 60 nm spherical polymersomes and 240 nm spherical polymersomes. b-c Cellular uptake was analysed by flow cytometry and normalised to number of particles internalised. **d)** Cellular uptake of rhodamine-labelled tubular polymersomes after 5 or 9 hours of incubation. Pictures represent a single Z slice around the nuclear region of the cells. From left to right: Rhodamine channel, merge rhodamine and DIC channels, rhodamine channel with FIRE LUT from ImageJ software. Scale bar: 30 $\mu$ m. **e)** 3D study of confocal Z stacks of single cells after 5 and 9 hours of incubation with tubular polymersomes. Left panels represent top projection of the cell (scale bar: 10  $\mu$ m) while middle panels show the cell from the side. Right images are from a single Z slice through the nucleus of the cell. Bottom panels are a montage showing the different Z slices through the cell. Scale bars: 5 $\mu$ m.







## 4.3 Discussion

The investigation conducted in this chapter aimed to outline the main characteristics of the uptake of PMPC-PDPA polymersomes in mammalian cells and to improve our knowledge in the impact that the physical properties of these nanoparticles have in their cellular uptake.

I have corroborated that the internalisation of polymersomes is a temperature-dependent process<sup>166</sup> (figure 4.1.a) with a fast onset (< 5 min), at least in the cancer cell line FaDu (figure 4.1.d), which is in agreement with previously published results showing enhanced uptake of this formulation in cancer cells in comparison with healthy cells<sup>176</sup>. This information together with the fact that we have observed internalisation of this polymersome formulation in any cell type tested on the laboratory (more than 23 different cell types) except red blood cells<sup>166</sup>, which are known for not undergoing endocytosis<sup>179,180</sup>, proves to a large extent that PMPC-PDPA polymersomes are internalised by an endocytic process in mammalian cells. It is important to consider that a diffusion or a fusion of these polymersomes with the plasma membrane would be quite unlikely taking into account their supramolecular structure and the high molecular weight of the polymers forming their entangled membranes<sup>196</sup>. As an example, a 200 nm PMPC-PDPA polymersome would be disassembled into  $1.7 \times 10^3$  copolymer chains, being the molecular weight of a standard PMPC<sub>25</sub>-PDPA<sub>70</sub> block copolymer chain equal to 22,3 kDa. Glucose, one of the biggest molecules able to diffuse through the membrane is 180 Da. In addition, particles made up of high molecular weight polymers are related to slow chain exchange and therefore high colloidal stability.

Taking maximum advantage of the knowledge acquired over the years working with polymersomes for biological applications and the tools at our disposal, I have studied the effect of polymersome size and shape in the nanoparticle internalisation. Nevertheless, to control polymersome production and to optimise nanoparticle purification in order to obtain polymersomes of a defined shape and a narrow size distribution is not a straightforward task. We have recently demonstrated how the physical characteristics of the polymersomes produced are affected by a complex combination of different parameters including the copolymers used and the degree of

polymerization of the polymers in their composition, the temperature, the pH and the ionic strength of the solution<sup>182</sup>; thus we are constantly monitoring and investigating polymersome production and purification in the laboratory in order to improve our control over these processes. Progress made in this sense during the course of the present research gave me the possibility to investigate the effect of polymersome size on nanoparticle internalisation at smaller nanoparticle sizes than it was done before and moreover, to study for the first time the effect of nanoparticle shape in PMPC-PDPA polymersomes uptake. We noticed that by using relatively mild cycles of centrifugation (from 5,000 RCF to 20,000 RCF, 20 minutes cycles) in a centrifuge with a fixed angle rotor we were able to separate fractions of nanoparticle dispersion enriched in different sizes, from  $240 \pm 30$  nm polymersomes to  $20 \pm 4$  nm polymeric micelles (figure 4.2.e-f). Although we realise that the centrifugal forces used are one order of magnitude smaller than the average RCFs in differential force ultracentrifugation, the technique of choice in the biology laboratory for the routine fractionation of subcellular structures in the same range of sizes as our polymersomes, our methodology allowed us to achieve some degree of purification (figure 4.3.b vs. figure 4.3.d). Interestingly, Liang *et al.*, pelleted 140 nm poly( $\gamma$ -glutamic acid)-poly(lactide) ( $\gamma$ PGA-PLA) nanoparticles after 20 minutes centrifugation at 20,000 RCF<sup>197</sup> while Kakizawa *et al.*, pulled down hybrid organic-inorganic nanoparticles, made up by poly(ethylene glycol)-block-poly(aspartic acid) (PEG-PAA) and calcium phosphate and diameters between 100-300 nm, by centrifugation at 15,000 rcf for 30 minutes<sup>198</sup>. These are just two examples of how by using sub-ultracentrifugation RCFs over relatively short period of time some groups have been able to spin down polymeric nanoparticles with sizes between 100 - 400 nm<sup>199-202</sup>. These experimental observations seem to indicate that polymeric nanoparticles could be pelleted by milder centrifugation cycles than usually expected and they might be the starting point for a systematic study in the use of simple centrifugation for the purification of polymeric soft nanoparticles.

Uptake experiments conducted with the aforementioned nanoparticle fractions led to the identification of the optimal diameter for the cellular internalisation of spherical PMPC-PDPA polymersomes, around 60 nm. Polymersomes of this size were more efficiently internalised, in terms of the relative number of nanoparticles taken up, than bigger ones (figure 4.3.c). This value is slightly bigger than the one predicted by our theoretical model for the cellular uptake of nanoparticles (approx. 44 nm)<sup>203</sup>. However, from that

work it was derived that the optimal nanoparticle size for endocytosis strongly depends on the number of receptors available at the cell surface. The total number of receptors expressed by a cell can vary between different cell types, and therefore the optimal polymersome size, experimentally obtained for PMPC-PDPA polymersome internalisation in FaDu cells could be slightly different from the one calculated using a standard approximation to that biological parameter.

Finally, it is important to have in mind that for nanoparticles intended as intracellular delivery systems it is necessary to balance the optimal particle size for uptake with the optimal particle size for efficient encapsulation of the cargo. In this sense although we have observed that micelles present a favourable uptake kinetic, just below the optimal polymersome fraction (figure 4.3.d), they are not as versatile as polymersomes for the encapsulation and intracellular delivery of diverse compounds.

It is now widely accepted that one of the features of nanoparticles that has a great influence over nanosystem-cellular interactions, apart from the size, is the particle shape. Studies looking at the biological performance of tubular soft polymeric nanoparticles have been mainly conducted in cylindrical micelles (also known as rod-like, worm-like or filomicelles) and they have demonstrated that these nanoparticles present a different *in vivo* behavior compared with their spherical counterparts. Filomicelles remained in blood circulation up to 10 times longer than spherical micelles<sup>144</sup>, tended to accumulate less in healthy tissues than spherical ones<sup>204</sup> and showed an enhanced drug-loading capacity<sup>205</sup>. According to this, elongated polymeric nanoparticles could offer different and interesting opportunities in comparison with their spherical counterparts to modulate the delivery of a cargo *in vivo*. To the best of our knowledge, there are no publications that specifically address the effects of tubular shape on the cellular internalisation of polymersomes. Nevertheless the production of stable tubular polymersomes in aqueous solutions with one of their dimensions in the nm range has been reported<sup>206-208</sup>. We have lately advanced in the knowledge of how to produce tubular PMPC-PDPA polymersomes with all their dimensions in the nanometer range<sup>194</sup> (figure 4.4.a), opportunity that I have used to investigate the uptake of these nanoparticles in mammalian cells. I have observed that tubular polymersomes present an uptake profile with two phases where an initial slow onset is followed by a great increase, in terms of the relative number of tubes internalised, approximately 5 hours after incubation with the nanoparticles (figure 4.4.b). This uptake kinetic is different

from the one observed for spherical polymersomes of the same diameter as the tubes, which present a continuous polymersome endocytosis with a fast onset and a single plateau (figure 4.4.c). On the other hand, tubes appear to be internalised better than spherical polymersomes with a diameter that mimics the average tube length, 240 nm (figure 4.4.c). This situation could arise from the fact that the tubes investigated are characterised by a diameter of 60 nm, which according to our results is optimal for inducing the endocytosis of PMPC-PDPA polymersomes (figure 4.3.c). The curvature of the system is therefore ideal for stimulating deformation of the plasma membrane around the diameter of the tube; in contrast the length of the tube is not facilitating the internalisation of the tubular nanoparticle. Consequently the balance between the tube diameter and the tube length could be shaping the kinetic curve observed for tubular PMPC-PDPA polymersomes. Following cellular treatment, polymeric tubes would bind to the cell surface promoting a deformation of the plasma membrane around the diameter of the tube that subsequently would progress to wrap all the soft nanotube, a process that is likely to take more time than for a 60 nm spherical polymersome and that could be reflected in the initial slow onset for the internalisation of tubes observed by flow cytometry and confocal microscopy (figures 4.3.b,d).

Finally, I have demonstrated that PMPC-PDPA tubular polymersomes are able, likewise spherical polymersomes (figure 4.5.a), to act as intracellular delivery vectors. Tubular polymersomes were able to deliver fluorescent BSA, previously encapsulated in them by electroporation, into cells (figure 4.5.b). Although the defined domains of high fluorescent intensity at the cell contours observed in figure 4.5.b could indicate frustrated tube endocytosis or unsuccessful cargo release, the diffuse fluorescence through the cell cytosol is an indication that some fluorescent protein was delivered inside the cells, and although early results, they are promising and reveal the potential of these tubular nanoparticles as intracellular delivery vectors.

The information gathered in this chapter corroborates the strong influence that polymersome physical properties have in PMPC-PDPA polymersome internalisation in mammalian cells, and reveals the possibility to gain a new level of control over the temporal delivery of a encapsulated cargo through the fine tune of nanoparticle size and shape since it has been observed that tubular polymersomes present a slower cellular uptake than their spherical counterparts and they seem to be able to act as intracellular delivery vectors.

# Chapter 5: Receptor-mediated endocytosis of PMPC-PDPA polymersomes by scavenger receptors and tetraspanins

Part of this chapter has been published as:

Polymersome-mediated delivery of combination anti-cancer therapy to head and neck cancer cells: 2D and 3D *in vitro* evaluation.

Helen E. Colley\*, Vanessa Hearnden\*, **Milagros Avila-Olias\***, Denis Cecchin, Irene Canton, Jeppe Madsen, Sheila MacNeil, Nicholas Warren, Ke Hu, Jane A. McKeating, Steven P. Armes, Craig Murdoch, Martin H. Thornhill, and Giuseppe Battaglia

Molecular Pharmaceutics **2014** 11 (4), 1176-1188

\* Authors contributed equally to this study

## 5.1 Introduction

PMPC-PDPA polymersomes have the ability to enter many different cell types including primary cells, STEM cells and cancer cell lines<sup>166</sup>. The enhanced uptake observed for this formulation is surprising given the properties of the polymer forming the external brush of the nanoparticles. The PMPC (poly(2-methacryloyloxyethyl phosphorylcholine)) is a biocompatible and fouling-resistant polymer. Due to this ability to avoid non-specific adsorption of proteins it is currently used for the coating of several medical devices/implants<sup>209,210</sup>. At the nanometer scale, polymeric nanoparticles with anti-fouling properties are often associated with increased blood circulation times<sup>211</sup>, this being the reason for the usual coating of nanoparticles with polyethylene glycol (PEG), the most well known biocompatible and fouling-resistant polymer at the present. As a trade-off, nanosystems with such properties frequently have reduced cellular uptake. Therefore, PEGylated nanoparticles tend to be decorated with ligands on their surface for the targeting of specific cellular receptors. The attachment of ligands enhances nanoparticle cellular-recognition and promotes the endocytosis of the particle<sup>212</sup>. Nevertheless we have observed a high cellular uptake for PMPC-PDPA

polymersomes, and when PEG-PDPA polymersomes were compared with PMPC-PDPA polymersomes, the cellular uptake for the PMPC formulation was more than 10 times higher<sup>166</sup>.

The fact that PMPC based polymersomes are easily taken up by different cell types could indicate a specific interaction with the cell through the targeting of specific membrane receptors. A literature search looking for potential receptors for PMPC based polymersomes was conducted and scavenger receptors (SCRs) emerged as the strongest candidates. SCRs are a large family of structurally unrelated transmembrane glycoproteins originally identified by Brown and Goldstein in 1979<sup>213,214</sup>. Eight classes have been defined so far, among them, SCRs classes A and B are the best characterised and different subtypes have been discovered within these two classes. While SCRs type B are almost ubiquitously found in mammalian cells<sup>215</sup>, with the exception of CD163 which is only expressed by macrophages and monocytes, expression of SCRs type A is more restricted to myeloid cells and specific endothelial and epithelial cells<sup>216,217</sup>. These receptors recognise with high specificity many different types of ligands such as polyanionic ligands (i.e. polynucleotides and anionic phospholipids), viruses, bacteria, and endogenous nanoscopic particles (chylomicrons, HDL, oxidised LDL and acetylated LDL)<sup>216,218</sup>. Moreover, they have been implicated in the cellular uptake of some synthetic nanoparticles<sup>219-223</sup>. Interestingly, viruses and endogenous particles recognised by these receptors share with PMPC-PDPA polymersomes crucial physical characteristics for cellular uptake such as shape and a nanometer size. Additionally, the PMPC external brush of our polymersomes is enriched in phosphocholine groups, a specific recognition motif in ligands targeting some SCRs class B<sup>224</sup>.

With the aim to investigate whether PMPC-PDPA polymersome internalisation is a receptor-mediated endocytic process in mammalian cells, facilitated at least to some extent by scavenger receptors, I conducted the experiments detailed below.



## 5.2 Results

### 5.2.1 Effect of ligands for scavenger receptors A and B in PMPC-PDPA polymersome uptake

To test our hypothesis that SCrs might mediate polymersome uptake, I pre-incubated different cells types including primary HDFs, epithelial cancer cell-lines such as FaDus, HeLas and Huh7, and immune cells like LADMACs and macrophages (I-11.15 macrophages) with Fucoidan and Polyinosinic acid, known ligands for SCrs. Polyinosinic acid is a single stranded polynucleotide of inosine that specifically targets SCrs type A<sup>225</sup>. Fucoidan is an anionic polysaccharide that binds to SCrs type A and SCrs type B<sup>226,227</sup>. It is important to specify that Fucoidan was considered a specific ligand for SCrs type A. Although some papers can be still found in which it is referred to as a specific ligand for SCrs type A, it has been demonstrated that Fucoidan binds also to SCrs type B and therefore it can be defined as a ligand for both scavenger receptors classes<sup>226,227</sup>. Following pre-incubation with SCrs ligands, cells were incubated with fluorescent-labelled polymersomes without removing the ligands from the media. Results are presented in figure 5.1. It can be observed how polymersome uptake was almost completely inhibited in the presence of Fucoidan, with fluorescence levels similar to cells that were not incubated with polymersomes. There was no statically significant difference between untreated cells and cells incubated with Fucoidan plus polymersomes for all the cell types with the exception of FaDus. Nonetheless, an inhibition around 80% in polymersome uptake was still observed on FaDu cells. On the other hand, pre-incubation with Polyinosinic acid did not produce a statistically significant inhibition in the cellular uptake of polymersomes except in the case of HeLas, where polymersome uptake was reduced by 40%.

The results obtained are a proof-of-concept that SCrs are indeed implicated in PMPC-PDPA polymersomes internalisation in mammalian cells, in addition, they point to SCrs type B as the ones associated with their cellular uptake.

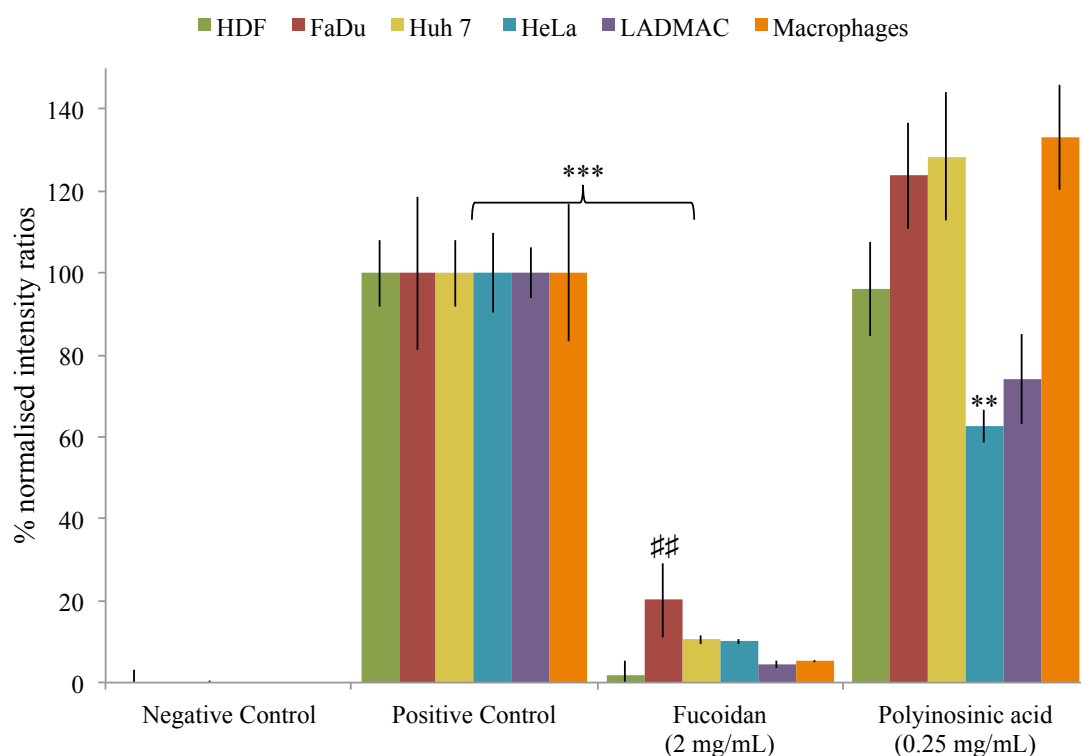


**Figure 5.1: Effect of Fucoïdan and Polyinosinic acid on polymersome uptake in different cell types**

Normalised MFI values obtained by flow cytometry for cells pre-incubated with either Fucoïdan or Polyinosinic acid for 1 hour followed by incubation with 1 mg/ml of fluorescent polymersomes for another hour. Negative control: cells incubated neither with scavenger receptors ligands nor with polymersomes. Positive control: cells not pre-incubated with F or PI. n=3 experiments. Error bars:  $\pm$  sem. Statistical analysis: one-way ANOVA plus Bonferroni post-test. # Represent statistically significant difference compared with the negative control. \* Represent statistically significant difference compared with the positive control,  $p < 0.01$  (\*\* or ##),  $p < 0.001$  (\*\*\*)

### 5.2.2 Scavenger receptors type B: Role of SR-BI, SR-BII and CD36 in PMPC-PDPA polymersomes uptake

Four subtypes of scavenger receptors B expressed at the cell surface have been identified and characterised: CD36, SR-BI (also referred as CLA-1) and its isoform SR-BII, and CD163 (5 isoforms). The narrow distribution of CD163, only expressed by monocytes and macrophages drew my attention towards the other two subtypes. CD36 and SR-BI comprise a glycosylated extracellular domain, two transmembrane regions, and cytoplasmic amino- and carboxyl-terminus. SR-BI and SR-BII are splice variants of the same gene with the same extracellular loop and different C-terminus<sup>228</sup>. SCrs type B are widely expressed across different cell types comprising phagocytic immune cells such as macrophages, neutrophils, and monocytes, adipocytes, and diverse endothelial and epithelial cells including hepatocytes. FaDus and HDFs are positive for the expression of SCrs B<sup>229</sup> (EMBL-EBI database). These receptors were first intensively studied in the uptake of modified lipoproteins, specially oxidised and acetylated LDL<sup>230</sup>. Since then, they have also been implicated in the removal of apoptotic cells and in the immune response by mediating the uptake of *Plasmodium falciparum* infected cells (CD36) and the cellular entry of different viruses and bacteria<sup>218,231</sup>. SR-BI and SR-BII are particularly recognised as the cellular receptors of HDL, being able to either mediate the internalisation of the particle, or the exchange of cholesterol between the HDL particle and the cell via their lipid exchange activity<sup>232-234</sup>. From a functional point of view, it appears that SR-BI and SR-BII accomplish the same functions although often they do it with different efficiency<sup>228</sup>. The experimental design for most of the experiments detailed in this section is based on the targeting of the extracellular loop of the SR-B receptors. According to the information just presented both SR-BI and SR-BII will be targeted by this means and consequently from now on I will refer to both of them as SR-Bs.

To differentiate which subtype of SCr type B is responsible for the binding of PMPC-PDPA polymersomes I tried to specifically block either the CD36 or the SR-Bs receptors and subsequently analyse polymersome internalisation under these conditions. The first study involved the use of the ketoamide ITX5061, a specific SR-Bs antagonist able to inhibit SR-Bs dependent uptake of HDL cholesterol esters and HCV infection<sup>235,236</sup>.

HDFs were pre-incubated with different ITX5061 concentrations (1  $\mu$ M, 10  $\mu$ M, 20  $\mu$ M) for one hour prior to incubation with rhodamine-labelled polymersomes for another hour in the presence of the antagonist. Flow cytometry results are shown in figure 5.2.a. Pre-incubation with ITX5061 produced a significant inhibition, close to 50%, in PMPC-PDPA polymersome internalisation. There was no noticeable difference in the inhibition achieved by increasing concentrations of the antagonist suggesting that only 1  $\mu$ M of the antagonist was enough to saturate SR-Bs receptors in HDFs.

A specific antibody against the extracellular loop of CD36 was used to investigate polymersome internalisation under conditions where this receptor was blocked. Fadu cells were pre-incubated with the anti-CD36 antibody prior to the addition of fluorescent polymersomes to the cells. Cells were then incubated in the presence of both the antibody and polymersomes for a further hour and nanoparticle uptake was investigated by flow cytometry. As it can be observed in figure 5.2.d there was almost no difference in polymersome internalisation between cells incubated in the presence or absence of anti-CD36. On the other hand, when an anti-SR-Bs antibody was used, a significant inhibition in polymersome internalisation, around 50%, was achieved. As observed in figure 5.2.e, this inhibition was further increased to 90% when the concentration of specific IgG was increased. It is important to point out that although a non-targeting IgG control produced an inhibition close to 50% this could be, at least to some extent, an artefact originating from the experimental procedure. The anti-SR-Bs antibody used on these studies is an antiserum preparation while the control IgG used is a pure IgG fraction with no other protein present in the commercial preparation, according to the information supplied by the manufacturer. Hence, for the same amount of IgG added to the cells the concentration of specific anti-SR-Bs IgG that the cells were incubated with is likely to be a low value, furthermore, this targeting IgG is surrounded by a heterogeneous protein mixture as it is characteristic for an antiserum preparation. On the other hand, in the case of the IgG control, cells were incubated with a high concentration of pure IgG that under those conditions could be easily sticking to the cell surface and strongly contributing to the inhibition observed. In any case, at equal IgG concentrations, the inhibition in polymersome internalisation observed under specific blocking of SR-Bs was significantly stronger than the inhibition detected when the non-specific IgG was used (figure 5.2.e).

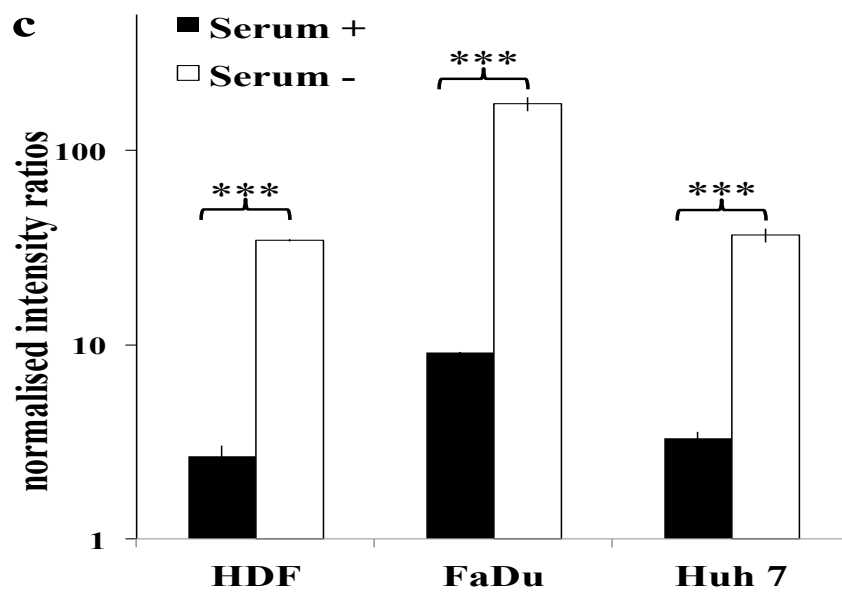
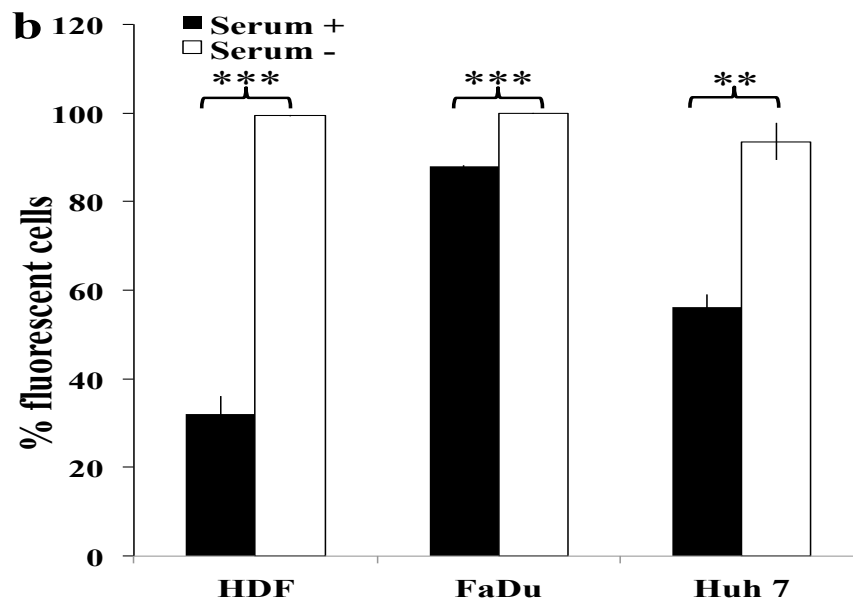
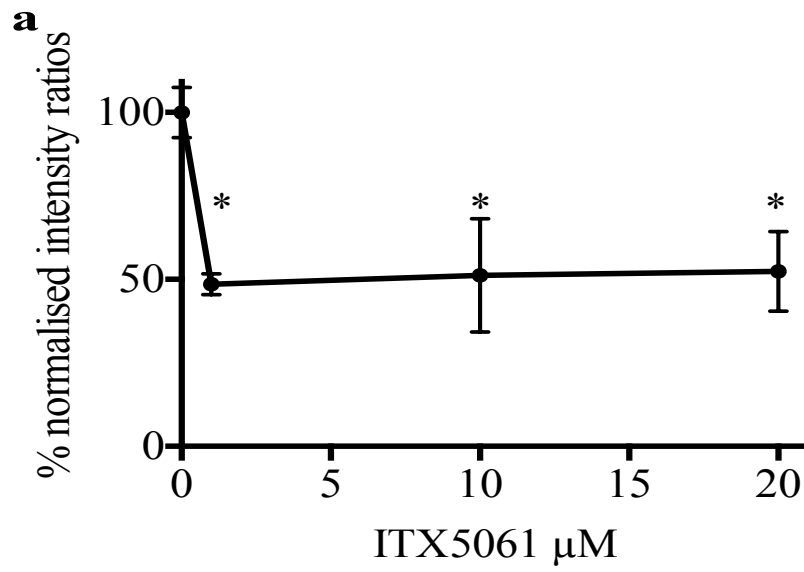
Even though blocking of CD36 did not produce an inhibition in polymersome uptake (figure 5.2.d), simultaneous blocking of CD36 and SR-Bs, using specific antibodies against each of them, resulted in significantly stronger inhibition than the one produced when only SR-Bs were neutralised. As it can be observed in figure 5.2.f, for the same concentration of specific IgG/well, inhibition of polymersome internalisation is close to 50% when only SR-Bs was blocked compared to more than 80% inhibition when the binding to both receptors was hindered. This result suggests that a role for CD36 in the uptake of PMPC-PDPA polymersomes should not be totally discarded at this stage.

The strong inhibition in PMPC-PDPA polymersome uptake observed under SR-Bs neutralising conditions either by the presence of a receptor antagonist or by a specific antibody led me to investigate the uptake of nanoparticles in SR-Bs knockdown cells. Knockdown of the scavenger receptors type B SR-Bs in FaDu cells was performed by electroporation using the NEON™ transfection system (Invitrogen). Effective knockdown of SR-Bs was accomplished after a process of optimization where different siRNA concentrations from 40 nM up to 160 nM were tested. Knockdown was investigated after 24, 36 and 48 hours post-transfection. Although knockdown levels were encouraging, there were still residual SR-Bs 24 hours after transfection (data not shown). By contrast, after 36 hours transfection with either 130 or 160 nM of siRNA, SR-Bs levels were almost zero as investigated by western blotting (figure 5.3.a); at 48 hours post-transfection proteins levels started to be recovered (figure 5.3.b). Therefore, transfection with 130 nM of siRNA during 36 hours was chosen as the ideal experimental set-up to study polymersome uptake in the absence of scavenger receptor SR-Bs.

Uptake of PMPC-PDPA polymersome in SR-Bs knockdown cells is shown in figure 5.3.c. Surprisingly, there was no significant inhibition of polymersome uptake when SR-Bs was knocked down, which contrasts with the results obtained when SR-Bs were present but blocked with an antibody. Nevertheless, although the inhibition was not significant, it was observed a tendency towards a reduced uptake (> 20%) in cells where the knockdown effectiveness was close to 100% (almost no detectable protein expression by western blotting, experiments 2 and 3) (figure 5.3.d-e).

The information derived from the inhibitory experiments performed, the blocking studies and the SR-Bs knockdown, points out a role for SR-Bs in PMPC-PDPA

polymersome uptake and at the same time it also highlights that it could be another receptor rather than SR-Bs and CD36 mediating polymersome internalisation in mammalian cells.



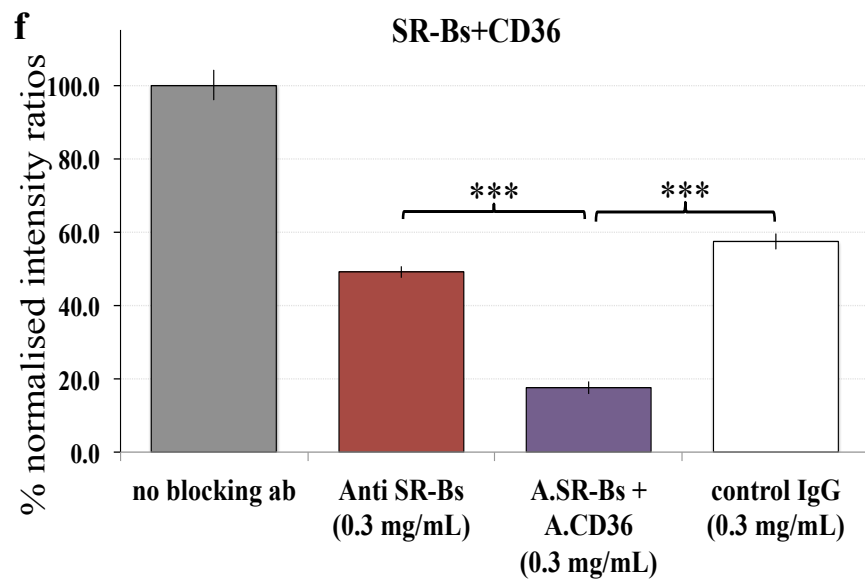
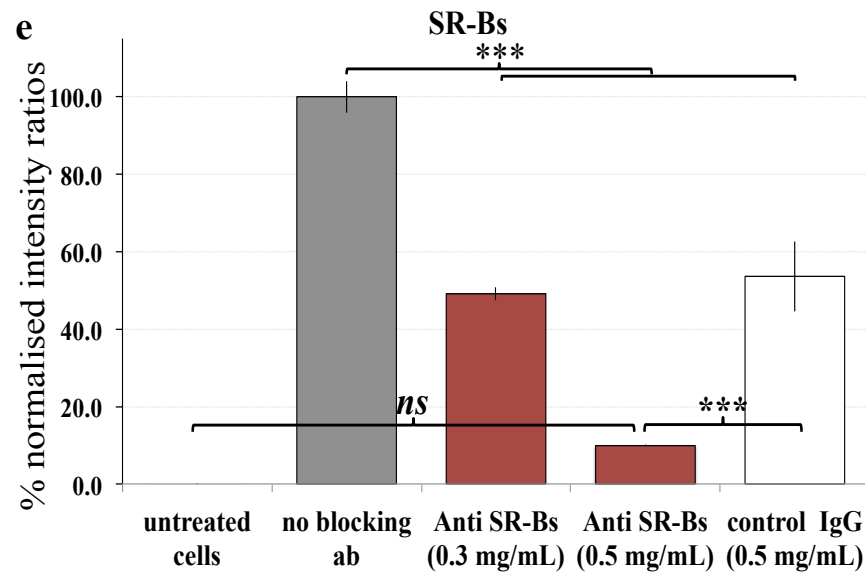
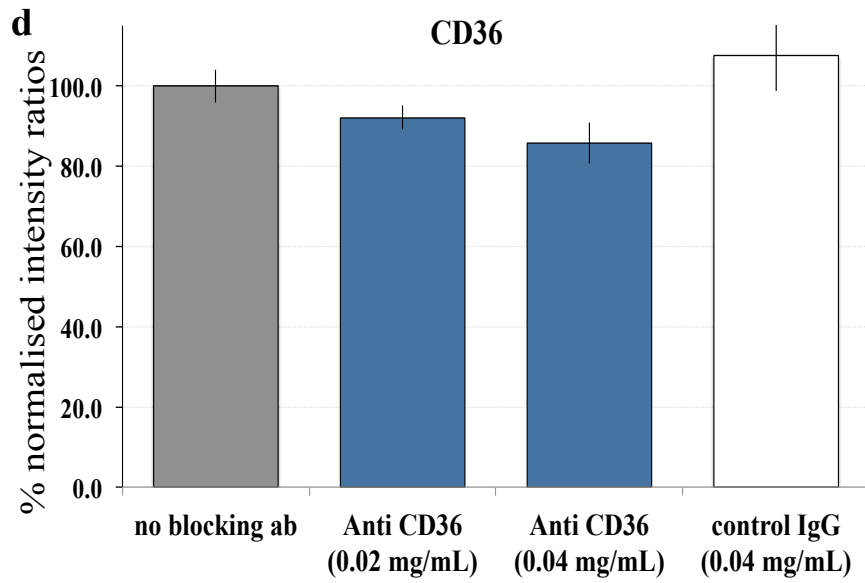




**Figure 5.2: Scavenger receptors type B: SR-BI, SR-BII and CD36 in polymersome uptake**

**a)** Inhibition of polymersome internalisation in the presence of the SR-Bs antagonist ITX5061 in HDFs. **b)** % Fluorescent cells after incubation with fluorescent polymersomes in the presence or absence of serum. **c)** Normalised MFI values associated with cells after incubation with fluorescent polymersomes in the presence or absence of serum. **d)** Uptake of polymersomes in cells pre-incubated with an antibody against SR-Bs (whole antiserum) or a non-specific IgG (pure IgG fraction). Cells incubated with polymersomes in the absence of antibody and cells incubated neither with antibody nor with polymersomes are included as controls. **e)** Uptake of polymersomes in cells pre-incubated with an antibody against CD36. Control wells as in d. **f)** Comparison of polymersomes uptake in cells pre-incubated with either an anti-SR-Bs or with a combination of anti-SR-Bs plus anti-CD36 antibodies; controls as in d. All experiments in the figure were analysed by flow cytometry; graphs display normalised MFI values except b) which shows % fluorescent cells. n=3 experiments. Error bars:  $\pm$  sem. Statistical analysis: one-way ANOVA plus Bonferroni.  $p < 0.05$  (\*),  $p < 0.01$  (\*\*),  $p < 0.001$  (\*\*\*)

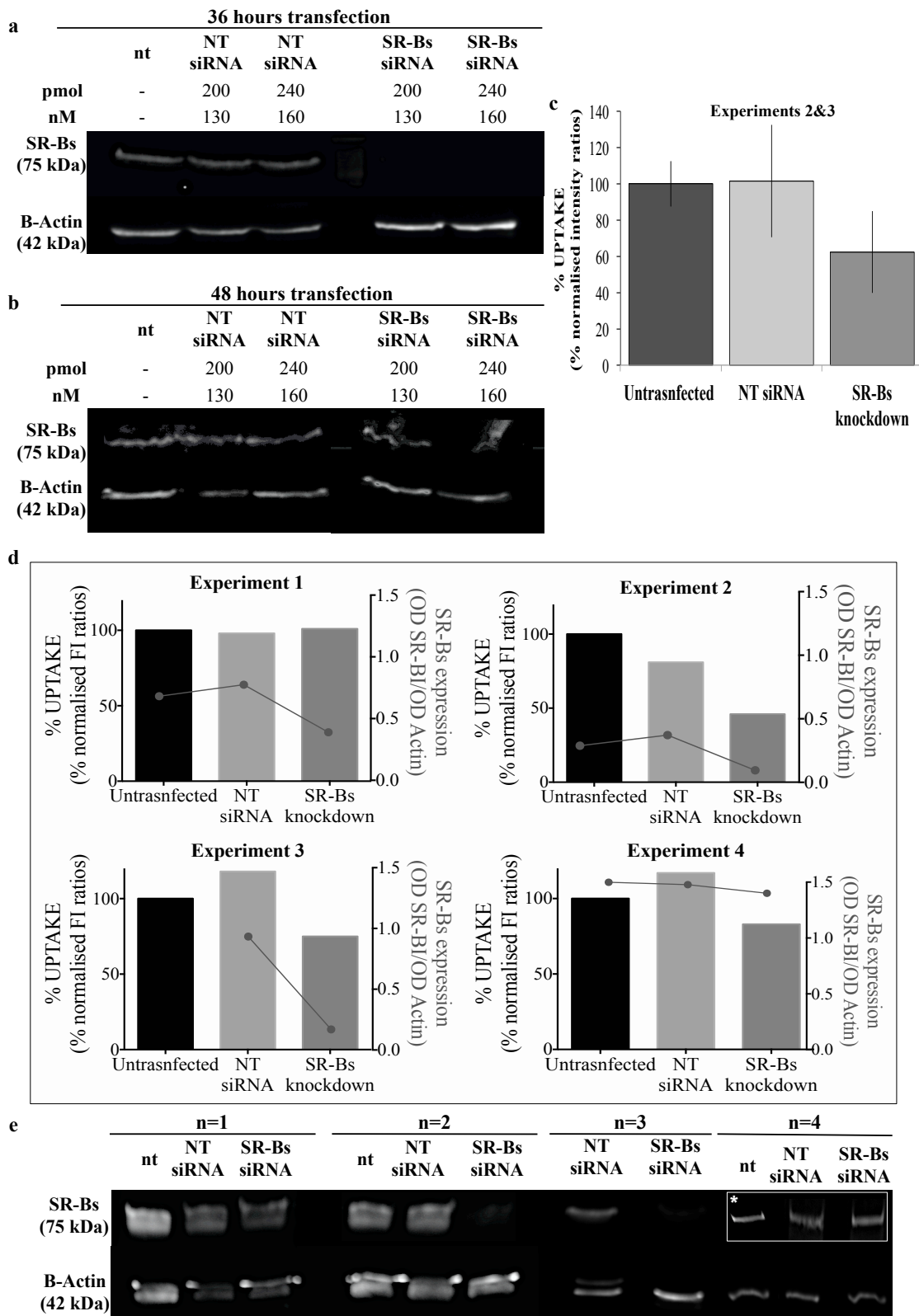


**Figure 5.3: Uptake of PMPC-PDPA polymersome in SR-Bs knockdown FaDu cells**

**a-b)** SR-Bs cellular levels by western blotting at 36 **a)** or 48 **b)** hours after transfection with two different concentrations of non-targeting or targeting siRNA. **c)** Flow cytometry results showing uptake of polymersomes in non-transfected cells, non-targeting siRNA transfected cells and SR-Bs knockdown cells. n=2experiments (experiments 2 and 3),  $\pm$  sem. **d)** Combined graphs showing uptake of polymersome (bar chart) and SR-Bs expression levels measured by western blotting (grey traces) for four individual knockdown experiments performed. **e)** Western blots from experiments in d. nt: non transfected cells. NT: cells transfected with non-targeting siRNA. \* 100-150 kDa band instead of 75 kDa.

### 5.2.3 Tetraspanin CD81 in PMPC-PDPA polymersome uptake

Tetraspanins are a family of transmembrane proteins discovered in 1990<sup>237,238</sup>. Members of this family present four transmembrane domains defining a small and a large extracellular loop with cytoplasmic N- and C-terminus. As many as thirty-three tetraspanins have been identified in mammals being in most of the cases widely expressed across all the spectra of mammalian cells, both intracellularly and at the plasma membrane. Tetraspanins often interact among themselves or with other proteins (i.e. integrins) forming tetraspanin-enriched domains<sup>105</sup> at the cell membrane, which are different to lipid rafts<sup>239</sup>. Nowadays tetraspanins attract great interest in two major biomedical areas, cancer and infection, with different viruses and bacteria targeting tetraspanins to enter host cells<sup>240</sup>. One example is the tetraspanin CD81, which is expressed by all mammalian cells investigated except red blood cells, platelets and neutrophils. CD81 is one of the best-studied tetraspanins due to its involvement in the internalisation of hepatitis C virus (HCV), where it is one of the main receptors implicated, together with the scavenger receptor SR-BI. Interestingly, this is not the only situation where CD81 and SR-BI have been identified as co-receptors of a specific ligand, both are also involved in the internalisation of *Plasmodium* sporozoites<sup>240,241</sup>.

The fact that scavenger receptor SR-BI and tetraspanin CD81 work together in the internalisation of some natural cargoes, which in turn are exogenous particles, one of them with all its dimensions in the nanometer range, and taking into account the results previously described in this chapter, we propose that CD81 is a good candidate for being a receptor implicated in PMPC-PDPA polymersome internalisation in mammalian cells.

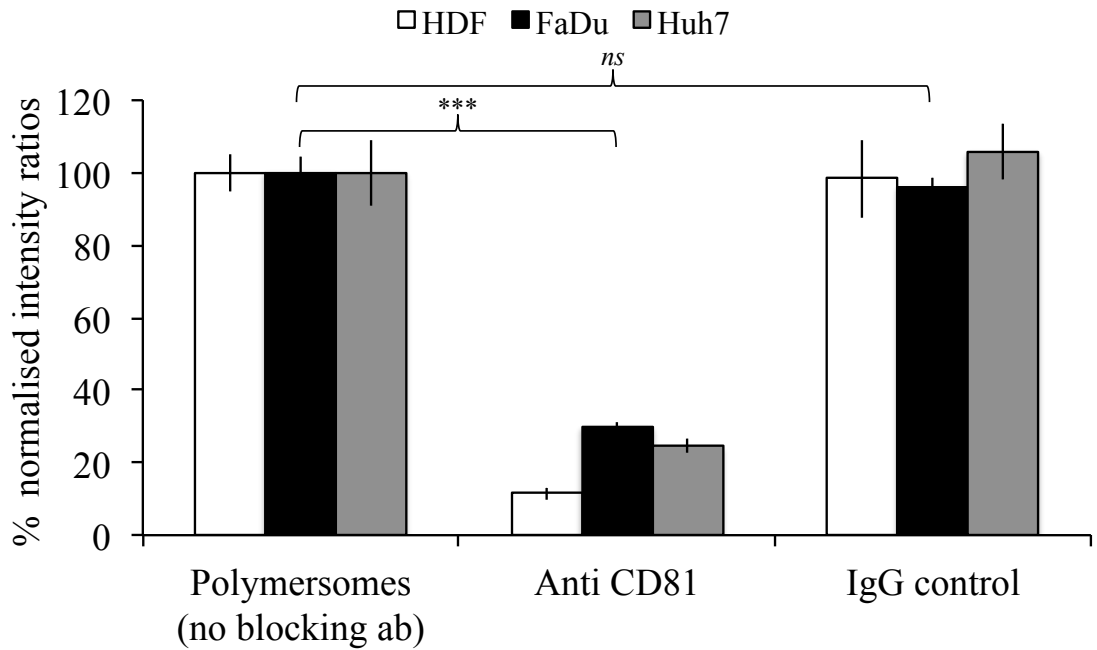
To investigate a possible role for the tetraspanin CD81 in polymersome internalisation I studied the cellular uptake of PMPC-PDPA polymersomes in HDF, FaDu and Huh7 cells previously incubated with a neutralising antibody anti-CD81. The results presented in figure 5.4 show a strong and significant inhibition of polymersome uptake in all the three cell types under study, 88%, 70% and 75% respectively, when CD81 was blocked highlighting a role for CD81 in the cellular uptake of the nanoparticle formulation.

Three receptors have been investigated in this chapter in relation with PMPC-PDPA polymersome uptake in mammalian cells: the scavenger receptors type B CD36 and SR-Bs, and the tetraspanin CD81. The same global effect, an inhibition in the cellular uptake of polymersome internalisation was observed across different cell types upon blocking of either scavenger receptors type B (figure 5.1) or tetraspanin CD81 (figure 5.4). On the other hand, I have often observed that PMPC-PDPA polymersomes are not taken up to the same degree, or with the same rate, by different cells types. Figure 5.2.c shows uptake of fluorescent-labelled polymersomes as measured by flow cytometry after 90 minutes incubation of HDF, FaDu and Huh7 cells. I believe that diverse cellular expression levels of the receptors investigated in here across the cell types could explain, at least in part, the differences in polymersome internalisation kinetics observed. In order to test this hypothesis the levels of CD36, SR-BI and CD81 at the plasma membrane of live HDF, FaDu and Huh7 cells were investigated by indirect immunofluorescence and flow cytometry. Results in figure 5.5.a shows how expression levels of CD36 among the different cells under study is almost equal while in the case of the tetraspanin CD81, it seems to be a higher concentration of receptor on the plasma membrane of primary HDF, compared with the cancer cells lines. Finally, the highest difference in receptor expression was observed with the scavenger receptors SR-Bs that appears to be enriched in the plasma membrane of Huh7 compared to FaDu (almost two fold increase) while HDFs express very low levels of this scavenger receptor at the cell surface. Therefore, the hepatocytes are the cell type under study, which present altogether higher expression of the receptors that seem to be regulating the endocytosis of PMPC-PDPA polymersomes. As a result, it could be expected a high avidity for polymersomes in Huh7 with a consequent enhanced uptake compared with HDF and FaDu cells. However as it can be seen in figure 5.2.c FaDu cells and not Huh7, are the ones showing an enhanced uptake of this formulation. A high expression at the plasma membrane of CD81 and SR-Bs does not therefore directly correlate with a higher uptake of PMPC-PDPA polymersomes.

The cellular expression of the tetraspanin and the scavenger receptors was further studied in FaDu cells by confocal microscopy. In order to obtain information not only of the expression of the receptors at the cell surface but also to learn whether there are intracellular pools of this receptors and how they are distributed inside the cell FaDu cells were fixed and permeabilised prior to performing indirect immunolabeling of the

receptors. Images in figure 5.5.b are Z projections from Z-stacks in a group of cells displaying the distribution of each receptor. The first thing that can be observed is that all cells within the group express the receptors, there are not subpopulations of cells that do not express a certain receptor, although in the case of CD36 the expression in some cells is very low. The second important point is that expression of the receptors seems enhanced in dividing cells compared with non dividing cells, this was specially noticeable for SR-Bs. This point was further verified by quantification of the fluorescence associated with dividing and non-dividing cells across different pictures. In the case of the SR-Bs expression of the receptors was significantly higher in dividing cells. Dividing cells also present enhanced expression of CD81 protein. On the contrary, there was no overall difference in expression levels in dividing vs. non-dividing cells in the case of CD36.

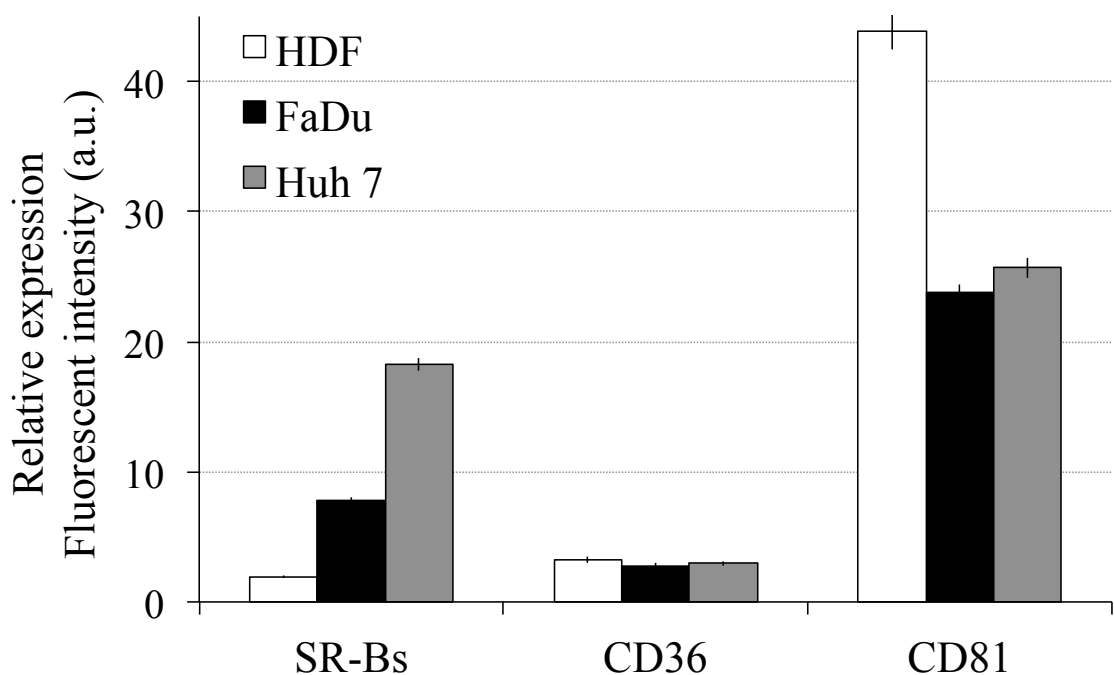
A detailed 3D analysis of the expression of each receptor in a single cell is shown in figures 5.5.c and 5.5.d. Comparing the single Z-slice montages in figure 5.5.d it can be seen how expression of the tetraspanin CD81 is almost restricted to the periphery of the cell while SR-Bs is evenly distributed through all the cell volume. The scavenger receptor CD36 is present both intracellularly and at the cell surface but it seems to be slightly more expressed at the plasma membrane. SR-Bs expression through the cell appears to be quite homogeneous and more diffuse compared with the other two receptors. In the case of CD81, it specially seems to be arranged into clusters or domains while CD36 distribution from this perspective would be a case in between the two expression patterns observed for SR-Bs and CD81.

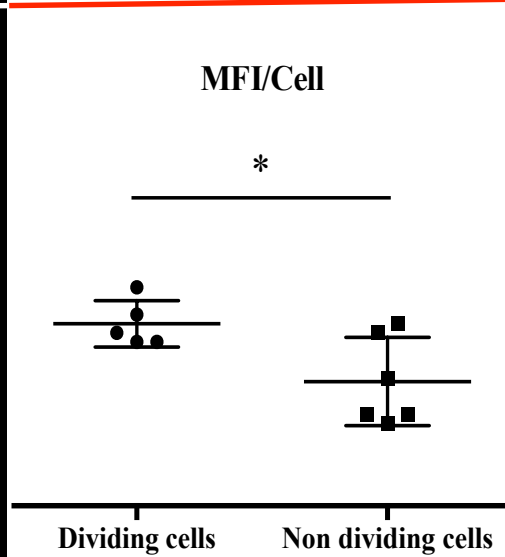
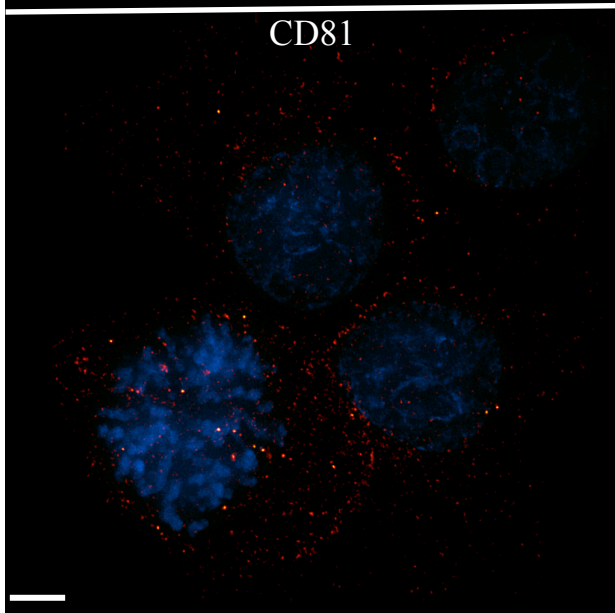
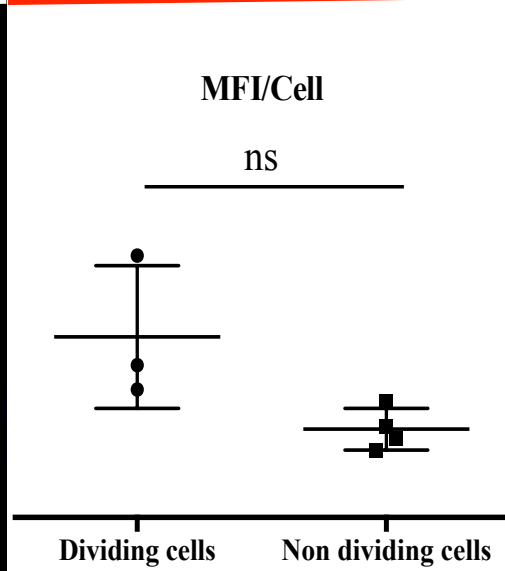
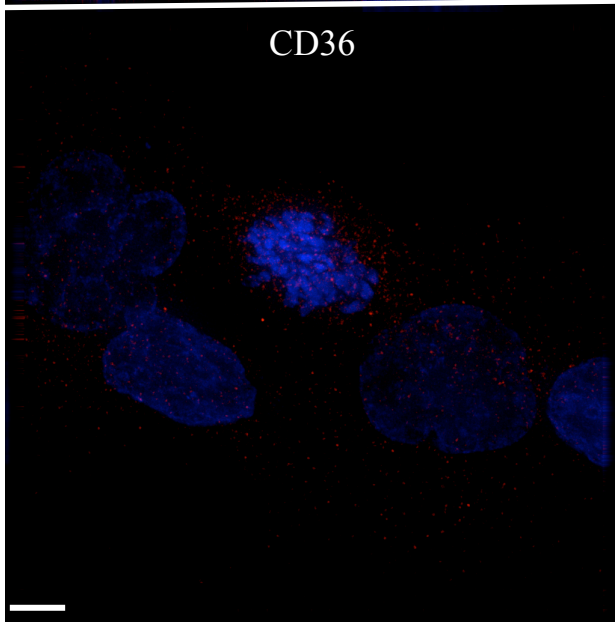
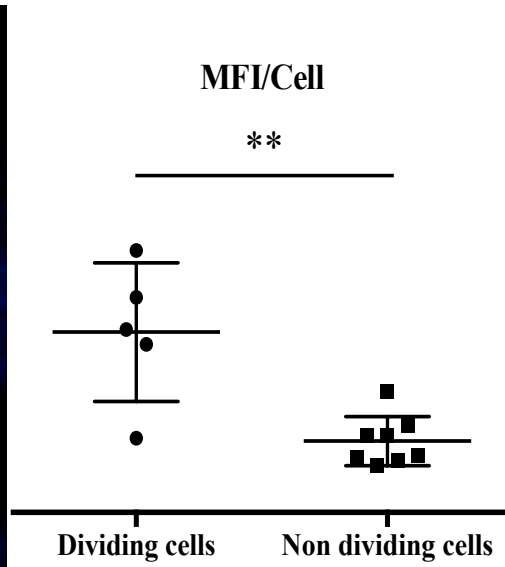
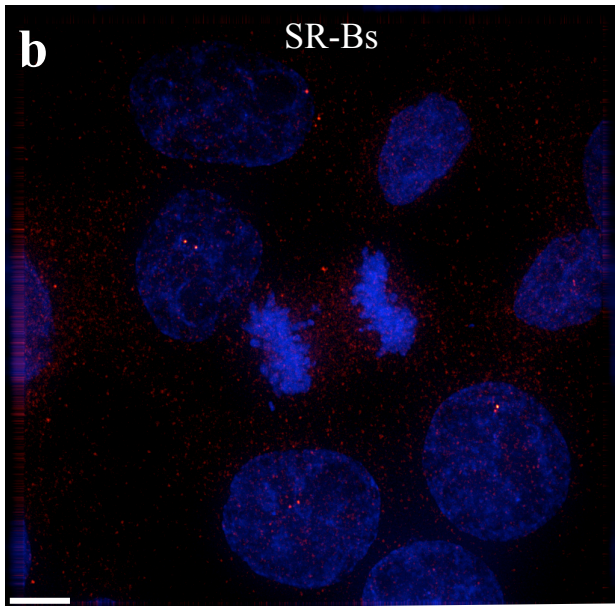


**Figure 5.4: Uptake of polymersomes in the presence of a blocking antibody against CD81**

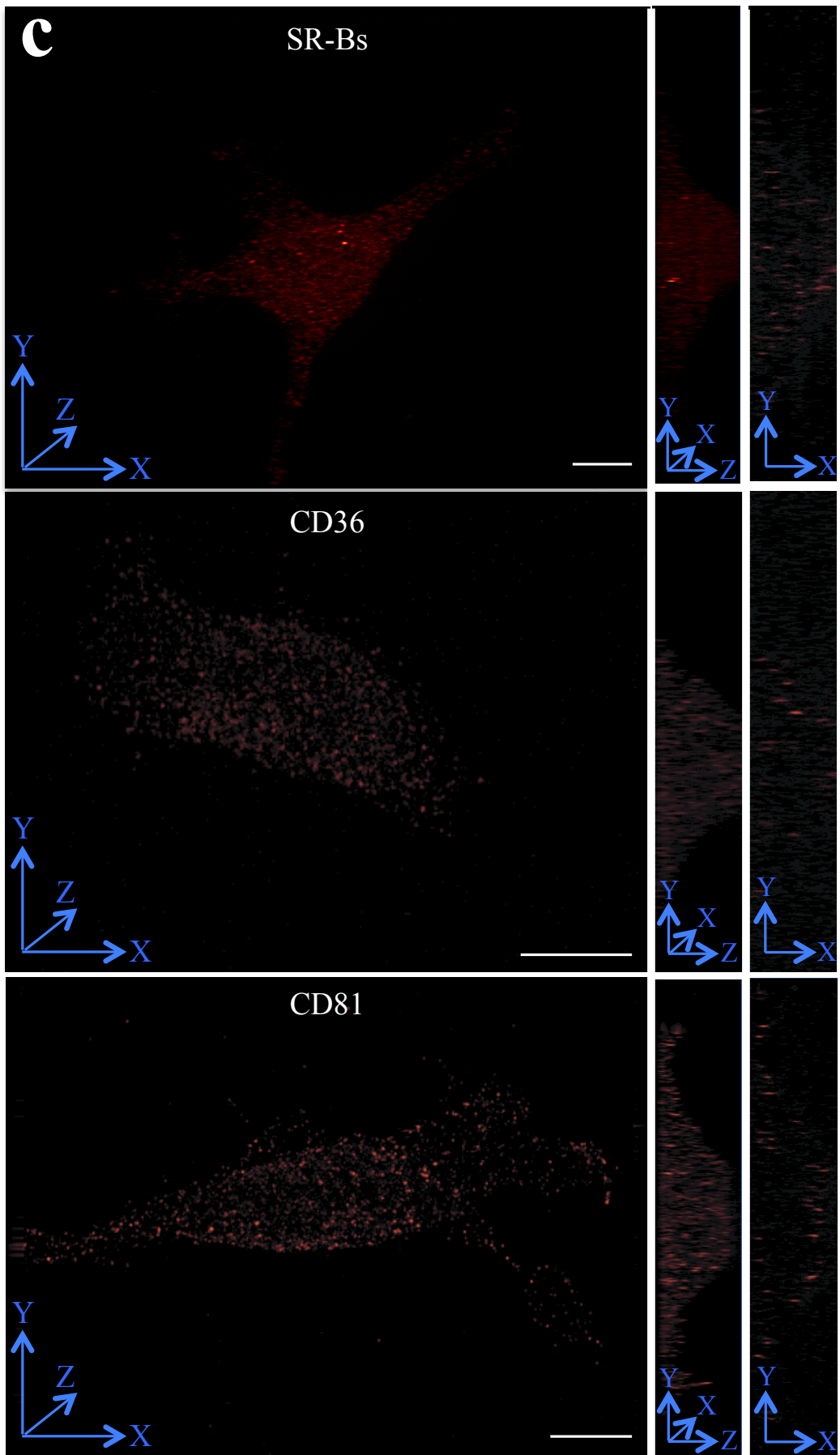
Normalised flow cytometry results comparing polymersome uptake in cells incubated with an antibody targeting the extracellular loop of CD81 vs. uptake in normal conditions (absence of antibody) or the presence of a control IgG (non-targeting IgG). n=3 experiments. Errors bars:  $\pm$  sem. Statistical analysis: one-way ANOVA plus Bonferroni post-test  $p < 0.001$  (\*\*\*).

**a**









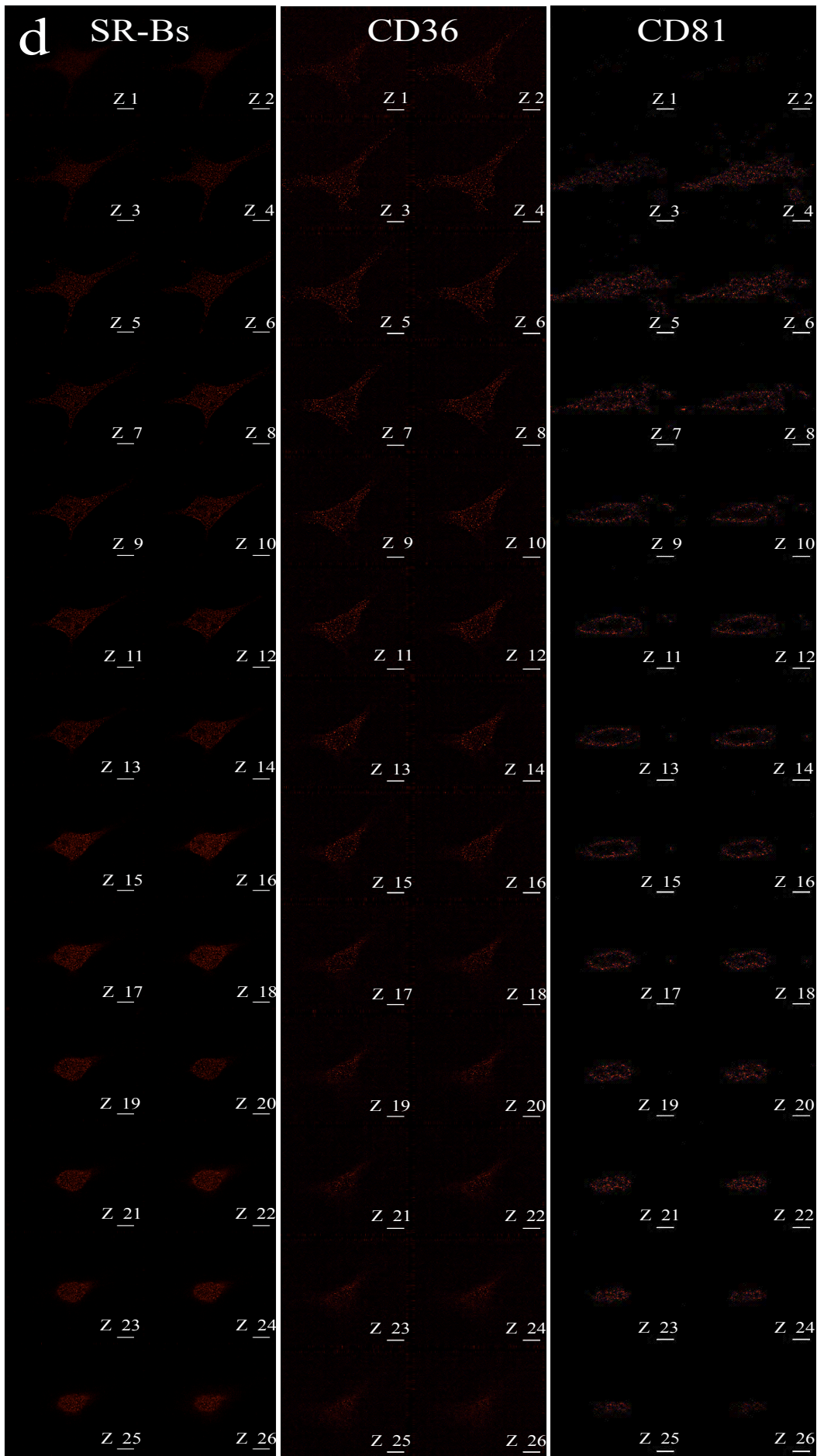


**Figure 5.5: Cellular expression of the scavenger receptors SR-Bs and CD36 and the tetraspanin CD81 in mammalian cells**

**a)** Plasma membrane levels of SR-Bs, CD36 and CD81 receptors in live HDFs, FaDu and Huh7 cells measured by flow cytometry. **b-d)** Cellular distribution of SR-Bs, CD36 and CD81 receptors by immunofluorescence in fixed FaDu cells. **b)** Confocal micrographs of the distribution of each receptor in a group of cells. Scale bars: 4  $\mu\text{m}$ . Right graphs: receptor expression (MFI per cell) in dividing cells vs. non-dividing cells. Mean  $\pm$  SD. Statistical significant difference (student's t-test, \*\*  $p < 0.01$ , \*  $p < 0.05$ ). **c)** Single cell detail of the distribution of each receptor by confocal microscopy. 3D reconstructions across the Z planes of the cells are shown from two perspectives: top projections (left panels) and side projections (central panels). Right panels represent a single Z slice through the nucleus of the cell. Scale bars: 5  $\mu\text{m}$ . **d)** Montage pictures of Z stacks in c displaying the single Z slices. Slice width: 0.28  $\mu\text{m}$  (SR-Bs), 0.22  $\mu\text{m}$  (CD36) and 0.28  $\mu\text{m}$  (CD81). Scale bars: 5  $\mu\text{m}$ .



## 5.3 Discussion

The aim of the present research, motivated by the favourable internalisation of PMPC-PDPA polymersomes observed in mammalian cells, was to investigate whether PMPC-PDPA polymersome uptake is a receptor-mediated endocytic process and whether this endocytosis is mediated by scavenger receptors in mammalian cells. With this in mind, I investigated uptake of polymersomes in serum free conditions and in cells where scavenger receptors were blocked or inhibited by different means.

I observed that polymersome uptake is enhanced in serum free conditions (figures 5.2.b and 5.2.c), which is in line with a role for SCrs in PMPC-PDPA polymersome internalisation. Although the exact composition of FCS (fetal calf serum) is not known, it is expected to be rich in lipoproteins that are natural ligands of SCrs. Therefore, it is reasonable to think that these lipoproteins could compete with polymersomes for the SCrs with a consequent higher nanoparticle uptake in serum free conditions. Interestingly, Patel *et al.*, have recently reported 150% higher uptake of their biofunctionalised nanoparticles in serum free conditions while investigating the SCrs mediated uptake of the nanoparticles. These results are agreement with my own observations.

A different interpretation of the results obtained would imply the adsorption of serum proteins to the polymersome surface, to form a protein corona. The protein corona will control the interactions of the nanoparticle with the surroundings, including the rate and the mechanism of cellular internalisation of the protein-polymer aggregate<sup>242</sup>. Nonetheless, results recently generated in our laboratory have shown, using isothermal titration calorimetry, that serum albumin, the most abundant protein in mammals blood<sup>243</sup>, as well as a standard IgG, does not interact with PMPC-PDPA polymersome surface (Prof. Battaglia unpublished data).

The fact that polymersome internalisation was almost completely abolished in the presence of Fucoidan, a ligand for SCrs type A and B (figure 5.1), in the six different cell types under study support receptor-mediated endocytosis as a common uptake mechanism for PMPC-PDPA polymersomes in mammalian cells. Additionally, the fact that nanoparticle endocytosis was inhibited in the presence of a ligand for SCrs type A and B but not in the presence of a specific ligand for SCrs type A led me to look into the

specific target receptor for the nanoparticles among three types of SCrs B expressed at the plasma membrane: SR-BI, SR-BII and CD36. SCrs type A have therefore not being further investigated in this thesis in relation with PMPC-PDPA polymersome internalisation although I realise that the inhibition observed in cells incubated with Fucoidan could be the result of the simultaneous blocking of both types of receptors. In any case, we found important evidence that SR-Bs receptors (SR-BI and SR-BII) are participating in the internalisation of this polymersome formulation since nanoparticle uptake is reduced to 50% in cells pre-incubated with ITX5061 (figure 5.2.a), an antagonist of SR-Bs receptors. Moreover blocking of SR-Bs using a specific antibody against the extracellular loop of these receptors inhibited polymersome uptake up to 80% in a concentration dependent manner (figure 5.2.d). The use of an antibody to block CD36 did not result in a significant inhibition of polymersome internalisation (figure 5.2.d). However, simultaneous blocking of SR-Bs and CD36 produced a stronger inhibition than the inhibition observed when only SR-Bs was blocked (figure 5.f), suggesting that CD36 could still have a role in PMPC-PDPA polymersome internalisation.

Surprisingly, the uptake of polymersomes in SR-Bs knockdown cells was not significantly perturbed. Nevertheless, we should not exclude a role for these receptors in PMPC-PDPA polymersome internalisation based on knockdown studies alone. It is not the first case reported where siRNA-mediated inhibition of SCrs did not result in the inhibition of the cellular uptake of an exogenous ligand otherwise strongly inhibited using another experimental approach. In 2006 Saleh *et al.*, were the first to link the uptake of exogenous double stranded RNA (dsRNA) with SCrs in *Drosophila S2* cells. They observed a strong inhibition in dsRNA endocytosis using a pharmacological approach but failed to replicate the inhibition by knocking down as many as 19 genes coding for SCrs. Neither the individual knockdown nor the simultaneous knockdown of the genes inhibited the cellular uptake of dsRNA<sup>244</sup>. More recently, in 2010, Patel *et al.*, discovered that specific biofunctionalised nanoparticles were taken up by SCrs in mammalian cells. Internalisation of oligonucleotide-funtionalised gold nanoparticles was reduced >60% in cells incubated with either Fucoidan or Polyinosinic acid. On the other hand knockdown of SCrs type A, SCrs type B or simultaneous knockdown of both types did not inhibit nanoparticle uptake<sup>219</sup>. In both cases, they concluded that simultaneous knockdown of different receptors was probably not enough to impair the uptake through remaining receptors at the cell surface, or that unidentified family

members were responsible for the effective cellular uptake. In line with this, Fucoidan and Polyinosinic acid could present a broader targeting ability as traditionally accepted being able to target other members of the scavenger family or even other receptors at the cell surface. It is known that Fucoidan can block selectins on the cell surface of leukocytes, platelets and red blood cells<sup>245</sup>. In addition, it has been recently discovered to be an agonist to C-type lectin-like receptor 2 (CLEC-2), present in platelets neutrophils and dendritic cells<sup>246</sup>. Although the cells used by Saleh and Patel in their studies do not fall into the range of cells expressing selectins or CLEC-2 receptor, it illustrates the possibility that the high inhibition observed upon pharmacological treatment could be strongly influenced by the blocking of unidentified cellular partners.

The use of different approaches to test the same hypothesis is part of a good scientific practice. Nonetheless, it can sometimes lead to apparently opposed results as it has happened to other groups before us. In our case the use of a neutralising antibody directed against SR-Bs receptors produced the strongest inhibition observed in PMPC-PDPA polymersome internalisation under neutralising conditions for a specific receptor, while the knockdown of SR-Bs did not produce a significant inhibition in polymersome uptake. The use of a blocking antibody against a specific SCr represents a fast and overall non-cell-disruptive way to specifically assess the implication of a receptor in polymersome internalisation. On the other hand, knocking down the protein under study offers the possibility to investigate polymersome uptake in the complete absence of the candidate receptor, in contrast with the previous approach where the receptor is present but blocked. However, to knockdown the expression of one of the constitutive elements of a cell can lead to off-target effects. A protein such a membrane receptor is often implicated in different functional networks and therefore it could be expected that the cell will try to compensate this absence by regulating the expression of other genes or the functions of other proteins. These off-targets effects will acquire more importance as the time that the cell remains in the absence of the protein increases and could dilute or mask the true effect of the receptor under study. The antibody approach is not exempt of possible off-target effects either. Sometimes antiserum preparations can contain together with the specific IgGs against the receptor under study, another non-reported IgGs targeting other surface molecules. Another possibility is that by specifically blocking the SR-Bs we are producing a non-specific block of another surface molecule working in partnership with the SR-Bs towards the internalisation of the nanoparticles.

In either case, the total inhibition achieved would be the result of the simultaneous blocking of a receptor complex and the knockdown of only one of the receptors implicated might be not enough to effectively inhibit polymersome internalisation. In agreement with this possibility I have found evidence that another receptor, tetraspanin CD81, is also implicated in PMPC-PDPA polymersome internalisation in mammalian cells (figure 5.4). Interestingly both SR-Bs and CD81 receptors seem to be upregulated, in terms of cellular protein levels, in dividing cells (figure 5.3.b), an observation that could shed some light into the reasons behind the enhanced uptake noticed for this formulation in cells with high dividing rates<sup>176</sup>.

One of the main characteristics of the tetraspanin family is their ability to physically interact with other proteins. Interestingly, the tetraspanin CD9 has been found to interact with the scavenger receptor CD5 in the plasma membrane of B cells<sup>247</sup>. Although a direct interaction between the tetraspanin CD81 and the scavenger receptors SR-BI/SR-BII has not been identified, CD81 and SR-BI have been found mediating the endocytosis of the same exogenous biological particles in the cases of HCV and the *Plasmodium* sporozite. To the best of our knowledge, this is the first time that a scavenger receptor and a tetraspanin are implicated together in the endocytosis of man-made nanoparticles. It is important to highlight that PMPC-PDPA polymersomes are completely synthetic nanoparticles that according to the results presented here are actively targeting biological receptors without been intentionally biofunctionalised for that purpose, as it has been the case for other nanoparticles taken up by SCrs<sup>248-250</sup>. Nonetheless, it is important to highlight that the phosphocholine groups repeated in the external brush of PMPC polymersomes are a common chemical group within natural systems, and we believe that these groups could be responsible, at least in part, for the biological targeting observed. In line with this, PMPC polymersomes targeting of SCrs and tetraspanin CD81 could be revealing a novel functionality of the PMPC polymer. Like PEG, PMPC is currently used in biomedical applications for its biocompatibility and non-fouling properties. This resistance to interact with biomolecules can get in conflict with any PMPC responsibility in specific molecular interactions with cellular receptors. Nonetheless, it might be possible that the special arrangement of the polymer in the surface of highly curved nanovesicles favours its interactions with specific receptors in the plasma membrane. Probably guided by a similar thought Choi *et al.*, have recently shown that the cellular uptake, through SCrs, of oligonucleotide-



functionalised gold nanoparticles seems to derive from the specific arrangement of the nucleotides in 3D structures<sup>251</sup>. In addition, our own previous results have shown that when PMPC distribution at the surface of the polymersomes is not continuous but patched, 25% PMPC-PDPA polymersomes *vs.* 100% PMPC-PDPA polymersomes, bigger patched particles can be taken up with the same efficiency as non-patched particles half in size<sup>165,166</sup>. With the identification of the specific receptors mediating the uptake of PMPC polymersomes this results could be indeed an indication that the specific targeting ability of the nanoparticles resides in the combination between the physical and the chemical properties of the formulation. This is just one of the interesting new lines of work derived from the results presented on this chapter where I have shown that PMPC-PDPA polymersome internalisation in mammalian cells is a receptor-mediated endocytic process regulated by two different transmembrane family proteins, with tetraspanin CD81 and SCRs type B identified as the specific molecular targets for this nanoparticle formulation.



# Chapter 6: Characterising the mechanism of receptor-mediated endocytosis of PMPC-PDPA polymersomes

## 6.1 Introduction

From a simple point of view, receptor-mediated endocytosis of cargo comprises a specific binding at the cell surface often followed by a local plasma membrane re-arrangement, and in any case, by a membrane deformation, with the consecutive pinching off, and subcellular trafficking, of the endocytic vesicle containing the cargo. Having identified at least some of the receptors involved in the first stage of PMPC-PDPA polymersome endocytosis, I aimed to characterise the subsequent mechanism of internalisation of this nanoparticle formulation.

In the previous chapter I have shown that the tetraspanin CD81 and the scavenger receptors SR-Bs facilitate the uptake of PMPC-PDPA polymersomes in mammalian cells. To gather information about the potential cellular structures defining the mechanism of polymersome endocytosis, we could consider the characteristics of the endocytic pathways triggered upon binding of recognised ligands of these two receptors. The best example is HCV, which directly interacts with the receptors SR-BI and CD81 at the cell surface. Bound HCV particles are then translocated to tight junctions, in a process that seems to be regulated by claudin 1 and occludin, where they are finally internalised by clathrin-mediated endocytosis (CME). Following internalisation, the decrease of the pH in the early endosomes triggers the fusion of the viral particle with the endosomal membrane and the subsequent release of nucleocapsid into the cell cytosol<sup>252</sup>.

When considering the possible endocytic pathways that a cargo interacting with CD81 and SR-BI could follow, it is also worth noticing that both transmembrane proteins have been found to bind cholesterol at the plasma membrane<sup>253,254</sup>, and that SR-BI has been shown to be associated with caveolae<sup>255</sup>, while CD81 is part of tetraspanin enriched

domains at the plasma membrane<sup>240</sup>. Therefore, a cargo using this set of receptors to gain cellular entry may use various endocytic routes to achieve this goal.

The ultimate role of PMPC-PDPA polymersomes is to be internalised by the cell and to release its cargo at a subcellular level. Nanoparticle endocytosis and its consequent subcellular sorting is a complex process to elucidate, with multiple cellular pathways often playing interconnecting roles. However, a full understanding of polymersome endocytosis will allow the rational improvement of the nanovector features and the establishment of the complete toxicological profile of the system. In order to characterise the pathway/s of PMPC-PDPA polymersome internalisation I have explored several experimental approaches whose results are detailed below.

## **6.2 Results**

### **6.2.1 Investigation of PMPC-PDPA polymersome endocytosis using chemical inhibitors**

Chemical inhibitors are compounds that once in contact with the cell will stop or hinder endocytosis, either by removing essential structures from the plasma membrane (i.e. cholesterol) or by interfering with the normal activity of certain molecules (i.e. dynamin). They have been used to study the internalisation mechanisms of different nanoparticles. The fact that these experiments are usually considered straightforward to perform and interpret, as well as economical, is behind their widespread usage. However, in the last few years, the awareness about the extra care needed when planning, performing and interpreting studies involving chemical inhibitors has grown considerably<sup>256,257</sup>. These concerns arise in part, from the fact that chemical inhibitors can easily induce cellular toxicity<sup>256</sup>. It is reasonable to think that the normal endocytosis of a cargo will be strongly affected if mechanisms of cellular stress and death are activated, with the consequent risk of achieving misleading results. Therefore, it is crucial to carefully select the concentrations of the chemicals and the time that the cells will be exposed to them. It is also clear that these compounds have cell specific effects<sup>256,258,259</sup>; in consequence, treatment conditions should be specifically determined for each cell type. Finally, chemical inhibitors have been always associated with a

certain lack of specificity<sup>256,257</sup> that is has been aggravated, as it has become clear that the boundaries between different endocytic routes are less rigid than it was thought a decade ago.

Taking into account the considerations mentioned above, the use of chemical inhibitors can be still a useful technique to first approach the characterisation of an endocytic pathway, especially as a way to narrow down the list of candidates mediating the internalisation. Accordingly, we decided to employ inhibitors to start characterising PMPC-PDPA polymersome uptake.

#### 6.2.1.1 Prescreen. Selection of chemical inhibitors to map different endocytic routes and definition of their treatment window

The range of available inhibitors to study the endocytosis of a system is large, as well as the experimental protocols and conditions at which they are used in some cases. To be able to investigate different endocytic routes I shortlisted 12 inhibitors, presented in table 6.1, together with their inhibitory effect on endocytosis and examples of the concentrations and the incubation times previously used in HeLa cells.

##### *6.2.1.1.1 MTT assays*

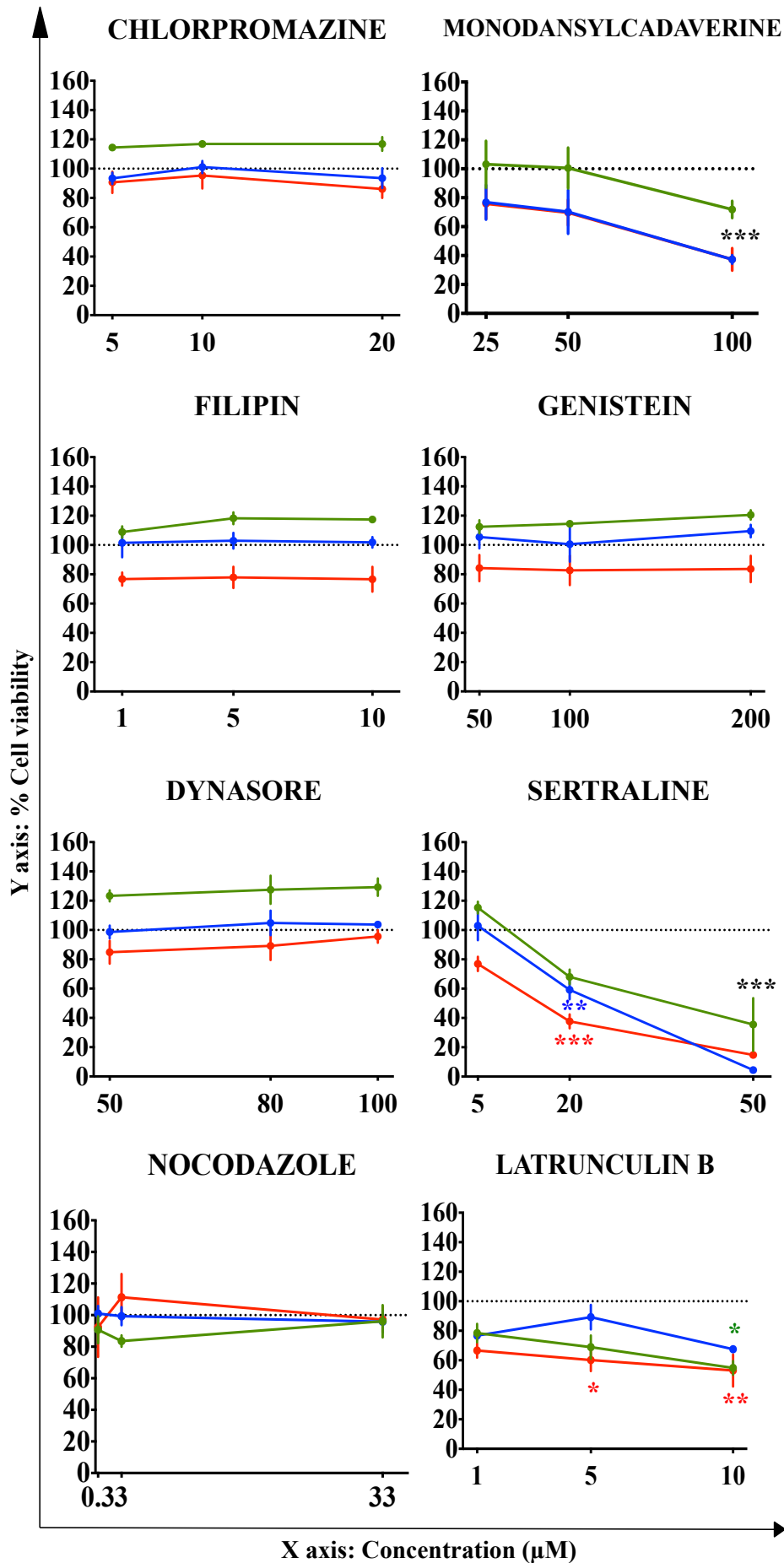
As mentioned before, chemical inhibitors are potentially cytotoxic; as a first step to be able to use them to investigate polymersome endocytosis, I screened the shortlisted agents for induced cellular toxicity. Based on reported treatments in the literature three concentrations were selected for each compound to be tested (table 6.1). In addition, each concentration was investigated at three different incubation times: 10, 30, and 60 minutes. Cellular viability levels after incubation with the inhibitors was explored using a MTT assay. Results are presented in figure 6.1.

<b>Inhibitor</b>	<b>Effect</b>	<b>Reported incubation in HeLa (37°C)</b>	<b>Concentrations to be tested</b>
<b>Chlorpromazine (CPZ)</b>	Prevents the assembly of coated pits at the plasma membrane. Promotes reversible translocation of clathrin and its adaptor protein from the plasma membrane to intracellular vesicles.	14µM 30 min <sup>260</sup>	5 µM 10 µM 20 µM
		20 µM 65 min (30 min pre-i.+35 min t.) <sup>261</sup>	
<b>Monodansylcadaverine (MDC)</b>	Competitive inhibitor of the enzyme transglutaminase. Transglutaminase is involved in the cross-linking of proteins during coated pit formation.	100 µM up to 1 h <sup>*262</sup>	25 µM 50 µM 100 µM
		400 µM 1 hr (30 min pre-i.+30 min t.) <sup>*263</sup>	
<b>Filipin (FLP)</b>	Sequesters cholesterol at the plasma membrane.	7,5 µM 30 min <sup>260</sup>	1 µM 5 µM 10 µM
		5µg/ml 50 min (30 min pre-i.+20 min t.) <sup>264</sup>	
<b>Genistein (GNT)</b>	Inhibits tyrosine protein kinase impairing actin and dynamin 2 recruitment to the endocytic site.	100 µg/ml (30 min pre-i.+20 min t.) <sup>264</sup>	50 µM 100 µM 200 µM
<b>Dynasore (DNY)</b>	Inhibits dynamin 1 and dynamin 2 GTPase activity.	50-80 µM 5 hrs <sup>265</sup>	50 µM 80 µM 100 µM
		80 µM 45 min (30 min pre-i.+15 min t.) <sup>*266</sup>	
		90µM 30 min <sup>260</sup>	
<b>Sertraline (SRT)</b>	Inhibits dynamin 1 and dynamin 2 GTPase activity.	20 µM 65 min (30 min pre-i.+35 min t.) <sup>261</sup>	5 µM 20 µM 50 µM
<b>Nocodazole (NCDZ)</b>	Disrupts cytoskeleton by promoting microtubule depolymerisation.	33 µM 70 min (10 min, 4 °C pre-i+1h t.) <sup>*267</sup>	0.3 µM 3 µM 33 µM
		33 µM 2 hrs (1hr pre-i+1h t.) <sup>166</sup>	

Inhibitor	Effect	Reported incubation in HeLa (37°C)	Concentrations to be tested
<b>Latrunculin B (LatB)</b>	Disruption of cytoskeleton by inhibiting actin filament assembly.	0.5 $\mu$ M 15 min <sup>268</sup> 2 $\mu$ M 1.7 hrs (40 min pre-i+1h t.) <sup>*267</sup>	1 $\mu$ M 5 $\mu$ M 10 $\mu$ M
<b>Cytochalasin D (Cyto-D)</b>	Disrupts cytoskeleton by inhibiting further actin polymerisation.	0.1 $\mu$ M 30 min <sup>269</sup> 0.2-4 $\mu$ M 60 min pre-i. <sup>270</sup> 1-5 $\mu$ M 1.5 hrs (30 min pre-i+1hr t.) <sup>*271</sup> 2 $\mu$ M 30 min <sup>260</sup>	0.1 $\mu$ M 1 $\mu$ M 2 $\mu$ M
<b>1,1'-Disulfaneyldinaphthalen-2-ol (IPA-3)</b>	Allosteric inhibitor of the serine/threonine kinase Pak1. Pak 1 is a regulator of the cytoskeleton dynamics through effectors such as BAR domain proteins.	5-25 $\mu$ M 1.5 hrs (30 min pre-i+1hr t.) <sup>*271</sup>	10 $\mu$ M 25 $\mu$ M 50 $\mu$ M
<b>5-(N-ethyl-N-isopropyl)amiloride (EIPA)</b>	Blocks the Na <sup>+</sup> /H <sup>+</sup> exchangers leading to mild acidification of the cytosol. Decreases plasma membrane ruffling often associated with macropinocytosis.	25,50 $\mu$ M 1.5 hrs (30 min pre-i+1hr t.) <sup>*271</sup> 100 $\mu$ M 10 min <sup>260</sup>	25 $\mu$ M 50 $\mu$ M 100 $\mu$ M
<b>Bafilomycin A1 (Baf-A)</b>	Inhibits the vacuolar ATPase hampering the acidification of the endosomal lumen.	2-100 mM 1.5 hrs (30 min pre-i+1hr t.) <sup>*271</sup> 8-200 nM, 60 min pre-i. <sup>270</sup>	10 nM 50 nM 100 nM

**Table 6.1: Chemical inhibitors of endocytosis**

Mechanisms of different inhibitors to perturb endocytosis, examples of inhibitory treatments (concentrations and incubation times) reported in the literature to investigate endocytosis in HeLa cells, and concentrations of each inhibitor to be tested in our laboratory. Legend: pre-incubation (pre-i.), treatment (t.), incubation with inhibitors was carried out in serum free media (\*).





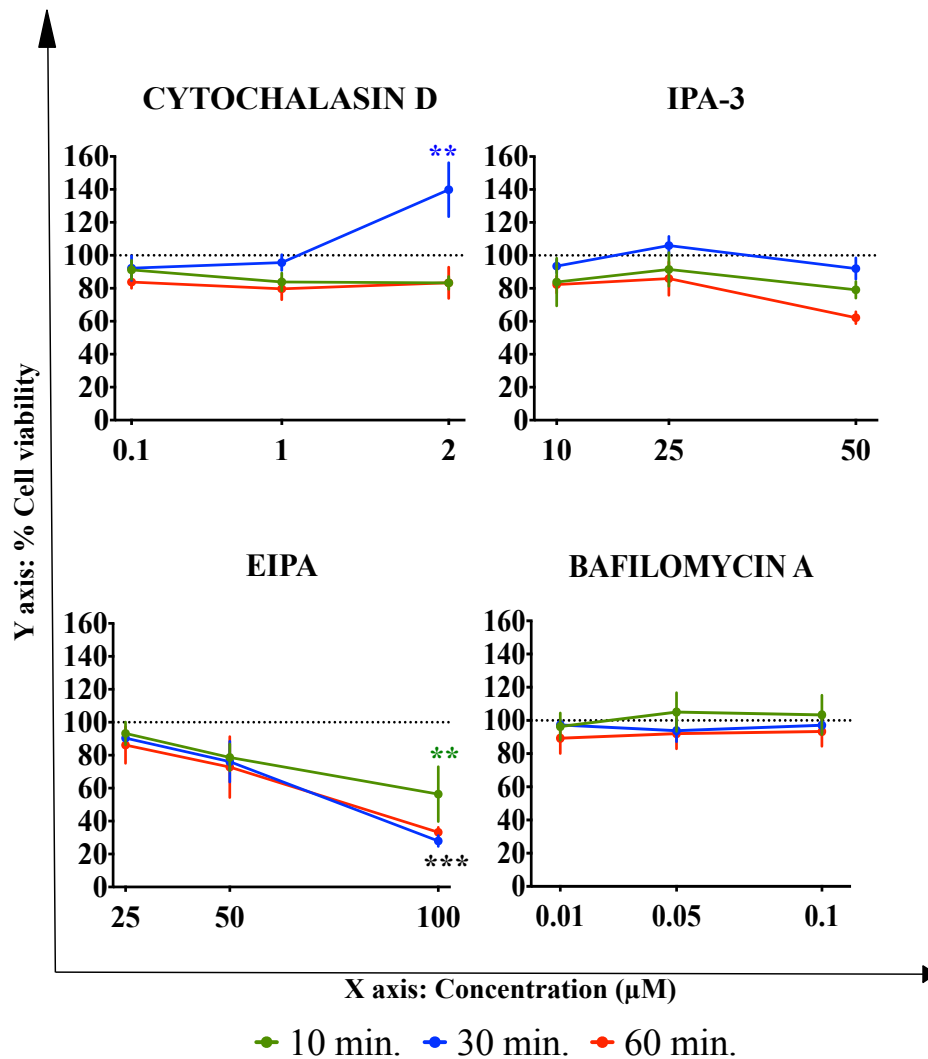


**Figure 6.1: Cell viability levels after incubation with inhibitors (MTT assays)**

HeLa cells were incubated with three different concentrations of each inhibitor for 10 minutes, 30 minutes or 1 hour. Cell viability was investigated by MTT. Cells incubated only with ultrapure water (main diluent added to the cells together with the inhibitors) were used as a control, and were set to represent 100% cellular viability (dashed line). n=3 experiments. Error bars:  $\pm$  sem. Statistical analysis: one-way ANOVA plus Bonferroni post-test. \* Represents statistically significant difference compared with control cells,  $p < 0.05$  (\*),  $p < 0.01$  (\*\*),  $p < 0.001$  (\*\*\*)

### *6.2.1.1.2 Live-Dead cell viability assays: flow cytometry and fluorescence microscopy*

Based on the MTT results I decided not to consider monodansylcadaverine, sertraline, latrunculin B and EIPA for further studies. On the other hand, the inhibitors and concentrations selected for the next screen are listed in table 6.2.

To verify further that the chosen compounds do not cause cell death or compromise the plasma membrane integrity, live/dead assays were performed. Propidium iodide (PI) is a red fluorescent intercalating agent (Em: 617 nm) that will not permeate intact cell membranes. Therefore, it is usually used to distinguish cells with a compromised membrane within a cell population. Using PI, and taking advantage of the possibility to analyse large cell populations by flow cytometry, I investigated the percentage of dead cells after 30 minutes incubation with the inhibitors at the concentrations listed in table 6.2. As figure 6.2 shows, the percentage of positive cells for PI staining after inhibitor treatment was always  $\leq 3\%$  (1.8% for untreated cells), in contrast with the nearly 30% observed when cells were incubated with 10% DMSO, a highly cytotoxic organic solvent at that percentage. Moreover, the cell population profile in terms of physical properties (cell size and granularity), was greatly altered in cells incubated with 10% DMSO, while it remained similar to untreated cells in the rest of the conditions.

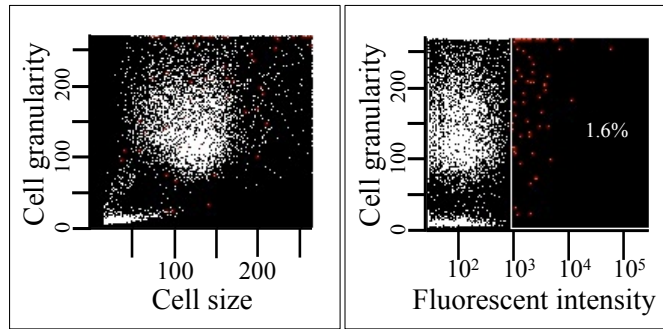
In a parallel study, following inhibitor treatment, the cells were incubated with PI and SYTO<sup>®</sup>9, a cell-permeable green fluorescent nucleic acid stain (Em: 500 nm). In this case, the cells were analysed by fluorescence microscopy to be able to visualise in detail any morphological change induced by the inhibitors. After incubation with both dyes, viable cells should be only stained by green SYTO<sup>®</sup>9, while dead cells or cells with a compromised plasma membrane will be simultaneously stained in red by PI. Pictures displayed in figure 6.3 demonstrate the low occurrence of cells with compromised plasma membrane, and the maintenance of normal cell morphology, in cells incubated with chemical inhibitors of endocytosis. On the other hand, cells incubated with 10% DMSO appeared as a homogenous cell mass where the nuclear membrane has disappeared. The percentage of damaged cells seems higher than the one obtained by flow cytometry. At 1% DMSO the previous damaging and drastic effects over cell morphology were not observed.

The results derived from the live/dead experiments show that for the proposed inhibitors, concentrations and incubation times, cell viability and plasma membrane integrity are maintained as normal.

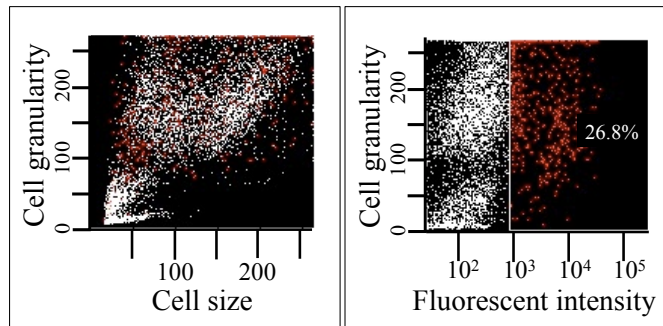
<b>Inhibitor</b>	<b>Concentration (<math>\mu</math>M)</b>	<b>Incubation time (min)</b>
Chlorpromazine	10	30
Filipin	5	30
Genistein	50	30
Dynasore	50	30
Nocodazole	33	30
Cytochalasin D	1	30
1,1'-Disulfanediyldinaphthalen-2-ol (IPA-3)	10	30
Bafilomycin A1	0.01	30

**Table 6.2: Selected inhibitors and their associated incubation conditions (concentration and time) for live/dead assays**

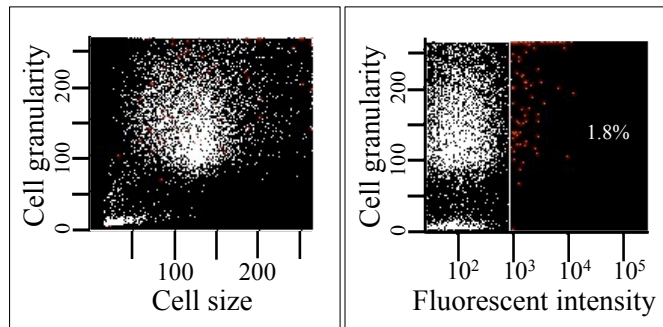
### UNTREATED CELLS



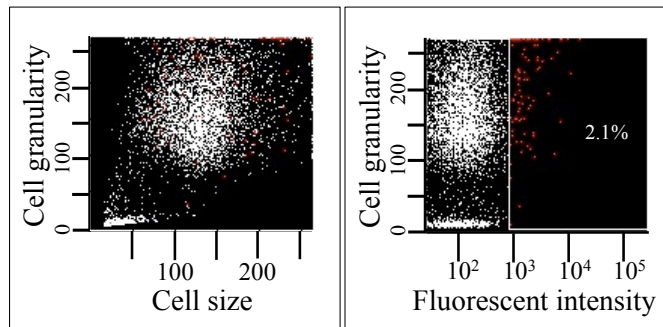
### 10% DMSO



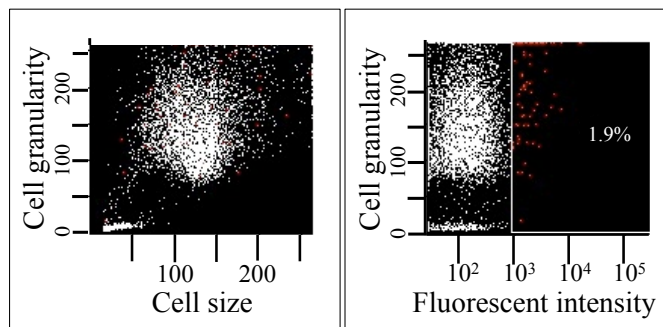
### 1% DMSO



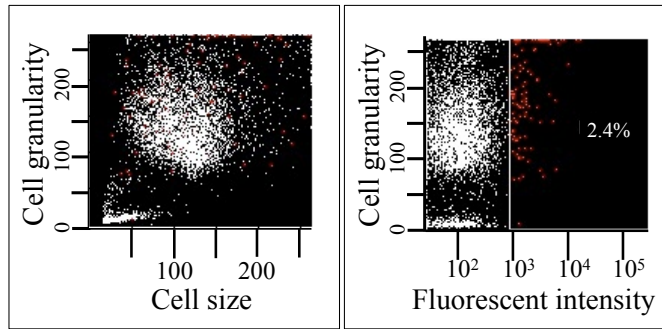
### CHLORPROMAZINE



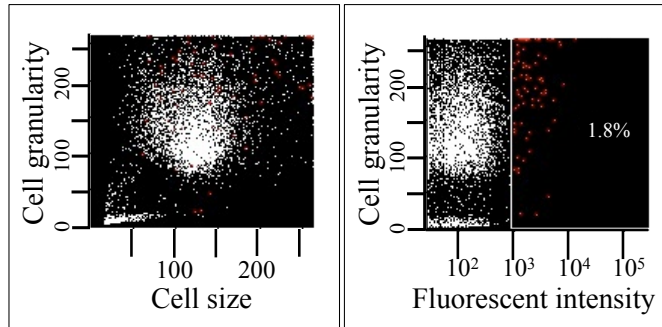
### FILIPIN



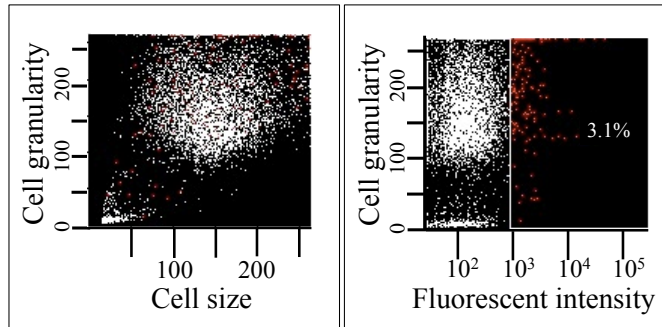
### GENISTEIN



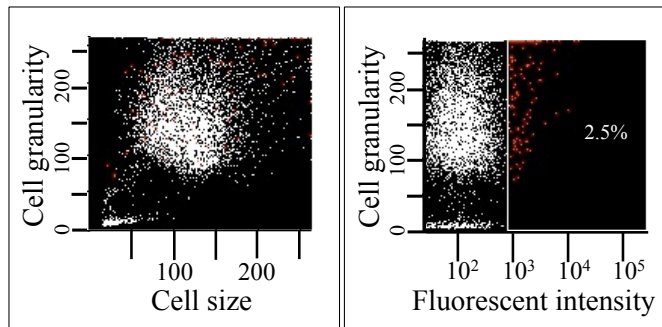
### DYNASORE



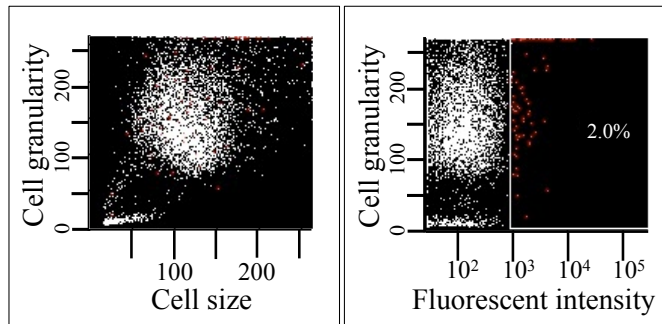
### CYTOCHALASIN D



### IPA-3



### BAFILOMYCIN A1



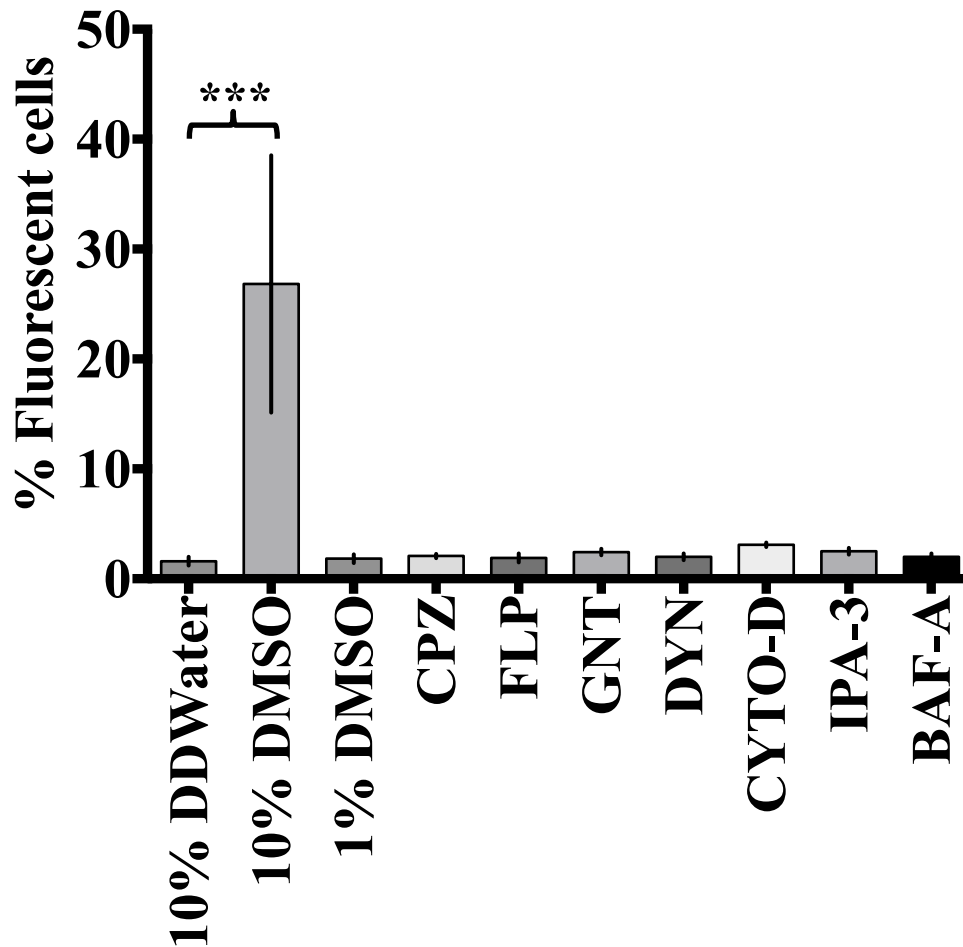
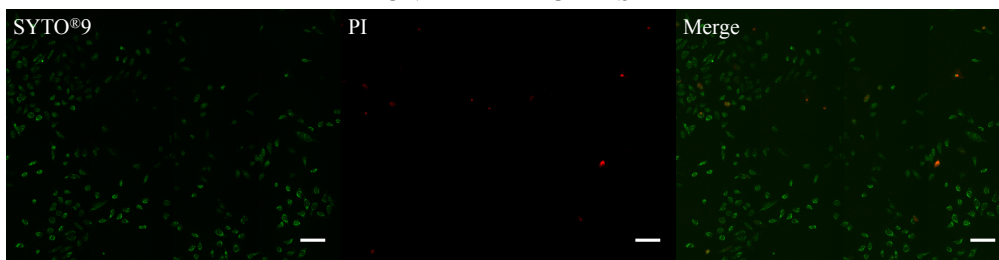


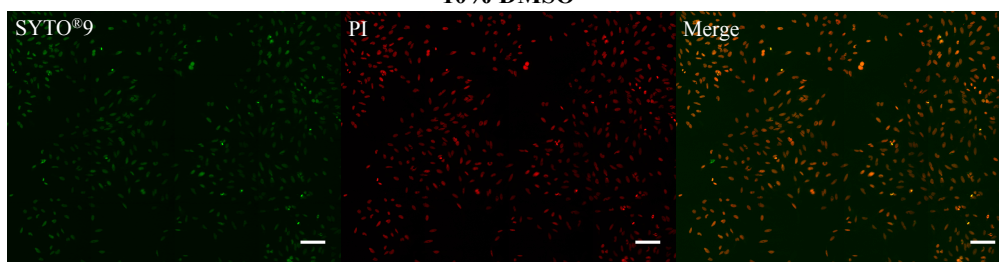
**Figure 6.2: Live-Dead experiments I. Flow cytometry**

The plasma membrane integrity of HeLa cells incubated with endocytic inhibitors was investigated using propidium iodide. Following incubation with inhibitors, cells were incubated with the red-fluorescent dye and the percentage of fluorescent cells (cells with a compromised plasma membrane) was explored by flow cytometry. Cells incubated with DMSO or ultrapure water were used as positive and negative controls for membrane damage. Dot plots on the left represent the cell population analysed, for each treatment, in terms of size (forward scatter) and granularity (side scatter). Dot plots on the right display cells with fluorescence over the threshold (red dots). Graphs correspond to 1 (of 3) experiment performed. The percentage shown in the graphs is the average fluorescent cell population from 3 independent experiments. Bar chart on the bottom summarises the data from the 3 experiments performed for each condition. Error bars:  $\pm$  sem. Statistical analysis: one-way ANOVA plus Bonferroni.  $p < 0.001$  (\*\*\*)

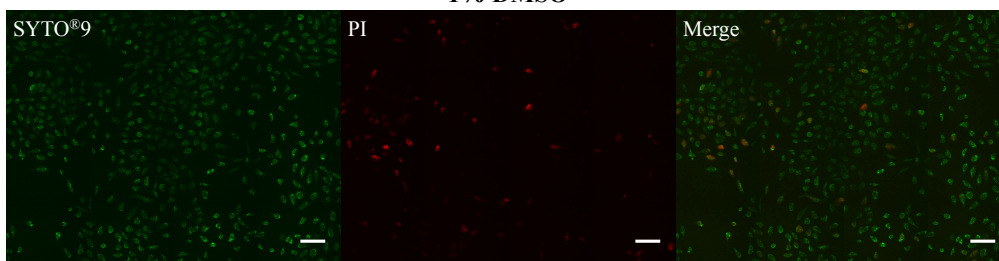
**UNTREATED CELLS**



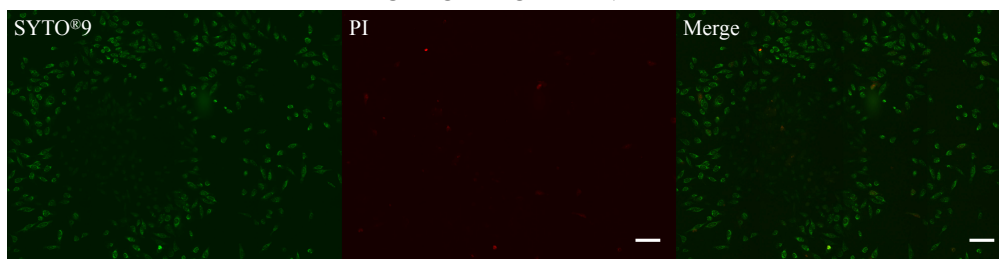
**10% DMSO**



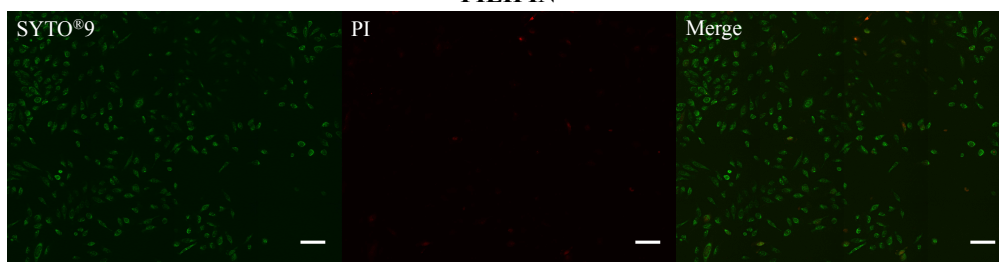
**1% DMSO**



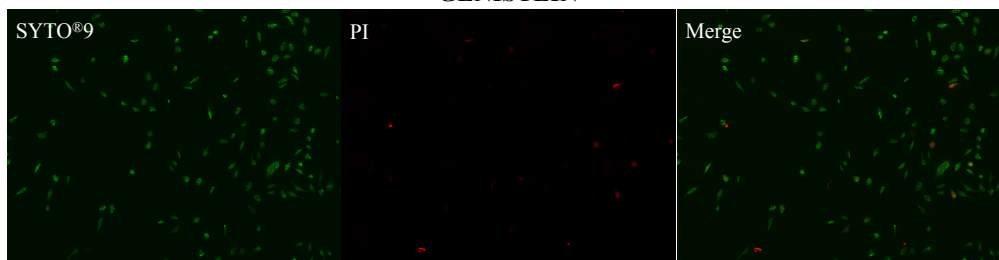
**CHLORPROMAZINE**



**FILIPIN**



**GENISTEIN**



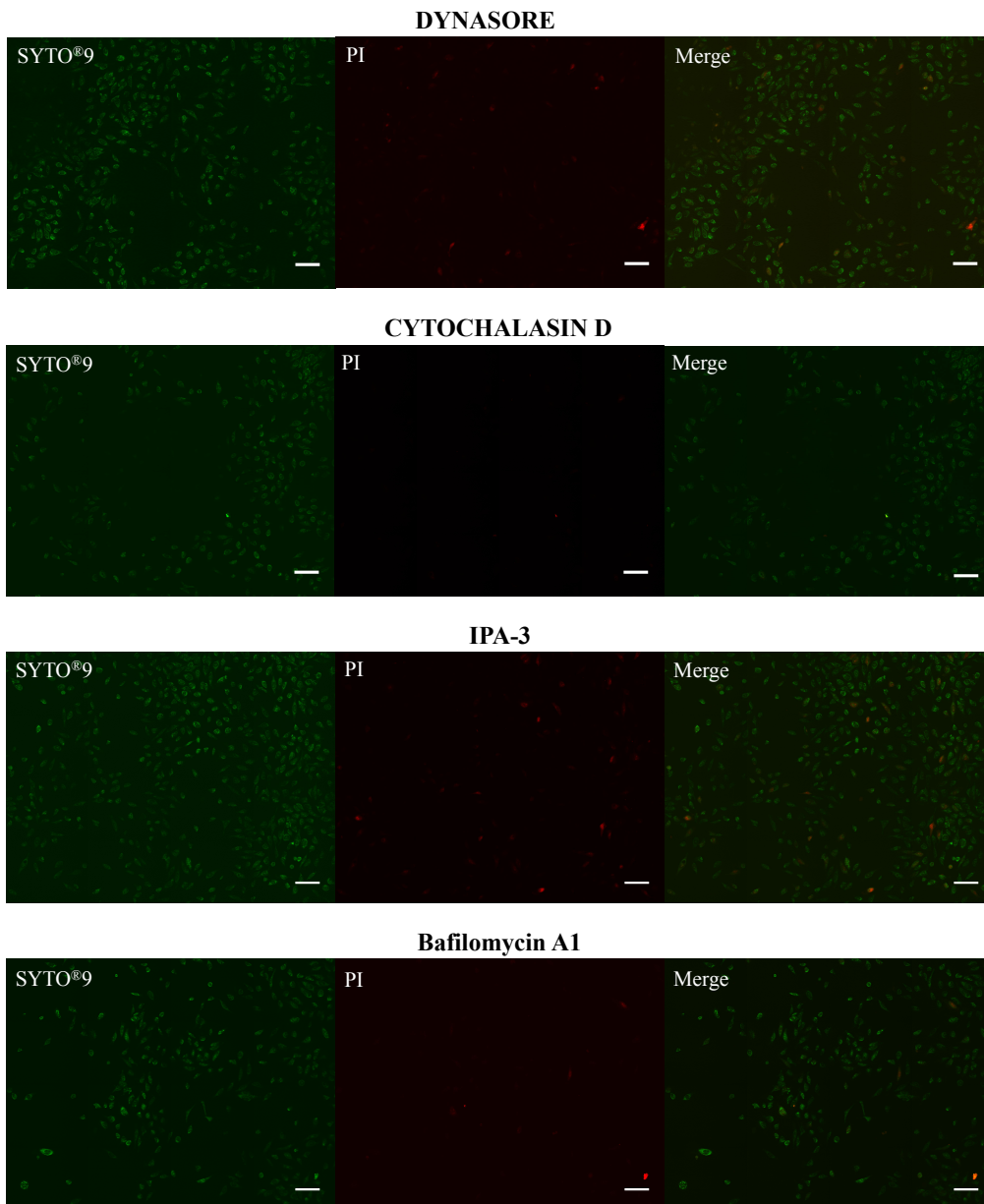


**Figure 6.3: Live-Dead experiments II. Fluorescence microscopy**

The plasma membrane integrity of HeLa cells incubated with endocytic inhibitors was investigated using propidium iodide and SYTO<sup>®</sup> 9. Following incubation with inhibitors, cells were incubated with the nucleic acids stain for 10 minutes before being imaged in a BD Pathway 855 spinning disk confocal using a 20X lens. Cells incubated with DMSO or ultrapure water were used as positive and negative controls for membrane damage. Representative images from 1 of the 3 experiments performed for each inhibitor are shown. Scale bars: 100  $\mu$ M.



### 6.2.1.2. Final screen

The final incubation conditions for the use of each chemical inhibitor were sometimes milder than the ones reported in the literature, since the practice to check the toxicity induced by these compounds, before using them to inhibit the endocytosis of a cargo, has not been very common in the past. Because of the inhibition produced by most of these agents is reversible<sup>256,266,272,273</sup>, they should be also present in the media during the incubation with polymersomes. The final layout of the screen, including inhibitors concentrations and incubation times is shown in table 6.3.

Control molecules, representative of different endocytic pathways, were selected to analyse their uptake, in parallel to polymersomes, in the presence of the inhibitors. Transferrin is considered a specific marker for clathrin-mediated endocytosis<sup>274</sup>. On the other hand, cholera toxin (CTxB) has been traditionally considered a marker for caveolae-mediated endocytosis<sup>275</sup>. However, recent studies suggest that this toxin may not be internalised by a canonical caveolae route. The internalisation path followed by CTxB could be more accurately defined as dependent on lipid rafts at the surface of the plasma membrane<sup>276,277</sup>, cholesterol dependent<sup>276,278</sup> and caveolae-independent but caveolin-1 regulated<sup>278,279</sup>. Finally, dextrans of the correct molecular weight are suitable markers for macropinocytosis the other major ubiquitous endocytic pathway identified to date. Dextrans are also considered markers for fluid phase endocytosis. Therefore, AlexaFluor<sup>®</sup> 647 conjugates of transferrin (5 µg/ml), cholera toxin subunit B (10 µg/ml) and 10kDa dextran (0.1 mg/ml) were used as control molecules in the present study.

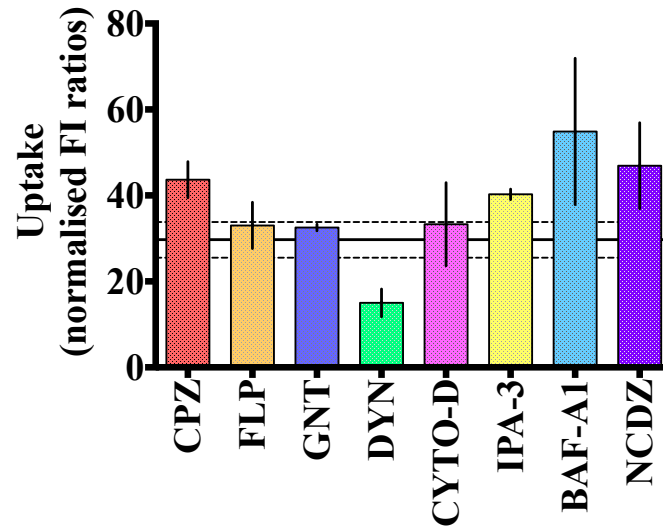
The results from the screen are shown in figure 6.4. Briefly, the cells were pre-incubated during 15 minutes with the inhibitors before addition of either rhodamine-labelled PMPC-PDPA polymersomes (0.2 mg/ml) or control molecules. Incubation was maintained for another 20 minutes without removing the inhibitors from the media. Afterwards, the media was aspirated and cells were thoroughly washed twice with PBS before being processed for flow cytometry.

<b>Inhibitor</b>	<b>Pre-incubation (15 minutes)</b>	<b>Incubation (20 minutes)</b>
Chlorpromazine	20 $\mu$ M	10 $\mu$ M
Filipin	10 $\mu$ M	5 $\mu$ M
Genistein	100 $\mu$ M	50 $\mu$ M
Dynasore	100 $\mu$ M	50 $\mu$ M
Nocodazole	66 $\mu$ M	33 $\mu$ M
Cytochalasin D	2 $\mu$ M	1 $\mu$ M
1,1'-Disulfanediyldinaphthalen-2-ol (IPA-3)	20 $\mu$ M	10 $\mu$ M
Bafilomycin A1	0.02 $\mu$ M	0.01 $\mu$ M

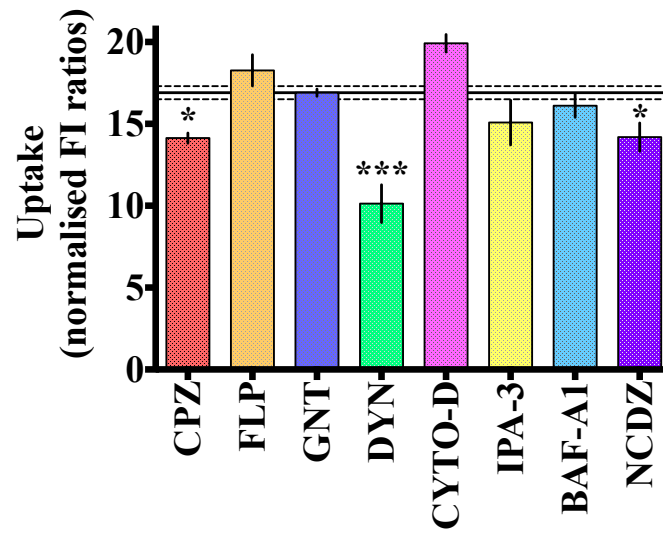
**Table 6.3: Selected inhibitors and their associated incubation conditions (concentration and time) to investigate the mechanism of PMPC-PDPA polymersome endocytosis in HeLa cells**

Cells will be pre-incubated with the indicated inhibitor concentrations for 15 minutes before the addition of polymersomes or control cargoes for different endocytic pathways. Incubation with polymersomes or controls was maintained for 20 minutes, in the presence of the inhibitors, at the listed concentrations.

**a POLYMERSOMES UPTAKE**



**b TRANSFERRIN UPTAKE**



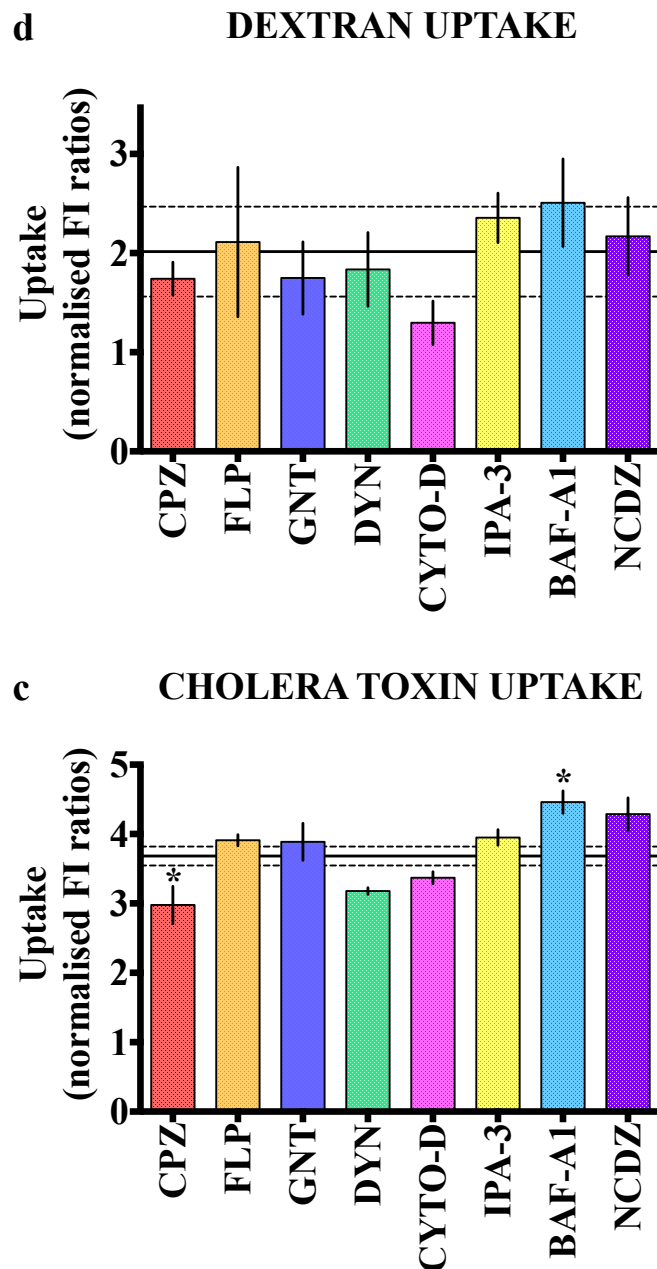


**Figure 6.4: Uptake of PMPC-PDPA polymersomes, transferrin, cholera toxin subunit B and dextran in the presence of inhibitors of endocytosis in HeLa cells**

Fluorescent intensity values normalised to control cells (cells incubated with PBS instead of inhibitors) of HeLa cells incubated with rhodamine-labelled polymersomes (200  $\mu\text{g}$ , **a**), or AlexaFluor<sup>®</sup> 647 conjugates of transferrin (8  $\mu\text{g}$ , **b**), cholera toxin subunit b (16  $\mu\text{g}$ , **c**) and 10 kDa dextran (100  $\mu\text{g}$ , **d**) in the presence of inhibitors of endocytosis. Cells were pre-incubated with the inhibitors for 15 minutes before being incubated with polymersomes or control cargoes for 20 minutes (in the presence of the inhibitors). Cells were analysed by flow cytometry.  $n=3$  experiments. Error bars:  $\pm\text{sem}$ . Control cells are represented by a black continuous line with its associated errors (dashed lines). Statistical analysis: one-way ANOVA plus Bonferroni.  $p < 0.05$  (\*),  $p < 0.001$  (\*\*\*)

## 6.2.2 Role of dynamin in PMPC-PDPA polymersome internalisation

According to the results presented in the previous section, none of the endocytic inhibitors used produced a statistically significant difference in polymersome uptake. Nonetheless, impairing the normal function of dynamin using the inhibitor dynasore showed a trend towards reduced polymersome uptake in HeLa cells. Consequently, I decided to investigate further the role of dynamin in PMPC-PDPA polymersome internalisation. In order to do that, I examined polymersome uptake in cells transiently transfected with a dominant negative dynamin. Dynamin K44A is a mutant form of the protein dynamin (dynamin 1) impaired in its ability to bind GTP. The mutation is localised in the Lysine 44 of the G1 region, in the GTPase domain. It has been demonstrated that efficient binding and hydrolysis of GTP are essential for dynamin-dependent endocytosis<sup>280</sup>.

HeLa cells were transfected with either wild type dynamin (WT) or mutant K44A dynamin (K44A) cDNA constructs inserted in a cytomegalovirus expression vector, using TurboFect<sup>TM</sup> for 8 hours. Afterwards, transfected cells were incubated with CellLuminate<sup>®</sup> (PMPC-PDPA polymersomes encapsulating rhodamine B octadecyl ester perchlorate) for one hour and imaged by confocal microscopy. In a parallel experiment transfected cells were incubated for 20 minutes with AlexaFluor<sup>®</sup>647 transferrin. Transferrin endocytosis is dynamin-dependent and the use of dynamin K44A has been previously demonstrated to reduce transferrin internalisation<sup>72,281</sup>. Due to the presence of a reporter gene encoded in the cDNA used for the transfection, transfected cells are fluorescent in blue and therefore, they can be identified under the microscope. Confocal micrographs displaying the extent of polymersome and transferrin internalisation in transfected cells are presented in figure 6.5.

The effect of the expression of a dominant negative dynamin in polymersome endocytosis was also investigated in FaDu cells. Following overnight transfection with Lipofectamine<sup>®</sup>2000, cells were incubated with rhodamine-labelled polymersomes for 1 hour and analysed by flow cytometry. In figure 6.6.a representative dot plots obtained by flow cytometry are shown. Using the appropriate gating I could segregate transfected cells (blue fluorescent cells) from untransfected ones, and investigate polymersome internalisation only in the former group. As figure 6.5.b shows there was no reduced

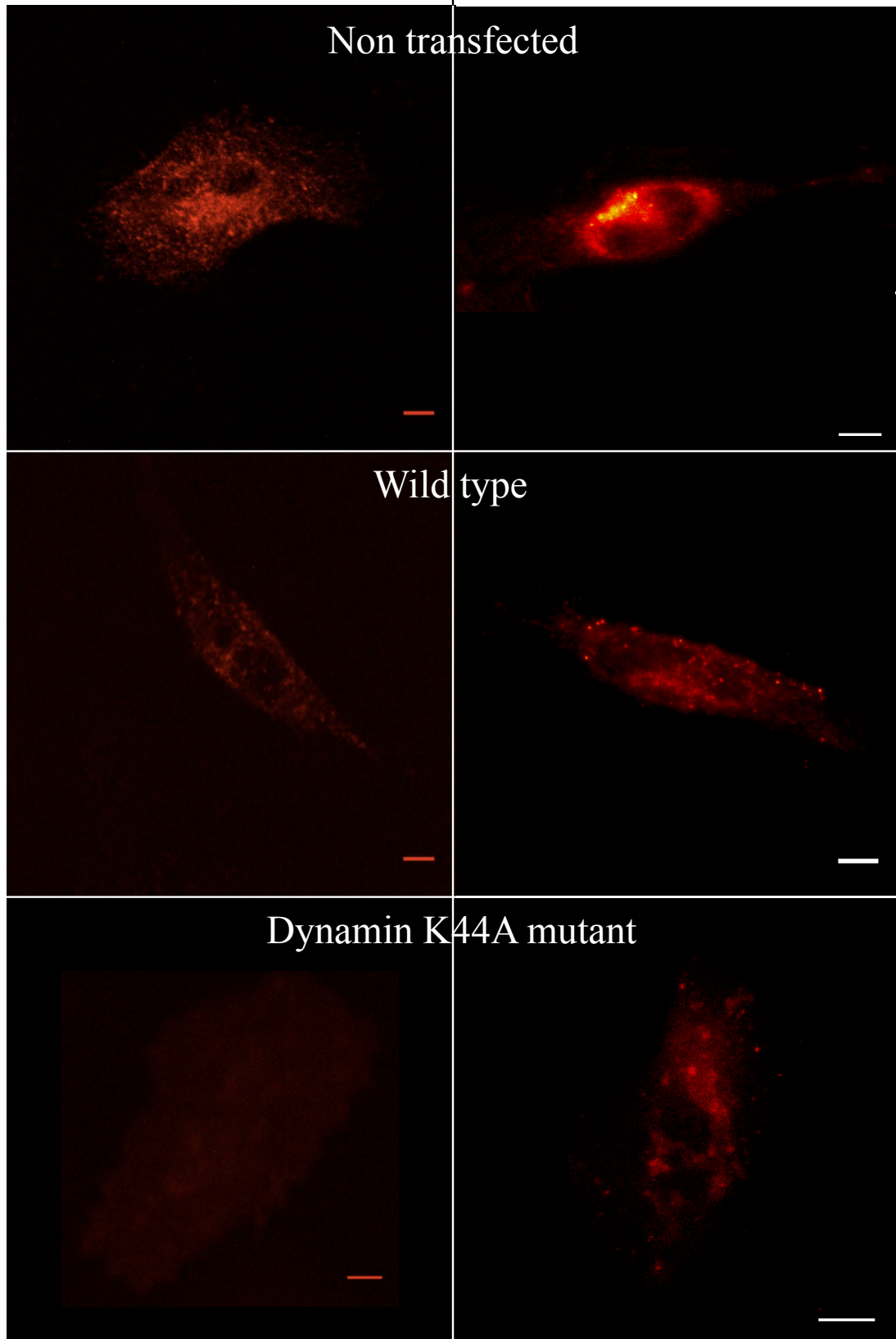
polymersome uptake in cells expressing dynamin K44A compared with WT cells. Unfortunately, it was not possible to verify the flow cytometry results by using fluorescence microscopy in FaDu cells due to technical difficulties. As noticed by flow cytometry, the transfection efficiency in FaDu cells was generally low ( $16 \pm 3.9$  for WT cells and  $12 \pm 2.4$  for K44A mutant cells), even though I tried to improve it by using two different vectors, Lipofectamine<sup>®</sup>2000 and TurboFect<sup>™</sup>, and a range of diverse experimental settings for each of them. In addition, I noticed that FaDu cells adhered with difficulty to dishes or slides for microscopy following transfection with Lipofectamine<sup>®</sup>2000 and TurboFect<sup>™</sup>. While FaDus grew very well in polystyrene tissue cultured 24 well plates, they did not attach to Ibidi<sup>®</sup> untreated glass bottom  $\mu$ -dishes neither to Ibidi<sup>®</sup>  $\mu$ -slides with plastic bottom. I then coated the surface of these dishes to improve cellular attachment but FaDus grew with an unusual morphology when cultured in poly-L-Lysine incubated  $\mu$ -dishes and collagen incubated  $\mu$ -dishes. Finally, I discovered that they attach to, and grow normally in Ibidi<sup>®</sup> tissue culture incubated  $\mu$ -dishes, which are compatible with high-resolution microscopy. Nevertheless, transfected FaDu were extremely photosensitive and developed very fast and intense phototoxicity after excitation with the 405 laser, which ultimately made it impossible to obtain quality confocal micrographs during the course of this thesis.

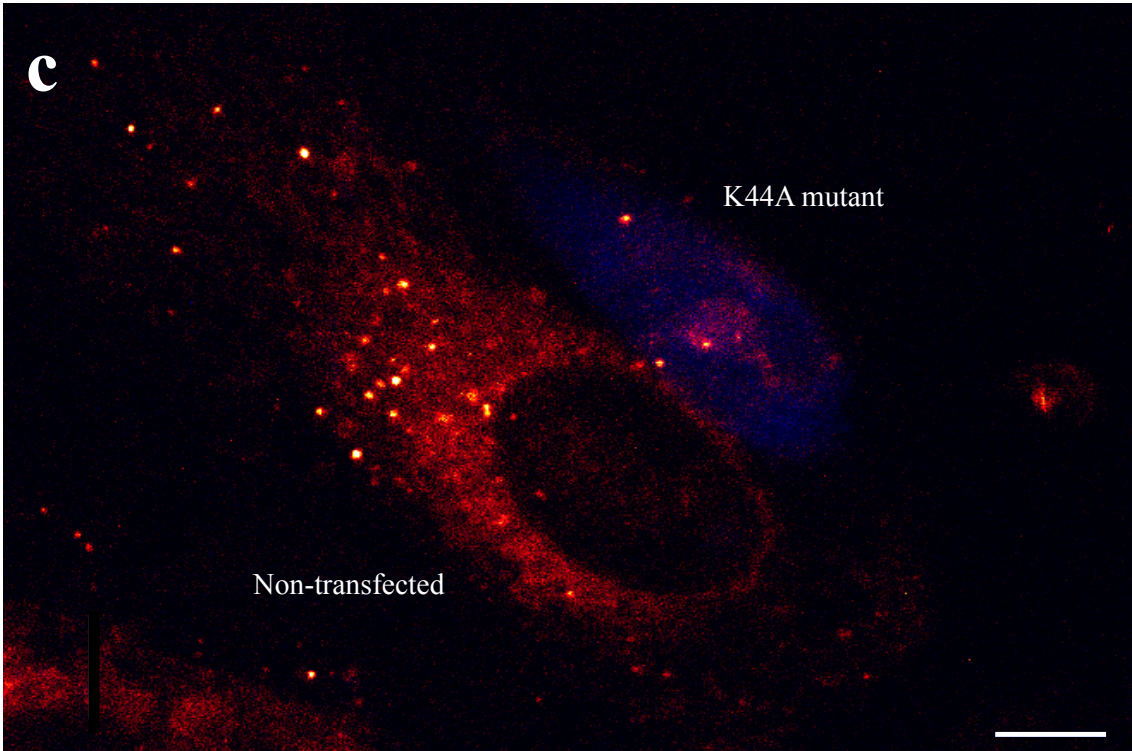
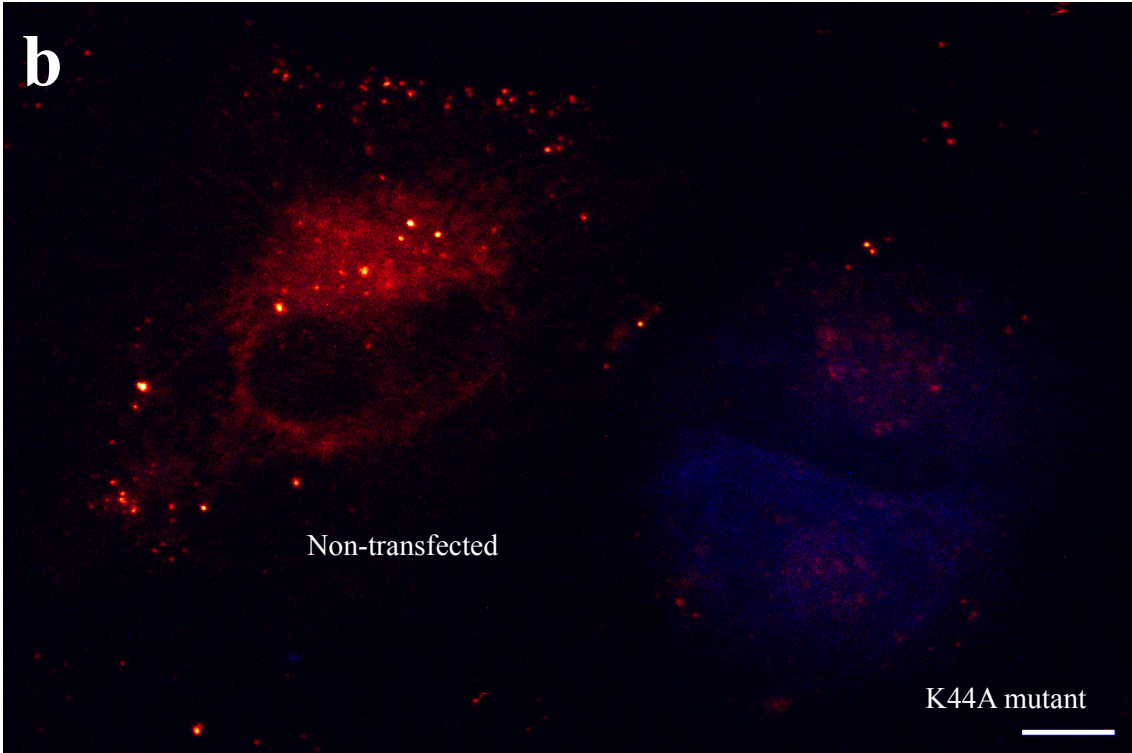
To summarise, the experiments conducted in this section showed that polymersome uptake was not significantly inhibited in cells where dynamin-dependent endocytosis was severely impaired due to the overexpression of the mutant K44A dynamin (K44A) compared with cells where dynamin-assisted internalisation was almost 100% operative (WT dynamin). This was more evident for FaDu cells (figure 6.5) than for HeLa cells. Although there was a reduction in polymersome uptake between WT and K44A dynamin HeLa cells (figure 6.4.a), the quantitative analysis of the micrographs indicated that it was minimal (figure 6.4.d). A more noticeable reduction was observed between dynamin K44A cells and non-transfected HeLas (figures 6.4.b-d). Nonetheless, it has been previously reported that cells overexpressing wild type dynamin present a reduced transferrin endocytosis compared to non-transfected cells<sup>281</sup>, something that we also qualitatively perceived (figure 6.4.a).

**a**

AlexaFluor®647  
Transferrin

Polymersomes  
encapsulating rhodamine







<b>d</b> INTENSITY PARAMETERS FROM MICROSCOPY ANALYSIS (POLYMERSOMES CHANNEL)						
Cell type	N	Min.	Max.	Median	Mode	Integrated density
Non-transfected	5	123 ± 67	596 ± 163	147 ± 72	139 ± 73	428.870
WT dynamin	3	115 ± 4	360 ± 130	146 ± 8.5	133 ± 4	152.289
K44A dynamin	5	73 ± 98	329 ± 43	98 ± 95	91 ± 99	107.896

**Figure 6.5: Polymersomes and transferrin uptake in mutant K44A dynamin HeLa cells**  
Cells expressing a dominant negative form of dynamin (K44A) were incubated either with PMPC-PDPA polymersomes encapsulating rhodamine B octadecyl ester perchlorate (CellLuminate<sup>®</sup>) (1 mg/ml, 1 hour) or with AlexaFluor<sup>®</sup> 647 transferrin (25 µg/ml, 20 minutes). Non-transfected cells and cells transfected with wild type dynamin were also incubated with the cargoes and used as controls. Cells were imaged in a Zeiss LSM510 Meta inverted confocal microscope using a 60X oil immersion lens. Transfected cells, encoding a blue fluorescent reporter gene, were identified using a 405 nm laser. **a)** Confocal micrographs displaying uptake of transferrin (left column) or polymersomes encapsulating a fluorescent dye (right column) in non-transfected cells, cells transfected with WT dynamin and cells transfected with mutant K44A dynamin. All cells shown in the *wild type* and *dynamin K44A mutant* panels were positive for expression of the blue fluorescent reporter. The blue channel has been omitted for clarity. Scales bars: 10 µM. **b-c)** Confocal pictures showing uptake of rhodamine-encapsulated polymersomes in adjacent cells. In both pictures, cells represented in blue are cells that express K44A dynamin. In both pictures, cells that are not represented in blue correspond to non-transfected cells. Non-transfected cells express only endogenous dynamin. Scale bars: 10 µM. **d)** Intensity parameters obtained from the analysis of confocal micrographs using ImageJ 1.48q software. N: number of cells analysed in each group. Min.&Max.: minimum and maximum grey values. Median: median grey value. Mode (mode grey value): most frequently occurring grey value. Integrated density: the sum of the values of the pixels.

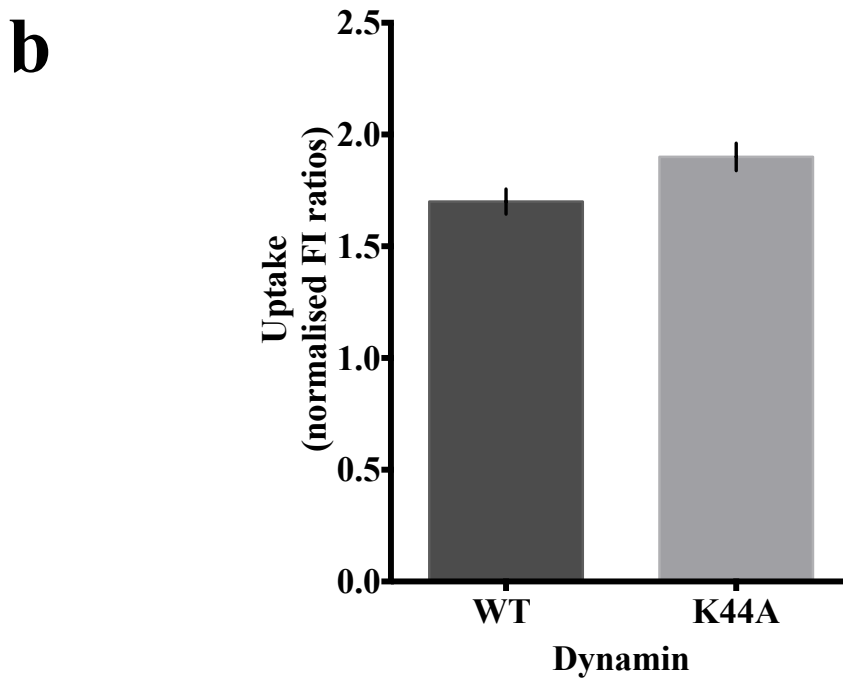
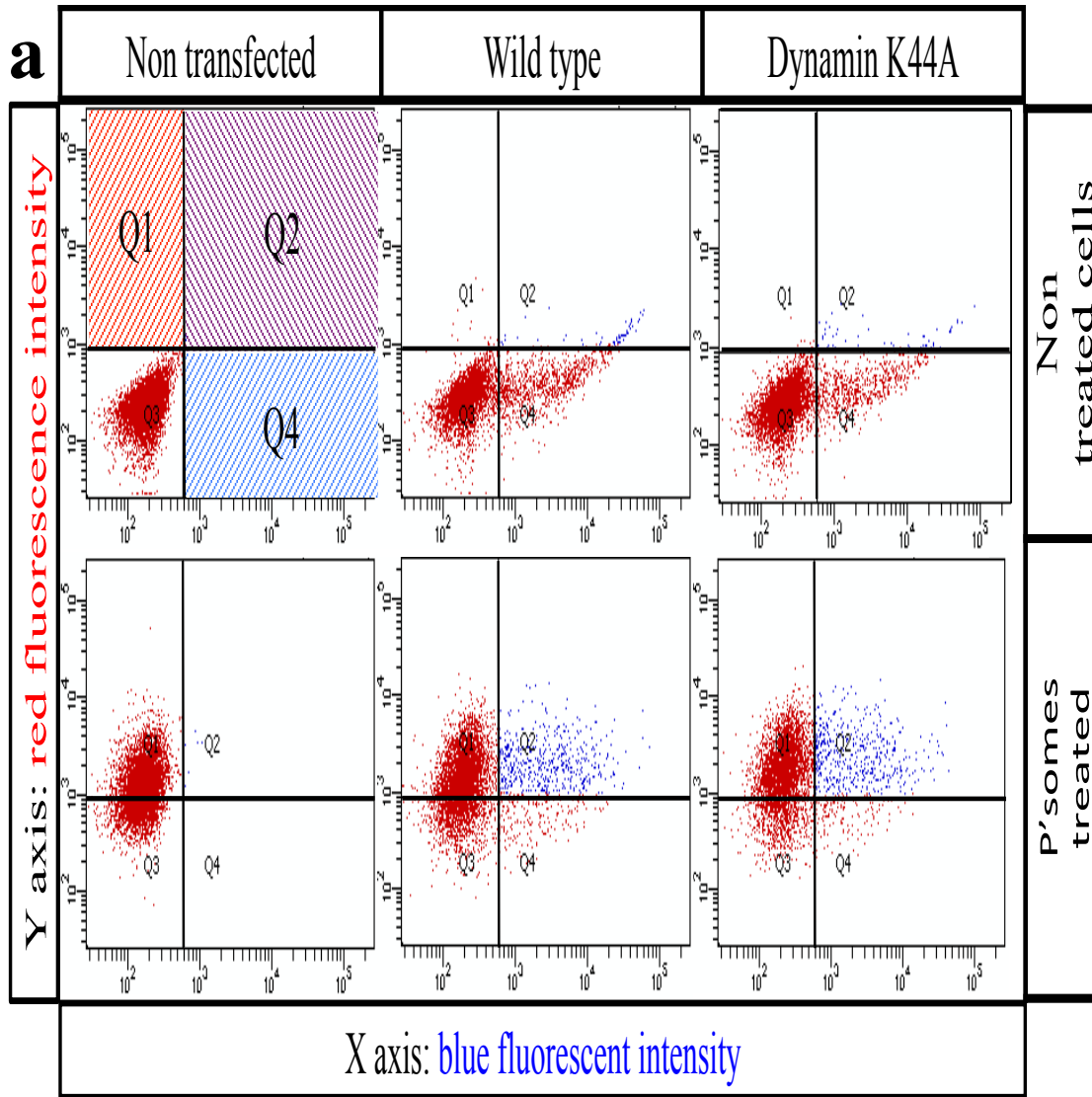


**Figure 6.6: Polymersome uptake in FaDu cells expressing mutant K44A dynamin**

FaDus transfected with mutant K44A dynamin cDNA were incubated with rhodamine-labelled PMPC-PDPA polymersomes (1mg/ml, 1 hour). Non-transfected cells and cells transfected with wild type dynamin were used as controls. Following treatment, cells were analysed by flow cytometry using a 405 laser to investigate the presence of transfected cells (fluorescent blue reporter gene encoded in the cDNA) and a 488 nm laser to assess cellular uptake of fluorescent polymersomes. a) Examples of flow cytometry plots obtained. Transfected cells are fluorescent in blue (X axis), cells positive for polymersome internalisation are fluorescent in red (Y axis). Therefore, transfected cells that have interacted with polymersomes are displayed in Q2, transfected cells that do not uptake polymersomes fall within Q4, and uptake of polymersome in non-transfected cells is represented in Q1. b) Median fluorescent intensities normalized to control cells (cells not incubated with polymersomes) obtained by flow cytometry for transfected FaDus after incubation with fluorescent polymersomes. n=3 experiments. Error bars:  $\pm$  sem.

### **5.2.3 BAR domain proteins in PMPC-PDPA polymersome internalisation. siRNA screening in Drosophila cells**

BAR domain proteins currently attract great attention in the field of endocytosis. Proteins belonging to this super family contain a BAR domain within their structure that allow them to sense and/or induce membrane curvature and therefore we were very interested to study them in relation with PMPC-PDPA polymersome internalisation. Since polymersomes are highly curved nanoparticles and the curvature of the system influences its uptake, as previously shown in chapter 4, we hypothesise that BAR domain proteins could play an important role in PMPC-PDPA polymersome endocytosis. To test this hypothesis we took advantage of the Drosophila siRNA screening facilities at The University of Sheffield. A small screen, comprising 19 Drosophila genes that are homologues of human genes coding for BAR domain proteins implicated in endocytosis and cellular trafficking, was designed. The screen was completed with another 13 genes coding for diverse proteins related to endocytosis in mammalian cells such as clathrin, protein kinase D, epsin, actin, and the identified PMPC-PDPA polymersomes receptors CD81 and SR-BI. All the Drosophila genes screened, their human homologues and associated human proteins are listed in table 6.4. Our aim with this experimental set up was to exploit the high susceptibility of SR2<sup>+</sup> Drosophila cells to gene inhibition by siRNA, to investigate polymersome uptake in Drosophila cells defective in a specific protein related to cellular trafficking, as a way to identify potential proteins regulating polymersome endocytosis in mammalian cells. Any hits from this screen would be further verified in a secondary screen in mammalian cells.

According to the standard protocol in the screening facility, SR2<sup>+</sup> cells were seeded in multiwell plates containing 0.25 µg of siRNA per well that is passively incorporated into the cells and depletes the expression of the targeted protein over a period of 3 days. Transfected cells were then incubated with 5 µg of rhodamine-labelled polymersomes for 1 hour before being fixed and imaged in a widefield high-content screening microscope (example of images obtained in figure 6.7). A high-content cellular imaging software (MetaXpress<sup>®</sup>) was used to process the images obtained. The software was set up to recognise individual cells within a micrograph and to quantify the rhodamine fluorescence associated with them.

The percentage of fluorescent cells and the fluorescent intensity values retrieved by the software were first used to investigate whether the transfection by itself has an effect on polymersome uptake. As figure 6.8 shows, around 50% of the cells in both groups, non-transfected and transfected with non-targeting siRNA, have become fluorescent after 1 hour incubation with polymersomes, although mean fluorescent intensity associated with transfected cells was slightly higher.

I next examined polymersome uptake in knockdown cells. The average cellular fluorescent intensity ( $\pm$  SD) for each transfection condition compared to control cells (cells transfected with non-targeting siRNA) is plotted in figure 6.9.a. Knockdown cells falling within the variability range of control cells were considered not to present a distorted polymersome uptake. As a consequence, cells above or below this threshold presented an enhanced/inhibited polymersome endocytosis. A secondary threshold, arbitrarily defined as control cells SD  $\pm$  5, was implemented in order to differentiate between genes that affect polymersomes endocytosis at a low extent and those that influence polymersome internalisation at a higher level.

The same data (average fluorescent intensity) was re-analysed and represented according to published methods for hit selection in RNAi high-throughput screens<sup>282</sup> (figures 6.9.b-c). A dual-flashlight chart was used to present at the same time, biological meaningful data (difference between the mean fluorescent intensity obtained for knockdown and control cells) and statistical information (SSDM). According to the guidelines provided in the literature<sup>282</sup>, and taking into account that my experimental design includes an average of 9 technical replicates for each gene, I use the following formula to calculate the strictly standardised mean difference (SSDM):

*Equation 4*

$$\frac{\bar{X}_i - \bar{X}_N}{\sqrt{s_i^2 + s_N^2}}$$

Where  $X_i$  is the mean fluorescent intensity from the replicates of the genes and  $X_N$  is the mean fluorescent intensity from the replicates of the control cells.  $S_i$  and  $S_N$  correspond to the standard deviations of the genes and the control replicates, respectively.

Genes with a fold change larger than  $\pm 10$  and a SSDM superior to  $\pm 1$  would be considered to code for proteins that are implicated in polymersome uptake in *Drosophila* cells (figure 6.9.b-c).

In general, polymersome uptake was reduced in cells lacking any of the genes studied except for Sar1 knockdown cells (gene 25), where the high variability across the repeated measurements was big enough to overshadow a biological effect. Polymersome uptake was specially reduced in cells missing Lfq (gene 21) and CG42388 (gene 19) genes, which correspond to the human proteins epsin and nostrin, respectively. Epsin is a protein with membrane-bending capacity that facilitates the formation of clathrin-coated invaginations through direct interaction with clathrin<sup>283</sup>. Nostrin is a peripheral cytoplasmic protein that functions as an adaptor of caveolin-1 and directly interacts with dynamin<sup>284</sup>. In addition, according to the strong inhibition observed after knockdown, the following proteins could be also assisting polymersome endocytosis in mammalian cells: Rho GTPase activating protein 10 (gene 13), which activates RhoA and Cdc42 (related to clathrin and caveolae-independent endocytosis), tetraspanin CD81 (gene 18), protein kinase D (gene 11) that is involved in many receptor-mediated signal transduction pathways<sup>285</sup>, sortin nexins 1, 2, 5 and 6 (gene 9) BAR domain proteins facilitating protein sorting, centaurin- $\gamma$ -2 (gene15) a GTPase activating protein of ARF1, which in turn is related to dynamin-independent endocytosis and the endo-lysosomal traffic of proteins through CME, and finally centaurin 1 (gene20) that interacts with protein kinase D.

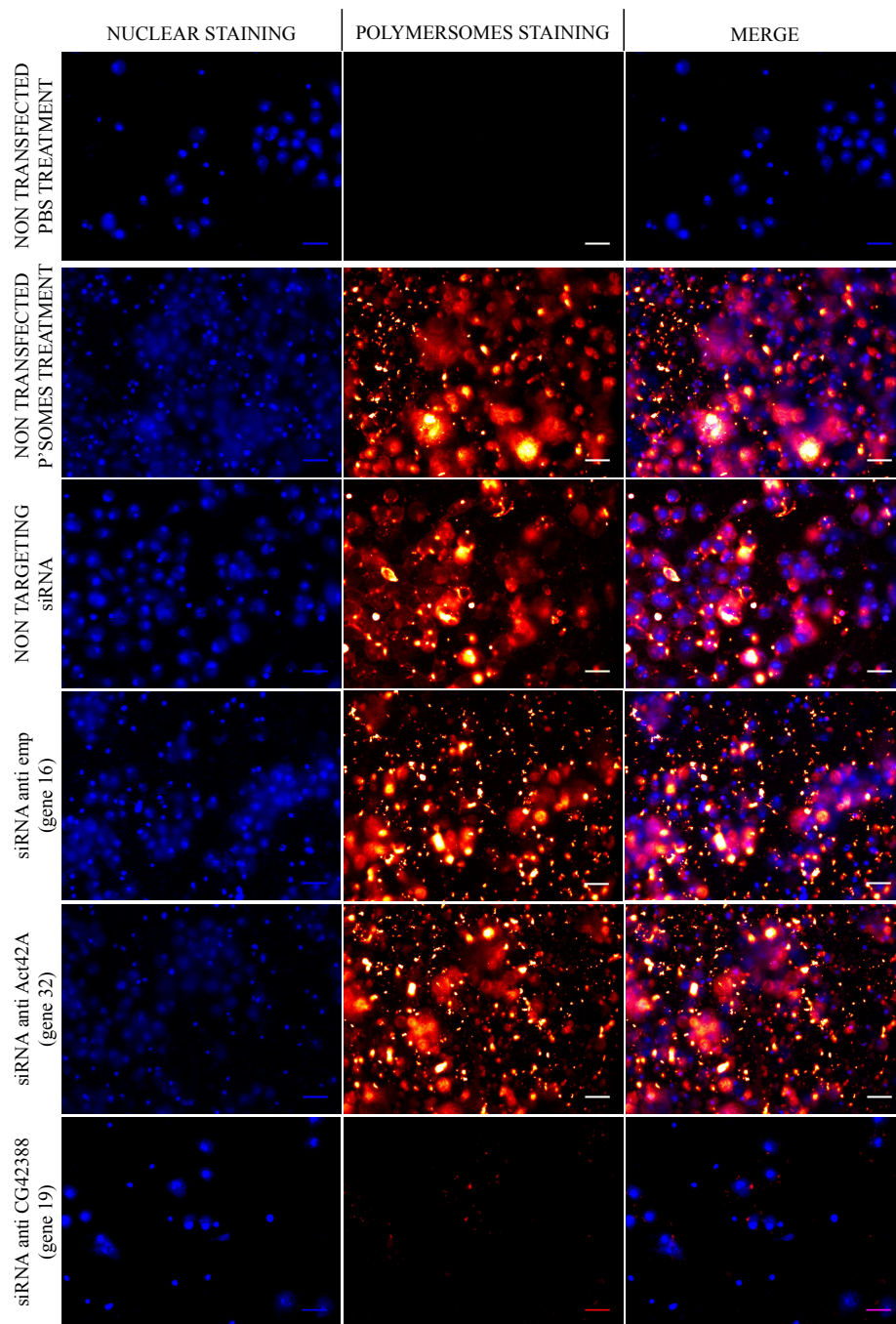
<b>Gene Number</b>	<b>Drosophila Gene</b>	<b>Human Homologue Gene</b>	<b>Human Protein</b>
1	emp (CG2727)	SCARB1	SR-BI
2*	CG8176	FCHo1, FCHo2	FCH domain only, proteins 1 and 2
3*	H3PX1/SH3PX1 (CG6757)	SNX 9, SNX 18	Sortin Nexins
4	Chc (CG9012)	CLTC	Clathrin
5*	CG32082	IRSp53/BAIAP2L2	BAI1-associated protein 2-like 2
6	Arf79F (CG8385)	ARF1	ADP-ribosylation factor 1 (ARF1)
7	nwk (CG43479)	FCHSD2/NWK, FCHSD1/NWK2	FCH and double SH3 domains proteins 1 and 2
8*	Cip4 (CG15015)	FNBP1L/TOCA-1	Formin-binding protein 1-like
9*	Snx6 (CG8282)	SNX 1 SNX 2 SNX 5 SNX 6	Sortin Nexins
10*	Appl (CG7727)	APPL2	Adaptor protein, phosphotyrosine interaction, PH domain and leucine zipper containing 2
11	PKD (CG7125)	PRKD1	Protein Kinase D
12*	Asap1 (CG30372)	ASAP2	Arf-GAP with SH3 domain, ANK repeat and PH domain containing-protein 2
13*	Graf (CG8948)	GRAF2	Rho GTPase activating protein 10
14*	CG17184	ARFIP1 ARFIP2	Arfaptin 1 (ADP-ribosylation factor interacting proteins 1 and 2)
15	cenG1A (CG31811)	AGAP1	Centaurin gamma 2 (Arf-GAP with GTPase, ANK repeat and PH domain- containing protein 1)
16	santa-maria (CG12789)	SCARB1	SR-BI
17*	mim (CG33558)	MTSS1L/ ABBA-1	Metastasis suppressor 1-like protein
18	Tsp96F (CG6120)	CD81	CD81
19*	CG42388	NOSTRIN	Nostrin
20*	CG8243	ADAP1	Centaurin 1 (Arf-GAP with dual PH domains containing protein 1)
21	Lfq (CG8532)	EPN1	Epsin

Gene Number	Drosophila Gene	Human Homologue Gene	Human Protein
22*	endoA (CG14296)	SH3GL2 SH3GL1 SH3GL3	Endophilins 1,2,3
23*	cenB1A (CG6742)	ACAP3	Arf-GAP with coiled-coil, ANK repeat and PH domains 3
24*	Amph (CG8604)	AMPH/BIN1	Amphiphysin
25*	Sar1 (CG7073)	Sar1A	GTP-binding protein SAR1a
26*	alphaTub84B (CG1913)	DNMBP/ TUBA	Dynamin binding protein
27	Act5C (CG4027)	ACTC1	Actin
28*	Synd (CG33094)	PACSIN1	Pacsin/ Syndapin
29	CG6120	CD81	CD81
30*	CG6167	PICK1	PRKCA-binding protein (protein interacting with C kinase 1)
31	lap (CG2520)	SNAP91	Clathrin coat assembly protein AP180
32	Act42A (CG12051)	ACTC1	Actin

**Table 6.4: Genes related to endocytosis and cellular trafficking investigated in a siRNA screening in SR2+ Drosophila cells**

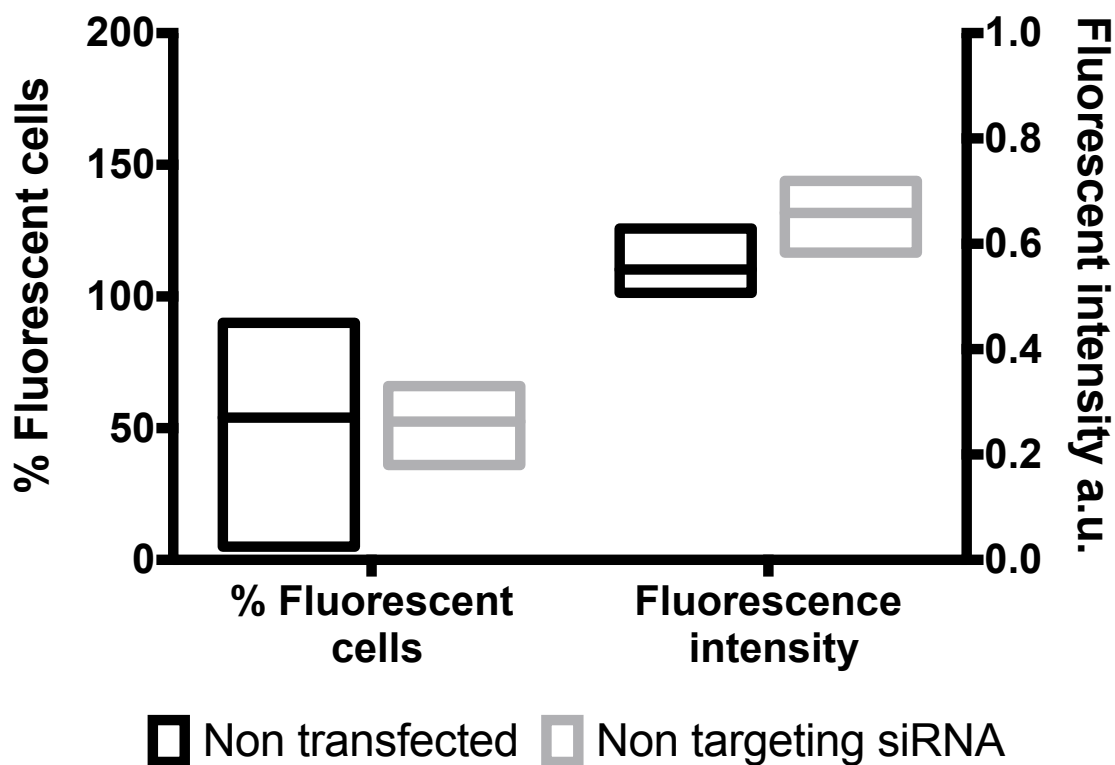
Drosophila genes knocked down, together with the identification number used in the screen, the human homologue gene and the corresponding human protein for each of them. \* Denotes BAR domain protein.





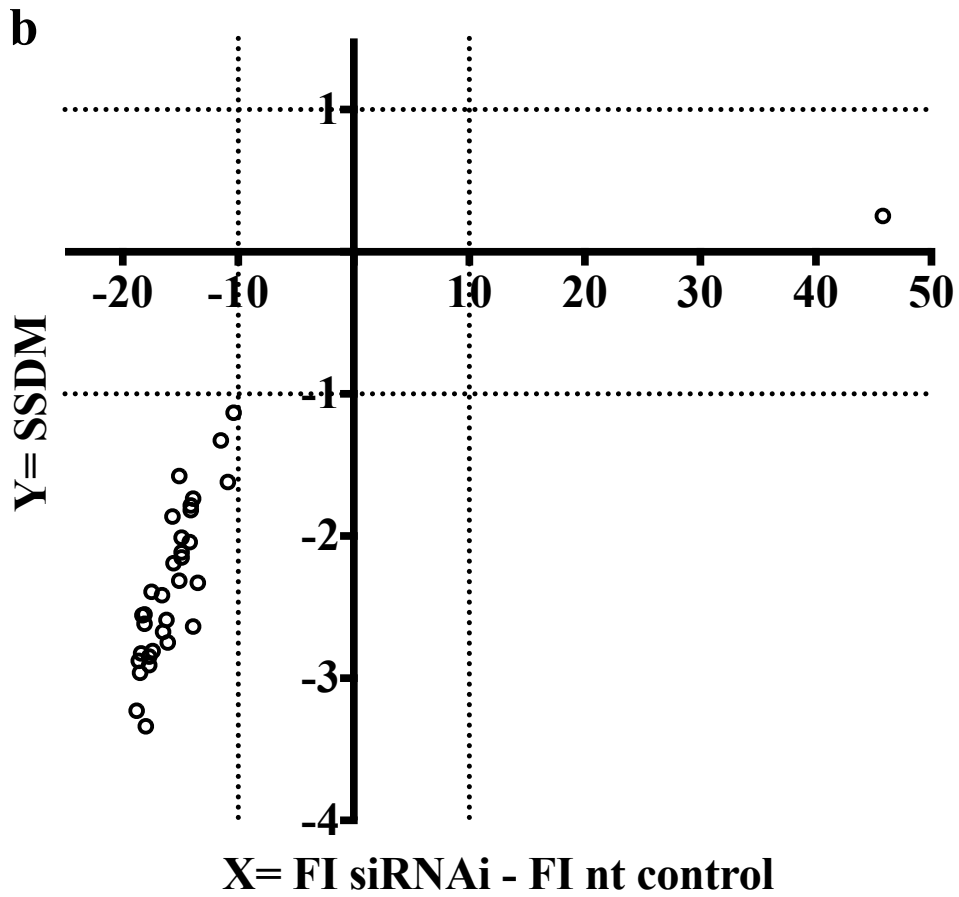
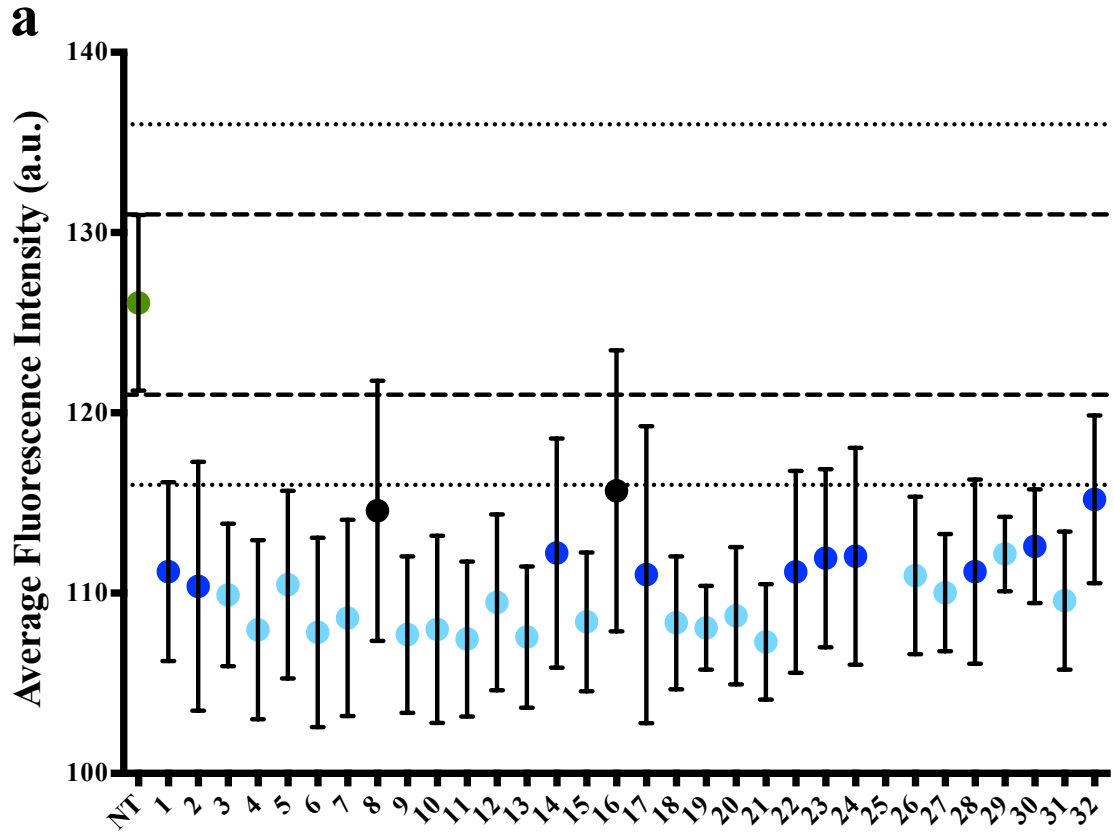
**Figure 6.7: Uptake of PMPC-PDPA polymersomes in knockdown SR2+ Drosophila cells. Fluorescent micrographs examples**

Interaction of rhodamine-labelled polymersomes with Drosophila cells where gene 32 and gene 5 were depleted is shown in the bottom panels. Uptake of polymersomes in cells transfected with non-targeting siRNA, and non-transfected cells are included for comparison. Cells non-incubated with polymersomes are shown as control. Images were acquired in an ImageXpress Micro XLS widefield high content screening system using a 40X objective and analysed using MetaXpress<sup>®</sup> and imageJ software packages. Scale bars: 20  $\mu$ m.



**Figure 6.8: Uptake of rhodamine-labelled PMPC-PDPA polymersomes in non-transfected, or transfected with non-targeting siRNA, SR2<sup>+</sup> Drosophila cells**

Graph displays cellular uptake, in terms of % fluorescent cells and fluorescent intensity, after incubation with rhodamine-labelled polymersomes in cells transfected with non-targeting siRNA compared with cells that were not transfected. Rectangles represent max. and min. values (upper and lower lines) and mean value (midline). Non-transfected: 28 technical replicates. Non-targeting siRNA: 63 technical replicates.



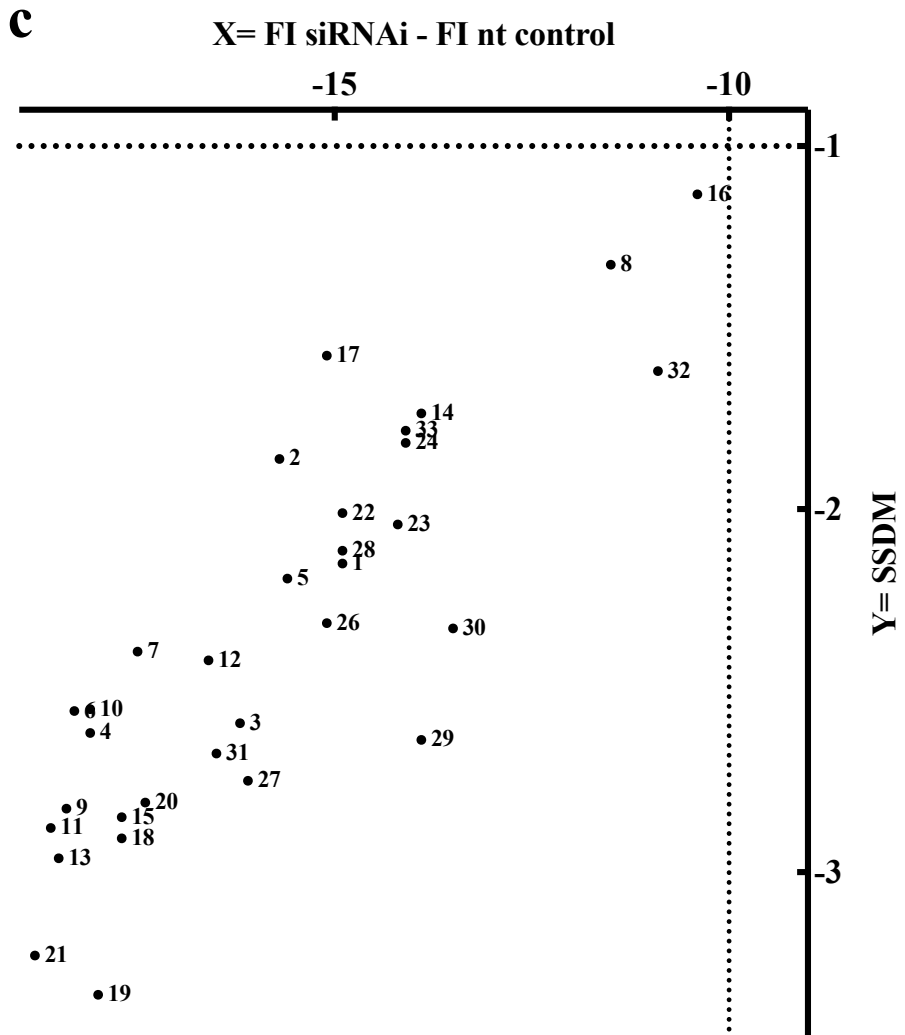


**Figure 6.9: Uptake of PMPC-PDPA polymersomes in knockdown SR2<sup>+</sup> Drosophila cells. Fluorescent intensity measurements**

32 genes coding for proteins related to endocytosis and cellular trafficking were knocked down in SR2<sup>+</sup> cells using siRNA. Transfected cells were incubated with 5 $\mu$ g of rhodamine-labelled polymersomes for 1 hour before being qualitatively and quantitatively analysed by high throughput microscopy. **a)** Average cellular fluorescent intensity for each transfection condition. Graph displays mean values  $\pm$  SD. An average of 9 technical repetitions for each gene was performed. The green dot represents cells transfected with non-targeting siRNA (control cells). Knockdown genes falling within the variability range of the control (thick dashed lines) are represented by black dots and do not present a distorted polymersome endocytosis. Narrow dashed lines denote control cells SD  $\pm$  5. Genes overlapping with this interval, but not with the previous one, present a decreased polymersome internalisation (dark blue dots). Knockdown genes that do not overlap with any of the thresholds mentioned are represented as light blue dots. A decreased polymersome internalisation is observed under these conditions, and the inhibition is stronger than the one observed after the knockdown of genes represented in dark blue. Note: Gene 25 is not represented as its SD exceeded the Y-axis. **b)** Dual-flashlight representation of SSDM vs. fold change. Strictly standardised mean difference (SSDM) is represented in the Y-axis. Mean cellular fluorescent intensity obtained for each gene minus the mean fluorescent intensity value for control cells (non-targeting siRNA) is represented in the X-axis. Vertical dashed lines represent average fold change  $\pm$  10. Horizontal dashed lines denote SSDM  $\pm$  1. Genes (empty circles) falling between the dashed lines and the axis are considered not to affect the normal endocytosis of polymersomes. **c)** Genes considered to facilitate polymersome endocytosis. The bottom left quadrant from graph **b** has been zoomed to visualise the genes distribution. The influence, in polymersome endocytosis, of the protein codified by each gene is higher as the gene appears more distant from the axis and the threshold lines.



## **6.3 Discussion**

Following the identification, in the previous chapter, of two specific receptors facilitating polymersome uptake in mammalian cells, I aimed to further characterise the endocytic pathway/s followed by the nanoparticles, with emphasis on the identification of the intracellular cell factors required for particle uptake. In order to do that, I perturbed endocytosis and assessed polymersome uptake, using different experimental approaches with increasing level of specificity towards a particular endocytic mechanism.

### **6.3.1 Investigation of PMPC-PDPA polymersome endocytosis through chemical inhibitors**

In the first instance, chemical compounds were used to inhibit/perturb different endocytic molecules. According to the extra care needed when using these agents to avoid misleading results, I performed an exhaustive pre-screen to select the inhibitors to use and their incubation conditions (figures 6.1-6.3, table 6.3). Consequently it was possible to explore polymersome uptake in cells incubated with inhibitors under conditions that resemble controls cells in terms of general cellular viability level and integrity of the plasma membrane. Surprisingly, a reduction in polymersome internalisation in cells pre-incubated with bafilomycin or nocodazole was not observed (figure 6.4). In the former case, the compound hinders the acidification of the endosomal lumen, which should prevent PMPC-PDPA polymersomes disassembly since they are pH responsive nanoparticles. However, it might be possible that 20 minutes incubation with fluorescent polymersomes is not enough to appreciate a difference in fluorescent intensity levels between control cells and cells where nanoparticle disassembly is reduced or inhibited. Following polymersome break up in endosomes and cytosol release, single amphiphilic copolymers chains are likely to be integrated within cellular membranes, staining them over time. Therefore, although the cell will get eventually stained, the fluorescence of the nanoparticles confined in endosomes will be initially diluted as they escape from the endocytic compartment. Providing bafilomycin did work, there is the possibility that cells containing non-acidified endocytic vesicles loaded with fluorescent polymersomes could have similar

overall fluorescent intensity to cells undergoing normal polymersome endocytosis and endosomal release for only 20 minutes. In the case of nocodazole, the present results contrast with results previously obtained in our group, where endocytosis of polymersomes was inhibited by 60% in HDFs after incubation with this microtubules depolymerising agent<sup>166</sup>. Apart from any cell type-dependent sensitivity to this compound, on that occasion cells were pre-incubated with nocodazole for 1 hour, compared with the 15 minutes pre-incubation protocol followed for the experiments reported in this chapter. Additionally, the argument put forward for bafilomycin could also apply here.

In the interest of avoiding cytotoxicity induced by chemical inhibitors I might have been too conservative with the pre-incubation times and the concentrations used (table 6.3). Judging from the inhibition observed for the control cargoes (figure 6.3), slightly longer pre-incubation times would probably have been necessary to allow the chemicals to exert their full inhibitory effect. For example, it could be expected that a reduction in Tf uptake would have been observed in cells incubated with cytochalasin D, since actin plays an important role in CME endocytosis<sup>286</sup>. However, it has also been reported that the effectiveness of this inhibitor to prevent Tf endocytosis is very cell type-dependent<sup>102</sup>. The introduction of a final acid wash step before flow cytometry analysis would have possibly amplified any difference in fluorescent intensity, between control cells and cells where endocytosis was partially inhibited, particularly if polymersomes were stacked at the plasma membrane or in invaginations connected with it. Finally, the experiments were conducted in the presence of serum, while in some experimental protocols involving the use of these inhibitors pre-incubation is carried out in serum free conditions (table 6.1), possibly to avoid any aggregation/precipitation of the chemicals that could diminish their effect.

In the case of cholera toxin it is difficult to discern whether the results obtained could include artefacts derived from the experimental protocol or not. According to the information presented in the results section, CTxB is very promiscuous regarding the endocytic mechanisms used. The significant reduction in toxin uptake in cells incubated with chlorpromazine is in agreement with reports showing CME endocytosis of CTxB<sup>275</sup>. Nevertheless CTxB has also been related to caveolae-mediated endocytosis<sup>287</sup>, in which case an effect in toxin uptake in cells incubated with filipin and/or genistein should have been observed. There are also contradictory reports showing dynamin-



dependent<sup>278</sup> and dynamin-independent<sup>275</sup> uptake of the toxin. According to the results presented, CTxB seems to be using CME endocytosis. However it would be recommended to repeat the experiments with the amendments to the experimental protocol mentioned above. CTxB was used as a control to compare its uptake to that of PMPC-PDPA polymersomes under the same inhibitory conditions. Figures 6.4.b,c shows that their endocytosis is not affected in the same way by the inhibition of the same cell factors. A comparison between the uptake profiles obtained for polymersomes and dextran in inhibited cells is more difficult. Little dextran internalisation was observed in control cells, and cells incubated with inhibitors. In addition, the results were highly variable (figure 6.4.d). A reason for this could be that macropinocytosis is a transient process in most cell types which gets commonly activated after growth factors stimulation<sup>288</sup>. Unstimulated HeLa cells were used and so, macropinocytosis could be not occurring at a significant level in them. Therefore, to be able to compare the uptake profile of polymersomes with that of dextran in inhibited cells I should have used stimulated cells (i.e. using epidermal growth factor).

This discussion illustrates the high number of variables to have in mind while designing and performing these experiments. Similarly, it highlights the fragile balance between effective inhibition of a certain endocytic route and promoting cytotoxic and off-target effects while working with chemical inhibitors.

### **6.3.2 Implication of dynamin in PMPC-PDPA polymersome internalisation**

Over the years dynamin has emerged as a very important molecule in endocytosis. It is the main force driving the pinching off the invaginated endocytic vesicles from the plasma membrane in some of the best-characterised endocytic mechanisms in mammalian cells such as CME and caveolae-mediated endocytosis, as well as in recently described endocytic pathways like RhoA and interleukin-2-mediated endocytosis<sup>15</sup>. Therefore, it was surprising to find out that dynamin seems not to be essential, or to be strongly implicated, in PMPC-PDPA polymersome endocytosis. I arrived to this conclusion after noticing similar nanoparticle uptake in cells overexpressing the mutant K44A dynamin (not able to bind GTP and therefore to

mediate the pinching off of vesicles from the plasma membrane) and a wild type dynamin. The same conclusion was obtained in two different cell lines using different experimental settings (CellLuminate<sup>®</sup> vs. rhodamine-labelled polymersomes and microscopy vs. flow cytometry). Nonetheless, in the case of HeLa cells I have drawn my conclusion from a very small number of observations and therefore it would be advisable to repeat the experiment looking at a larger population in order to investigate whether the small reduction observed is diluted or it becomes significant. It is also important to consider that the inhibition of dynamin-dependent process could up-regulate dynamin-independent process, as it has been previously observed<sup>289</sup>. This would mask the true level of dynamin implication in PMPC-PDPA polymersome endocytosis providing the nanoparticles can use both, dynamin-dependent and dynamin-independent internalisation routes. PMPC-PDPA polymersome could be using one of the dynamin-independent pathways described to date, such as Cdc42 and Arf6-mediated endocytosis<sup>15</sup>. Macropinocytosis and flotillin-mediated endocytosis, where there is some controversy about their dependence on dynamin, could be also possible routes for the cellular internalisation of these polymersomes. The involvement of these pathways in polymersome uptake could be investigated under the microscope, looking for the early localisation of fluorescent polymersomes in cells transfected to express fluorescent-labelled markers, such as Cdc42, Arf6, or flotillin.

The experiments performed in this section raise the interesting question of which molecules, rather than dynamin, could be mediating the detachment of the endocytic vesicle containing the nanoparticles from the plasma membrane. The actin cytoskeleton and BAR domain proteins are potential candidates. They play a main role in dynamin-independent endocytosis as well as being normally implicated in dynamin-dependent processes<sup>74,93,96</sup>. Their implication in PMPC-PDPA polymersome uptake has been investigated to some extent in this chapter by means of the actin inhibitor cytochalasin D, which did not affect polymersome internalisation, and by siRNA knockdown of actin and BAR domain proteins, discussed below.

### **6.3.3 BAR domain proteins in PMPC-PDPA polymersome internalisation. siRNA screening in Drosophila cells**

The possibility to test almost simultaneously, and in a comparable manner, the impact that different single proteins have in polymersome endocytosis, drove the design of a screen with chemical inhibitors. Unfortunately, I did not obtain as much information as I was expecting from it, possibly influenced by the experimental considerations previously mentioned. Nevertheless, a screen is one of the most interesting ways to explore polymersome internalisation. In this sense, the possibilities offered by high-throughput screening are exceptional. The opportunity to automate almost every step of the protocol marks it as a high reproducible methodology. In addition, the amount of biological information both, at a single cell level and at a population level, provided by this kind of screen is outstanding. Therefore, I decided to take advantage of the screening facilities for genome wide screens in Drosophila cells at The University of Sheffield to study polymersome endocytosis. Due to the time limit of this thesis I had just enough time to start exploring the suitability of this technique to characterise polymersome uptake, and to set up a small preliminary screen. Surprisingly, almost all the genes investigated came out as positive hits (figure 6.9), meaning that the proteins that they code for would be implicated in PMPC-PDPA polymersome internalisation or subcellular trafficking (figure 6.9). This is not usual. Although SR2<sup>+</sup> cells are easily transfectable it is unlikely that the knockdown was 100% effective in all the cases. Moreover, the high number of hits raises the question of whether the control could be an outlier. This is probably the weakest point of the screen. Although the use of cells transfected with siRNA for *Caenorhabditis elegans* genes with no homology with Drosophila cells is adequate, the presence of more controls would have been necessary. The screen could be further optimised in the future by including scramble siRNA and siRNA coding for housekeeping genes not related to endocytosis or subcellular trafficking. Besides siRNA controls, it would be suitable to include cells incubated with a cytotoxic agent at a toxic dose, to be able to compare fluorescent signal associated with dead cells or cells with a compromised membrane to that of healthy transfected cells undergoing endocytosis. This control would be useful to rule out not optimal transfected cells from the final results.

Having pointed out the main limitations of the screen and how they could be overcome in the future, there is also the possibility that the high number of hits is a natural consequence, or highly influenced by redundant functions among the group of genes comprising the screen. Most of the genes investigated code for proteins able to sense and induce membrane curvature. If our hypothesis is true, and polymersome endocytosis is strongly driven by the curvature of the particle, it is reasonable to expect that the knockdown of proteins able to sense plasma membrane deformation would, in most of the cases, have an effect in polymersome uptake.

Actin, another candidate to mediate the detachment of the endocytic vesicle containing the polymersomes from the plasma membrane, is represented in the screen by two genes (32, 27), while one of them came out as a relative strong hit, the other one did not, leaving very much unresolved actin implication in PMPC-PDPA polymersome uptake. On the other hand, the tetraspanin CD81 (genes 18 and 29) emerged as strong hit, in agreement with the results previously obtained in mammalian cells. Intriguingly, none of the two genes coding for SR-BI (genes 16 and 1) were strong hits on the screen. This could be due to different receptor requirements in mammal and insect cells and highlights the necessity to characterise in detail PMPC-PDPA polymersome uptake in *Drosophila* cells. It would be advisable to repeat Fucoïdan and Polyinosinic acid experiments in SR2<sup>+</sup> cells, to investigate further the implication of scavenger receptors in nanoparticle internalisation in this cell type. It also raises the question of whether it would be better to continue with the screen in mammalian cells rather than in *Drosophila* cells, if there are such important differences in PMPC-PDPA polymersome endocytosis between the two cell types.

#### **6.3.4 Final remarks**

Although some of the experiments presented in this chapter have clear limitations and would require additional optimisation, I believe that the overall picture indicates that PMPC-PDPA polymersomes exhibit a high level of plasticity in their mechanism of cellular entry. In addition, polymersome endocytosis is a dynamin-independent process in FaDu cells, and most likely in HeLa cells, which often defines very unique endocytic routes where the cargo features play a central role. Consequently, I propose a cargo-

driven endocytic mechanism for PMPC-PDPA polymersomes where the nanoparticle high curvature and the specific nanoparticle binding to the cell surface are crucial. The model for the endocytosis of PMPC-PDPA polymersomes, based on the information gathered by the experiments conducted in this thesis, would be described and discussed in detail in the following chapter.



# **Chapter 7: Conclusions, final discussion and future perspectives**

The aim of this thesis was to extend our knowledge of the internalisation mechanism followed by PMPC-PDPA polymersomes in mammalian cells, which was minimal at the beginning of the present research. This has been fulfilled with the acquisition of important pieces of information that have made us understand the reason behind the enhanced uptake of this formulation, and how to properly balance key polymersome properties in order to better control their internalisation, opening new and interesting lines of work to be developed in the future.

## **7.1 Summary of findings**

### **7.1.1 Effects of polymersome size and shape in PMPC-PDPA polymersome uptake**

Taking advantage of the specific physical properties that different production methods imprint in PMPC-PDPA polymersomes, and exploring sequential centrifugation as a technique for the purification of bulk polymersome dispersion, the important effect of particle size on polymersome uptake kinetics has been corroborated and extended. Moreover, the impact of nanoparticle shape in PMPC-PDPA polymersome uptake has been investigated for the first time. Importantly, we have discovered that a diameter of approximately 60 nm corresponds to the optimal nanoparticle size for the uptake of spherical PMPC-PDPA polymersomes (relative number of particles taken up) in mammalian cells. This result, obtained in the cancer cell line FaDu (presented in this thesis), and in a parallel study conducted by another PhD student in primary neutrophils, is in agreement with the optimum particle diameter for the receptor-mediated endocytosis of nanoparticles reported by different groups<sup>142,290-293</sup>. Complementing this finding, we have demonstrated that polymersome uptake is highly influenced by nanoparticle shape. Uptake profiles are different for spherical and tubular nanoparticles. Elongated particles show a biphasic uptake and a delayed internalisation

when compared to spherical polymersomes of the same diameter. This, together with the discovery that tubular PMPC-PDPA polymersomes present higher encapsulation ability than their spherical counterparts<sup>194</sup>, and are able to act as intracellular delivery vectors, could be translated into new possibilities to modulate the temporal delivery of a cargo *in vivo*. Therefore, the next step will be to compare the uptake profiles of spherical and tubular PMPC-PDPA polymersomes *in vivo* animal models. Polymeric filomicelles present enhanced circulation times *in vivo*<sup>144</sup>, and we would like to investigate if this is also the case for tubular polymersomes. In addition, it would be quite interesting to compare the biodistribution profiles of spherical and tubular polymersomes, in order to explore whether some level of control over polymersomes sites of action *in vivo* could be achieved by fine-tuning of the nanoparticle shape.

### **7.1.2 Identification of the cellular receptors targeted by PMPC-PDPA polymersomes**

One of the most important contributions of this thesis to the understanding of cell-PMPC-PDPA polymersome interactions has been the identification of receptor-mediated endocytosis as a common pathway for the internalisation of these nanoparticles in mammalian cells. Using different molecules, from antagonists to neutralising antibodies, to impair/block endocytosis through specific receptors, I have found strong evidence that tetraspanin CD81 and scavenger receptors SR-BI/SR-BII (the methodology followed did not allow us to distinguish between them) are mediating PMPC-PDPA polymersome uptake in mammalian cells. A role for scavenger receptor CD36 in polymersome internalisation is also possible following consideration of the results obtained. This could be investigated further in CD36 knockdown cells. It would be also important to verify, in knockdown cells, the strong polymersome inhibition observed when a neutralising antibody anti-CD81 was used, and most interesting would be to study polymersome uptake in cells simultaneously deprived of the expression of all three receptors. Moreover, we would like to learn about the interactions established among these receptors in the context of PMPC-PDPA polymersome endocytosis, and the specific role that each one plays in polymersome uptake. In the case of HCV endocytosis, the sequential involvement of the different receptors (SR-BI, and CD81) and other cell surface factors mediating viral internalisation has been determined by



incubating the cells with specific neutralising antibodies at different time points, before and after viral binding. It has been demonstrated that SR-BI acts both in early viral binding to the cell, and at later stages of viral infection<sup>181,294,295</sup>. We could adapt the experimental procedure followed in those studies to explore at what time the different receptors are being used in PMPC-PDPA polymersome endocytosis. In addition, we could investigate the existence of direct interactions between CD81, SR-BI, SR-BII and CD36 before and after polymersome incubation using immunoprecipitation protocols. It is exciting to discover the ability of PMPC-PDPA polymersomes to target specific receptors at the cell surface, mimicking the interactions established by natural nanoparticles with the cells. The finding that the endocytosis of this formulation is greatly enhanced in serum free conditions is an additional indication that the targeting of the receptors is directly mediated by polymersome surface and not through nanoparticle association with the proteins present in the media.

### **7.1.3 Dynamin-independent internalisation of PMPC-PDPA polymersomes**

Another important aspect of the cellular uptake of PMPC-PDPA polymersomes revealed by the research presented in here, is that receptor-mediated endocytosis of these nanoparticles could be a dynamin-independent process in mammalian cells. This conclusion was achieved after investigating, by flow cytometry, the uptake of rhodamine-labelled polymersomes in FaDu cells expressing a dominant negative dynamin. The same result although less convincing than in the previous cell line due to the reduced sample size, was obtained in K44A mutant HeLa cells incubated with unlabelled-polymersomes encapsulating a fluorescent dye and analysed by confocal fluorescence microscopy. The slightly different experiment setups and the different detection techniques used strengthen the common observation. It would be important to complement these observations by studying the participation of dynamin in polymersome uptake in primary cells. In addition, it would be interesting to repeat these experiments using tubular polymersomes instead of spherical ones, since we have already noticed a difference between their internalisation kinetics.

Finally, the involvement of specific endocytic pathways such as CME, caveolae-mediated endocytosis and macropinocytosis, in PMPC-PDPA polymersome uptake, as well as the participation of BAR domain proteins in nanoparticle internalisation has been investigated to some extent in this thesis. Although, as discussed on the previous chapter, these experiments would require further optimisation and therefore are not fully conclusive at this stage, we believe that, so far, the emerging picture points to the possibility that PMPC-PDPA polymersomes use multiple endocytic pathways to enter the cells.

## 7.2 Final discussion and future perspectives

Taking into account the findings summarised above and acknowledging the limitations of some of the results presented, I propose that the endocytic uptake of PMPC-PDPA polymersomes is characterised by:

a) A high level of promiscuity. Polymersomes would be able to take advantage of any endocytic process operating at the cell surface at a given time. For example, it is known that caveolae are constantly present at the cell surface where they help to counteract membrane tension through different mechanisms including their endocytosis<sup>296</sup>. In addition, it has been demonstrated that clathrin coated pits start to assemble at the plasma membrane in the absence of any cargo, rapidly aborting the nucleation after a short period of time or committing to the next endocytic step only after cargo stimulation<sup>297,298</sup>. The ability of PMPC-PDPA polymersome to enter a high number of heterogeneous cell types could be a consequence of their promiscuous behaviour. Most endocytic routes are ubiquitous in mammalian cells, but interestingly we have reported here, high polymersome uptake in Huh7 cells, which present very low levels of caveolins and are negative for caveolae expression<sup>299</sup>. Additionally, experimental data generated in the laboratory, although not by this thesis, has revealed that polymersomes could enter the cells via phagocytosis in neutrophils. These observations nourish my hypothesis of polymersome endocytosis being characterised by a high level of promiscuity, for which there are also biological precedents. Some pathogens have been proven to enter the cell following a wide range of different endocytic routes. One of the best examples is cholera toxin (CTxB). As previously

pointed out in this thesis, CTxB can enter the cell via caveolae-mediated endocytosis, CME, and caveolae and clathrin-independent endocytosis<sup>300</sup>. Likewise Shiga toxin (STx) and simian virus 40 (SV40) have been shown to gain cellular access through different endocytic routes<sup>301-303</sup>. Furthermore, the research conducted by Prof. Ludger Johannes group (Institut Curie, Paris) has demonstrated the ability of all these exogenous particles to induce their own endocytosis, without the help of any cytosolic endocytic machinery<sup>304,305</sup>. They have shown that CTxB, STx and SV40 bind to specific glycolipids receptors (GM1, Gb3, GM1 respectively) through pentameric protein scaffolds, leading to lipid reorganisation and membrane clustering, which in turn is translated into cellular membrane invagination and formation of tight tubular invaginations containing the toxins or the viral particles. Based on experiments conducted in model (giant unilamellar vesicles, GUVs) and cellular membranes Prof. Johannes group proposed that the kinetics of the tubule nucleation is controlled by a free energy barrier, which is strongly influenced by the cost of membrane deformation at the invagination neck. The intrinsic high curvature of the viral particles (SV40, 45 nm in diameter) is enough to trigger tubule nucleation at the membrane within seconds of incubation with the virus. This process is delayed (minutes) in the case of small toxins (STx, CTxB), which lack the ability of simultaneously imposing membrane deformation as they adhere to the cell surface<sup>305</sup>. Finally, they have shown that detachment of the endocytic vesicle from the plasma membrane is dynamin and actin-dependent in the case of STx<sup>304</sup> and actin-dependent but dynamin-independent for SV40<sup>305</sup>. Nonetheless, there are also reports demonstrating a dynamin-independent internalisation for all three particles<sup>300,302,303</sup>.

b) The ability of PMPC-PDPA polymersomes to induce their own endocytosis. Similarly to the natural particles just presented, the promiscuous behaviour of this nanoparticle formulation could be also the reflection of their inherent facility to promote their endocytosis. In order to do that, a first step of docking to the plasma membrane seems to be a logical prerequisite. In the case of PMPC-PDPA polymersomes it is fulfilled with the binding to tetraspanin CD81 and specific scavenger receptors B. The capacity to induce an inward membrane deformation as the nanoparticle binds to the plasma membrane, or shortly after it, seems to be also essential. This thesis has produced evidence of the importance of nanoparticle curvature in PMPC-PDPA

endocytosis. Spherical polymersomes 60 nm in diameter, the ones with the optimal curvature at the contact point with the cell investigated, were the most effectively and rapidly internalised. Therefore, the ability of PMPC-PDPA polymersome to induce their endocytosis would be the result of the balance between polymersome-receptors interactions and the energy necessary to deform the membrane. Such balance would be strongly dependent on the inherent polymersome curvature and influenced by polymersome shape. In fact, tubular PMPC-PDPA polymersomes show a slower cellular uptake than their spherical counterparts. In order to directly test the ability of PMPC-PDPA polymersome to induce membrane invagination and the physico-chemical characteristics of those invaginations (shape of the bud and lipid composition) we could replicate the work done by Prof. Johannes group in model membranes. Using GUVs we could study the potential of these polymersome formulation to induce local rearrangement of the membrane and lipid clustering. The direct observation of the type of invaginations at which polymersomes are found at the cellular plasma membrane would be a milestone. During the course of this thesis, we have unsuccessfully tried to visualise these early events using transmission electron microscopy and resin-embedded cellular samples. Recent developments in microscopy have made it possible to combine fluorescence microscopy and electron microscopy to visualise the same area of a sample on a grid by both techniques, with a total resolution below 100 nm<sup>306,307</sup>. Such powerful systems would be ideal to investigate the molecular architecture of the membrane invaginations associated with polymersomes of different sizes and shapes. Moreover, combining it with immunolabelling we could assess the participation of specific cell factors, from clathrin to BAR domain proteins and actin, at different stages of polymersome endocytosis. Until these techniques become more readily available and we can have access to them, we could attempt to directly visualise polymersomes attachment to the plasma membrane, invaginations containing the nanoparticles and subcellular sorting of the endocytic vesicles using cryogenic electron microscopy (CryoEM).

An interesting question arising from the work presented in here, is related to the molecular force driven the detachment of the endocytic vesicle containing the nanoparticles from the plasma membrane, since PMPC-PDPA polymersome internalisation seems to be a dynamin-independent process, consistent with our current results. Apart from dynamin, there are other proteins that could assist this process such

as actin<sup>96</sup>, epsin<sup>93</sup>, Eps15 homology (EH)-domain (EHD)-containing proteins<sup>308</sup>, even BAR domain proteins<sup>93</sup>. In fact, according to the preliminary data obtained from the siRNA screening conducted in drosophila cells, it seems that epsin, actin, and BAR domain proteins are implicated in the internalisation of this nanoparticle formulation. The involvement of these molecules in polymersome endocytosis could be explored further by investigating nanoparticle uptake in knockdown cells, cells transfected with dominant negative versions of these proteins or transfected to express a fluorescent version of these molecules, ideally using high-throughput imaging. In addition to proteins, the biophysical properties of the plasma membrane also play an important role in vesicle fission<sup>67,113</sup>. Research conducted by Prof. Aurelien Roux (University of Geneva) has shown that phase separation of membrane lipids, either by specific lipid clustering or by induced membrane tubulation, promotes the local fission of membranes *in vitro*<sup>309</sup>. As mentioned above, cargo binding can directly induce membrane rearrangement, lipid clustering, even membrane tubulation. In addition, it has been observed that the interaction of some nanoparticles with phospholipid models membranes, and more recently with cellular membranes in live cells, resulted in effective vesicle severing and nanoparticle endocytosis<sup>310,311</sup>. It would be interesting to investigate if membrane invaginations containing PMPC-PDPA polymersomes could be detached from parent membranes without the need of any cell factor. This could be studied in GUVs. A totally cargo-driven membrane scission in cells would be *a priori* more difficult, since the cortical actin meshwork and the highly crowded and viscous cytoplasm would present a high resistance to it, nonetheless it is a stimulating scenario for further research.

According to the findings and the conclusions presented, PMPC-PDPA polymersomes seem to mimic the ability of pathogens to guarantee their cellular uptake by taking maximum advantage of cellular endocytosis. The similarity is especially interesting in the case of PMPC-PDPA polymersomes and HCV, as both nanoparticles target the scavenger receptor SR-BI and the tetraspanin CD81. Accordingly, PMPC-PDPA polymersomes could compete with HCV for their common receptors, with the possibility of observing a reduced viral uptake in the presence of these polymersomes. We have already started to test this hypothesis, in collaboration with Prof. McKeating (The University of Birmingham), with promising results so far. Viral infection,

measured by cellular luciferase expression 72 hours after treatment with HCV pseudoparticles encoding a luciferase reporter gene, was reduced by approximately 50% in cells simultaneously incubated with viral particles and empty PMPC-PDPA polymersomes (2 independent experiments performed by Mrs. Ke Hu at The University of Birmingham). It is important to remember that we have previously investigated the toxicological profile of PMPC-PDPA polymersomes in cell cultures, without finding any indication of significant cellular toxicity induced by these nanoparticles<sup>166,173</sup>. Moreover, we have recently explored the expression of genes involved in the interferon- $\alpha$  and interferon- $\beta$  immune responses, which are normally activated in cells after viral exposure and that are critical for host defense, finding out that incubation with empty PMPC-PDPA polymersomes induce a non-specific antiviral state on the cells (Dr. Patikarnmonthon and Prof. Battaglia unpublished data). This is very interesting, since one of the tricks that virus, such as HCV, play on their hosts to avoid their clearance is to switch off this antiviral cellular state<sup>312</sup>. According to these results, polymersomes could prevent HCV infection, to some extent, using multiple mechanisms, competition for plasma membrane receptors and induction of an antiviral state on the cells. We are currently continuing this line of work, that ascribed a possible antiviral activity to PMPC-PDPA polymersomes, and we will soon be repeating the competition studies for the third time. If the data shows again an inhibition of viral infection in cells simultaneously incubated with polymersomes, it is our intention to repeat this study *in vivo*, to investigate whether these nanoparticles are able to significantly reduce HCV infection in animal models. At the same time, it would be important, to monitor the health profile of the animal after different polymersome administration regimes. This is definitely one of the most exciting lines of work derived from this thesis due to the high clinical impact of the possible outcome. Hepatitis C virus infection is a major global health problem with 150 million people chronically infected, and more than 350,000 deaths per year from hepatitis C-related liver diseases (WHO 2013). There is not a preventive vaccine available and the mainstay of standard-of-care for HCV, interferon- $\alpha$  plus ribavirin, is effective only in approximately 50% of the patients<sup>313,314</sup>, highlighting the necessity to improve current HCV treatments.

In addition, if our hypothesis were true, it would be revealing a novel and revolutionary property of PMPC-PDPA polymersomes. From being the intracellular delivery vector encapsulating the prophylactic/therapeutic molecule, the polymersome itself could also be an active compound with prophylactic/therapeutic activity. One cannot but get

excited imagining the long-term possibilities that such a finding could bring, for example, HCV patients could be treated with PMPC-PDPA polymersomes loaded with an antiviral drug, reducing the chances of cellular re-infection and cell-to-cell viral spread (extracellular action) and treating the cells (intracellular action) at the same time, with the same nanoparticle. This research could be also extended to test the capacity of PMPC-PDPA polymersomes to effectively reduce other viral infections, in this sense, it is our intention to investigate in the near future whether human immunodeficiency virus<sup>283</sup> infection is affected by the presence of PMPC-PDPA polymersomes





## References

- 1 Ledet G, M. Nanomedicine: Emerging Therapeutics for the 21st Century *US Pharm.* 37, 7-11,**2012**.
- 2 Beija, M., Salvayre, R., Lauth-de Viguerie, N. & Marty, J. D. Colloidal systems for drug delivery: from design to therapy. *Trends Biotechnol* 30, 485-496,**2012**.
- 3 Chen, H., Khemtong, C., Yang, X., Chang, X. & Gao, J. Nanonization strategies for poorly water-soluble drugs. *Drug Discov Today* 16, 354-360,**2011**.
- 4 Pisal, D. S., Kosloski, M. P. & Balu-Iyer, S. V. Delivery of therapeutic proteins. *J Pharm Sci* 99, 2557-2575,**2010**.
- 5 Verma, I. M. & Somia, N. Gene therapy -- promises, problems and prospects. *Nature* 389, 239-242,**1997**.
- 6 Bumcrot, D., Manoharan, M., Koteliansky, V. & Sah, D. W. RNAi therapeutics: a potential new class of pharmaceutical drugs. *Nat Chem Biol* 2, 711-719,**2006**.
- 7 Zhang, L., Gu, F. X., Chan, J. M., Wang, A. Z., Langer, R. S. & Farokhzad, O. C. Nanoparticles in medicine: therapeutic applications and developments. *Clin Pharmacol Ther* 83, 761-769,**2008**.
- 8 Wang, T., Upponi, J. R. & Torchilin, V. P. Design of multifunctional non-viral gene vectors to overcome physiological barriers: dilemmas and strategies. *Int J Pharm* 427, 3-20,**2012**.
- 9 Ludlow, M., Allen, I. & Schneider-Schaulies, J. Systemic spread of measles virus: overcoming the epithelial and endothelial barriers. *Thromb Haemostasis* 102, 1050-1056,**2009**.
- 10 Diamond, M. S. & Klein, R. S. West Nile virus: crossing the blood-brain barrier. *Nat Med* 10, 1294-1295,**2004**.
- 11 Grove, J. & Marsh, M. The cell biology of receptor-mediated virus entry. *J Cell Biol* 195, 1071-1082,**2011**.
- 12 Avila-Olias, M., Pegoraro, C., Battaglia, G. & Canton, I. Inspired by nature: fundamentals in nanotechnology design to overcome biological barriers. *Ther Deliv* 4, 27-43,**2013**.
- 13 Alberts B, J. A., Lewis J, et al. . in *Mol Biol Cell* (ed Garland Science) (2002).
- 14 De Duve, C., Ciba Foundation. (ed Margaret P. Cameron Anthony V. S. De Reuck).
- 15 Doherty, G. J. & McMahon, H. T. Mechanisms of endocytosis. *Annu Rev Biochem* 78, 857-902,**2009**.
- 16 Gruenberg, J. & van der Goot, F. G. Mechanisms of pathogen entry through the endosomal compartments. *Nat Rev Mol Cell Bio* 7, 495-504,**2006**.
- 17 Marsh, M. & Helenius, A. Virus entry: Open sesame. *Cell* 124, 729-740,**2006**.
- 18 Shapero, K., Fenaroli, F., Lynch, I., Cottell, D. C., Salvati, A. & Dawson, K. A. Time and space resolved uptake study of silica nanoparticles by human cells. *Mol Biosyst* 7, 371-378,**2011**.
- 19 Decuzzi, P. & Ferrari, M. The receptor-mediated endocytosis of nonspherical particles. *Biophys J* 94, 3790-3797,**2008**.
- 20 Jutras, I. & Desjardins, M. Phagocytosis: at the crossroads of innate and adaptive immunity. *Annu Rev Cell Dev Biol* 21, 511-527,**2005**.
- 21 Tuma, P. & Hubbard, A. L. Transcytosis: crossing cellular barriers. *Physiol Rev* 83, 871-932,**2003**.
- 22 Lewis, W. H. Pinocytosis. *B Johns Hopkins Hosp* 49, 17-27,**1931**.

- 23 Swanson, J. A. Shaping cups into phagosomes and macropinosomes. *Nat Rev Mol Cell Bio* 9, 639-649,**2008**.
- 24 Roth, T. F. & Porter, K. R. Yolk Protein Uptake in the Oocyte of the Mosquito *Aedes Aegypti*. *J Cell Biol* 20, 313-332,**1964**.
- 25 Daumke, O., Roux, A. & Haucke, V. BAR Domain Scaffolds in Dynamin-Mediated Membrane Fission. *Cell* 156, 882-892,**2014**.
- 26 Liu, Y. W., Su, A. I. & Schmid, S. L. The evolution of dynamin to regulate clathrin-mediated endocytosis: speculations on the evolutionarily late appearance of dynamin relative to clathrin-mediated endocytosis. *Bioessays* 34, 643-647,**2012**.
- 27 Griffiths, G., Back, R. & Marsh, M. A quantitative analysis of the endocytic pathway in baby hamster kidney cells. *J Cell Biol* 109, 2703-2720,**1989**.
- 28 Goldstein, J. L., Anderson, R. G. & Brown, M. S. Coated pits, coated vesicles, and receptor-mediated endocytosis. *Nature* 279, 679-685,**1979**.
- 29 Bretscher, M. S. Endocytosis: relation to capping and cell locomotion. *Science* 224, 681-686,**1984**.
- 30 Palade, G. E. An electron microscope study of the mitochondrial structure. *J Histochem Cytochem* 1, 188-211,**1953**.
- 31 Yamada, E. The fine structure of the gall bladder epithelium of the mouse. *J Biophys Biochem Cytol* 1, 445-458,**1955**.
- 32 Rothberg, K. G., Heuser, J. E., Donzell, W. C., Ying, Y. S., Glenney, J. R. & Anderson, R. G. Caveolin, a protein component of caveolae membrane coats. *Cell* 68, 673-682,**1992**.
- 33 Thomsen, P., Roepstorff, K., Stahlhut, M. & van Deurs, B. Caveolae are highly immobile plasma membrane microdomains, which are not involved in constitutive endocytic trafficking. *Mol Biol Cell* 13, 238-250,**2002**.
- 34 Ikonen, E. & Parton, R. G. Caveolins and cellular cholesterol balance. *Traffic* 1, 212-217,**2000**.
- 35 Parton, R. G. & del Pozo, M. A. Caveolae as plasma membrane sensors, protectors and organizers. *Nat Rev Mol Cell Bio* 14, 98-112,**2013**.
- 36 Minshall, R. D., Sessa, W. C., Stan, R. V., Anderson, R. G. W. & Malik, A. B. Caveolin regulation of endothelial function. *Am J Physiol-Lung C* 285, L1179-L1183,**2003**.
- 37 Howes, M. T., Kirkham, M., Riches, J., Cortese, K., Walser, P. J., Simpson, F., Hill, M. M., Jones, A., Lundmark, R., Lindsay, M. R., Hernandez-Deviez, D. J., Hadzic, G., McCluskey, A., Bashir, R., Liu, L. B., Pilch, P., McMahon, H., Robinson, P. J., Hancock, J. F., Mayor, S. & Parton, R. G. Clathrin-independent carriers form a high capacity endocytic sorting system at the leading edge of migrating cells. *Journal of Cell Biology* 190, 675-691,**2010**.
- 38 Hansen, C. G. & Nichols, B. J. Molecular mechanisms of clathrin-independent endocytosis. *J Cell Sci* 122, 1713-1721,**2009**.
- 39 Glebov, O. O., Bright, N. A. & Nichols, B. J. Flotillin-1 defines a clathrin-independent endocytic pathway in mammalian cells. *Nat Cell Biol* 8, 46-U16,**2006**.
- 40 Frick, M., Bright, N. A., Riento, K., Bray, A., Merrified, C. & Nichols, B. J. Coassembly of flotillins induces formation of membrane microdomains, membrane curvature, and vesicle budding. *Curr Biol* 17, 1151-1156,**2007**.
- 41 Otto, G. P. & Nichols, B. J. The roles of flotillin microdomains--endocytosis and beyond. *J Cell Sci* 124, 3933-3940,**2011**.

- 42 Sabharanjak, S., Sharma, P., Parton, R. G. & Mayor, S. GPI-anchored proteins are delivered to recycling endosomes via a distinct cdc42-regulated, clathrin-independent pinocytic pathway. *Dev Cell* 2, 411-423,**2002**.
- 43 Donaldson, J. G. Multiple roles for Arf6: sorting, structuring, and signaling at the plasma membrane. *The Journal of biological chemistry* 278, 41573-41576,**2003**.
- 44 Lundmark, R., Doherty, G. J., Vallis, Y., Peter, B. J. & McMahon, H. T. Arf family GTP loading is activated by, and generates, positive membrane curvature. *The Biochemical journal* 414, 189-194,**2008**.
- 45 Grassart, A., Dujancourt, A., Lazarow, P. B., Dautry-Varsat, A. & Sauvonnnet, N. Clathrin-independent endocytosis used by the IL-2 receptor is regulated by Rac1, Pak1 and Pak2. *EMBO Rep* 9, 356-362,**2008**.
- 46 Basquin, C., Malarde, V., Mellor, P., Anderson, D. H., Meas-Yedid, V., Olivo-Marin, J. C., Dautry-Varsat, A. & Sauvonnnet, N. The signalling factor PI3K is a specific regulator of the clathrin-independent dynamin-dependent endocytosis of IL-2 receptors. *J Cell Sci* 126, 1099-1108,**2013**.
- 47 Lamaze, C., Dujancourt, A., Baba, T., Lo, C. G., Benmerah, A. & Dautry-Varsat, A. Interleukin 2 receptors and detergent-resistant membrane domains define a clathrin-independent endocytic pathway. *Mol Cell* 7, 661-671,**2001**.
- 48 Praefcke, G. J. & McMahon, H. T. The dynamin superfamily: universal membrane tubulation and fission molecules? *Nat Rev Mol Cell Biol* 5, 133-147,**2004**.
- 49 Chen, M. S., Obar, R. A., Schroeder, C. C., Austin, T. W., Poodry, C. A., Wadsworth, S. C. & Vallee, R. B. Multiple forms of dynamin are encoded by shibire, a Drosophila gene involved in endocytosis. *Nature* 351, 583-586,**1991**.
- 50 Vanderblik, A. M. & Meyerowitz, E. M. Dynamin-Like Protein Encoded by the Drosophila-Shibire Gene Associated with Vesicular Traffic. *Nature* 351, 411-414,**1991**.
- 51 Smistad, G., Jacobsen, J. & Sande, S. A. Multivariate toxicity screening of liposomal formulations on a human buccal cell line. *Int J Pharm* 330, 14-22,**2007**.
- 52 Chappie, J. S., Acharya, S., Leonard, M., Schmid, S. L. & Dyda, F. G domain dimerization controls dynamin's assembly-stimulated GTPase activity. *Nature* 465, 435-440,**2010**.
- 53 Faelber, K., Posor, Y., Gao, S., Held, M., Roske, Y., Schulze, D., Haucke, V., Noe, F. & Daumke, O. Crystal structure of nucleotide-free dynamin. *Nature* 477, 556-560,**2011**.
- 54 Ford, M. G., Jenni, S. & Nunnari, J. The crystal structure of dynamin. *Nature* 477, 561-566,**2011**.
- 55 Zheng, J., Cahill, S. M., Lemmon, M. A., Fushman, D., Schlessinger, J. & Cowburn, D. Identification of the binding site for acidic phospholipids on the pH domain of dynamin: implications for stimulation of GTPase activity. *J Mol Biol* 255, 14-21,**1996**.
- 56 Vallis, Y., Wigge, P., Marks, B., Evans, P. R. & McMahon, H. T. Importance of the pleckstrin homology domain of dynamin in clathrin-mediated endocytosis. *Current biology : CB* 9, 257-260,**1999**.
- 57 Ramachandran, R., Pucadyil, T. J., Liu, Y. W., Acharya, S., Leonard, M., Lukiyanchuk, V. & Schmid, S. L. Membrane Insertion of the Pleckstrin Homology Domain Variable Loop 1 Is Critical for Dynamin-catalyzed Vesicle Scission. *Mol Biol Cell* 20, 4630-4639,**2009**.

- 58 Ferguson, S. M. & De Camilli, P. Dynamin, a membrane-remodelling GTPase. *Nat Rev Mol Cell Biol* 13, 75-88,**2012**.
- 59 Ramachandran, R., Surka, M., Chappie, J. S., Fowler, D. M., Foss, T. R., Song, B. D. & Schmid, S. L. The dynamin middle domain is critical for tetramerization and higher-order self-assembly. *Embo J* 26, 559-566,**2007**.
- 60 Gao, S., von der Malsburg, A., Paeschke, S., Behlke, J., Haller, O., Kochs, G. & Daumke, O. Structural basis of oligomerization in the stalk region of dynamin-like MxA. *Nature* 465, 502-506,**2010**.
- 61 Stowell, M. H., Marks, B., Wigge, P. & McMahon, H. T. Nucleotide-dependent conformational changes in dynamin: evidence for a mechanochemical molecular spring. *Nat Cell Biol* 1, 27-32,**1999**.
- 62 Oh, P., McIntosh, D. P. & Schnitzer, J. E. Dynamin at the neck of caveolae mediates their budding to form transport vesicles by GTP-driven fission from the plasma membrane of endothelium. *Journal of Cell Biology* 141, 101-114,**1998**.
- 63 Henley, J. R., Krueger, E. W. A., Oswald, B. J. & McNiven, M. A. Dynamin-mediated internalization of caveolae. *Journal of Cell Biology* 141, 85-99,**1998**.
- 64 Sweitzer, S. M. & Hinshaw, J. E. Dynamin undergoes a GTP-dependent conformational change causing vesiculation. *Cell* 93, 1021-1029,**1998**.
- 65 Ferguson, S., Raimondi, A., Paradise, S., Shen, H. Y., Mesaki, K., Ferguson, A., Destaing, O., Ko, G., Takasaki, J., Cremona, O., O'Toole, E. & De Camilli, P. Coordinated Actions of Actin and BAR Proteins Upstream of Dynamin at Endocytic Clathrin-Coated Pits. *Dev Cell* 17, 811-822,**2009**.
- 66 Pucadyil, T. J. & Schmid, S. L. Real-time visualization of dynamin-catalyzed membrane fission and vesicle release. *Cell* 135, 1263-1275,**2008**.
- 67 Lenz, M., Morlot, S. & Roux, A. Mechanical requirements for membrane fission: Common facts from various examples. *Febs Lett* 583, 3839-3846,**2009**.
- 68 Morlot, S. & Roux, A. Mechanics of Dynamin-Mediated Membrane Fission. *Annu Rev Biophys* 42, 629-649,**2013**.
- 69 Hinshaw, J. E. & Schmid, S. L. Dynamin Self-Assembles into Rings Suggesting a Mechanism for Coated Vesicle Budding. *Nature* 374, 190-192,**1995**.
- 70 Doherty, G. J. & McMahon, H. T. Mediation, modulation, and consequences of membrane-cytoskeleton interactions. *Annual review of biophysics* 37, 65-95,**2008**.
- 71 Qualmann, B., Kessels, M. M. & Kelly, R. B. Molecular links between endocytosis and the actin cytoskeleton. *Journal of Cell Biology* 150, F111-F116,**2000**.
- 72 Hill, E., van Der Kaay, J., Downes, C. P. & Smythe, E. The role of dynamin and its binding partners in coated pit invagination and scission. *J Cell Biol* 152, 309-323,**2001**.
- 73 Takei, K., Slepnev, V. I., Haucke, V. & De Camilli, P. Functional partnership between amphiphysin and dynamin in clathrin-mediated endocytosis. *Nat Cell Biol* 1, 33-39,**1999**.
- 74 Morlot, S., Galli, V., Klein, M., Chiaruttini, N., Manzi, J., Humbert, F., Dinis, L., Lenz, M., Cappello, G. & Roux, A. Membrane Shape at the Edge of the Dynamin Helix Sets Location and Duration of the Fission Reaction. *Cell* 151, 619-629,**2012**.
- 75 Suetsugu, S. & Gautreau, A. Synergistic BAR-NPF interactions in actin-driven membrane remodeling. *Trends Cell Biol* 22, 141-150,**2012**.

- 76 Peter, B. J., Kent, H. M., Mills, I. G., Vallis, Y., Butler, P. J. G., Evans, P. R. & McMahon, H. T. BAR domains as sensors of membrane curvature: The amphiphysin BAR structure. *Science* 303, 495-499, **2004**.
- 77 Weissenhorn, W. Crystal structure of the endophilin-A1 BAR domain. *J Mol Biol* 351, 653-661, **2005**.
- 78 Zhu, G., Chen, J., Liu, J., Brunzelle, J. S., Huang, B., Wakeham, N., Terzyan, S., Li, X., Rao, Z., Li, G. & Zhang, X. C. Structure of the APPL1 BAR-PH domain and characterization of its interaction with Rab5. *Embo J* 26, 3484-3493, **2007**.
- 79 Li, J., Mao, X., Dong, L. Q., Liu, F. & Tong, L. Crystal structures of the BAR-PH and PTB domains of human APPL1. *Structure* 15, 525-533, **2007**.
- 80 Pylypenko, O., Lundmark, R., Rasmuson, E., Carlsson, S. R. & Rak, A. The PX-BAR membrane-remodeling unit of sorting nexin 9. *Embo J* 26, 4788-4800, **2007**.
- 81 Henne, W. M., Kent, H. M., Ford, M. G., Hegde, B. G., Daumke, O., Butler, P. J., Mittal, R., Langen, R., Evans, P. R. & McMahon, H. T. Structure and analysis of FCHO2 F-BAR domain: a dimerizing and membrane recruitment module that effects membrane curvature. *Structure* 15, 839-852, **2007**.
- 82 Millard, T. H., Bompard, G., Heung, M. Y., Dafforn, T. R., Scott, D. J., Machesky, L. M. & Futterer, K. Structural basis of filopodia formation induced by the IRSp53/MIM homology domain of human IRSp53. *Embo J* 24, 240-250, **2005**.
- 83 Mattila, P. K., Pykalainen, A., Saarikangas, J., Paavilainen, V. O., Vihinen, H., Jokitalo, E. & Lappalainen, P. Missing-in-metastasis and IRSp53 deform PI(4,5)P2-rich membranes by an inverse BAR domain-like mechanism. *J Cell Biol* 176, 953-964, **2007**.
- 84 Suetsugu, S., Murayama, K., Sakamoto, A., Hanawa-Suetsugu, K., Seto, A., Oikawa, T., Mishima, C., Shirouzu, M., Takenawa, T. & Yokoyama, S. The RAC binding domain/IRSp53-MIM homology domain of IRSp53 induces RAC-dependent membrane deformation. *The Journal of biological chemistry* 281, 35347-35358, **2006**.
- 85 Frost, A., Perera, R., Roux, A., Spasov, K., Destaing, O., Egelman, E. H., De Camilli, P. & Unger, V. M. Structural basis of membrane invagination by F-BAR domains. *Cell* 132, 807-817, **2008**.
- 86 Mim, C. & Unger, V. M. Membrane curvature and its generation by BAR proteins. *Trends Biochem Sci* 37, 526-533, **2012**.
- 87 Shimada, A., Niwa, H., Tsujita, K., Suetsugu, S., Nitta, K., Hanawa-Suetsugu, K., Akasaka, R., Nishino, Y., Toyama, M., Chen, L., Liu, Z. J., Wang, B. C., Yamamoto, M., Terada, T., Miyazawa, A., Tanaka, A., Sugano, S., Shirouzu, M., Nagayama, K., Takenawa, T. & Yokoyama, S. Curved EFC/F-BAR-domain dimers are joined end to end into a filament for membrane invagination in endocytosis. *Cell* 129, 761-772, **2007**.
- 88 Mim, C., Cui, H., Gawronski-Salerno, J. A., Frost, A., Lyman, E., Voth, G. A. & Unger, V. M. Structural basis of membrane bending by the N-BAR protein endophilin. *Cell* 149, 137-145, **2012**.
- 89 Gallop, J. L., Jao, C. C., Kent, H. M., Butler, P. J., Evans, P. R., Langen, R. & McMahon, H. T. Mechanism of endophilin N-BAR domain-mediated membrane curvature. *Embo J* 25, 2898-2910, **2006**.
- 90 Frost, A., Unger, V. M. & De Camilli, P. The BAR domain superfamily: membrane-molding macromolecules. *Cell* 137, 191-196, **2009**.

- 91 Itoh, T., Erdmann, K. S., Roux, A., Habermann, B., Werner, H. & De Camilli, P. Dynamin and the actin cytoskeleton cooperatively regulate plasma membrane invagination by BAR and F-BAR proteins. *Dev Cell* 9, 791-804,**2005**.
- 92 Tarricone, C., Xiao, B., Justin, N., Walker, P. A., Rittinger, K., Gamblin, S. J. & Smerdon, S. J. The structural basis of Arfaptin-mediated cross-talk between Rac and Arf signalling pathways. *Nature* 411, 215-219,**2001**.
- 93 Boucrot, E., Pick, A., Camdere, G., Liska, N., Evergren, E., McMahon, H. T. & Kozlov, M. M. Membrane fission is promoted by insertion of amphipathic helices and is restricted by crescent BAR domains. *Cell* 149, 124-136,**2012**.
- 94 Campelo, F., McMahon, H. T. & Kozlov, M. M. The hydrophobic insertion mechanism of membrane curvature generation by proteins. *Biophys J* 95, 2325-2339,**2008**.
- 95 Dominguez, R. & Holmes, K. C. Actin structure and function. *Annual review of biophysics* 40, 169-186,**2011**.
- 96 Romer, W., Pontani, L. L., Sorre, B., Rentero, C., Berland, L., Chambon, V., Lamaze, C., Bassereau, P., Sykes, C., Gaus, K. & Johannes, L. Actin Dynamics Drive Membrane Reorganization and Scission in Clathrin-Independent Endocytosis. *Cell* 140, 540-553,**2010**.
- 97 Jaumouille, V. & Grinstein, S. Receptor mobility, the cytoskeleton, and particle binding during phagocytosis. *Curr Opin Cell Biol* 23, 22-29,**2011**.
- 98 Lim, J. P. & Gleeson, P. A. Macropinocytosis: an endocytic pathway for internalising large gulps. *Immunol Cell Biol* 89, 836-843,**2011**.
- 99 Sinha, B., Koster, D., Ruez, R., Gonnord, P., Bastiani, M., Abankwa, D., Stan, R. V., Butler-Browne, G., Védie, B., Johannes, L., Morone, N., Parton, R. G., Raposo, G., Sens, P., Lamaze, C. & Nassoy, P. Cells Respond to Mechanical Stress by Rapid Disassembly of Caveolae. *Cell* 144, 402-413,**2011**.
- 100 Muriel, O., Echarri, A., Hellriegel, C., Pavon, D. M., Beccari, L. & Del Pozo, M. A. Phosphorylated filamin A regulates actin-linked caveolae dynamics. *J Cell Sci* 124, 2763-2776,**2011**.
- 101 Mooren, O. L., Galletta, B. J. & Cooper, J. A. Roles for actin assembly in endocytosis. *Annu Rev Biochem* 81, 661-686,**2012**.
- 102 Fujimoto, L. M., Roth, R., Heuser, J. E. & Schmid, S. L. Actin assembly plays a variable, but not obligatory role in receptor-mediated endocytosis in mammalian cells. *Traffic* 1, 161-171,**2000**.
- 103 Aghamohammadzadeh, S. & Ayscough, K. R. Differential requirements for actin during yeast and mammalian endocytosis. *Nat Cell Biol* 11, 1039-1042,**2009**.
- 104 Kaksonen, M., Toret, C. P. & Drubin, D. G. A modular design for the clathrin- and actin-mediated endocytosis machinery. *Cell* 123, 305-320,**2005**.
- 105 Smaczynska-de, R., II, Allwood, E. G., Aghamohammadzadeh, S., Hettema, E. H., Goldberg, M. W. & Ayscough, K. R. A role for the dynamin-like protein Vps1 during endocytosis in yeast. *J Cell Sci* 123, 3496-3506,**2010**.
- 106 Gu, C., Yaddanapudi, S., Weins, A., Osborn, T., Reiser, J., Pollak, M., Hartwig, J. & Sever, S. Direct dynamin-actin interactions regulate the actin cytoskeleton. *Embo J* 29, 3593-3606,**2010**.
- 107 Mooren, O. L., Kotova, T. I., Moore, A. J. & Schafer, D. A. Dynamin2 GTPase and cortactin remodel actin filaments. *The Journal of biological chemistry* 284, 23995-24005,**2009**.
- 108 Orth, J. D. & McNiven, M. A. Dynamin at the actin-membrane interface. *Curr Opin Cell Biol* 15, 31-39,**2003**.

- 109 Merrifield, C. J., Perrais, D. & Zenisek, D. Coupling between clathrin-coated-pit invagination, cortactin recruitment, and membrane scission observed in live cells. *Cell* 121, 593-606,**2005**.
- 110 Boulant, S., Kural, C., Zeeh, J. C., Ubelmann, F. & Kirchhausen, T. Actin dynamics counteract membrane tension during clathrin-mediated endocytosis. *Nat Cell Biol* 13, 1124-1131,**2011**.
- 111 Yao, L. H., Rao, Y., Bang, C., Kurilova, S., Varga, K., Wang, C. Y., Weller, B. D., Cho, W., Cheng, J. & Gong, L. W. Actin polymerization does not provide direct mechanical forces for vesicle fission during clathrin-mediated endocytosis. *J Neurosci* 33, 15793-15798,**2013**.
- 112 Baumgart, T., Hess, S. T. & Webb, W. W. Imaging coexisting fluid domains in biomembrane models coupling curvature and line tension. *Nature* 425, 821-824,**2003**.
- 113 Liu, J., Kaksonen, M., Drubin, D. G. & Oster, G. Endocytic vesicle scission by lipid phase boundary forces. *Proc Natl Acad Sci U S A* 103, 10277-10282,**2006**.
- 114 Campelo, F. & Malhotra, V. Membrane fission: the biogenesis of transport carriers. *Annu Rev Biochem* 81, 407-427,**2012**.
- 115 Kozlov, M. M., McMahon, H. T. & Chernomordik, L. V. Protein-driven membrane stresses in fusion and fission. *Trends Biochem Sci* 35, 699-706,**2010**.
- 116 Akinc, A. & Battaglia, G. Exploiting endocytosis for nanomedicines. *Cold Spring Harb Perspect Biol* 5, a016980,**2013**.
- 117 Bangham, A. D. & Horne, R. W. Negative Staining of Phospholipids and Their Structural Modification by Surface-Active Agents as Observed in the Electron Microscope. *J Mol Biol* 8, 660-668,**1964**.
- 118 Pan, B. T. & Johnstone, R. M. Fate of the transferrin receptor during maturation of sheep reticulocytes in vitro: selective externalization of the receptor. *Cell* 33, 967-978,**1983**.
- 119 They, C., Regnault, A., Garin, J., Wolfers, J., Zitvogel, L., Ricciardi-Castagnoli, P., Raposo, G. & Amigorena, S. Molecular characterization of dendritic cell-derived exosomes. Selective accumulation of the heat shock protein hsc73. *J Cell Biol* 147, 599-610,**1999**.
- 120 Sun, D., Zhuang, X., Xiang, X., Liu, Y., Zhang, S., Liu, C., Barnes, S., Grizzle, W., Miller, D. & Zhang, H. G. A novel nanoparticle drug delivery system: the anti-inflammatory activity of curcumin is enhanced when encapsulated in exosomes. *Molecular therapy : the journal of the American Society of Gene Therapy* 18, 1606-1614,**2010**.
- 121 Alvarez-Erviti, L., Seow, Y., Yin, H., Betts, C., Lakhali, S. & Wood, M. J. Delivery of siRNA to the mouse brain by systemic injection of targeted exosomes. *Nat Biotechnol* 29, 341-345,**2011**.
- 122 Buhleier, E., Wehner, W. & Vogtle, F. Cascade-Chain-Like and Nonskid-Chain-Like Syntheses of Molecular Cavity Topologies. *Synthesis-Stuttgart*, 155-158,**1978**.
- 123 Bawarski, W. E., Chidlow, E., Bharali, D. J. & Mousa, S. A. Emerging nanopharmaceuticals. *Nanomedicine : nanotechnology, biology, and medicine* 4, 273-282,**2008**.
- 124 Radowski, M. R., Shukla, A., von Berlepsch, H., Bottcher, C., Pickaert, G., Rehage, H. & Haag, R. Supramolecular aggregates of dendritic multishell architectures as universal nanocarriers. *Angew Chem Int Ed Engl* 46, 1265-1269,**2007**.

- 125 Jones, A. T. & Sayers, E. J. Cell entry of cell penetrating peptides: tales of tails wagging dogs. *Journal of controlled release : official journal of the Controlled Release Society* 161, 582-591,**2012**.
- 126 Silhol, M., Tyagi, M., Giacca, M., Lebleu, B. & Vives, E. Different mechanisms for cellular internalization of the HIV-1 Tat-derived cell penetrating peptide and recombinant proteins fused to Tat. *Eur J Biochem* 269, 494-501,**2002**.
- 127 Berry, C. C. Intracellular delivery of nanoparticles via the HIV-1 tat peptide. *Nanomedicine (Lond)* 3, 357-365,**2008**.
- 128 Santra, S., Yang, H., Dutta, D., Stanley, J. T., Holloway, P. H., Tan, W., Moudgil, B. M. & Mericle, R. A. TAT conjugated, FITC doped silica nanoparticles for bioimaging applications. *Chem Commun (Camb)*, 2810-2811,**2004**.
- 129 Zhang, L. & Eisenberg, A. Multiple Morphologies of "Crew-Cut" Aggregates of Polystyrene-b-poly(acrylic acid) Block Copolymers. *Science* 268, 1728-1731,**1995**.
- 130 Discher, B. M., Won, Y. Y., Ege, D. S., Lee, J. C., Bates, F. S., Discher, D. E. & Hammer, D. A. Polymersomes: tough vesicles made from diblock copolymers. *Science* 284, 1143-1146,**1999**.
- 131 Nagle, J. F. Phospholipid-Bilayers - Physical Principles and Models - Cevc,G, Marsh,D. *Nature* 329, 682-682,**1987**.
- 132 Battaglia, G. & Ryan, A. J. Bilayers and interdigitation in block copolymer vesicles. *J Am Chem Soc* 127, 8757-8764,**2005**.
- 133 Discher, D. E. & Ahmed, F. Polymersomes. *Annu Rev Biomed Eng* 8, 323-341,**2006**.
- 134 LoPresti, C., Lomas, H., Massignani, M., Smart, T. & Battaglia, G. Polymersomes: nature inspired nanometer sized compartments. *J Mater Chem* 19, 3576-3590,**2009**.
- 135 Canton, I. & Battaglia, G. Endocytosis at the nanoscale. *Chem Soc Rev* 41, 2718-2739,**2012**.
- 136 Christian, D. A., Cai, S., Bowen, D. M., Kim, Y., Pajerowski, J. D. & Discher, D. E. Polymersome carriers: from self-assembly to siRNA and protein therapeutics. *Eur J Pharm Biopharm* 71, 463-474,**2009**.
- 137 Pratt, L. R. Molecular theory of hydrophobic effects: "She is too mean to have her name repeated." *Annu Rev Phys Chem* 53, 409-436,**2002**.
- 138 Israelachvili, J. N., Mitchell, D. J. & Ninham, B. W. Theory of Self-Assembly of Hydrocarbon Amphiphiles into Micelles and Bilayers. *J Chem Soc Farad T* 72, 1525-1568,**1976**.
- 139 Pearson, R. T., Avila-Olias, M., Joseph, A.S., Nyberg, S., Battaglia, G., in *Smart Materials for Drug Delivery* Vol. 1 (ed RSC Publishing) Ch. 7, 179-207 (RSC Publishing, 2013).
- 140 Prabha, S., Zhou, W. Z., Panyam, J. & Labhasetwar, V. Size-dependency of nanoparticle-mediated gene transfection: studies with fractionated nanoparticles. *Int J Pharm* 244, 105-115,**2002**.
- 141 Desai, M. P., Labhasetwar, V., Walter, E., Levy, R. J. & Amidon, G. L. The mechanism of uptake of biodegradable microparticles in Caco-2 cells is size dependent. *Pharm Res* 14, 1568-1573,**1997**.
- 142 Chithrani, B. D. & Chan, W. C. Elucidating the mechanism of cellular uptake and removal of protein-coated gold nanoparticles of different sizes and shapes. *Nano Lett* 7, 1542-1550,**2007**.



- 143 Chithrani, B. D., Ghazani, A. A. & Chan, W. C. Determining the size and shape dependence of gold nanoparticle uptake into mammalian cells. *Nano Lett* 6, 662-668,**2006**.
- 144 Geng, Y., Dalhaimer, P., Cai, S., Tsai, R., Tewari, M., Minko, T. & Discher, D. E. Shape effects of filaments versus spherical particles in flow and drug delivery. *Nat Nanotechnol* 2, 249-255,**2007**.
- 145 Champion, J. A. & Mitragotri, S. Role of target geometry in phagocytosis. *Proc Natl Acad Sci U S A* 103, 4930-4934,**2006**.
- 146 Gratton, S. E., Napier, M. E., Ropp, P. A., Tian, S. & DeSimone, J. M. Microfabricated particles for engineered drug therapies: elucidation into the mechanisms of cellular internalization of PRINT particles. *Pharm Res* 25, 2845-2852,**2008**.
- 147 Rabenstein, D. L. Heparin and heparan sulfate: structure and function. *Nat Prod Rep* 19, 312-331,**2002**.
- 148 Parimi, S., Barnes, T. J. & Prestidge, C. A. PAMAM dendrimer interactions with supported lipid bilayers: a kinetic and mechanistic investigation. *Langmuir* 24, 13532-13539,**2008**.
- 149 Leroueil, P. R., Hong, S., Mecke, A., Baker, J. R., Jr., Orr, B. G. & Banaszak Holl, M. M. Nanoparticle interaction with biological membranes: does nanotechnology present a Janus face? *Acc Chem Res* 40, 335-342,**2007**.
- 150 Lin, J., Zhang, H., Chen, Z. & Zheng, Y. Penetration of lipid membranes by gold nanoparticles: insights into cellular uptake, cytotoxicity, and their relationship. *Acs Nano* 4, 5421-5429,**2010**.
- 151 Miller, C. R., Bondurant, B., McLean, S. D., McGovern, K. A. & O'Brien, D. F. Liposome-cell interactions in vitro: effect of liposome surface charge on the binding and endocytosis of conventional and sterically stabilized liposomes. *Biochemistry* 37, 12875-12883,**1998**.
- 152 Kelly, C., Jefferies, C. & Cryan, S. A. Targeted liposomal drug delivery to monocytes and macrophages. *J Drug Deliv* 2011, 727241,**2011**.
- 153 Rathore, S. S. & Ghosh, P. C. Effect of surface charge and density of distearylphosphatidylethanolamine-mPEG-2000 (DSPE-mPEG-2000) on the cytotoxicity of liposome-entrapped ricin: effect of lysosomotropic agents. *Int J Pharm* 350, 79-94,**2008**.
- 154 Blanz, A., Massignani, M., Battaglia, G., Armes, S. P. & Ryan, A. J. Tailoring Macromolecular Expression at Polymersome Surfaces. *Adv Funct Mater* 19, 2906-2914,**2009**.
- 155 Mecke, A., Majoros, I. J., Patri, A. K., Baker, J. R., Jr., Holl, M. M. & Orr, B. G. Lipid bilayer disruption by polycationic polymers: the roles of size and chemical functional group. *Langmuir* 21, 10348-10354,**2005**.
- 156 Kean, T., Roth, S. & Thanou, M. Trimethylated chitosans as non-viral gene delivery vectors: cytotoxicity and transfection efficiency. *Journal of controlled release : official journal of the Controlled Release Society* 103, 643-653,**2005**.
- 157 He, C., Hu, Y., Yin, L., Tang, C. & Yin, C. Effects of particle size and surface charge on cellular uptake and biodistribution of polymeric nanoparticles. *Biomaterials* 31, 3657-3666,**2010**.
- 158 Gratton, S. E., Ropp, P. A., Pohlhaus, P. D., Luft, J. C., Madden, V. J., Napier, M. E. & DeSimone, J. M. The effect of particle design on cellular internalization pathways. *Proc Natl Acad Sci U S A* 105, 11613-11618,**2008**.
- 159 Merhi, M., Dombu, C. Y., Brient, A., Chang, J., Platel, A., Le Curieux, F., Marzin, D., Nessler, F. & Betbeder, D. Study of serum interaction with a

- cationic nanoparticle: Implications for in vitro endocytosis, cytotoxicity and genotoxicity. *Int J Pharm* 423, 37-44,**2012**.
- 160 Doorley, G. W. & Payne, C. K. Cellular binding of nanoparticles in the presence of serum proteins. *Chem Commun (Camb)* 47, 466-468,**2011**.
- 161 Walczyk, D., Bombelli, F. B., Monopoli, M. P., Lynch, I. & Dawson, K. A. What the cell "sees" in bionanoscience. *J Am Chem Soc* 132, 5761-5768,**2010**.
- 162 You, C. C., De, M. & Rotello, V. M. Monolayer-protected nanoparticle-protein interactions. *Curr Opin Chem Biol* 9, 639-646,**2005**.
- 163 Doorley, G. W. & Payne, C. K. Nanoparticles act as protein carriers during cellular internalization. *Chem Commun (Camb)* 48, 2961-2963,**2012**.
- 164 Verma, A., Uzun, O., Hu, Y. H., Hu, Y., Han, H. S., Watson, N., Chen, S. L., Irvine, D. J. & Stellacci, F. Surface-structure-regulated cell-membrane penetration by monolayer-protected nanoparticles. *Nat Mater* 7, 588-595,**2008**.
- 165 LoPresti, C., Massignani, M., Fernyhough, C., Blanazs, A., Ryan, A. J., Madsen, J., Warren, N. J., Armes, S. P., Lewis, A. L., Chirasatitsin, S., Engler, A. J. & Battaglia, G. Controlling polymersome surface topology at the nanoscale by membrane confined polymer/polymer phase separation. *Acs Nano* 5, 1775-1784,**2011**.
- 166 Massignani, M., LoPresti, C., Blanazs, A., Madsen, J., Armes, S. P., Lewis, A. L. & Battaglia, G. Controlling cellular uptake by surface chemistry, size, and surface topology at the nanoscale. *Small* 5, 2424-2432,**2009**.
- 167 Du, J., Tang, Y., Lewis, A. L. & Armes, S. P. pH-sensitive vesicles based on a biocompatible zwitterionic diblock copolymer. *J Am Chem Soc* 127, 17982-17983,**2005**.
- 168 Goda, T. & Ishihara, K. Soft contact lens biomaterials from bioinspired phospholipid polymers. *Expert Rev Med Devices* 3, 167-174,**2006**.
- 169 Lewis, A. L., Tolhurst, L. A. & Stratford, P. W. Analysis of a phosphorylcholine-based polymer coating on a coronary stent pre- and post-implantation. *Biomaterials* 23, 1697-1706,**2002**.
- 170 Moro, T., Takatori, Y., Ishihara, K., Konno, T., Takigawa, Y., Matsushita, T., Chung, U. I., Nakamura, K. & Kawaguchi, H. Surface grafting of artificial joints with a biocompatible polymer for preventing periprosthetic osteolysis. *Nat Mater* 3, 829-836,**2004**.
- 171 Kobayashi, K., Ohuchi, K., Hoshi, H., Morimoto, N., Iwasaki, Y. & Takatani, S. Segmented polyurethane modified by photopolymerization and cross-linking with 2-methacryloyloxyethyl phosphorylcholine polymer for blood-contacting surfaces of ventricular assist devices. *J Artif Organs* 8, 237-244,**2005**.
- 172 Bories-Azeau, X., Armes, S. P. & van den Haak, H. J. W. Facile synthesis of zwitterionic diblock copolymers without protecting group chemistry. *Macromolecules* 37, 2348-2352,**2004**.
- 173 Lomas, H., Massignani, M., Abdullah, K. A., Canton, I., Lo Presti, C., MacNeil, S., Du, J., Blanazs, A., Madsen, J., Armes, S. P., Lewis, A. L. & Battaglia, G. Non-cytotoxic polymer vesicles for rapid and efficient intracellular delivery. *Faraday Discuss* 139, 143-159; discussion 213-128, 419-120,**2008**.
- 174 Massignani, M., Canton, I., Sun, T., Hearnden, V., Macneil, S., Blanazs, A., Armes, S. P., Lewis, A. & Battaglia, G. Enhanced fluorescence imaging of live cells by effective cytosolic delivery of probes. *PLoS One* 5, e10459,**2010**.
- 175 Wayakanon, K., Thornhill, M. H., Douglas, C. W., Lewis, A. L., Warren, N. J., Pinnock, A., Armes, S. P., Battaglia, G. & Murdoch, C. Polymersome-mediated intracellular delivery of antibiotics to treat Porphyromonas gingivalis-infected

- oral epithelial cells. *FASEB journal : official publication of the Federation of American Societies for Experimental Biology* 27, 4455-4465, **2013**.
- 176 Pegoraro, C., Cecchin, D., Gracia, L. S., Warren, N., Madsen, J., Armes, S. P., Lewis, A., MacNeil, S. & Battaglia, G. Enhanced drug delivery to melanoma cells using PMPC-PDPA polymersomes. *Cancer Lett* 334, 328-337, **2013**.
- 177 Lomas, H., Canton, I., MacNeil, S., Du, J., Armes, S. P., Ryan, A. J., Lewis, A. L. & Battaglia, G. Biomimetic pH sensitive polymersomes for efficient DNA encapsulation and delivery. *Adv Mater* 19, 4238-+, **2007**.
- 178 Canton, I., Massignani, M., Patikarnmonthon, N., Chierico, L., Robertson, J., Renshaw, S. A., Warren, N. J., Madsen, J. P., Armes, S. P., Lewis, A. L. & Battaglia, G. Fully synthetic polymer vesicles for intracellular delivery of antibodies in live cells. *FASEB journal : official publication of the Federation of American Societies for Experimental Biology* 27, 98-108, **2013**.
- 179 Haldar, K., Samuel, B. U., Mohandas, N., Harrison, T. & Hiller, N. L. Transport mechanisms in Plasmodium-infected erythrocytes: lipid rafts and a tubovesicular network. *Int J Parasitol* 31, 1393-1401, **2001**.
- 180 Groebel, K., Hoelzle, K., Wittenbrink, M. M., Ziegler, U. & Hoelzle, L. E. Mycoplasma suis invades porcine erythrocytes. *Infect Immun* 77, 576-584, **2009**.
- 181 Sourisseau, M., Michta, M. L., Zony, C., Israelow, B., Hopcraft, S. E., Narbus, C. M., Martin, A. P. & Evans, M. J. Temporal Analysis of Hepatitis C Virus Cell Entry with Occludin Directed Blocking Antibodies. *Plos Pathog* 9, **2013**.
- 182 Pearson, R. T., Warren, N. J., Lewis, A. L., Armes, S. P. & Battaglia, G. Effect of pH and Temperature on PMPC-PDPA Copolymer Self-Assembly. *Macromolecules* 46, 1400-1407, **2013**.
- 183 Madsen, J., Warren, N. J., Armes, S. P. & Lewis, A. L. Synthesis of rhodamine 6G-based compounds for the ATRP synthesis of fluorescently labeled biocompatible polymers. *Biomacromolecules* 12, 2225-2234, **2011**.
- 184 Wilson, G. K. *Mechanism(s) of hepatitis C virus induced liver injury* PhD thesis, The University of Birmingham, (2012).
- 185 Wang, L. G., Chierico, L., Little, D., Patikarnmonthon, N., Yang, Z., Azzouz, M., Madsen, J., Armes, S. P. & Battaglia, G. Encapsulation of Biomacromolecules within Polymersomes by Electroporation. *Angew Chem Int Edit* 51, 11122-11125, **2012**.
- 186 Bradford, M. M. A rapid and sensitive method for the quantitation of microgram quantities of protein utilizing the principle of protein-dye binding. *Anal Biochem* 72, 248-254, **1976**.
- 187 Mosmann, T. Rapid colorimetric assay for cellular growth and survival: application to proliferation and cytotoxicity assays. *J Immunol Methods* 65, 55-63, **1983**.
- 188 Ale, M. T., Mikkelsen, J. D. & Meyer, A. S. Important determinants for fucoidan bioactivity: a critical review of structure-function relations and extraction methods for fucose-containing sulfated polysaccharides from brown seaweeds. *Mar Drugs* 9, 2106-2130, **2011**.
- 189 Johannes, L. & Mayor, S. Induced domain formation in endocytic invagination, lipid sorting, and scission. *Cell* 142, 507-510, **2010**.
- 190 Rangan, S. R. S. New Human Cell Line (Fadu) from a Hypopharyngeal Carcinoma. *Cancer* 29, 117-&, **1972**.
- 191 Murdoch, C., Reeves, K. J., Hearnden, V., Colley, H., Massignani, M., Canton, I., Madsen, J., Blanzas, A., Armes, S. P., Lewis, A. L., MacNeil, S., Brown, N. J., Thornhill, M. H. & Battaglia, G. Internalization and biodistribution of

- polymersomes into oral squamous cell carcinoma cells in vitro and in vivo. *Nanomedicine (Lond)* 5, 1025-1036,**2010**.
- 192 Smart, T. P., Mykhaylyk, O. O., Ryan, A. J. & Battaglia, G. Polymersomes hydrophilic brush scaling relations. *Soft Matter* 5, 3607-3610,**2009**.
- 193 Battaglia, G. & Ryan, A. J. Bilayers and interdigitation in block copolymer vesicles. *J Am Chem Soc* 127, 8757-8764,**2005**.
- 194 Robertson, J. D., Yealland, G., Avila-Olias, M., Chierico, L., Bandmann, O., Renshaw, S. A. & Battaglia, G. pH-Sensitive Tubular Polymersomes: Formation and Applications in Cellular Delivery. *Acs Nano*,**2014**.
- 195 Mayor, S. & Pagano, R. E. Pathways of clathrin-independent endocytosis. *Nat Rev Mol Cell Biol* 8, 603-612,**2007**.
- 196 Ahmed, F., Pakunlu, R. I., Srinivas, G., Brannan, A., Bates, F., Klein, M. L., Minko, T. & Discher, D. E. Shrinkage of a rapidly growing tumor by drug-loaded polymersomes: pH-triggered release through copolymer degradation. *Mol Pharm* 3, 340-350,**2006**.
- 197 Liang, H. F., Yang, T. F., Huang, C. T., Chen, M. C. & Sung, H. W. Preparation of nanoparticles composed of poly( $\gamma$ -glutamic acid)-poly(lactide) block copolymers and evaluation of their uptake by HepG2 cells. *Journal of controlled release : official journal of the Controlled Release Society* 105, 213-225,**2005**.
- 198 Kakizawa, Y., Furukawa, S. & Kataoka, K. Block copolymer-coated calcium phosphate nanoparticles sensing intracellular environment for oligodeoxynucleotide and siRNA delivery. *Journal of controlled release : official journal of the Controlled Release Society* 97, 345-356,**2004**.
- 199 Vila, A., Sanchez, A., Janes, K., Behrens, I., Kissel, T., Jato, J. L. V. & Alonso, M. J. Low molecular weight chitosan nanoparticles as new carriers for nasal vaccine delivery in mice. *European Journal of Pharmaceutics and Biopharmaceutics* 57, 123-131,**2004**.
- 200 d'Angelo, I., Garcia-Fuentes, M., Parajo, Y., Welle, A., Vantus, T., Horvath, A., Bokonyi, G., Keri, G. & Alonso, M. J. Nanoparticles Based on PLGA:Poloxamer Blends for the Delivery of Proangiogenic Growth Factors. *Mol Pharm* 7, 1724-1733,**2010**.
- 201 Barati, R., Johnson, S. J., McCool, S., Green, D. W., Willhite, G. P. & Liang, J. T. Fracturing Fluid Cleanup by Controlled Release of Enzymes from Polyelectrolyte Complex Nanoparticles. *J Appl Polym Sci* 121, 1292-1298,**2011**.
- 202 Italia, J. L., Yahya, M. M., Singh, D. & Kumar, M. N. V. R. Biodegradable Nanoparticles Improve Oral Bioavailability of Amphotericin B and Show Reduced Nephrotoxicity Compared to Intravenous FungizoneA (R). *Pharm Res* 26, 1324-1331,**2009**.
- 203 Chaudhuri, A., Battaglia, G. & Golestanian, R. The effect of interactions on the cellular uptake of nanoparticles. *Phys Biol* 8,**2011**.
- 204 Christian, D. A., Cai, S., Garbuzenko, O. B., Harada, T., Zajac, A. L., Minko, T. & Discher, D. E. Flexible filaments for in vivo imaging and delivery: persistent circulation of filomicelles opens the dosage window for sustained tumor shrinkage. *Mol Pharm* 6, 1343-1352,**2009**.
- 205 Cai, S., Vijayan, K., Cheng, D., Lima, E. M. & Discher, D. E. Micelles of different morphologies--advantages of worm-like filomicelles of PEO-PCL in paclitaxel delivery. *Pharm Res* 24, 2099-2109,**2007**.
- 206 Reiner, J. E., Wells, J. M., Kishore, R. B., Pfefferkorn, C. & Helmerson, K. Stable and robust polymer nanotubes stretched from polymersomes. *Proc Natl Acad Sci U S A* 103, 1173-1177,**2006**.

- 207 van Oers, M. C., Rutjes, F. P. & van Hest, J. C. Tubular polymersomes: a cross-linker-induced shape transformation. *J Am Chem Soc* 135, 16308-16311,**2013**.
- 208 Grumelard, J., Taubert, A. & Meier, W. Soft nanotubes from amphiphilic ABA triblock macromonomers. *Chem Commun (Camb)*, 1462-1463,**2004**.
- 209 Ishihara, K., Nomura, H., Mihara, T., Kurita, K., Iwasaki, Y. & Nakabayashi, N. Why do phospholipid polymers reduce protein adsorption? *J Biomed Mater Res* 39, 323-330,**1998**.
- 210 Lewis, A. L. Phosphorylcholine-based polymers and their use in the prevention of biofouling. *Colloids Surf B Biointerfaces* 18, 261-275,**2000**.
- 211 Li, S. D. & Huang, L. Pharmacokinetics and biodistribution of nanoparticles. *Mol Pharm* 5, 496-504,**2008**.
- 212 Jokerst, J. V., Lobovkina, T., Zare, R. N. & Gambhir, S. S. Nanoparticle PEGylation for imaging and therapy. *Nanomedicine (Lond)* 6, 715-728,**2011**.
- 213 Goldstein, J. L., Ho, Y. K., Basu, S. K. & Brown, M. S. Binding site on macrophages that mediates uptake and degradation of acetylated low density lipoprotein, producing massive cholesterol deposition. *Proc Natl Acad Sci U S A* 76, 333-337,**1979**.
- 214 Brown, M. S., Goldstein, J. L., Krieger, M., Ho, Y. K. & Anderson, R. G. Reversible accumulation of cholesteryl esters in macrophages incubated with acetylated lipoproteins. *J Cell Biol* 82, 597-613,**1979**.
- 215 Janssen, K. P., Rost, R., Eichinger, L. & Schleicher, M. Characterization of CD36/LIMPII homologues in Dictyostelium discoideum. *The Journal of biological chemistry* 276, 38899-38910,**2001**.
- 216 Pluddemann, A., Neyen, C. & Gordon, S. Macrophage scavenger receptors and host-derived ligands. *Methods* 43, 207-217,**2007**.
- 217 Stephen, S. L., Freestone, K., Dunn, S., Twigg, M. W., Homer-Vanniasinkam, S., Walker, J. H., Wheatcroft, S. B. & Ponnambalam, S. Scavenger receptors and their potential as therapeutic targets in the treatment of cardiovascular disease. *Int J Hypertens* 2010, 646929,**2010**.
- 218 Baranova, I. N., Vishnyakova, T. G., Bocharov, A. V., Leelahavanichkul, A., Kurlander, R., Chen, Z., Souza, A. C., Yuen, P. S., Star, R. A., Csako, G., Patterson, A. P. & Eggerman, T. L. Class B scavenger receptor types I and II and CD36 mediate bacterial recognition and proinflammatory signaling induced by Escherichia coli, lipopolysaccharide, and cytosolic chaperonin 60. *J Immunol* 188, 1371-1380,**2012**.
- 219 Patel, P. C., Giljohann, D. A., Daniel, W. L., Zheng, D., Prigodich, A. E. & Mirkin, C. A. Scavenger receptors mediate cellular uptake of polyvalent oligonucleotide-functionalized gold nanoparticles. *Bioconjug Chem* 21, 2250-2256,**2010**.
- 220 Ezzat, K., Helmfors, H., Tudoran, O., Juks, C., Lindberg, S., Padari, K., El-Andaloussi, S., Pooga, M. & Langel, U. Scavenger receptor-mediated uptake of cell-penetrating peptide nanocomplexes with oligonucleotides. *FASEB journal : official publication of the Federation of American Societies for Experimental Biology* 26, 1172-1180,**2012**.
- 221 Zhang, L. W. & Monteiro-Riviere, N. A. Mechanisms of quantum dot nanoparticle cellular uptake. *Toxicol Sci* 110, 138-155,**2009**.
- 222 Kanno, S., Furuyama, A. & Hirano, S. A murine scavenger receptor MARCO recognizes polystyrene nanoparticles. *Toxicol Sci* 97, 398-406,**2007**.

- 223 Wang, H. Y., Wu, L. X. & Reinhard, B. M. Scavenger Receptor Mediated Endocytosis of Silver Nanoparticles into J774A.1 Macrophages Is Heterogeneous. *Acs Nano* 6, 7122-7132,**2012**.
- 224 Boullier, A., Friedman, P., Harkewicz, R., Hartvigsen, K., Green, S. R., Almazan, F., Dennis, E. A., Steinberg, D., Witztum, J. L. & Quehenberger, O. Phosphocholine as a pattern recognition ligand for CD36. *J Lipid Res* 46, 969-976,**2005**.
- 225 Marshall-Clarke, S., Downes, J. E., Haga, I. R., Bowie, A. G., Borrow, P., Pennock, J. L., Grecnis, R. K. & Rothwell, P. Polyinosinic acid is a ligand for toll-like receptor 3. *J Biol Chem* 282, 24759-24766,**2007**.
- 226 Husemann, J., Loike, J. D., Kodama, T. & Silverstein, S. C. Scavenger receptor class B type I (SR-BI) mediates adhesion of neonatal murine microglia to fibrillar beta-amyloid. *J Neuroimmunol* 114, 142-150,**2001**.
- 227 Terpstra, V. & van Berkel, T. J. Scavenger receptors on liver Kupffer cells mediate the in vivo uptake of oxidatively damaged red blood cells in mice. *Blood* 95, 2157-2163,**2000**.
- 228 Webb, N. R., Connell, P. M., Graf, G. A., Smart, E. J., de Villiers, W. J., de Beer, F. C. & van der Westhuyzen, D. R. SR-BII, an isoform of the scavenger receptor BI containing an alternate cytoplasmic tail, mediates lipid transfer between high density lipoprotein and cells. *The Journal of biological chemistry* 273, 15241-15248,**1998**.
- 229 Terpstra, V., van Amersfoort, E. S., van Velzen, A. G., Kuiper, J. & van Berkel, T. J. Hepatic and extrahepatic scavenger receptors: function in relation to disease. *Arterioscler Thromb Vasc Biol* 20, 1860-1872,**2000**.
- 230 Endemann, G., Stanton, L. W., Madden, K. S., Bryant, C. M., White, R. T. & Protter, A. A. Cd36 Is a Receptor for Oxidized Low-Density-Lipoprotein. *J Biol Chem* 268, 11811-11816,**1993**.
- 231 Scarselli, E., Ansuini, H., Cerino, R., Roccasecca, R. M., Acali, S., Filocamo, G., Traboni, C., Nicosia, A., Cortese, R. & Vitelli, A. The human scavenger receptor class B type I is a novel candidate receptor for the hepatitis C virus. *Embo J* 21, 5017-5025,**2002**.
- 232 Acton, S., Rigotti, A., Landschulz, K. T., Xu, S. Z., Hobbs, H. H. & Krieger, M. Identification of scavenger receptor SR-BI as a high density lipoprotein receptor. *Science* 271, 518-520,**1996**.
- 233 Eckhardt, E. R., Cai, L., Sun, B., Webb, N. R. & van der Westhuyzen, D. R. High density lipoprotein uptake by scavenger receptor SR-BII. *The Journal of biological chemistry* 279, 14372-14381,**2004**.
- 234 Rohrl, C. & Stangl, H. HDL endocytosis and resecretion. *Biochim Biophys Acta* 1831, 1626-1633,**2013**.
- 235 Masson, D., Koseki, M., Ishibashi, M., Larson, C. J., Miller, S. G., King, B. D. & Tall, A. R. Increased HDL Cholesterol and ApoA-I in Humans and Mice Treated With a Novel SR-BI Inhibitor. *Arterioscl Throm Vas* 29, 2054-U2170,**2009**.
- 236 Syder, A. J., Lee, H., Zeisel, M. B., Grove, J., Soulier, E., Macdonald, J., Chow, S., Chang, J., Baumert, T. F., McKeating, J. A., McKelvy, J. & Wong-Staal, F. Small molecule scavenger receptor BI antagonists are potent HCV entry inhibitors. *J Hepatol* 54, 48-55,**2011**.
- 237 Wright, M. D., Henkle, K. J. & Mitchell, G. F. An Immunogenic-Mr 23,000 Integral Membrane-Protein of Schistosoma-Mansoni Worms That Closely

- Resembles a Human Tumor-Associated Antigen. *J Immunol* 144, 3195-3200,**1990**.
- 238 Oren, R., Takahashi, S., Doss, C., Levy, R. & Levy, S. Tapa-1, the Target of an Antiproliferative Antibody, Defines a New Family of Transmembrane Proteins. *Mol Cell Biol* 10, 4007-4015,**1990**.
- 239 Charrin, S., Le Naour, F., Silvie, O., Milhiet, P. E., Boucheix, C. & Rubinstein, E. Lateral organization of membrane proteins: tetraspanins spin their web. *Biochem J* 420, 133-154,**2009**.
- 240 Monk, P. N. & Partridge, L. J. Tetraspanins: gateways for infection. *Infect Disord Drug Targets* 12, 4-17,**2012**.
- 241 Yalaoui, S., Huby, T., Franetich, J. F., Gego, A., Rametti, A., Moreau, M., Collet, X., Siau, A., van Gemert, G. J., Sauerwein, R. W., Luty, A. J., Vaillant, J. C., Hannoun, L., Chapman, J., Mazier, D. & Froissard, P. Scavenger receptor BI boosts hepatocyte permissiveness to Plasmodium infection. *Cell Host Microbe* 4, 283-292,**2008**.
- 242 Nel, A. E., Madler, L., Velegol, D., Xia, T., Hoek, E. M., Somasundaran, P., Klaessig, F., Castranova, V. & Thompson, M. Understanding biophysicochemical interactions at the nano-bio interface. *Nat Mater* 8, 543-557,**2009**.
- 243 Sugio, S., Kashima, A., Mochizuki, S., Noda, M. & Kobayashi, K. Crystal structure of human serum albumin at 2.5 angstrom resolution. *Protein Eng* 12, 439-446,**1999**.
- 244 Saleh, M. C., van Rij, R. P., Hekele, A., Gillis, A., Foley, E., O'Farrell, P. H. & Andino, R. The endocytic pathway mediates cell entry of dsRNA to induce RNAi silencing. *Nat Cell Biol* 8, 793-802,**2006**.
- 245 Fitton, J. H. Therapies from Fucoidan; Multifunctional Marine Polymers. *Mar Drugs* 9, 1731-1760,**2011**.
- 246 Manne, B. K., Getz, T. M., Hughes, C. E., Alshehri, O., Dangelmaier, C., Naik, U. P., Watson, S. P. & Kunapuli, S. P. Fucoidan Is a Novel Platelet Agonist for the C-type Lectin-like Receptor 2 (CLEC-2). *J Biol Chem* 288, 7717-7726,**2013**.
- 247 Figdor, C. G. & van Sriel, A. B. Fungal pattern-recognition receptors and tetraspanins: partners on antigen-presenting cells. *Trends Immunol* 31, 91-96,**2010**.
- 248 Nagayama, S., Ogawara, K., Minato, K., Fukuoka, Y., Takakura, Y., Hashida, M., Higaki, K. & Kimura, T. Fetuin mediates hepatic uptake of negatively charged nanoparticles via scavenger receptor. *Int J Pharm* 329, 192-198,**2007**.
- 249 Broz, P., Benito, S. M., Saw, C., Burger, P., Heider, H., Pfisterer, M., Marsch, S., Meier, W. & Hunziker, P. Cell targeting by a generic receptor-targeted polymer nanocontainer platform. *J Control Release* 102, 475-488,**2005**.
- 250 Chnari, E., Nikitzuk, J. S., Wang, J. Z., Uhrich, K. E. & Moghe, P. V. Engineered polymeric nanoparticles for receptor-targeted blockage of oxidized low density lipoprotein uptake and atherogenesis in macrophages. *Biomacromolecules* 7, 1796-1805,**2006**.
- 251 Choi, C. H., Hao, L., Narayan, S. P., Auyeung, E. & Mirkin, C. A. Mechanism for the endocytosis of spherical nucleic acid nanoparticle conjugates. *Proc Natl Acad Sci U S A* 110, 7625-7630,**2013**.
- 252 Scheel, T. K. H. & Rice, C. M. Understanding the hepatitis C virus life cycle paves the way for highly effective therapies. *Nat Med* 19, 837-849,**2013**.
- 253 Assanasen, C., Mineo, C., Seetharam, D., Yuhanna, I. S., Marcel, Y. L., Connelly, M. A., Williams, D. L., de la Llera-Moya, M., Shaul, P. W. & Silver,

- D. L. Cholesterol binding, efflux, and a PDZ-interacting domain of scavenger receptor-BI mediate HDL-initiated signaling. *J Clin Invest* 115, 969-977,**2005**.
- 254 Charrin, S., Manie, S., Thiele, C., Billard, M., Gerlier, D., Boucheix, C. & Rubinstein, E. A physical and functional link between cholesterol and tetraspanins. *Eur J Immunol* 33, 2479-2489,**2003**.
- 255 Babitt, J., Trigatti, B., Rigotti, A., Smart, E. J., Anderson, R. G. W., Xu, S. Z. & Krieger, M. Murine SR-BI, a high density lipoprotein receptor that mediates selective lipid uptake, is N-glycosylated and fatty acylated and colocalizes with plasma membrane caveolae. *J Biol Chem* 272, 13242-13249,**1997**.
- 256 Vercauteren, D., Vandenbroucke, R. E., Jones, A. T., Rejman, J., Demeester, J., De Smedt, S. C., Sanders, N. N. & Braeckmans, K. The Use of Inhibitors to Study Endocytic Pathways of Gene Carriers: Optimization and Pitfalls. *Mol Ther* 18, 561-569,**2010**.
- 257 Al-Soraj, M. H., Watkins, C. L., Vercauteren, D., De Smedt, S. C., Braeckmans, K. & Jones, A. T. siRNA versus pharmacological inhibition of endocytic pathways for studying cellular uptake of cell penetrating peptides. *Journal of controlled release : official journal of the Controlled Release Society* 148, e86-87,**2010**.
- 258 Sandgren, K. J., Wilkinson, J., Miranda-Saksena, M., McInerney, G. M., Byth-Wilson, K., Robinson, P. J. & Cunningham, A. L. A Differential Role for Macropinocytosis in Mediating Entry of the Two Forms of Vaccinia Virus into Dendritic Cells. *Plos Pathog* 6,**2010**.
- 259 Al Soraj, M., He, L., Peynshaert, K., Cousaert, J., Vercauteren, D., Braeckmans, K., De Smedt, S. C. & Jones, A. T. siRNA and pharmacological inhibition of endocytic pathways to characterize the differential role of macropinocytosis and the actin cytoskeleton on cellular uptake of dextran and cationic cell penetrating peptides octaarginine (R8) and HIV-Tat. *Journal of controlled release : official journal of the Controlled Release Society* 161, 132-141,**2012**.
- 260 Sun, V. Z., Li, Z. B., Deming, T. J. & Kamei, D. T. Intracellular Fates of Cell-Penetrating Block Copolypeptide Vesicles. *Biomacromolecules* 12, 10-13,**2011**.
- 261 Takahashi, K., Miyoshi, H., Otomo, M., Osada, K., Yamaguchi, N. & Nakashima, H. Suppression of dynamin GTPase activity by sertraline leads to inhibition of dynamin-dependent endocytosis. *Biochem Biophys Res Commun.* 391, 382-387. Epub 2009 Nov 2012.,**2010**.
- 262 Schutze, S., Machleidt, T., Adam, D., Schwandner, R., Wiegmann, K., Kruse, M. L., Heinrich, M., Wickel, M. & Kronke, M. Inhibition of receptor internalization by monodansylcadaverine selectively blocks p55 tumor necrosis factor receptor death domain signaling. *J Biol Chem* 274, 10203-10212,**1999**.
- 263 Zhang, X., Jin, Y., Plummer, M. R., Pooyan, S., Gunaseelan, S. & Sinko, P. J. Endocytosis and membrane potential are required for HeLa cell uptake of R.I.-CKTat9, a retro-inverso Tat cell penetrating peptide. *Mol Pharm* 6, 836-848,**2009**.
- 264 Torgersen, M. L., Skretting, G., van Deurs, B. & Sandvig, K. Internalization of cholera toxin by different endocytic mechanisms. *J Cell Sci.* 114, 3737-3747.,**2001**.
- 265 Ravikumar, B., Moreau, K., Jahreiss, L., Puri, C. & Rubinsztein, D. C. Plasma membrane contributes to the formation of pre-autophagosomal structures. *Nat Cell Biol.* 12, 747-757. Epub 2010 Jul 2018.,**2010**.



- 266 Kirchhausen, T., Macia, E. & Pelish, H. E. Use of dynasore, the small molecule inhibitor of dynamin, in the regulation of endocytosis. *Method Enzymol* 438, 77-93,**2008**.
- 267 Contreras, J., Xie, J., Chen, Y. J., Pei, H., Zhang, G., Fraser, C. L. & Hamm-Alvarez, S. F. Intracellular uptake and trafficking of difluoroboron dibenzoylmethane-poly lactide nanoparticles in HeLa cells. *ACS Nano.* 4, 2735-2747.,**2010**.
- 268 Carvou, N., Holic, R., Li, M., Futter, C., Skippen, A. & Cockcroft, S. Phosphatidylinositol- and phosphatidylcholine-transfer activity of PITPbeta is essential for COPI-mediated retrograde transport from the Golgi to the endoplasmic reticulum. *J Cell Sci.* 123, 1262-1273. Epub 2010 Mar 1223.,**2010**.
- 269 Hattula, K., Furuholm, J., Tikkanen, J., Tanhuanpaa, K., Laakkonen, P. & Peranen, J. Characterization of the Rab8-specific membrane traffic route linked to protrusion formation. *J Cell Sci.* 119, 4866-4877. Epub 2006 Nov 4814.,**2006**.
- 270 Patel, P. C., Giljohann, D. A., Daniel, W. L., Zheng, D., Prigodich, A. E. & Mirkin, C. A. Scavenger Receptors Mediate Cellular Uptake of Polyvalent Oligonucleotide-Functionalized Gold Nanoparticles. *Bioconjug Chem* 11, 11,**2010**.
- 271 Kalin, S., Amstutz, B., Gastaldelli, M., Wolfrum, N., Boucke, K., Havenga, M., DiGennaro, F., Liska, N., Hemmi, S. & Greber, U. F. Macropinocytotic uptake and infection of human epithelial cells with species B2 adenovirus type 35. *J Virol* 84, 5336-5350,**2010**.
- 272 de Vries, E., Tscherne, D. M., Wienholts, M. J., Cobos-Jimenez, V., Scholte, F., Garcia-Sastre, A., Rottier, P. J. & de Haan, C. A. Dissection of the influenza A virus endocytic routes reveals macropinocytosis as an alternative entry pathway. *Plos Pathog* 7, e1001329,**2011**.
- 273 Peterson, J. R. & Mitchison, T. J. Small molecules, big impact: a history of chemical inhibitors and the cytoskeleton. *Chem Biol* 9, 1275-1285,**2002**.
- 274 Hansen, S. H., Sandvig, K. & Vandeurs, B. Internalization Efficiency of the Transferrin Receptor. *Exp Cell Res* 199, 19-28,**1992**.
- 275 Torgersen, M. L., Skretting, G., van Deurs, B. & Sandvig, K. Internalization of cholera toxin by different endocytic mechanisms. *J Cell Sci* 114, 3737-3747,**2001**.
- 276 Chinnapen, D. J., Chinnapen, H., Saslowsky, D. & Lencer, W. I. Rafting with cholera toxin: endocytosis and trafficking from plasma membrane to ER. *FEMS Microbiol Lett* 266, 129-137,**2007**.
- 277 Wolf, A. A., Fujinaga, Y. & Lencer, W. I. Uncoupling of the cholera toxin-G(M1) ganglioside receptor complex from endocytosis, retrograde Golgi trafficking, and downstream signal transduction by depletion of membrane cholesterol. *The Journal of biological chemistry* 277, 16249-16256,**2002**.
- 278 Lajoie, P., Kojic, L. D., Nim, S., Li, L., Dennis, J. W. & Nabi, I. R. Caveolin-1 regulation of dynamin-dependent, raft-mediated endocytosis of cholera toxin-B sub-unit occurs independently of caveolae. *J Cell Mol Med* 13, 3218-3225,**2009**.
- 279 Lajoie, P. & Nabi, I. R. Lipid Rafts, Caveolae, and Their Endocytosis. *Int Rev Cel Mol Bio* 282, 135-163,**2010**.
- 280 Marks, B., Stowell, M. H. B., Vallis, Y., Mills, I. G., Gibson, A., Hopkins, C. R. & McMahon, H. T. GTPase activity of dynamin and resulting conformation change are essential for endocytosis. *Nature* 410, 231-235,**2001**.

- 281 van der Blik, A. M., Redelmeier, T. E., Damke, H., Tisdale, E. J., Meyerowitz,  
E. M. & Schmid, S. L. Mutations in human dynamin block an intermediate stage  
in coated vesicle formation. *J Cell Biol* 122, 553-563,**1993**.
- 282 Zhang, X. D. Illustration of SSMD, z score, SSMD\*, z\* score, and t statistic for  
hit selection in RNAi high-throughput screens. *J Biomol Screen* 16, 775-  
785,**2011**.
- 283 Sen, A., Madhivanan, K., Mukherjee, D. & Aguilar, R. C. The epsin protein  
family: coordinators of endocytosis and signaling. *Biomol Concepts* 3, 117-  
126,**2012**.
- 284 Zimmermann, K., Opitz, N., Dedio, J., Renne, C., Muller-Esterl, W. & Oess, S.  
NOSTRIN: A protein modulating nitric oxide release and subcellular  
distribution of endothelial nitric oxide synthase. *Proc Natl Acad Sci U S A* 99,  
17167-17172,**2002**.
- 285 Schelhaas, M. Come in and take your coat off - how host cells provide  
endocytosis for virus entry. *Cell Microbiol* 12, 1378-1388,**2010**.
- 286 Robertson, A. S., Smythe, E. & Ayscough, K. R. Functions of actin in  
endocytosis. *Cell Mol Life Sci* 66, 2049-2065,**2009**.
- 287 Pelkmans, L. & Helenius, A. Endocytosis via caveolae. *Traffic* 3, 311-320,**2002**.
- 288 Mercer, J. & Helenius, A. Virus entry by macropinocytosis. *Nat Cell Biol* 11,  
510-520,**2009**.
- 289 Damke, H., Baba, T., Vanderblik, A. M. & Schmid, S. L. Clathrin-Independent  
Pinocytosis Is Induced in Cells Overexpressing a Temperature-Sensitive Mutant  
of Dynamin. *Journal of Cell Biology* 131, 69-80,**1995**.
- 290 Jiang, W., Kim, B. Y., Rutka, J. T. & Chan, W. C. Nanoparticle-mediated  
cellular response is size-dependent. *Nat Nanotechnol* 3, 145-150,**2008**.
- 291 Yuan, H. Y. & Zhang, S. L. Effects of particle size and ligand density on the  
kinetics of receptor-mediated endocytosis of nanoparticles. *Appl Phys Lett*  
96,**2010**.
- 292 Gao, H., Shi, W. & Freund, L. B. Mechanics of receptor-mediated endocytosis.  
*Proc Natl Acad Sci U S A* 102, 9469-9474,**2005**.
- 293 Zhang, S., Li, J., Lykotrafitis, G., Bao, G. & Suresh, S. Size-Dependent  
Endocytosis of Nanoparticles. *Adv Mater* 21, 419-424,**2009**.
- 294 Catanese, M. T., Loureiro, J., Jones, C. T., Dorner, M., von Hahn, T. & Rice, C.  
M. Different requirements for scavenger receptor class B type I in hepatitis C  
virus cell-free versus cell-to-cell transmission. *J Virol* 87, 8282-8293,**2013**.
- 295 Zahid, M. N., Turek, M., Xiao, F., Thi, V. L., Guerin, M., Fofana, I., Bachellier,  
P., Thompson, J., Delang, L., Neyts, J., Bankwitz, D., Pietschmann, T., Dreux,  
M., Cosset, F. L., Grunert, F., Baumert, T. F. & Zeisel, M. B. The postbinding  
activity of scavenger receptor class B type I mediates initiation of hepatitis C  
virus infection and viral dissemination. *Hepatology* 57, 492-504,**2013**.
- 296 Sinha, B., Koster, D., Ruez, R., Gonnord, P., Bastiani, M., Abankwa, D., Stan,  
R. V., Butler-Browne, G., Védie, B., Johannes, L., Morone, N., Parton, R. G.,  
Raposo, G., Sens, P., Lamaze, C. & Nassoy, P. Cells respond to mechanical  
stress by rapid disassembly of caveolae. *Cell* 144, 402-413,**2011**.
- 297 Ehrlich, M., Boll, W., Van Oijen, A., Hariharan, R., Chandran, K., Nibert, M. L.  
& Kirchhausen, T. Endocytosis by random initiation and stabilization of  
clathrin-coated pits. *Cell* 118, 591-605,**2004**.
- 298 Cureton, D. K., Harbison, C. E., Cocucci, E., Parrish, C. R. & Kirchhausen, T.  
Limited Transferrin Receptor Clustering Allows Rapid Diffusion of Canine  
Parvovirus into Clathrin Endocytic Structures. *J Virol* 86, 5330-5340,**2012**.

- 299 Vainio, S., Heino, S., Mansson, J. E., Fredman, P., Kuismanen, E., Vaarala, O. & Ikonen, E. Dynamic association of human insulin receptor with lipid rafts in cells lacking caveolae. *EMBO Rep* 3, 95-100,**2002**.
- 300 Chinnapen, D. J. F., Chinnapen, H., Saslowsky, D. & Lencer, W. I. Rafting with cholera toxin: endocytosis and trafficking from plasma membrane to ER. *FEMS Microbiol Lett* 266, 129-137,**2007**.
- 301 Sandvig, K., Olsnes, S., Brown, J. E., Petersen, O. W. & van Deurs, B. Endocytosis from coated pits of Shiga toxin: a glycolipid-binding protein from *Shigella dysenteriae* 1. *J Cell Biol* 108, 1331-1343,**1989**.
- 302 Damm, E. M., Pelkmans, L., Kartenbeck, J., Mezzacasa, A., Kurzchalia, T. & Helenius, A. Clathrin- and caveolin-1-independent endocytosis: entry of simian virus 40 into cells devoid of caveolae. *J Cell Biol* 168, 477-488,**2005**.
- 303 Lauvrak, S. U., Torgersen, M. L. & Sandvig, K. Efficient endosome-to-Golgi transport of Shiga toxin is dependent on dynamin and clathrin. *J Cell Sci* 117, 2321-2331,**2004**.
- 304 Romer, W., Berland, L., Chambon, V., Gaus, K., Windschiegl, B., Tenza, D., Aly, M. R. E., Fraissier, V., Florent, J. C., Perrais, D., Lamaze, C., Raposo, G., Steinem, C., Sens, P., Bassereau, P. & Johannes, L. Shiga toxin induces tubular membrane invaginations for its uptake into cells. *Nature* 450, 670-U673,**2007**.
- 305 Ewers, H., Romer, W., Smith, A. E., Bacia, K., Dmitrieff, S., Chai, W., Mancini, R., Kartenbeck, J., Chambon, V., Berland, L., Oppenheim, A., Schwarzmann, G., Feizi, T., Schwille, P., Sens, P., Helenius, A. & Johannes, L. GM1 structure determines SV40-induced membrane invagination and infection. *Nat Cell Biol* 12, 11-18; sup pp 11-12,**2010**.
- 306 Schorb, M. & Briggs, J. A. Correlated cryo-fluorescence and cryo-electron microscopy with high spatial precision and improved sensitivity. *Ultramicroscopy*,**2013**.
- 307 Kukulski, W., Schorb, M., Welsch, S., Picco, A., Kaksonen, M. & Briggs, J. A. Correlated fluorescence and 3D electron microscopy with high sensitivity and spatial precision. *J Cell Biol* 192, 111-119,**2011**.
- 308 Daumke, O., Lundmark, R., Vallis, Y., Martens, S., Butler, P. J. G. & McMahon, H. T. Architectural and mechanistic insights into an EHD ATPase involved in membrane remodelling. *Nature* 449, 923-U915,**2007**.
- 309 Roux, A., Cuvelier, D., Nassoy, P., Prost, J., Bassereau, P. & Goud, B. Role of curvature and phase transition in lipid sorting and fission of membrane tubules. *Embo Journal* 24, 1537-1545,**2005**.
- 310 Zhao, Y., Sun, X., Zhang, G., Trewyn, B. G., Slowing, II & Lin, V. S. Interaction of mesoporous silica nanoparticles with human red blood cell membranes: size and surface effects. *Acs Nano* 5, 1366-1375,**2011**.
- 311 Le Bihan, O., Bonnafous, P., Marak, L., Bickel, T., Trepout, S., Mornet, S., De Haas, F., Talbot, H., Taveau, J. C. & Lambert, O. Cryo-electron tomography of nanoparticle transmigration into liposome. *J Struct Biol* 168, 419-425,**2009**.
- 312 Kawai, T. & Akira, S. Innate immune recognition of viral infection. *Nat Immunol* 7, 131-137,**2006**.
- 313 Urquijo, J. J., Diago, M., Boadas, J., Planas, R., Sola, R., Del Olmo, J. A., Crespo, J., Erdozain, J. C., Anton, M. D., Arocena, C., Suarez, D., Gine, J., Barrera, J. M., Gracia-Samaniego, J., Perez, R., Dalmau, B. & Montoro, M. Safety and efficacy of treatment with pegylated interferon alpha-2a with ribavirin in chronic hepatitis C genotype 4. *Ann Hepatol* 12, 30-35,**2013**.

- 314 Feuerstadt, P., Bunim, A. L., Garcia, H., Karlitz, J. J., Massoumi, H., Thosani, A. J., Pellecchia, A., Wolkoff, A. W., Gaglio, P. J. & Reinus, J. F. Effectiveness of hepatitis C treatment with pegylated interferon and ribavirin in urban minority patients. *Hepatology* 51, 1137-1143, **2010**.